DOE/CE/23810-102

# Elastohydrodynamic Lubrication with Polyolester Lubricants and HFC Refrigerants

## Final Report

**Volume I**

**April 1999**

Selda Gunsel
Michael Pozebanchuk

Pennzoil Products Company
Technology Center
1520 Lake Front Circle
The Woodlands, TX 77380 USA

**Prepared for:**
**The Air Conditioning and Refrigeration Technology Institute**
under
ARTI MCLR Project Number 670-54400

"This research project is supported, in whole or in part, by U.S. Department of Energy grant number DE-FG02-91CE23810: Materials Compatibilities and Lubricants Research (MCLR) on CFC-Refrigerant Substitutes. Federal funding supporting the MCLR program constitutes 93.57% of allowable costs. Funding from the air-conditioning and refrigeration industry supporting the MCLR program consists of direct cost sharing of 6.43% of allowable costs and significant in-kind contributions."

## DISCLAIMER

The U.S. Department of Energy's and the air-conditioning industry's support for the Materials Compatibility and Lubricants Research (MCLR) program does not constitute an endorsement by the U.S. Department of Energy, nor by the air-conditioning and refrigeration industry, of the views expressed herein.

## NOTICE

This report was prepared on account of work sponsored by the United States Government. Neither the United States Government, nor the Department of Energy, nor the Air Conditioning and Refrigeration Technology Institute, nor any of their employees, nor any of their contractors, subcontractors, or their employees, makes any warranty, expressed or implied, or assumes any legal liability or responsibility for the accuracy, completeness, or usefulness of any information, apparatus, product or process disclosed or represents that its use would not infringe privately-owned rights.

## DISCLAIMER

This report was prepared by Pennzoil Products Company for the Air Conditioning and Refrigeration Technology Institute. The material in it reflects Pennzoil Products Company's best judgment in light of the information available to it at the time of preparation. Any use which a third party makes of this report, or any reliance on or decisions to be made based on it, are the responsibility of such third party. Pennzoil Products Company accepts no responsibility for damages, if any, suffered by any third party as a result of decisions made or actions taken based on this report.

## ACKNOWLEDGEMENT

The authors would like to express their thanks to Glenn Hourahan (ARTI) for his support and assistance throughout this study. The authors also thank Richard Ernst (Trane), Robert Doerr (Trane), Arthur Butterworth (Trane), Phillip Johnson (Frick), Alex Lifson (Carlyle Compressor Co.), S. Ganesan Sundaresan (Copeland Corporation), Thomas E. Watson (McQuay International), Robert Yost (ICI), Mirjam Wilson (ICI), Aditi Mulay (Copeland), Victor Cheng (Mobil), and Lori Homolish (Idemitsu-Kosan) for solubility, viscosity and density information and helpful discussions. The authors appreciate the assistance of Sylvia Reneau in preparing this report.

## TABLE OF CONTENTS

**VOLUME I**

**VOLUME II**

Raw Data

Note: Raw Data is contained in a separate volume (Volume II).

## LIST OF TABLES

## LIST OF FIGURES

## 1.0 EXECUTIVE SUMMARY

Lubrication properties of refrigeration lubricants were investigated in high pressure nonconforming contacts under different conditions of temperature, rolling speed, and refrigerant concentration. The program was based upon the recognition that the lubrication regime in refrigeration compressors is generally elastohydrodynamic or hydrodynamic, as determined by the operating conditions of the compressor and the properties of the lubricant. Depending on the compressor design, elastohydrodynamic lubrication conditions exist in many rolling and sliding elements of refrigeration compressors such as roller element bearings, gears, and rotors.

The formation of an elastohydrodynamic film separating rubbing surfaces is important in preventing the wear and failure of compressor elements. It is, therefore, important to predict the elastohydrodynamic (EHD) performance of lubricants under realistic tribocontact conditions. This is, however, difficult as the lubricant properties that control film formation are critically dependent upon pressure and shear, and cannot be evaluated using conventional laboratory instruments.

In this study, the elastohydrodynamic behavior of refrigeration lubricants with and without the presence of refrigerants was investigated using the ultrathin film EHD interferometry technique. This technique enables very thin films, down to less than 5 nm, to be measured accurately within an EHD contact under realistic conditions of temperature, shear, and pressure. The technique was adapted to the study of lubricant/refrigerant mixtures. Film thickness measurements were obtained on refrigeration lubricants as a function of speed, temperature, and refrigerant concentration. The effects of lubricant viscosity, temperature, rolling speed, and refrigerant concentration on EHD film formation were investigated. From the film thickness measurements, effective pressure-viscosity coefficients were calculated.

The lubricants studied in this project included two naphthenic mineral oils (NMO), four polyolesters (POE), and two polyvinyl ether (PVE) fluids. These fluids represented viscosity grades of ISO 32 and ISO 68 and are shown in the table below. Refrigerants studied included

R-22, R-134a, and R-410A. Film thickness measurements were conducted at 23 °C, 45 °C, and 65 °C with refrigerant concentrations ranging from zero to 60% by weight.

| Refrigerant | Lubricant | Commercial Identification |
|---|---|---|
| R-22 | ISO 32 Naphthenic Mineral Oil (NMO-32) | Suniso 3GS |
| | ISO 68 Naphthenic Mineral Oil (NMO-68) | Suniso 4GS |
| R-134a | ISO 32 Polyolester (POE-32) | ICI Emkarate RL 32H |
| | ISO 32 Polyvinyl Ether (PVE-32) | Idemitsu Kosan FVC 32B |
| | ISO 68 Polyolester A (POE-68A) | ICI Emkarate RL 68H |
| | ISO 68 Polyolester B (POE-68B) | Mobil EAL 68 |
| | ISO 68 Polyolester C (POE-68C) | CPI Solest 68 |
| | ISO 68 Polyvinyl Ether (PVE-68) | Idemitsu Kosan FVC 68B |
| R-410A | ISO 32 Polyolester (POE-32) | ICI Emkarate RL 32H |
| | ISO 32 Polyvinyl Ether (PVE-32) | Idemitsu Kosan FVC 32B |
| | ISO 68 Polyolester A (POE-68A) | ICI Emkarate RL 68H |
| | ISO 68 Polyvinyl Ether (PVE-68) | Idemitsu Kosan FVC 68B |

All of the lubricants studied behaved as expected from the EHD theory under air. EHD film thickness increased with speed and dynamic viscosity and decreased with temperature. Effective pressure-viscosity coefficients ($\alpha$) calculated from the film thickness data showed the effect of chemical structure on the pressure-viscosity characteristics of the fluids. The fluids were ranked with respect to their pressure-viscosity coefficients in the following order:

naphthenic mineral oils > polyvinyl ethers > polyolesters.

Differences were observed in the pressure-viscosity characteristics of the polyolesters studied. This was related to the degree of branching in the ester structure. Esters with branching have higher $\alpha$-values than those with linear structure. Effective pressure-viscosity coefficients also change with temperature, decreasing as the temperature increases.

Refrigerants have a significant effect on reducing the EHD film formation ability of lubricants. EHD film thickness decreases drastically in the contact as the refrigerant concentration in the lubricant increases. Even at the low refrigerant concentration of 10%, the reduction in film thickness ranges from 30 to 65% depending on the test temperature. Refrigerants reduce dynamic viscosity as well as the pressure-viscosity coefficients of lubricants. However, this effect decreases as the temperature increases. The thickness of the

EHD film formed by the lubricant/refrigerant mixtures show a similar dependence on speed as that of the lubricant itself. Under some conditions (high refrigerant concentrations, high temperatures and pressures), some deviations were observed from the EHD theoretical slope for the film thickness/speed relationship.

Effective pressure-viscosity coefficients for the lubricant/refrigerant mixtures were calculated from the film thickness data using the theoretical relationship of Dowson-Hamrock and dynamic viscosity data available for the mixtures in the literature. The accuracy of the calculated pressure-viscosity coefficients depends strongly on the accuracy of the dynamic viscosity data used in the calculations.

For a given refrigerant and lubricant mixture, pressure-viscosity coefficient increases linearly in proportion to the logarithm of dynamic viscosity as shown below. This finding suggests that the same fundamental molecular properties govern changes in both dynamic viscosity and pressure-viscosity properties of fluids.

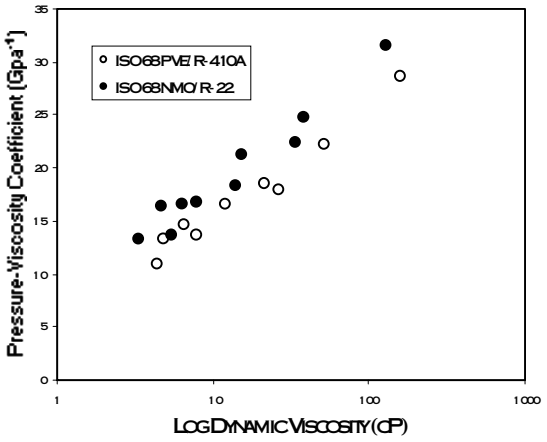


The ranking obtained with respect to the pressure-viscosity characteristics of the lubricants under air was also observed under refrigerant environments. However, the differences became smaller as the refrigerant concentration and the temperature increased. In general, refrigerant (R-134a or R-410A) mixtures with polyvinyl ethers have higher $\alpha$-values than those with polyolesters. Mixtures of naphthenic mineral oil and R-22 have higher $\alpha$-values than those of polyolesters or polyvinyl ethers and R-134a or R-410A.

The presence of R-410A in the lubricants (polyolesters or polyvinyl ethers) results in thinner EHD films, as shown below, than those produced by the same lubricants in the presence of R-134a.

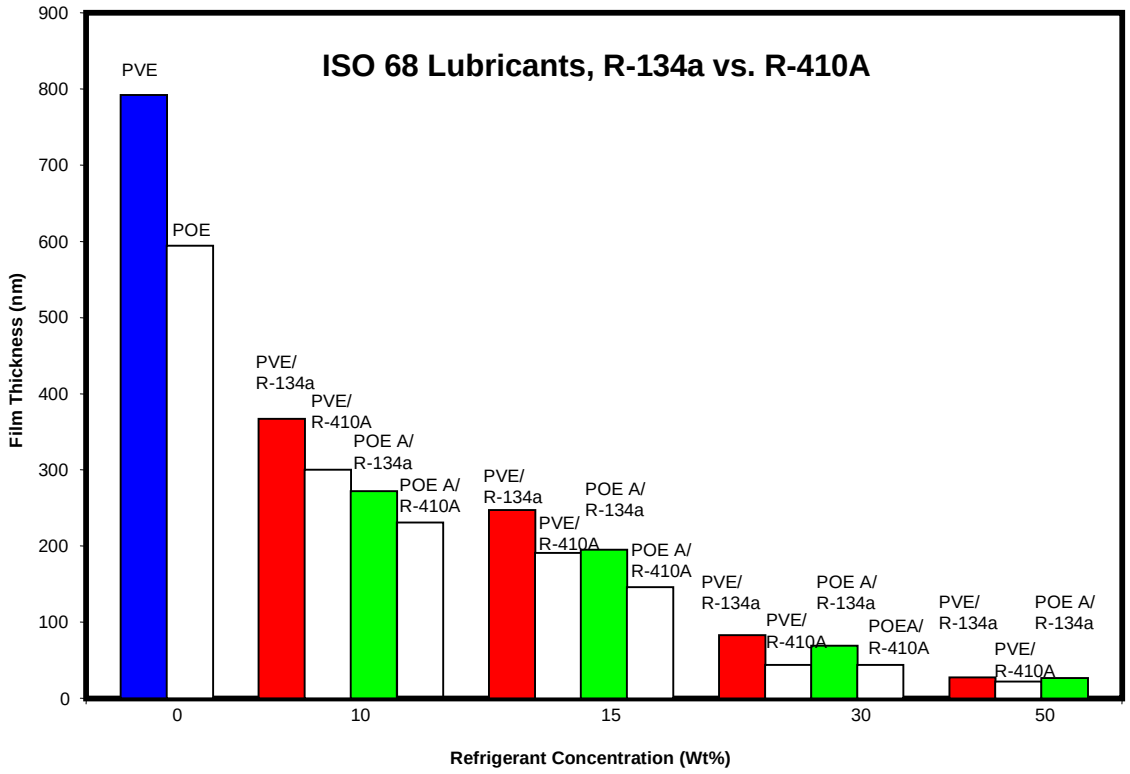


A graphical ranking of all the tested lubricant/refrigerant combinations is shown in the charts below. The film thickness data reported in these charts were obtained under the same conditions of temperature (22.5 °C) and speed (0.8 m/s) for ISO 32 and ISO 68 lubricants and their mixtures with refrigerants.

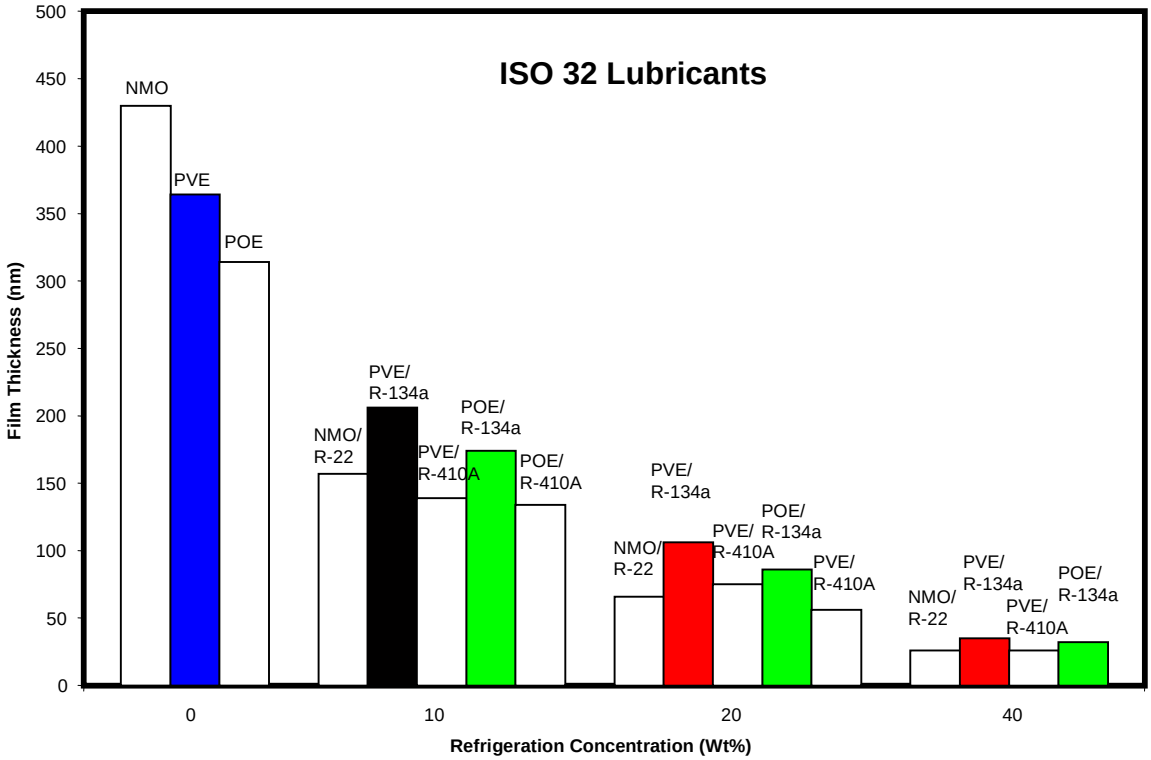


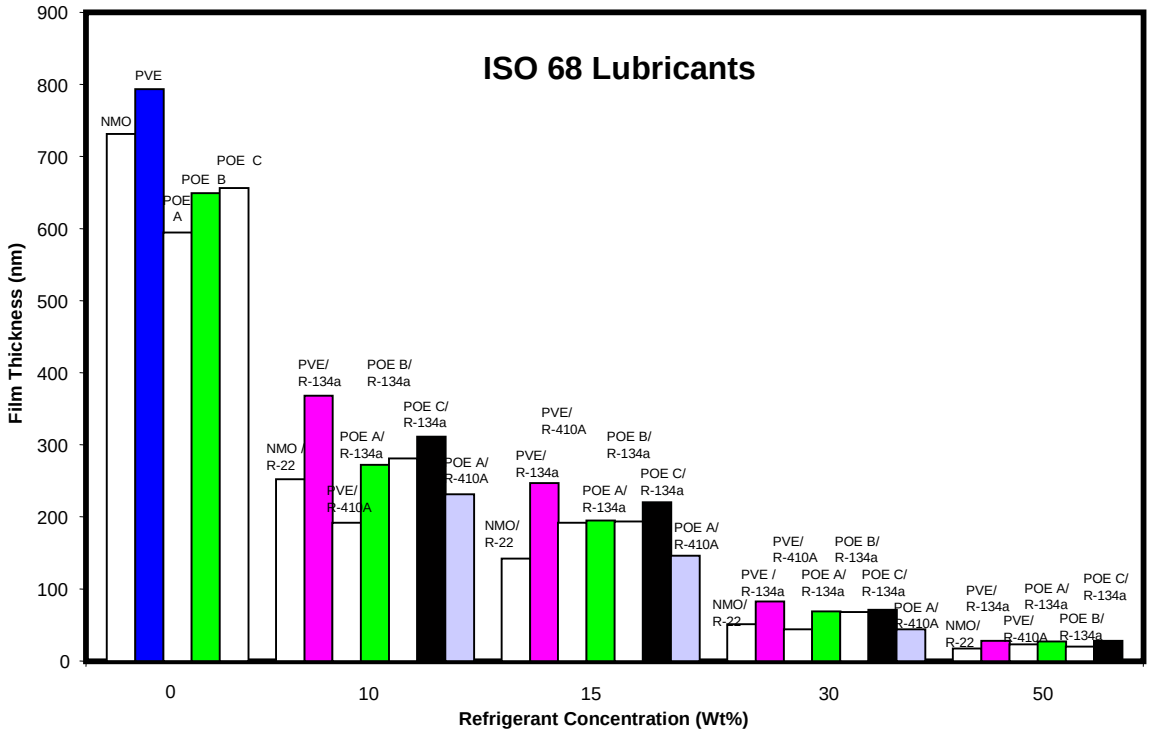


Based on the results of the current study, future areas of investigation were identified. These areas concentrate on 1) ways to improve the accuracy of the dynamic viscosity and

pressure-viscosity coefficient determinations on lubricant/refrigerant mixtures, and 2) evaluation of EHD friction (traction) properties of lubricant/refrigerant mixtures. This work would be useful for modeling viscosity and pressure-viscosity characteristics of lubricant/refrigerant mixtures, and for determining and optimizing lubricant behavior in EHD contacts of refrigeration compressors.

## 2.0 INTRODUCTION

The primary role of a refrigeration lubricant is to provide satisfactory lubrication to the moving parts of the compressor by reducing friction and wear of the rubbing surfaces. In addition, the refrigeration lubricant has important secondary functions such as the removal of heat from the hot compressor parts and to act as a sealing aid for the compression space and the valves.

Refrigeration lubricants represent a special case of lubricants due to their interactions with the refrigerants. These lubricants must perform their functions in the presence of refrigerants. Hence, in addition to the conventional lubricant properties such as viscosity, viscosity index, lubricity, stability, low temperature flow properties, compatibility with system materials, volatility, etc., interactions with the refrigerants should also be considered in the selection of refrigeration lubricants (1-3). There have been a number of studies reported in the literature on the interactions of refrigerants with lubricants concerning the effects on physical/chemical properties and performance (4-13).

The lubricant/refrigerant interactions are determined by the stability, solubility, miscibility, and surface tension properties of the lubricant/refrigerant mixture. Special problems that can arise from such interactions include the dilution of the lubricant by the refrigerant. It has been shown that a small amount of refrigerant in the lubricant can significantly reduce viscosity, since the viscosities of the refrigerants are much lower than those of the lubricants (14). This could adversely influence the lubrication properties of refrigeration oils as well as their heat transfer and sealing properties. On the other hand, viscosity reduction may improve oil return from the evaporator to the compressor. The interactions between the lubricant and the refrigerant can also result in reaction products which could lead to the formation of sludge, deposits, and copperplating. These could increase wear and result in mechanical failures.

Refrigeration lubricants provide lubrication to the moving parts of the compressor by forming a film that separates the surfaces and limits their contact and adhesion. This film can vary in thickness from a few monolayers as found under ***boundary lubrication*** conditions to hundreds and thousands of nanometers of hydrodynamically entrained lubricant as found under ***elastohydrodynamic (EHD)*** and ***hydrodynamic (HD) lubrication*** conditions. It has been recognized that the lubrication regime in refrigeration compressors is generally elastohydrodynamic and hydrodynamic, depending on the operating conditions (pressure, speed, temperature) and lubricant properties (1-3, 15). Elastohydrodynamic lubrication conditions may exist in many rolling and sliding elements of refrigeration compressors such as roller element bearings, gears, and rotors. Boundary lubrication may also exist under insufficient lubrication and compressor overload conditions, and during start-up and shutdown procedures.

It has been long recognized that the formation of EHD films separating rubbing surfaces is important in preventing wear and failure of machine elements. Therefore, it is of considerable practical importance to be able to measure film thickness in lubricated contacts in order to evaluate the effectiveness of lubricants and to test or validate the predictive theories.

The objective of this study was to investigate the film formation properties of refrigeration lubricants using the ultrathin film EHD interferometry technique and to study the effects of refrigerants on film formation. Film thickness measurements were conducted as a function of lubricant viscosity, speed, temperature, and refrigerant concentration. Based on the EHD film thickness data, effective pressure-viscosity coefficients were calculated for the test fluids at different temperatures and the effects of refrigerants on pressure-viscosity properties were investigated.

## 3.0 BACKGROUND

### 3.1 Changes in Refrigerant Technology – Impact on Lubrication

A wide variety of lubricants have been used in the lubrication of refrigeration compressors. These include mineral oils, synthetic hydrocarbons (alkylbenzenes and polyalphaolefins), polyalkylglycols, esters, and polyvinyl ethers (2, 3, 16, 17). The choice of the lubricant depends on the type of refrigerant used and whether it is polar in nature. Until recently, the most commonly used refrigerants included ammonia, hydrochlorofluorocarbons (HCFCs), and chlorofluorocarbons (CFCs). Due to the environmental hazards imposed by the CFCs and HCFCs, these refrigerants are now being replaced by hydrofluorocarbons (HFCs). There has been a lot of work done in recent years in order to find acceptable substitutes for CFCs and HCFCs (18-25).

The use of new refrigerants presents many challenges to the industry which include design changes in the refrigeration systems, materials, and lubricants. Tribological problems are expected since the candidate refrigerants do not possess the same lubrication and miscibility properties as the previous ones. For example, the refrigerant CFC-12 (R-12), which has been widely used in household refrigerators and automobile air conditioners, has good miscibility with mineral oils and alkylbenzenes. This refrigerant also makes a significant contribution to lubricity due to the presence of chlorine in its structure (26-29). Chlorine-containing compounds are well known for their extreme-pressure (EP) properties; they can react with the metals and form protective surfaces composed of metal chlorides.

On the other hand, the refrigerant R-134a, which is considered as a substitute for CFC-12, does not have chlorine and is not miscible with mineral oils. Therefore, an EP function cannot be expected from this refrigerant. Immiscibility with mineral oils also presents oil starvation related lubrication problems in the critical compressor parts. Polyalkylglycols (PAG) and polyolesters (POE) have been considered as potential lubricants to be used with R-134a due to their good miscibility (16, 18). However, boundary lubrication studies indicate that in order to achieve the same lubricity level of R-12/mineral oil or R-12/alkylbenzene systems, EP additives must be added to PAG/R-134a and POE/R-134a systems. Another approach may be the use of self-lubricating materials on the critical compressor components (30). The viscosity of the lubricant may also need to be adjusted to maintain the hydrodynamic film thickness

similar to those obtained with the R-12/mineral oil systems. Similar issues are also valid for R-22, a widely used refrigerant for air-conditioning units, which will also be phased-out due to environmental considerations.

There have been some studies reported in the literature on the boundary lubrication properties of refrigeration lubricants and refrigerants (26-29). However, there has been very little experimental work conducted on the EHD properties of refrigeration lubricants. Significant contributions in this area were recently made by Jonsson (31) and Akei et al (32, 33).

In order to ensure satisfactory operation of refrigeration compressors, the sliding and rolling components must be designed to operate under EHD or HD conditions. In the design calculations, HD and EHD theories are applied to estimate the lubrication conditions of compressors. However, the validity of these theories for non-homogeneous systems is questionable. Bearing lubrication studies by Jacobson (34) indicate that under certain conditions the behavior of the oil/refrigerant mixture deviates from the EHD theory. Therefore, it is important to be able to experimentally verify the calculated EHD film thickness. Recent studies of Wardle et al (35), Jonsson et al (31, 36), and Akei et al (32, 33) also indicate the need for further research in this area.

### 3.2 Elastohydrodynamic Lubrication

There are many rolling or sliding contacts in engineering where high loads are spread over small contact areas, for example in gears and bearings. In such nonconforming contacts, called elastohydrodynamic (EHD) or concentrated contacts, the lubricating film is exposed to extreme conditions of pressure and shear. In refrigeration compressors, EHD contacts can be found in the rolling element bearings, gears, rotors, or wherever rigid counterformal surfaces are loaded and move relative to one another. The pressures generated in EHD contacts can be on the order of 0.5 to 2.4 GPa. The high pressures within the contact have two beneficial effects, elastically flattening the surfaces, and hence reducing contact pressure, and increasing oil viscosity in the contact. The overall effect of these two is to permit the formation of thin EHD oil films in such contacts, typically 50 - 1000 nm (0.05 - 1 micron) thick. This is of the same order as the roughness of engineering surfaces which makes EHD oil film thickness an important practical value in predicting the performance of bearings and gears. A widely used term in this context is the specific film thickness, $\lambda$, which is defined as:

$$\lambda = \frac{h}{\sigma}$$ **Equation 1**

where h is the lubricant film thickness and $\sigma$ is the composite surface roughness of the two rubbing surfaces. The composite roughness is defined as:

$$\sigma = \sqrt{\sigma_1^2 + \sigma_2^2}$$ **Equation 2**

where $\sigma_1$, $\sigma_2$ are the root mean square (RMS) roughnesses of the two rubbing surfaces. The specific film thickness describes the thickness of the lubricant film in relation to the roughness of the lubricated surfaces. As the $\lambda$ value increases, there is less contact between the two surfaces. The surfaces are in contact at some point or points nearly all the time when $\lambda < 1$, and are almost never in contact when $\lambda > 4$. The specific film thickness parameter correlates with the function of a lubricant to prevent or minimize wear, scuffing, and to minimize rolling contact fatigue.

Theoretical calculation of EHD lubricant film thickness requires the simultaneous solution of hydrodynamic flow equations based on Reynolds' theory, surface elasticity equations based on Hertzian theory, and lubricant pressure-viscosity equations. This problem cannot be solved analytically, but successful numerical solutions were found by Archard (37), Dowson and Hamrock (38), and Foord and Cameron (39). These solutions are presented in the form of regression equations based on numerical solutions. The predicted film thickness is expressed in terms of three non-dimensional groups: speed, material, and load. These are shown below in the Dowson and Hamrock equation for central film thickness:

$$\frac{h_c}{R'} = 2.69 \left\{\frac{U\mu_0}{E'R'}\right\}^{0.67} \left\{\alpha E'\right\}^{0.53} \left\{\frac{W}{E'R'^2}\right\}^{-0.067} \left\{1-0.61e^{-0.73k}\right\}$$ **Equation 3**

where $h_c$ = central film thickness

U = mean surface speed of the two surfaces

R' = reduced radius of the two surfaces

E' = reduced Young's modulus

W = applied load

k = ellipticity parameter

$\mu_0$ = dynamic viscosity of the oil at atmospheric pressure and the test temperature

$\alpha$ = pressure-viscosity coefficient of the oil

The existing EHD design equations to calculate film thickness are based on the assumptions that the lubricant is both homogeneous and exists as a continuum. These assumptions may not be valid for lubricant and refrigerant mixtures. Also, under very thin film conditions, where film thickness is comparable to surface roughness, these assumptions may break down and the existing theories may not be valid. An alternative approach is to measure EHD film thickness directly from within the contact under realistic conditions of pressure and shear.

### 3.3 Film Thickness Measurements

A number of test methods have been developed to measure film thickness in hydrodynamic and EHD contacts (40-46). These are mostly based on electrical or electromagnetic radiation measurements and include techniques such as capacitance, resistance, fluorescence, x-ray, and inductance. Among these, the most widely used technique is the capacitance method. The advantage of this technique is that it can be applied to realistic metal-to-metal contacts. Capacitance has been used to measure film thickness in bearings and piston liner/rings (47, 48). One method that has proven particularly effective for measuring lubricant film thickness in model contacts is optical interferometry (39, 49). This technique has the advantage over the capacitance method in that it relies upon the refractive index of the separating film rather than its dielectric constant. Refractive index is much less variable with film composition than dielectric constant.

Figure 1 shows the principles of optical interferometry as applied to an EHD contact. The EHD contact can be formed by a steel ball loaded against a flat disc as a contact geometry equivalent to many nonconforming contacts of practical importance. Either the ball or the disc can be driven to give varying slide-to-roll ratios, simulating conditions found in practice. The disc is transparent to visible light, and the EHD film generated is measured by the observation of interference color within the contact. This technique has been very useful in studying EHD behavior of lubricants since the wavelength of light is of the same order as a typical EHD lubricant film.

The surface of the glass disc shown in Figure 1 is coated with a thin (20 nm) semi-reflecting chromium layer. Light is shone into the contact through the glass disc. Some of this light is reflected from the underside of the disc and some passes through the lubricant's film and is reflected back from the steel surface. Since the two beams of light travel different distances, when they recombine they interfere either constructively or destructively, according to Equations 4 and 5 below, and produce colored interference patterns which are characteristic of the lubricant film thickness. The lubricant film thickness, which is represented by the optical path difference between the two beams, is determined by studying the intensity of the recombined beam.

Destructive interference:

$$h_{oil} = \frac{(N + \tfrac{1}{2} - \phi)\,\lambda}{2n \cos\theta} \qquad N = 0,1,2 \qquad \textbf{Equation 4}$$

Constructive interference:

$$h_{oil} = \frac{(N - \phi)\,\lambda}{2n \cos\theta} \qquad N = 1,2,3 \qquad \textbf{Equation 5}$$

where h = lubricant film thickness

N = fringe order

$\phi$ = net phase change

$\lambda$ = wavelength of interfered light

n = refractive index of lubricant

$\theta$ = angle of incidence

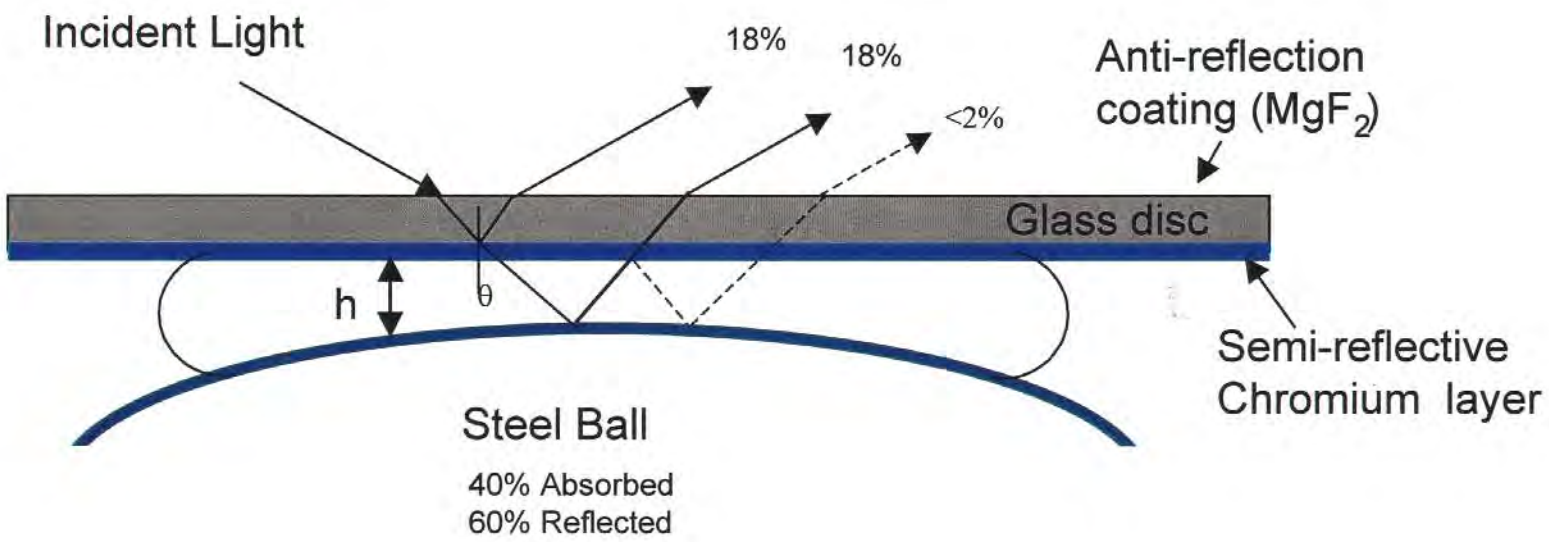


Figure 1. Principle of optical interferometry

The optical interferometry technique has been a useful tool for measuring lubricant film thickness in EHD contacts. This technique, however, also has some significant limitations with respect to the thickness of the films measured and the precision of the measurements. For example, for vertical illumination Equation 4 reduces down to the following equation for the first fringe:

$$nh_{oil} = \frac{\lambda}{4} \qquad \textbf{Equation 6}$$

This indicates that the first fringe occurs at the wavelength of visible light divided by four, which means that the thinnest films that can be measured by conventional optical interferometry are around 80 to 100 nanometers. This limitation has been overcome by the development of the "ultrathin film EHD interferometry" technique which is described in Section 5.0 (50).

### 3.4 Pressure-Viscosity Coefficient

Pressure-viscosity coefficient is an important rheological property of a lubricant that shows the dependence of viscosity on pressure and is defined as follows:

$$\alpha = \frac{1}{\mu}\left[\frac{\partial \mu}{\partial \rho}\right]_T \qquad \textbf{Equation 7}$$

where $\alpha$ is the pressure-viscosity coefficient, $\mu$ is the dynamic viscosity, and $\rho$ is the pressure.

Pressure-viscosity coefficient is of particular importance for applications when the lubricants are subjected to high local pressures, such as those found in EHD contacts. The knowledge of the pressure-viscosity coefficient for a particular lubricant system and its variation with temperature provides valuable design data and is essential if the EHD film thickness is to be calculated from theory. It can be seen from Equation 3 above that the EHD film thickness depends on two lubricant properties, $\mu$ and $\alpha$. $\mu_0$ is the ambient pressure oil viscosity in the inlet zone, and can be measured using conventional viscometers. The measurement of $\alpha$, on the other hand, is more complicated. However, it can be conveniently determined from the measured EHD film thickness by comparing the results to a reference oil with a known $\alpha$ value as shown below:

From the Dowson-Hamrock equation for EHD central film thickness:

$$h_c = k\alpha^{0.53} (U\mu_0)^{0.67} \qquad \textbf{Equation 8}$$

where k = constant, depending on load, geometry, and material properties.

Comparison of the film thickness for the test oil and the reference oil gives:

$$\frac{h_{ref}}{h_{test}} = \left[ \frac{\alpha_{ref}}{\alpha_{test}} \right]^{0.53} \qquad \textbf{Equation 9}$$

Pressure-Viscosity coefficient for the test oil is given by:

$$\alpha_{test} = \alpha_{ref} \left[ \frac{h_{test}}{h_{ref}} \right]^{\frac{1}{0.53}} \qquad \textbf{Equation 10}$$

## 4.0 SCOPE AND TECHNICAL APPROACH

The scope of this project was to investigate the film formation properties of refrigeration lubricants and is primarily concerned with measuring EHD film thickness of refrigeration lubricants and understanding the contribution of refrigerants to film formation. The lubricants studied included ISO 32 and ISO 68 viscosity grades of naphthenic mineral oils, polyolesters, and polyvinyl ethers. The refrigerants studied included R-22 (with mineral oils), R-134a (with polyolesters and polyvinyl ether lubricants), and R-410A (with polyolester and polyvinyl ether lubricants).

The technical approach taken was to investigate the EHD behavior of refrigeration lubricants, with and without the presence of refrigerants, using the "ultrathin film EHD" technique. This technique enables very thin films, down to less than 5 nm, to be measured accurately within an EHD contact under realistic conditions of shear and pressure. The effects of lubricant viscosity, temperature, rolling speed, and refrigerant concentration on EHD film formation were investigated. Effective pressure-viscosity coefficients were calculated for the fluids studied. The information generated as a result of this study is expected to aid in the selection of lubricants in refrigeration systems and also in the development of improved bearing designs.

The project was conducted according to the Tasks outlined below for the refrigerant and lubricant combinations listed in Table 2 (page 29).

**Task 1: Visit Manufacturers of Air-Conditioning and Refrigeration Compressors**

Visit one or more manufacturers to acquire more information about the specific lubrication requirements of air-conditioning and refrigeration compressors. Also gather information regarding the handling of refrigerants to assist with charging the EHD Tester and for conducting tests with various refrigerant concentrations.

**Task 2: Modify the EHD Test Apparatus to Contain Refrigerant Pressure**

Modify the ultrathin film EHD rig to operate at pressures above the vapor pressure of the refrigerants at the test temperatures.

**Task 3: Conduct Baseline Tests on Lubricants in Air**

Determine baseline EHD film thickness and pressure-viscosity coefficient for the ISO 32 and 68 lubricants (i.e., two mineral oils, four polyolester lubricants, and two polyvinyl ether lubricants) as a function of rolling speed over the temperature range 25 to 65 °C.

**Task 4: Conduct Tests on R-22 Refrigerant and Mineral Oil (Baseline)**

Determine EHD film thickness and pressure-viscosity coefficient for R-22 with the ISO 32 and 68 mineral oils as a function of rolling speed over the temperature range 25 to 65 °C and at refrigerant concentrations from 10 to 50%.

**Task 5: Conduct Tests on R-134a and Polyolester and Polyvinyl Ether Lubricants**

Determine EHD film thickness and pressure-viscosity coefficient for R-134a with the indicated ISO 32 and 68 lubricants as a function of rolling speed over the temperature range 25 to 65 °C and at refrigerant concentrations from 10 to 50%.

**Task 6: Conduct Tests on R-410A and Polyolester and Polyvinyl Ether Lubricants**

Determine EHD film thickness and pressure-viscosity coefficient for R-410A with the indicated ISO 32 and 68 lubricants as a function of rolling speed over the temperature range 25 to 65 °C and at refrigerant concentrations from 10 to 50%.

## 5.0 TEST METHOD

### 5.1 Ultrathin Film Interferometry Method – Lubricant Film Thickness Measurements

Ultrathin film interferometry method (50) was adapted to measure film thickness of lubricant and refrigerant mixtures. This method is an extension of conventional optical interferometry that permits very thin films, down to less than 5 nm, to be measured accurately within an EHD contact. This technique can be used to study lubricant behavior in EHD as well as in mixed lubrication regimes. It is particularly useful for measuring film thickness for low viscosity fluids and/or under high temperatures. It has been successfully applied to study the EHD behavior of lubricant base oils, antiwear additives, metalworking fluids and polymers used as viscosity index improvers in lubricants (51-57). Some preliminary studies were also conducted on refrigeration lubricants (58).

The test set-up is shown schematically in Figure 2. A highly polished steel ball (AISI 52100, 19.05 mm diameter, 11 nm RMS surface roughness) is loaded against the underside

flat surface of a rotating transparent glass disc to form a circular concentrated EHD contact. The underside of the chromium-plated glass disc is coated with a spacer layer of transparent silica of about 500 nm thickness. The composite surface roughness of the undeformed surfaces is 11 nm.

The ball is contained in a lubricant bath and is driven by the disc in nominally pure rolling. The lubricant is filled halfway to the top of the ball, so that the lubricant is entrained into the contact by the rolling motion of the ball. The test lubricant is enclosed in a stainless steel chamber and a heat insulation lid sits on top of the glass disc. This helps to maintain constant test temperature and protects the lubricant from exposure to the outside environment. The test temperature is controlled using heating rods embedded in the chamber walls and is monitored near the contact inlet using a digital thermometer. The temperature can be controlled to a set value within ± 0.5 °C.

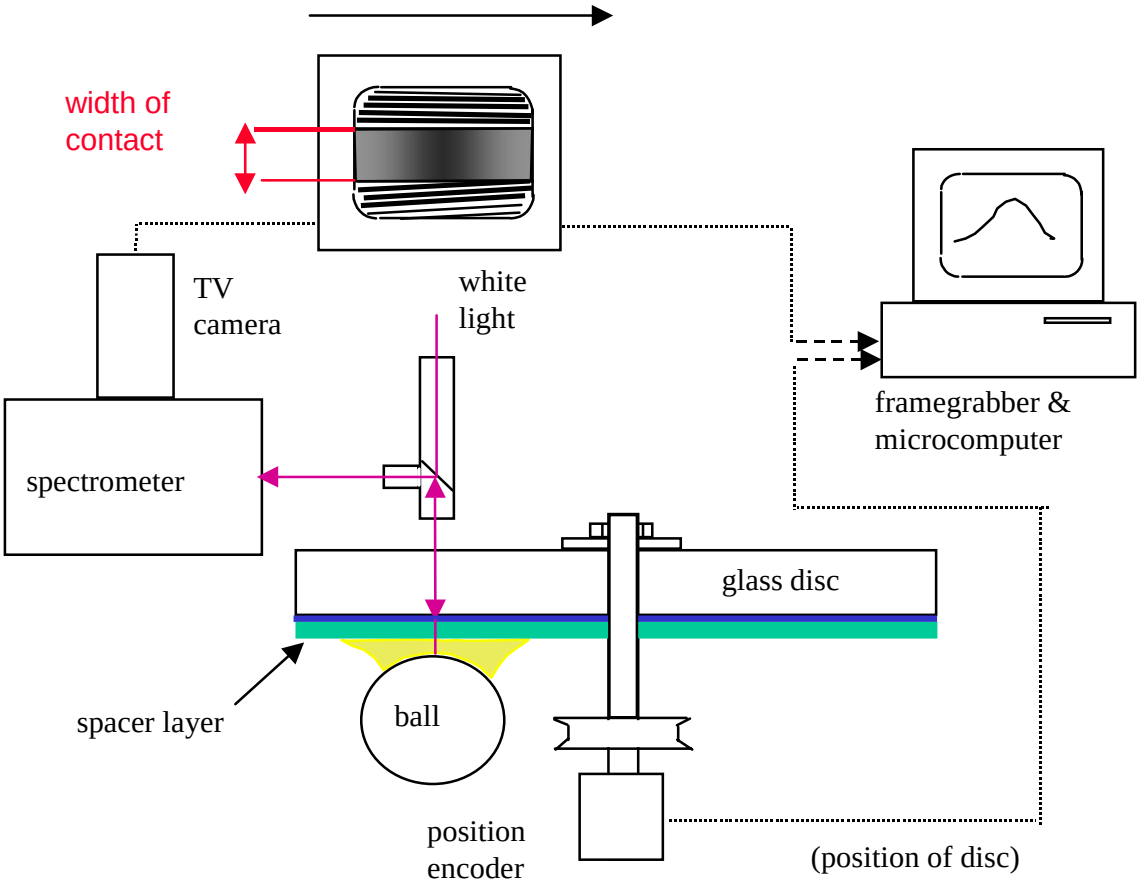


Figure 2. Schematic set-up for ultrathin film interferometry

Lubricant film thickness is determined by optical interferometry as shown schematically in Figure 3. White light is shone into the contact and some is reflected from the chromium layer, while some passes through the silica spacer layer and any lubricant film present to be reflected from the ball. The two beams recombine and interfere. The interfered light from the contact is passed into a spectrometer where it is dispersed and detected by a solid state, black and white TV camera as shown in Figure 2. A framegrabber is used to capture this image and a microcomputer program determines the wavelength of maximum constructive interference in the central region of the contact. In this case, the maximum constructive interference of spacer layer plus lubricant film occurs when:

$$n_{oil}\, h_{oil} + n_{sp}\, h_{sp} = \frac{(N - \phi)\, \lambda_{sp + oil}}{2 \cos \theta} \qquad N = 1,2,3 \qquad \textbf{Equation 11}$$

Maximum constructive interference of spacer layer occurs when:

$$n_{sp}\, h_{sp} = \frac{(N - \phi)\, \lambda_{sp}}{2 \cos \theta} \qquad N = 1,2,3 \qquad \textbf{Equation 12}$$

The lubricant film thickness is then calculated from the difference between the measured film thickness and the thickness of the silica spacer layer:

$$h_{oil} = \frac{(N_{sp + oil}\, \lambda_{sp + oil} - N_{sp}\, \lambda_{sp})}{2 n_{oil}} \qquad N = 1,2,3 \qquad \textbf{Equation 13}$$

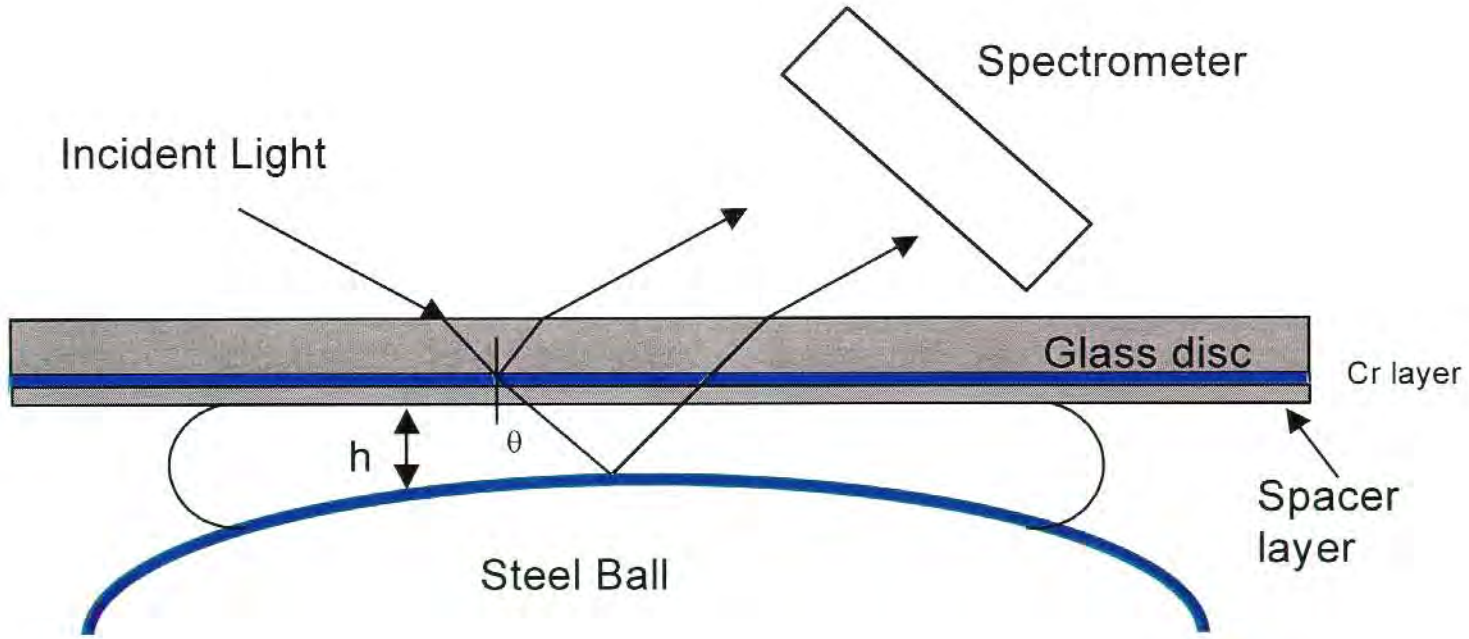


Figure 3. Principle of ultrathin film interferometry

The ultrathin film technique incorporates two important advances over conventional optical interferometry. The first one is the use of a transparent silica spacer layer which acts like a supplementary oil film, enabling optical interference to be observed even when the actual oil film present is very thin. This overcomes a major limitation of conventional optical interferometry, that it cannot easily measure film below approximately one quarter the wavelength of visible light. Thus, lubricant films less than 100 nm (0.1 micron) thick cannot be measured using the conventional method. The second advance is that the reflected interfered light is dispersed by a spectrometer rather than being observed by the eye, as is done in conventional optical interferometry. The dispersed spectrum is computer-analyzed to identify the wavelength of light that is most constructively interfered. This greatly increases the precision of the method compared to conventional optical interferometry.

## 5.2 Film Thickness Measurements for Lubricant/Refrigerant Mixtures

### 5.2.1 Pressurized Test Rig

The ultrathin film EHD rig was modified to operate at pressures above the vapor pressure of the refrigerants at the test temperatures. For this purpose, a new stainless steel test chamber with thicker walls (20 mm) was constructed. This chamber was fitted with a heavy section bolt-down lid with a nitrile O-ring and a small (25 mm diameter) fused silica insert to view the contact, as shown in Figure 4. The fused silica window was sealed with a nitrile O-ring and a copper washer to prevent stress cracking of the window due to misalignment. The optics were adjusted to compensate for the longer focal length as compared to the atmospheric system. The chamber was fitted with a new shaft and seal assembly. The seal assembly consisted of a high pressure bellows seal with graphite face. A solid-based chamber with no aperture for the load system was designed. A spring loading system with parallel leafs was fitted inside the chamber. When the ball and disc were placed and clamped in the chamber, the springs deflected and applied a constant load of 20N to the contact. The chamber was fitted with heating rods, cooling galleries, an inlet valve, an adjustable pressure relief valve, and an emergency burst valve.

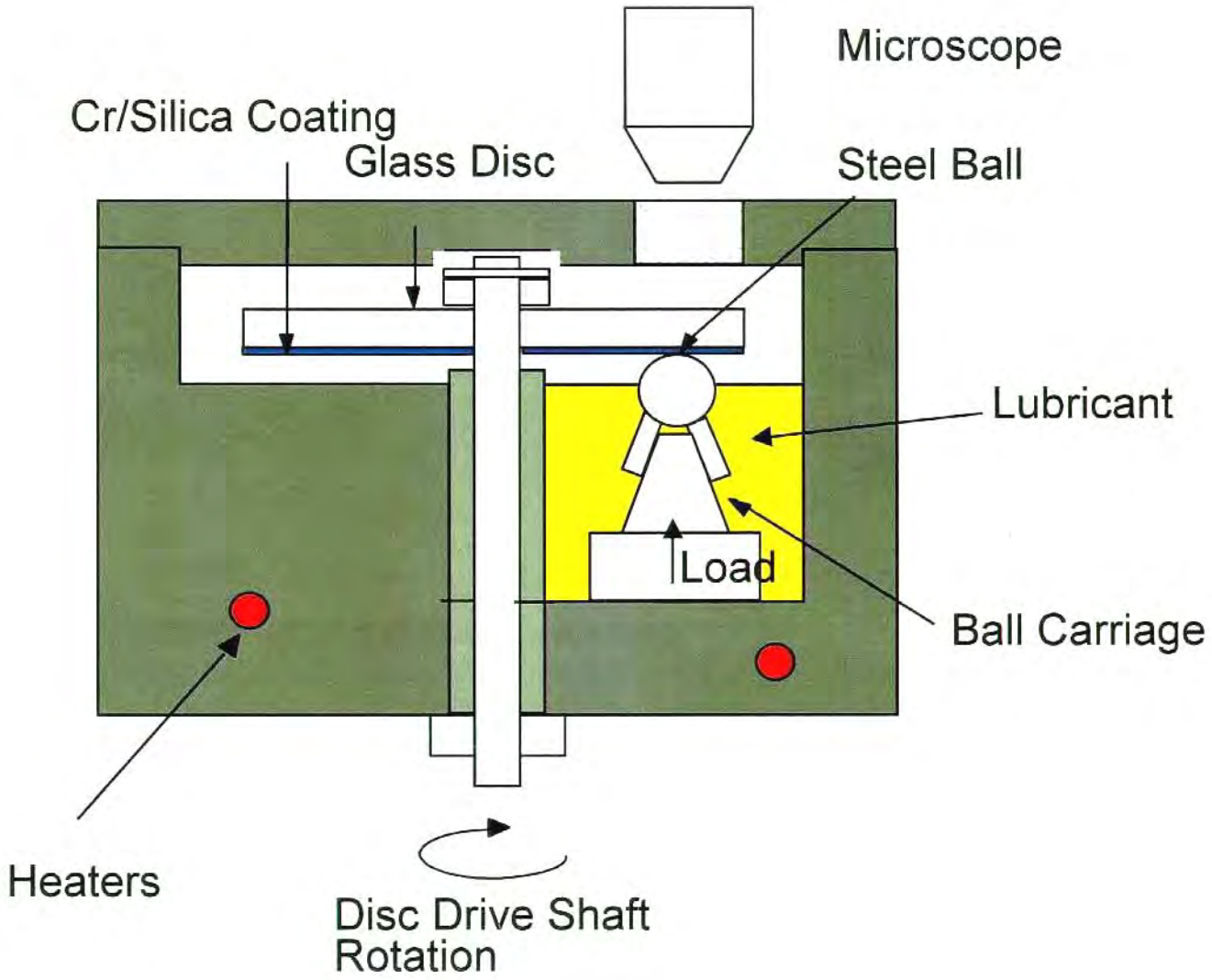


Figure 4. Pressurized Ultrathin Film Interferometry Rig

Figure 5 is a simplified diagram showing the test set-up for refrigerant/lubricant mixtures. The refrigerant cylinder was placed on a balance with a resolution of ± 0.05 g. The cylinder was connected to the test chamber by a 4.76 mm ID flexible stainless steel tubing. A known amount of refrigerant was introduced into the test chamber by a needle valve, V2. The system was designed to operate under 25 bars of pressure. The externally adjustable pressure relief valve was set at 35 bars. The emergency burst valve was rated at 50 bars. The system was fitted with vent and vacuum lines with needle valves for degassing the lubricant and discharging the refrigerant.

### 5.2.2 Test Procedure and Conditions

The test conditions are shown in Table 1. Film thicknesses of lubricants and refrigerant/lubricant mixtures were measured between the ball and the disc using ultrathin film interferometry as described above at a series of rolling speeds ranging from 0.01 m/s (2 rpm-disc rotational speed) to about 2 m/s (460 rpm). All of the tests were carried out at a load of 20N. For the glass-on-steel contact, this load resulted in a maximum Hertz contact pressure of 0.54 GPa.

**Table 1. Test Conditions and Materials**

| | |
|---|---|
| Contact Materials | 52100 steel ball (19 mm diameter)<br>$SiO_2$ coating (~ 400 nm) on Cr coated glass disc |
| Contact Load | 20 N |
| Maximum Contact Pressure | 0.54 GPa |
| Rolling Speed | 0.01 to 2 m/s |
| Bulk Temperature | 23 °C, 45 °C, 65 °C |

The film thickness was measured at three fluid temperatures: ambient, 45 °C, and 65 °C. The ambient temperature varied from 22 °C to 25 °C between tests. The variation in the ambient temperature for each test was within ± 0.5 °C. The average temperature for each ambient temperature test was reported along with the data. The test temperature of 45 °C

and 65 °C was controlled to a set value within ± 0.5 °C using a small K-type thermocouple with a resolution of 0.1 °C near the contact inlet. A new steel ball of RMS surface roughness of 11 nm was used for each test.

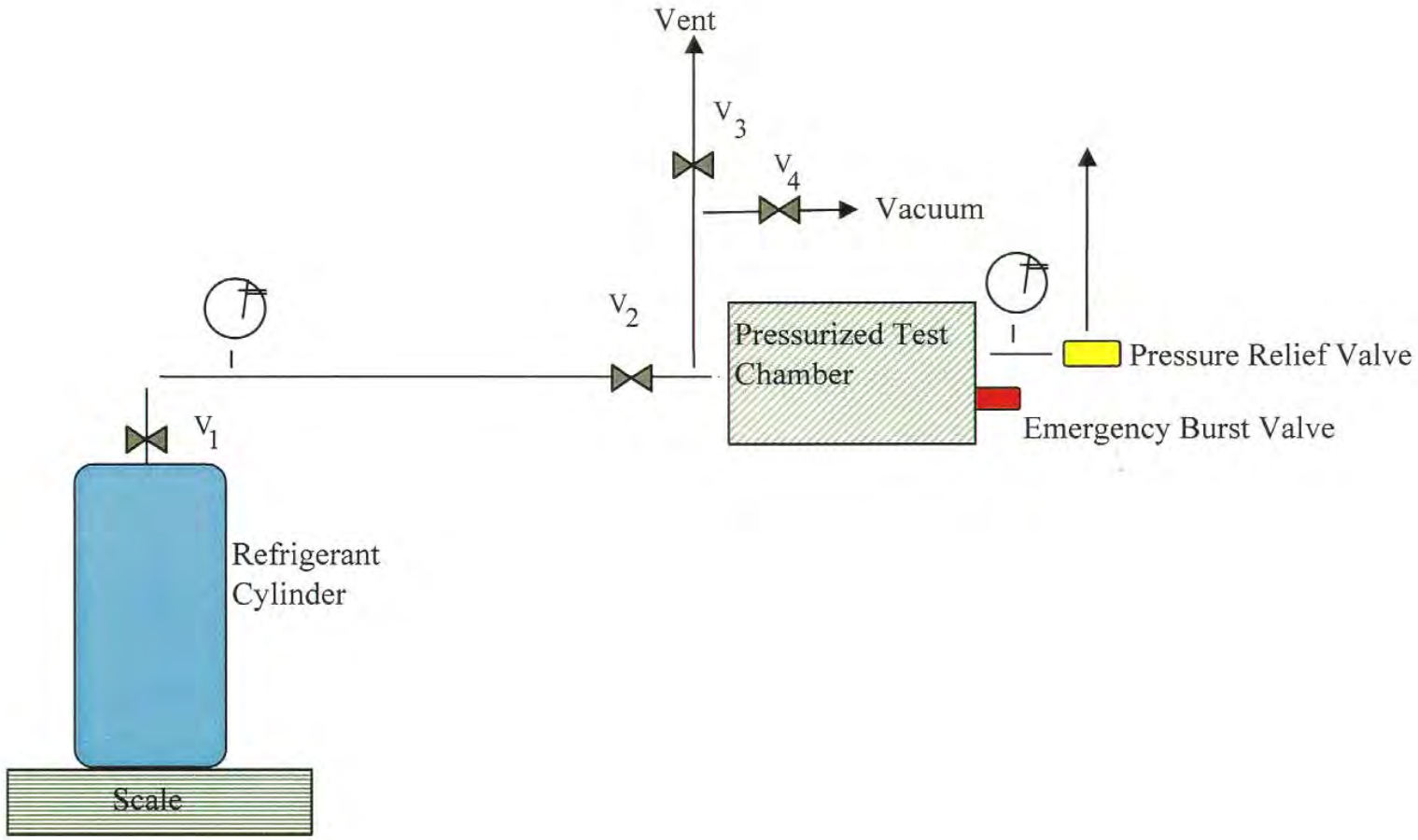


Figure 5. Pressurized Ultrathin Film Interferometry Rig

Lubricant and refrigerant were supplied separately to the test chamber. After placing the ball and disc in place, a known volume of test lubricant was charged into the chamber. The lid was bolted down using a torque wrench. The chamber was then evacuated to 350 microns to degas the oil. During evacuation, the refrigerant cylinder valve (V1) and the vent valve (V3) (Figure 5) were closed, and the chamber valve (V2) and the vacuum line valve (V4) were opened. After evacuation of the system, valves V2 and V4 were closed. Valve V1 was then opened and refrigerant was introduced into the line connecting the cylinder to the test chamber. The cylinder pressure and weight were recorded. Valve V2 was then opened and the desired weight of the refrigerant was added into the test chamber. The amount of the refrigerant charged into the chamber varied depending on the refrigerant concentration tested. Once the refrigerant was introduced into the test chamber, the chamber pressure would increase and then gradually decrease over time due to the dissolution of the refrigerant into the lubricant. The concentration of the refrigerant in the lubricant was determined by weighing the lubricant and the refrigerant added to the test chamber, and measuring the temperature and pressure of the chamber at equilibrium conditions. Daniel charts are used to determine the solubility and viscosity characteristics of the refrigerant and lubricant mixtures. The chamber pressure was monitored using a high precision gauge with an accuracy of ± 0.25%. An electronic halogen leak detector was used to ensure that no refrigerant leaked during the test. Film thickness measurements were taken after the pressure reached steady state. The time required for the system to reach steady state took from three to twenty-four hours, depending on the concentration and type of the refrigerant and lubricant tested.

As described in Section 3.3 above, the refractive index of the test fluid is necessary to calculate film thickness in optical interferometry. A method for calculating the refractive index (RI) of the lubricant/refrigerant mixtures was developed and given in Appendix A. However, the repeatability of the measurements was poor (i.e., greater than the RI differences caused by the addition of the refrigerant to the lubricant). This could be improved by changes in the optics and the software. This work is planned in future studies. Previous studies by Akei et al (32, 33) on similar lubricant/refrigerant mixtures indicate that the refractive indices of lubricants decrease slightly up to a maximum deviation of 1.7% with increasing refrigerant concentration of up to 40% by weight. Therefore, it was assumed in this study that the refractive index change due to refrigerants was negligible. For all the lubricants tested, the effect of contact pressure on refractive index was calculated and corrected using the Lorentz-Lorentz equation and Hartung's formula (39) as shown in Appendix B.

### 5.3 Test Fluids

The lubricants and refrigerants used in this study are shown in Table 2. Three different refrigerants were used: R-22, R-134a and R-410A. The lubricants studied included naphthenic mineral oils, polyolesters, and polyvinyl ethers of two different viscosity grades: ISO 32 and ISO 68. Table 3 shows some of the physical properties of the lubricants used.

**Table 2. Lubricants and Refrigerants Used**

| Refrigerant | Lubricant | Commercial Identification |
|---|---|---|
| R-22 | ISO 32 Naphthenic Mineral Oil (NMO-32)<br>ISO 68 Naphthenic Mineral Oil (NMO-68) | Suniso 3GS<br>Suniso 4GS |
| R-134a | ISO 32 Polyolester (POE-32)<br>ISO 32 Polyvinyl Ether (PVE-32)<br>ISO 68 Polyolester A (POE-68A)<br>ISO 68 Polyolester B (POE-68B)<br>ISO 68 Polyolester C (POE-68C)<br>ISO 68 Polyvinyl Ether (PVE-68) | ICI Emkarate RL 32H<br>Idemitsu Kosan FVC 32B<br>ICI Emkarate RL 68H<br>Mobil EAL 68<br>CPI Solest 68<br>Idemitsu Kosan FVC 68B |
| R-410A | ISO 32 Polyolester (POE-32)<br>ISO 32 Polyvinyl Ether (PVE-32)<br>ISO 68 Polyolester A (POE-68A)<br>ISO 68 Polyvinyl Ether (PVE-68) | ICI Emkarate RL 32H<br>Idemitsu Kosan FVC 32B<br>ICI Emkarate RL 68H<br>Idemitsu Kosan FVC 68B |

**Table 3. Physical Properties of Lubricants**

| Lubricant | Kinematic Viscosity, cSt | | Density, g/ml | | | Refractive Index | | |
|---|---|---|---|---|---|---|---|---|
| | 40 °C | 100 °C | 25 °C | 45 °C | 65 °C | 25 °C | 45 °C | 65 °C |
| NMO-32 | 29.73 | 4.36 | 0.9025 | 0.8890 | 0.8756 | 1.4954 | 1.4887 | 1.4814 |
| NMO-68 | 55.40 | 6.13 | 0.9069 | 0.8932 | 0.8797 | 1.4980 | 1.4910 | 1.4839 |
| POE-32 | 31.89 | 5.72 | 0.9745 | 0.9590 | 0.9435 | 1.4510 | 1.4440 | 1.4370 |
| POE-68A | 62.42 | 9.02 | 0.9781 | 0.9626 | 0.9471 | 1.4536 | 1.4468 | 1.4406 |
| POE-68B | 63.45 | 8.32 | 0.9599 | 0.9445 | 0.9292 | 1.4516 | 1.4445 | 1.4384 |
| POE-68C | 67.37 | 9.02 | 0.9544 | 0.9394 | 0.9245 | 1.4531 | 1.4465 | 1.4396 |
| PVE-32 | 31.03 | 4.94 | 0.9154 | 0.9003 | 0.8845 | 1.4394 | 1.4321 | 1.4256 |
| PVE-68 | 72.55 | 8.56 | 0.9288 | 0.9132 | 0.8977 | 1.4420 | 1.4350 | 1.4281 |

## 6.0 RESULTS

### 6.1 Film Thickness Measurements on Lubricants Under Air

Baseline film thickness measurements were conducted on two naphthenic mineral oils, four polyolester lubricants, and two polyvinyl ether lubricants as a function of rolling speed at ambient (22-25 °C), 45 and 65 °C. The results for each lubricant are reported below.

#### 6.1.1 Naphthenic Mineral Oils

Figures 6 and 7 show the results for the ISO 32 and ISO 68 naphthenic mineral oils in the form of plots of log (film thickness) vs. log (rolling speed). According to the Dowson and Hamrock film thickness equation described in Section 3.2, the relationship between lubricant film thickness and entrainment speed should obey the relationship:

$$h \alpha U^{0.67} \qquad \textbf{Equation 14}$$

The slopes of the lines in Figures 6 and 7 conform to Equation 14, lying in the range of 0.69 to 0.75. The film thickness behavior with rolling speed followed Equation 14 up to the highest speeds (2 m/s) measured. It is predicted that significant thermal effects, such as inlet shear heating, will not occur until the entrainment speed approaches 5 m/s (59).

The data also shows a rapid fall in film thickness with rising temperature, which is predicted to occur from the EHD theory due to a decrease in both the bulk-viscosity and pressure-viscosity coefficient of the lubricant with increasing temperature.

Figure 8 compares the film thickness measurements obtained on the two mineral oils and shows the effects of viscosity on film thickness measurements. As expected, the ISO 32 mineral oil forms thinner films (about half the thickness) in the contact than the ISO 68 mineral oil due to its lower viscosity.

### 6.1.2 Polyolesters

Figures 9 through 12 show the film thickness data as a function of rolling speed and temperature for the four polyolesters tested. The gradients of the plots vary from 0.67 to 0.71 and agree with the theoretical EHD slope. The data shows similar trends to those observed with the mineral oils above. Figure 13 shows the effects of lubricant viscosity on film thickness and compares the data obtained on ISO 32 and ISO 68 polyolesters. As expected, the lower viscosity ester forms thinner films in the contact than the higher viscosity fluid. Figure 14 compares the data obtained on the three ISO 68 polyolesters: A, B and C. The film thickness of the three fluids appear to be comparable to each other at the temperatures tested.

### 6.1.3 Polyvinyl Ethers

Figures 15 and 16 show the film thickness data as a function of rolling speed and temperature for the two polyvinyl ethers tested. Similar to the results reported above on mineral oils and polyolesters, the gradients of the plots show a good agreement with the EHD theory. Figure 17 shows the effects of lubricant viscosity on film thickness and compares the data obtained on ISO 32 and ISO 68 polyvinyl ethers. Overall, the data shows similar trends to those observed with the mineral oils and polyolesters above.

**Figure 6. Film Thickness Data for ISO 32 Naphthenic Mineral Oil**

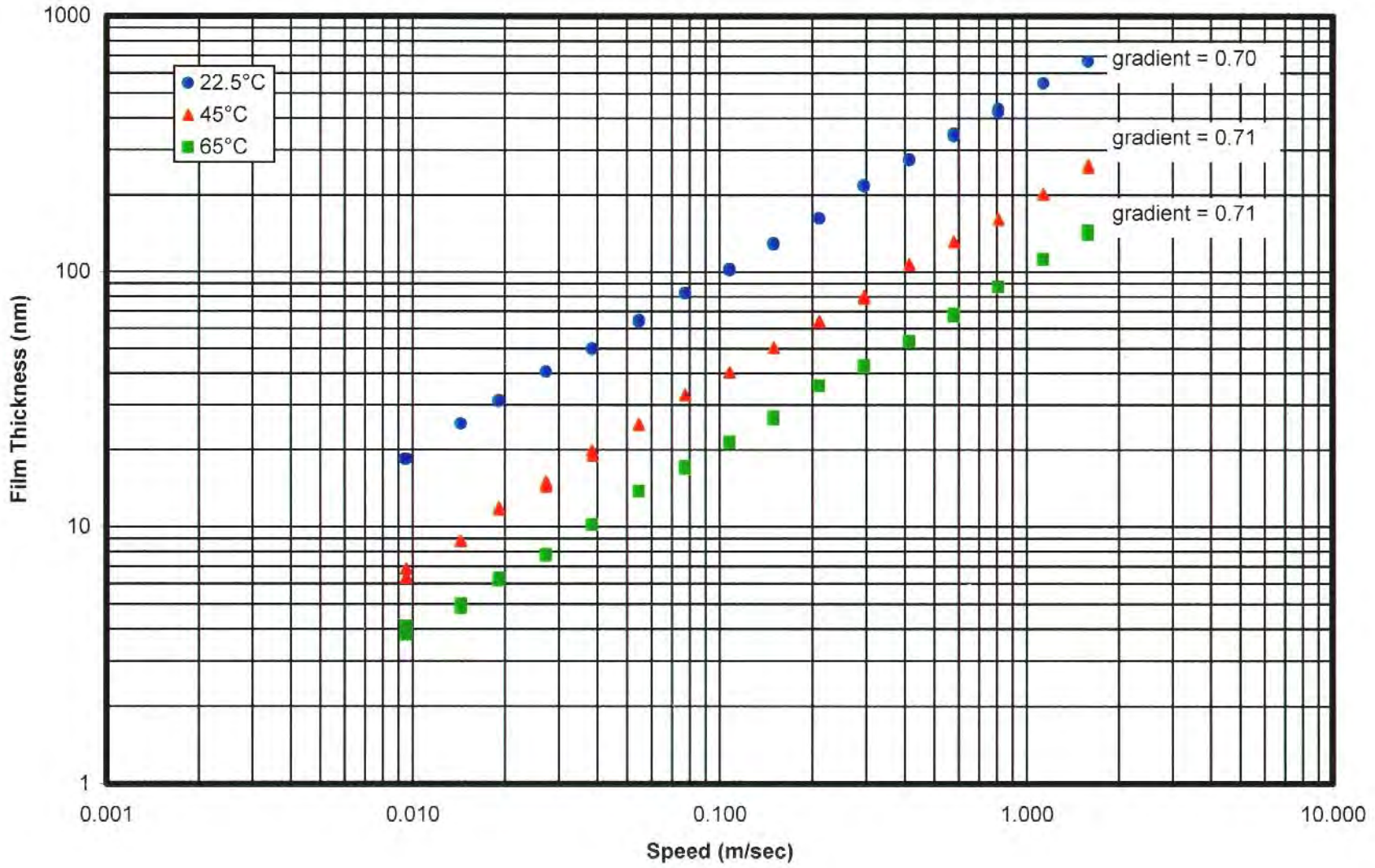

**Figure 7. Film Thickness Data for ISO 68 Naphthenic Mineral Oil**

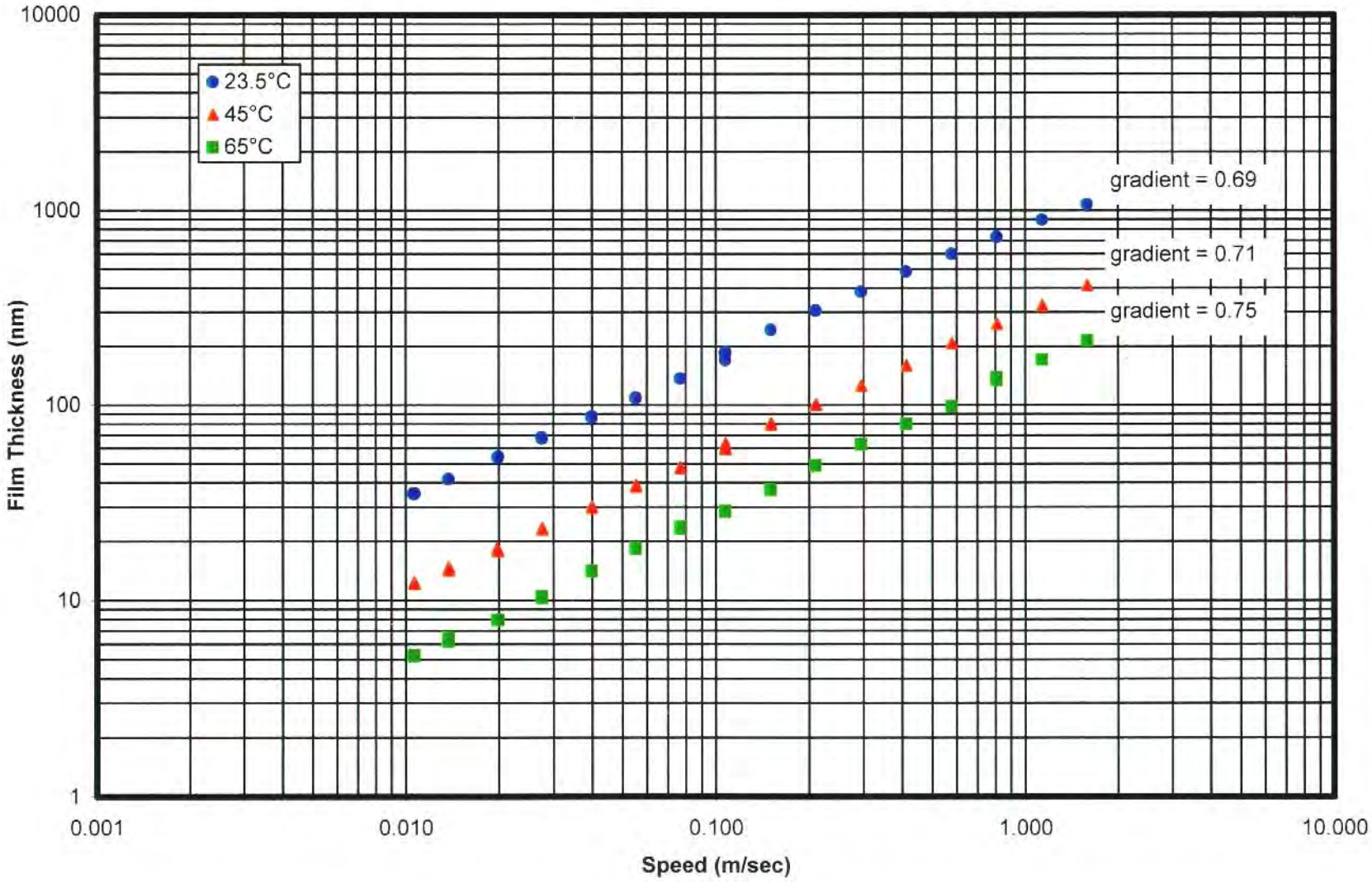

**Figure 8. Comparison of Film Thickness Data for ISO 32 and ISO 68 Naphthenic Mineral Oils**
**Effect of Viscosity on Film Thickness**

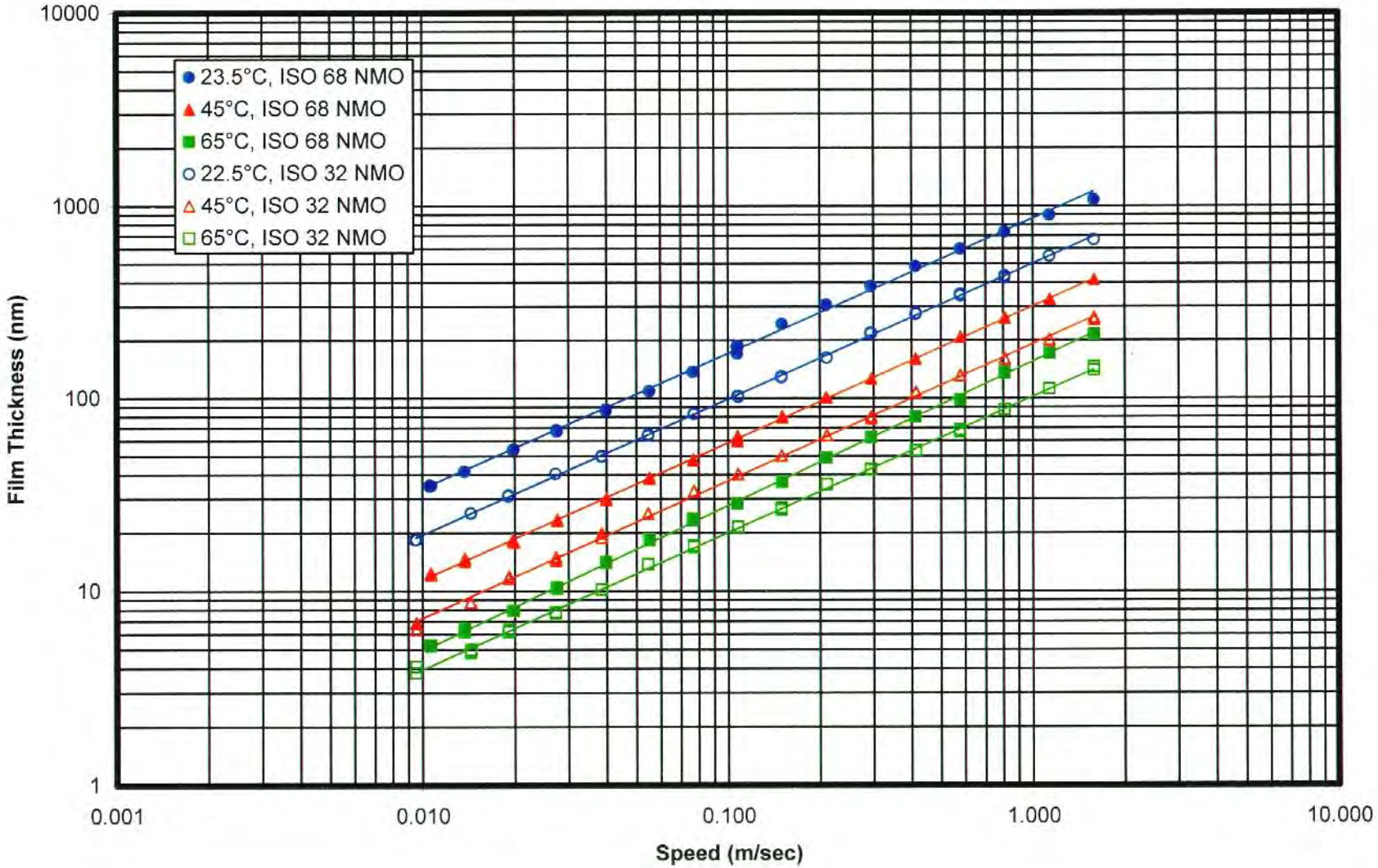

**Figure 9. Film Thickness Data for ISO 32 Polyolester**

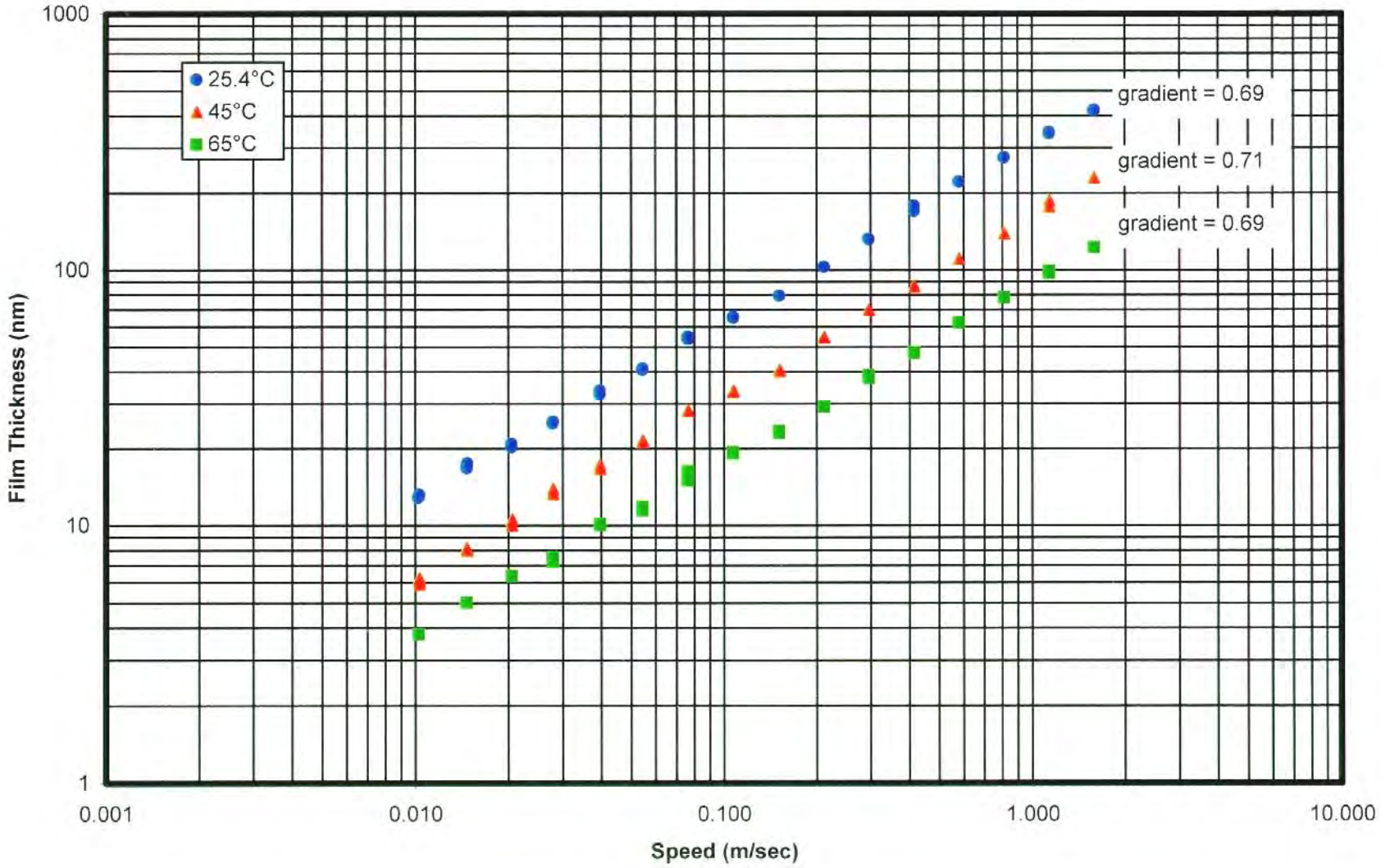

**Figure 10. Film Thickness Data for ISO 68 Polyolester A**

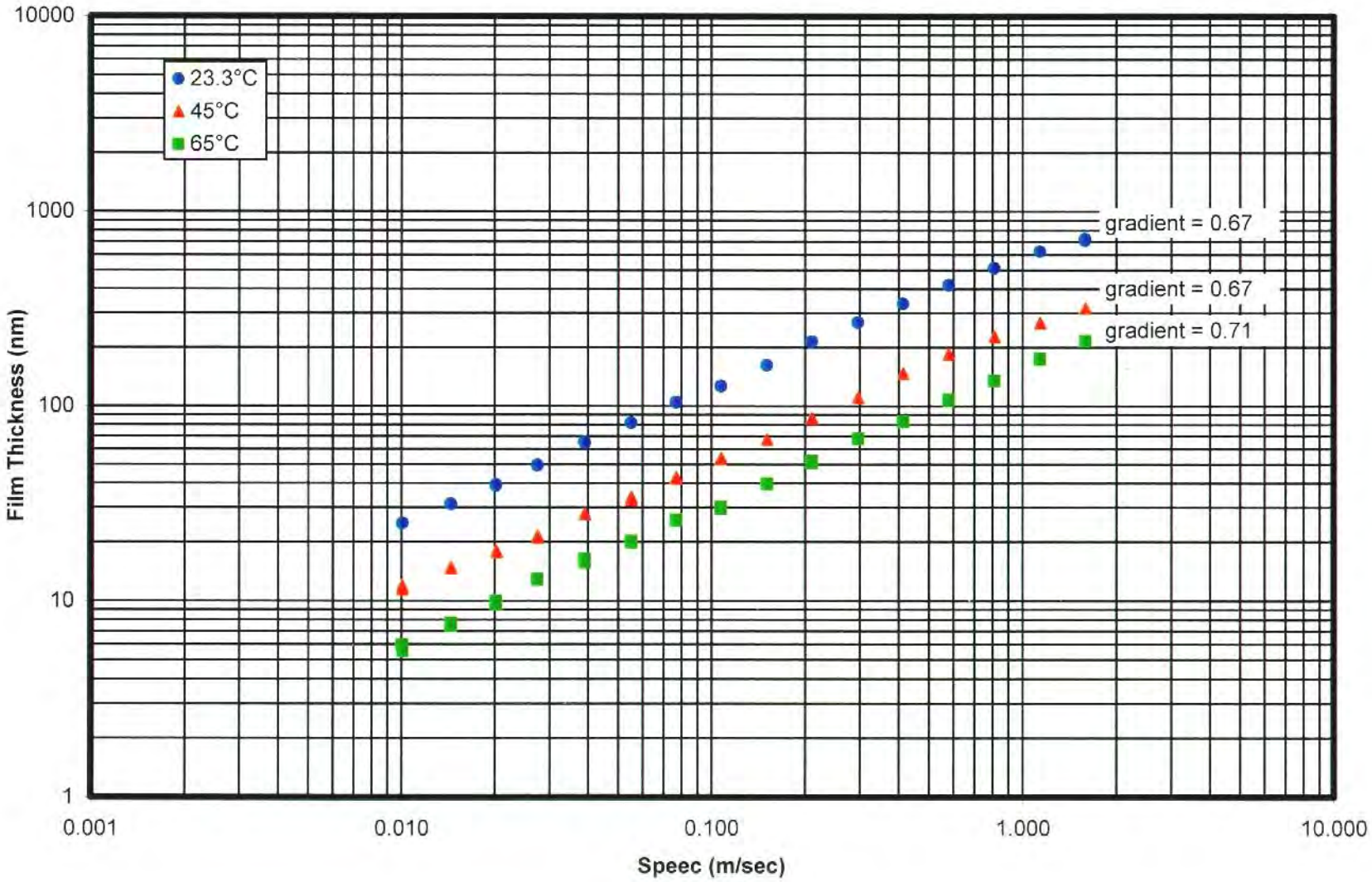

**Figure 11. Film Thickness Data for ISO 68 Polyolester B**

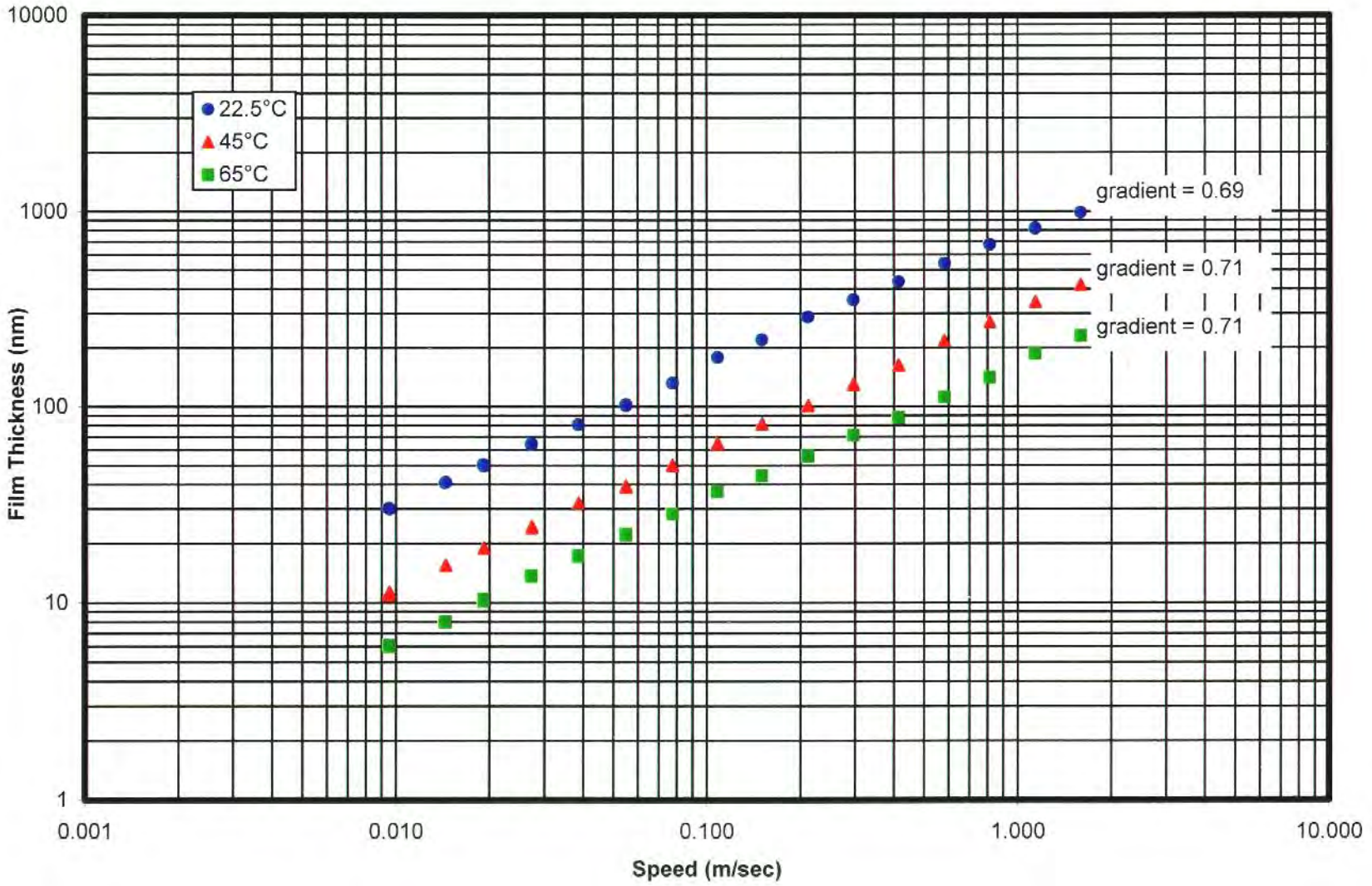

**Figure 12. Film Thickness Data for ISO 68 Polyolester C**

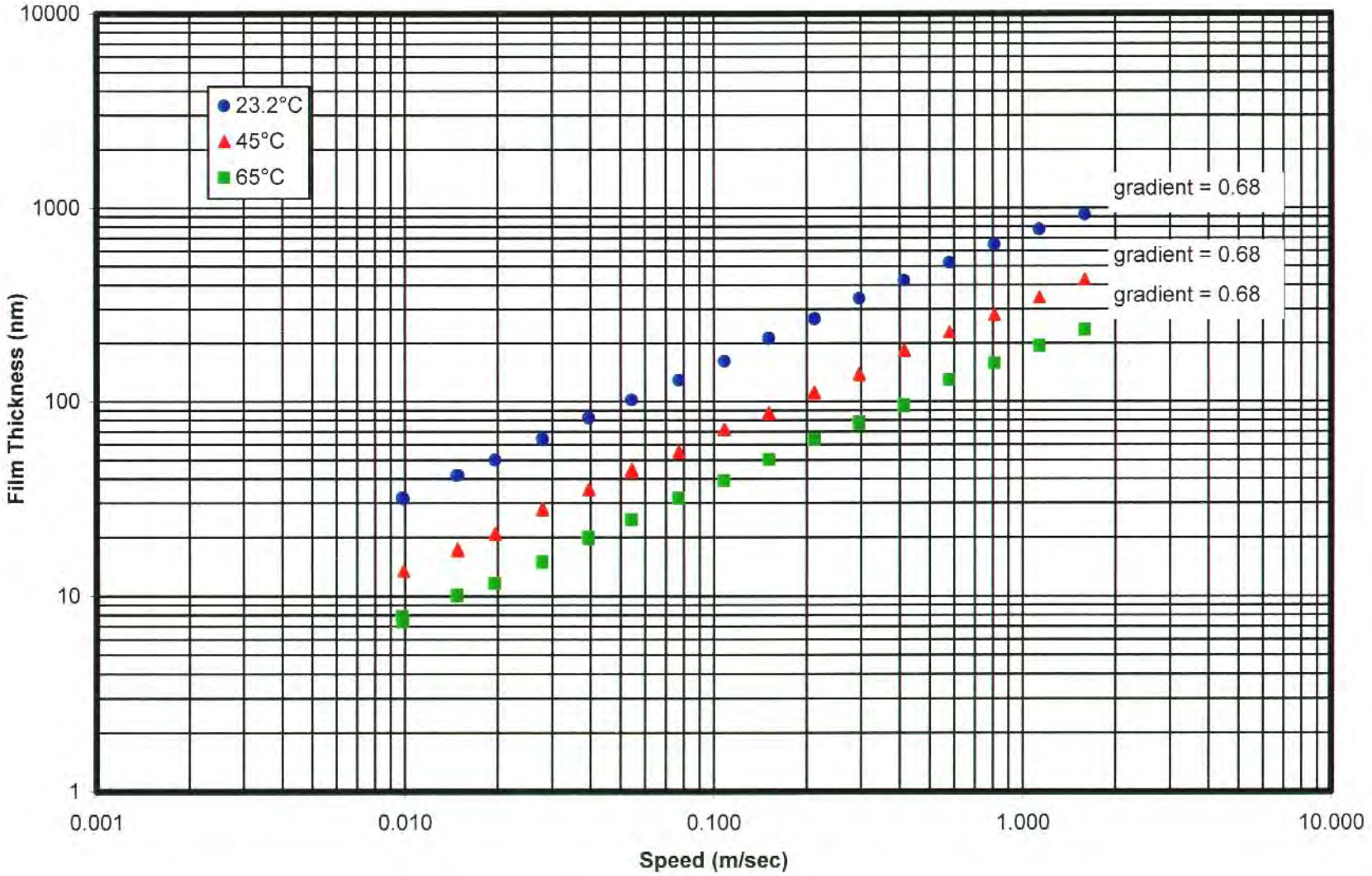

**Figure 13. Comparison of Film Thickness Data for ISO 32 Polyolester and ISO 68 Polyolester A - Effect of Viscosity on Film Thickness**

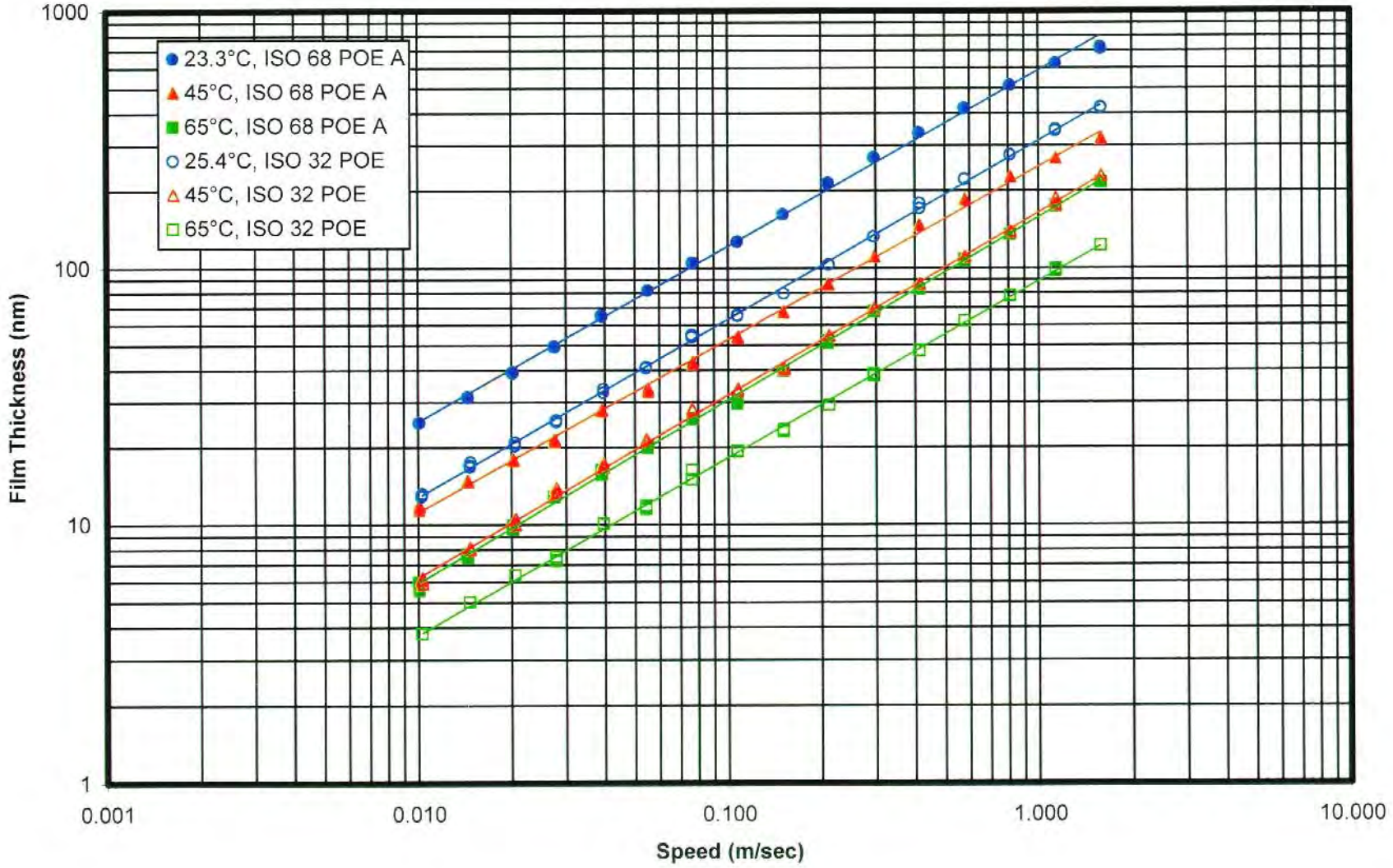

**Figure 14. Comparison of Film Thickness Data for ISO 68 Polyolesters**

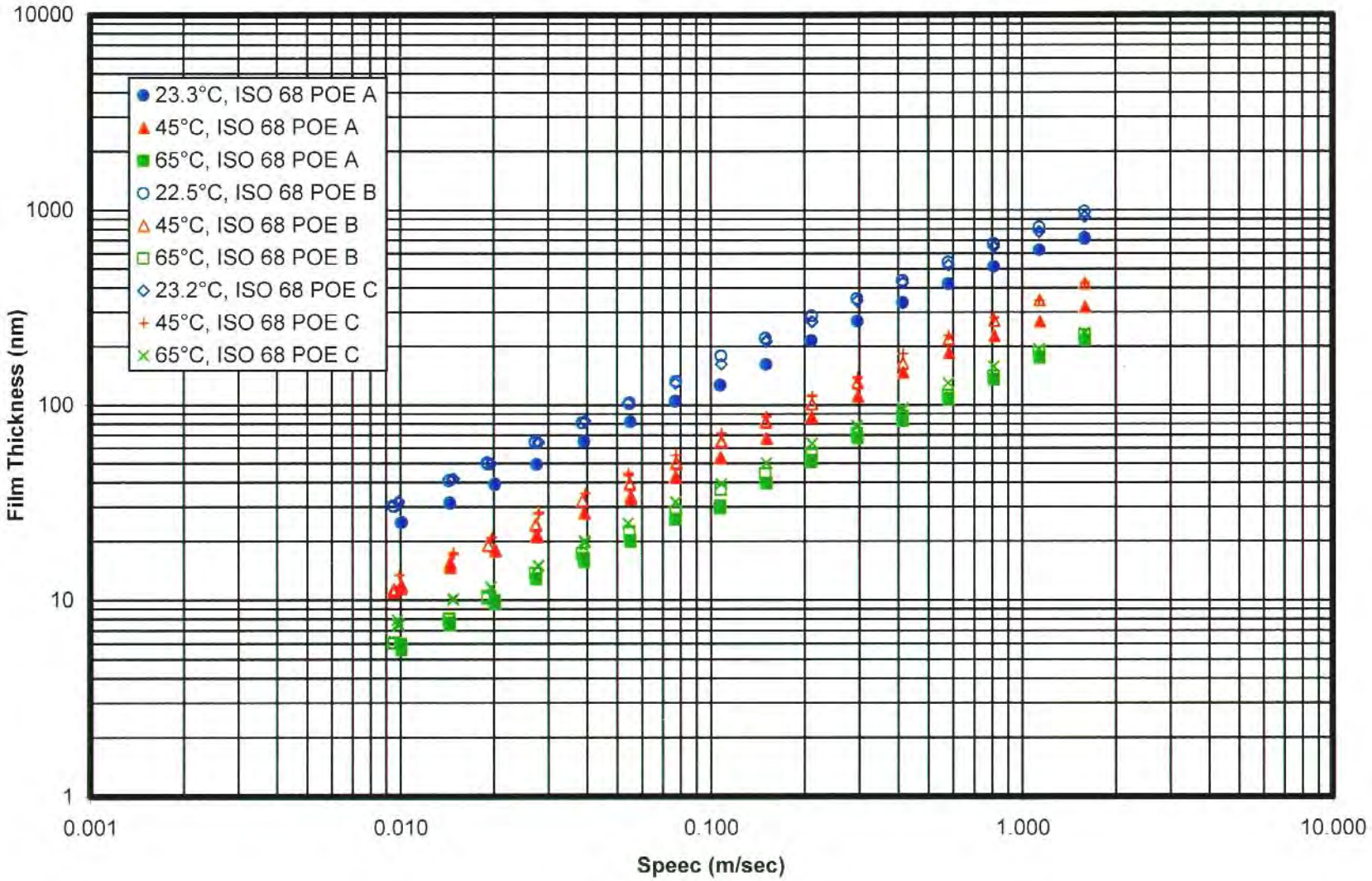

**Figure 15. Film Thickness Data for ISO 32 Polyvinyl Ether**

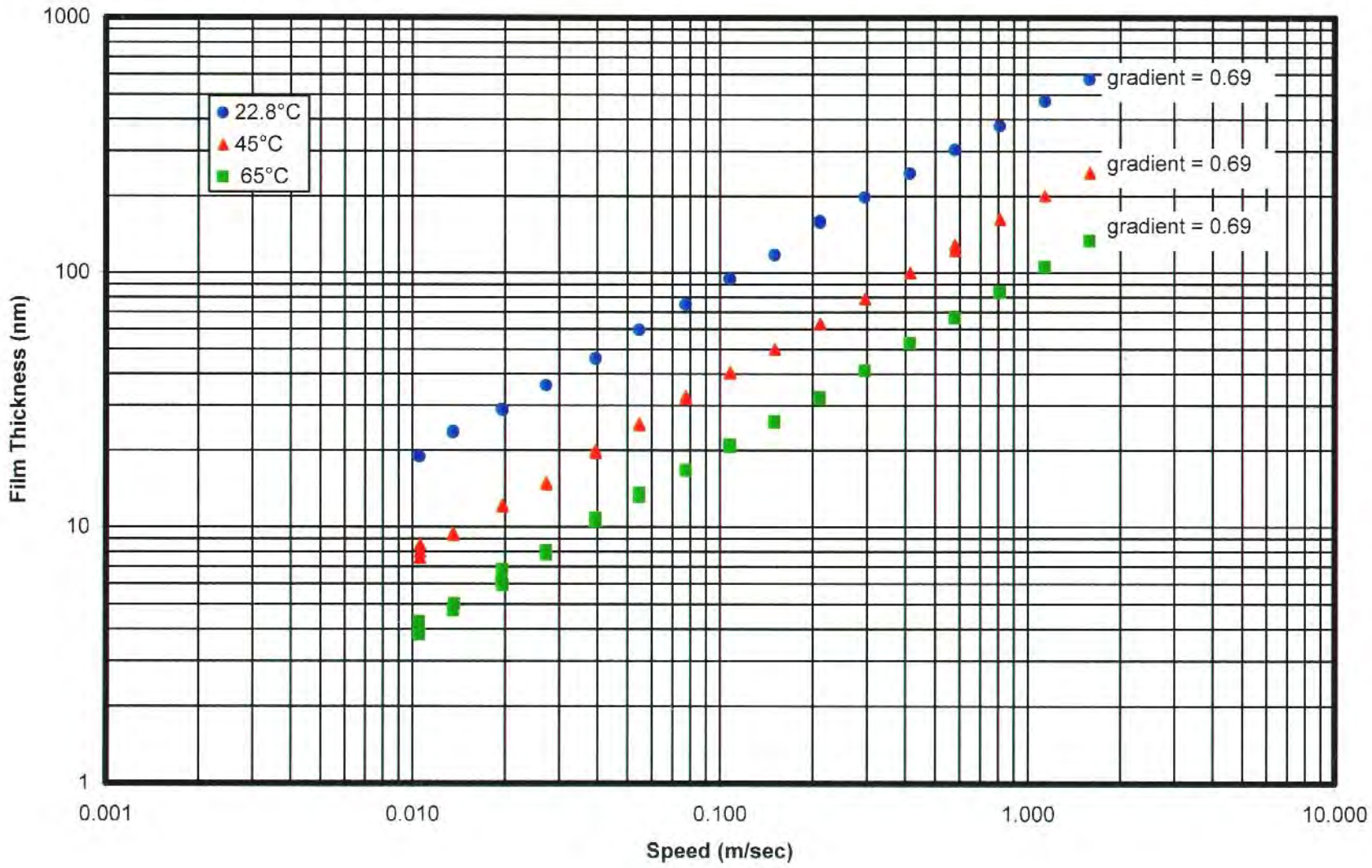

**Figure 16. Film Thickness Data for ISO 68 Polyvinyl Ether**

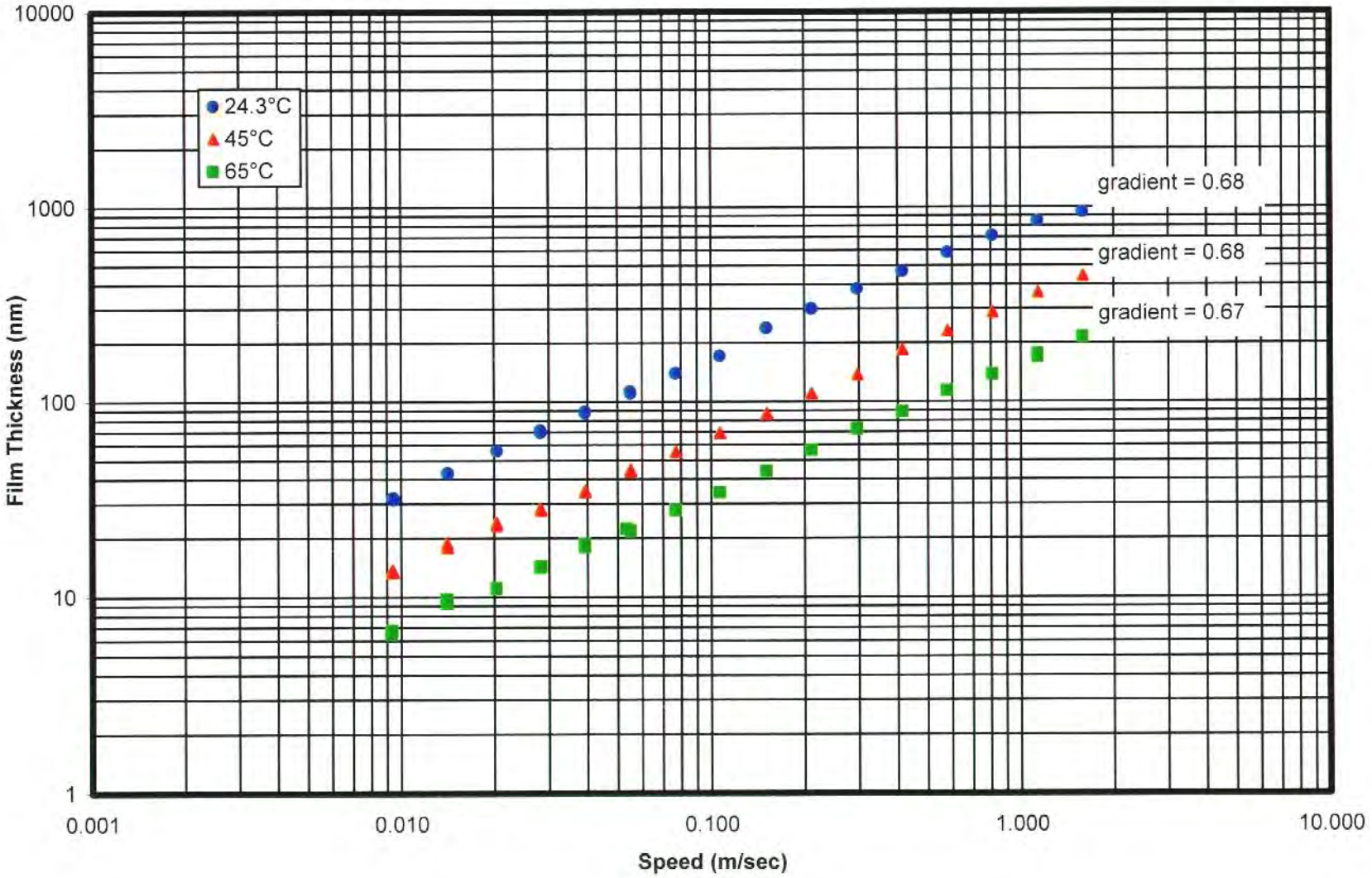

**Figure 17. Comparison of Film Thickness Data for ISO 32 and ISO 68 Polyvinyl Ethers**
**Effect of Viscosity on Film Thickness**

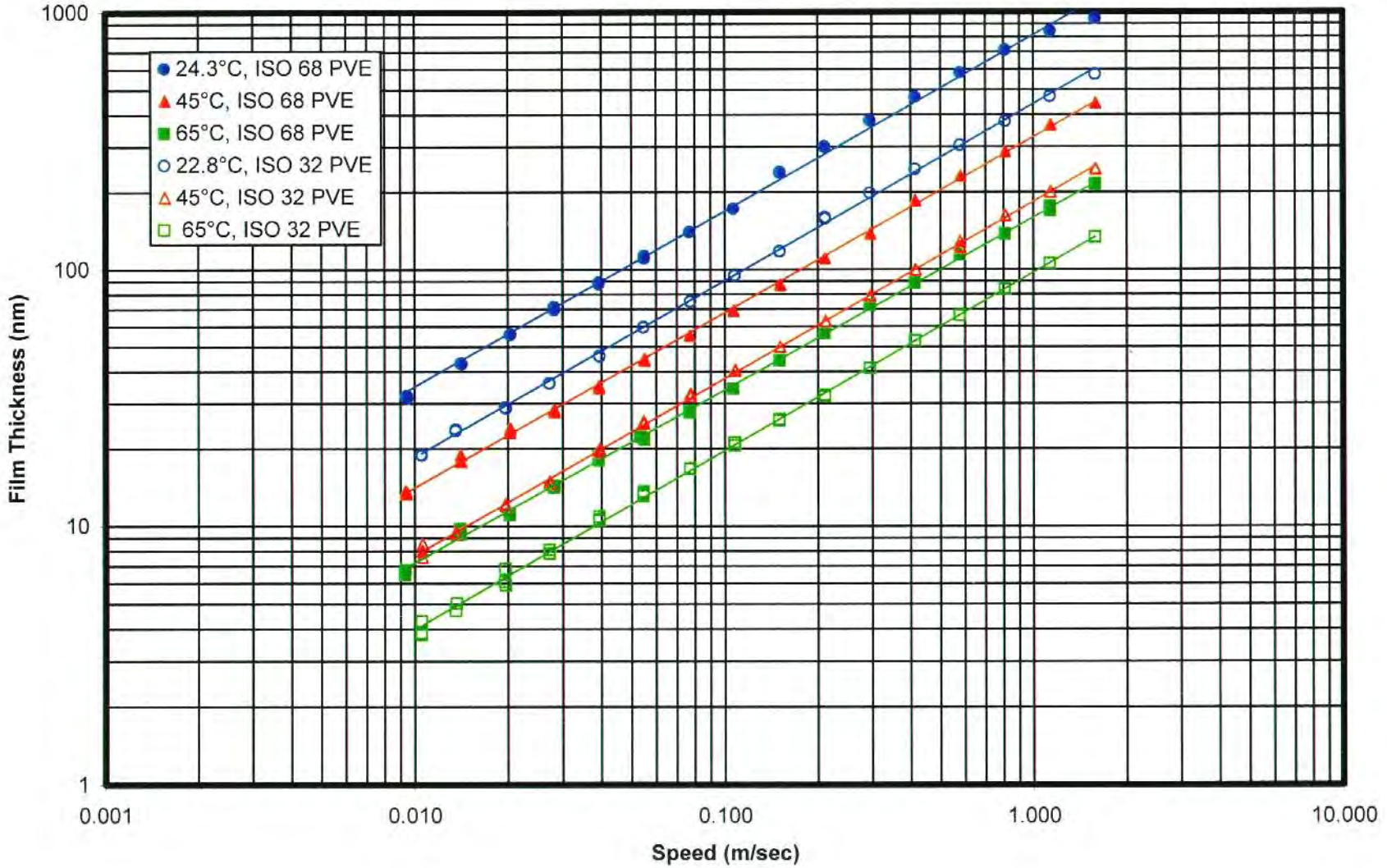

### 6.1.4 Repeatability of Measurements

The repeatability of the film thickness measurements by ultrathin film interferometry was determined to be ± 1 nm below 5 nm and ± 5% above 5 nm in previous studies (55). The repeatability of the film thickness measurements in this study was determined for two different conditions. First, the film thickness measurements obtained in the old test chamber (i.e. atmospheric) and the new test chamber (i.e. modified to operate under pressure) were compared to verify the operation of the new chamber. For this purpose, tests were conducted in air under identical test conditions. Second, the repeatability of the measurements in the new test chamber was investigated by conducting duplicate measurements on a number of test fluids.

Figures 18 through 21 show the repeatability of the film thickness measurements obtained in the old and the modified chamber for two naphthenic mineral oils and two polyolesters at three different test temperatures. The results indicate good agreement between the measurements and confirm the successful operation of the new rig.

Figures 22 to 25 show the repeatability of the film thickness measurements in the new rig for duplicate tests on two polyolesters and two polyvinyl ethers. The results indicate that the measurements are repeatable within 3%. This agrees with the previous studies which indicate an overall repeatability of 3-5% for the ultrathin film interferometry method (54-57).

## 6.2 Effective Pressure-Viscosity Coefficients

The effective pressure-viscosity coefficients ($\alpha$-value) of the test fluids were calculated from the measured film thickness values as described in Section 3.4 above. The reference oil used for this procedure, obtained from Imperial College, U.K., was a well characterized synthetic hydrocarbon with a viscosity of 13.86 cp and a pressure-viscosity coefficient of 13.5 $GPa^{-1}$ at 40 °C. Since the $\alpha$-values determined in this report depend upon a reference fluid, these values should be considered accurate relative to each other, but not as absolute values.

The effective pressure-viscosity coefficients calculated for the lubricants from the measured film thickness data at the three test temperatures are given in Table 4. The pressure-viscosity coefficient reported in the table is an average value determined from

duplicate film thickness measurements. The repeatability in the pressure-viscosity coefficients was determined to be ± 3 $GPa^{-1}$.

Figures 26 and 27 show the variation of $\alpha$-value with temperature for the ISO 32 and ISO 68 test fluids, respectively. These figures also show the effect of chemical structure on pressure-viscosity characteristics and rank the lubricants with respect to their $\alpha$-values. The mineral oils give the highest $\alpha$-values, followed by polyvinyl ethers. Among the lubricants tested, the polyolesters have the lowest $\alpha$-values.

Molecular characteristics and shape factors, such as flexibility and the presence of short, rigid side groups, influence pressure-viscosity properties (60). Pressure-viscosity characteristics of fluids depend on the chemical structure and the steric nature of the molecules. In general, fluids with ring structures or bulky side groups have higher $\alpha$-values than those with flexible, straight chain molecules (61). In Eyring's model of viscous flow, $\alpha$-value depends upon the activation flow volume which is a measure of the size of hole required to be created in a fluid against pressure for the activated jump to occur (62). The size of this hole will depend upon the size of a flow unit within a molecule and thus directly upon the rigidity and shape of the molecule (63). The data given in Table 4 and Figures 26 and 27 show that the naphthenic oils with ring structures have the highest $\alpha$-values. Esters, on the other hand, have low pressure-viscosity coefficients. This finding agrees with the existing literature on similar fluids (64, 65). Differences were observed in the pressure-viscosity characteristics of the polyolesters tested. This is probably due to the differences in the degree of branching in the ester structure. Polyolester B, which has the highest percent of branched acids (~ 84%), has higher $\alpha$-values than polyolesters A (~ 51% branched acids) and C (~ 67% branched acids). Esters with more linear structure (POE-32 and POE-68A) have the lowest $\alpha$-values.

Pressure-viscosity coefficients also change with temperature as shown in Figures 26 and 27. As the temperature increases, alpha value decreases. This is due to the reduced interaction between the molecules at the higher temperatures.

### 6.3 Film Thickness Measurements on Mixtures of Naphthenic Mineral Oils and R-22

Film thickness measurements were conducted on mixtures of ISO 32 and ISO 68 naphthenic mineral oils as a function of rolling speed, temperature and refrigerant concentration. The results are reported in the following sections.

**Table 4. Effective Pressure-Viscosity Coefficients of Lubricants**

| Lubricant | Temperature (°C) | Effective Pressure-Viscosity Coefficient (± 3 $GPa^{-1}$) |
|---|---|---|
| NMO-32 | 23 | 31.3 |
| | 45 | 24.0 |
| | 65 | 21.5 |
| POE-32 | 23 | 16.9 |
| | 45 | 14.8 |
| | 65 | 12.4 |
| PVE-32 | 23 | 25.5 |
| | 45 | 21.3 |
| | 65 | 17.0 |
| NMO-68 | 23 | 31.5 |
| | 45 | 24.7 |
| | 65 | 21.2 |
| POE-68A | 23 | 19.6 |
| | 45 | 17.8 |
| | 65 | 15.9 |
| POE-68B | 23 | 24.4 |
| | 45 | 20.5 |
| | 65 | 18.4 |
| POE-68C | 23 | 21.0 |
| | 45 | 18.9 |
| | 65 | 17.7 |
| PVE-68 | 23 | 28.5 |
| | 45 | 22.2 |
| | 65 | 18.5 |

**Figure 18. Film Thickness Data for ISO 32 Naphthenic Mineral Oil**
**Comparison Between Old and New Test Chamber**

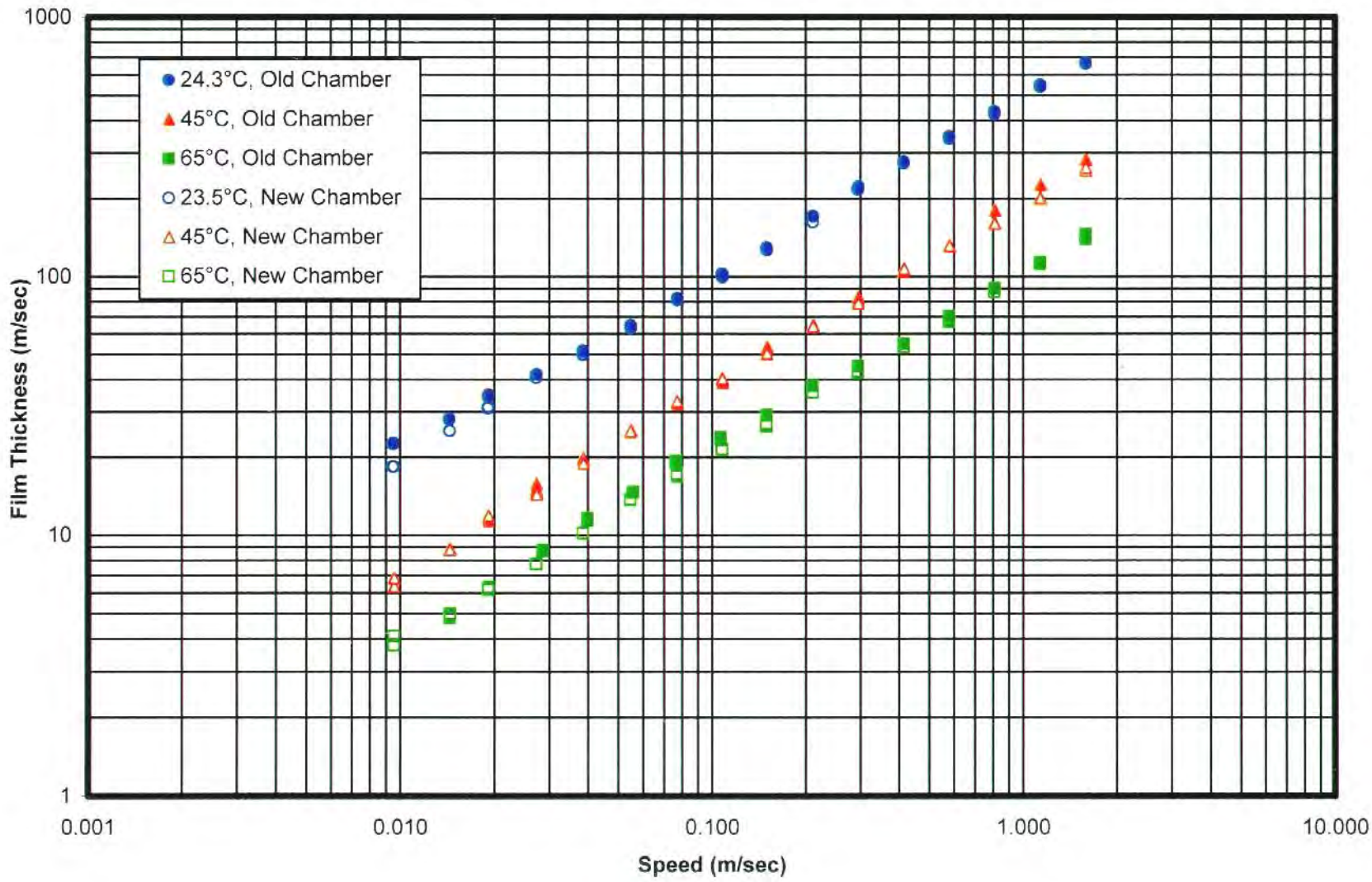

**Figure 19. Film Thickness Data for ISO 68 Naphthenic Mineral Oil - Comparison Between Old and New Test Chamber**

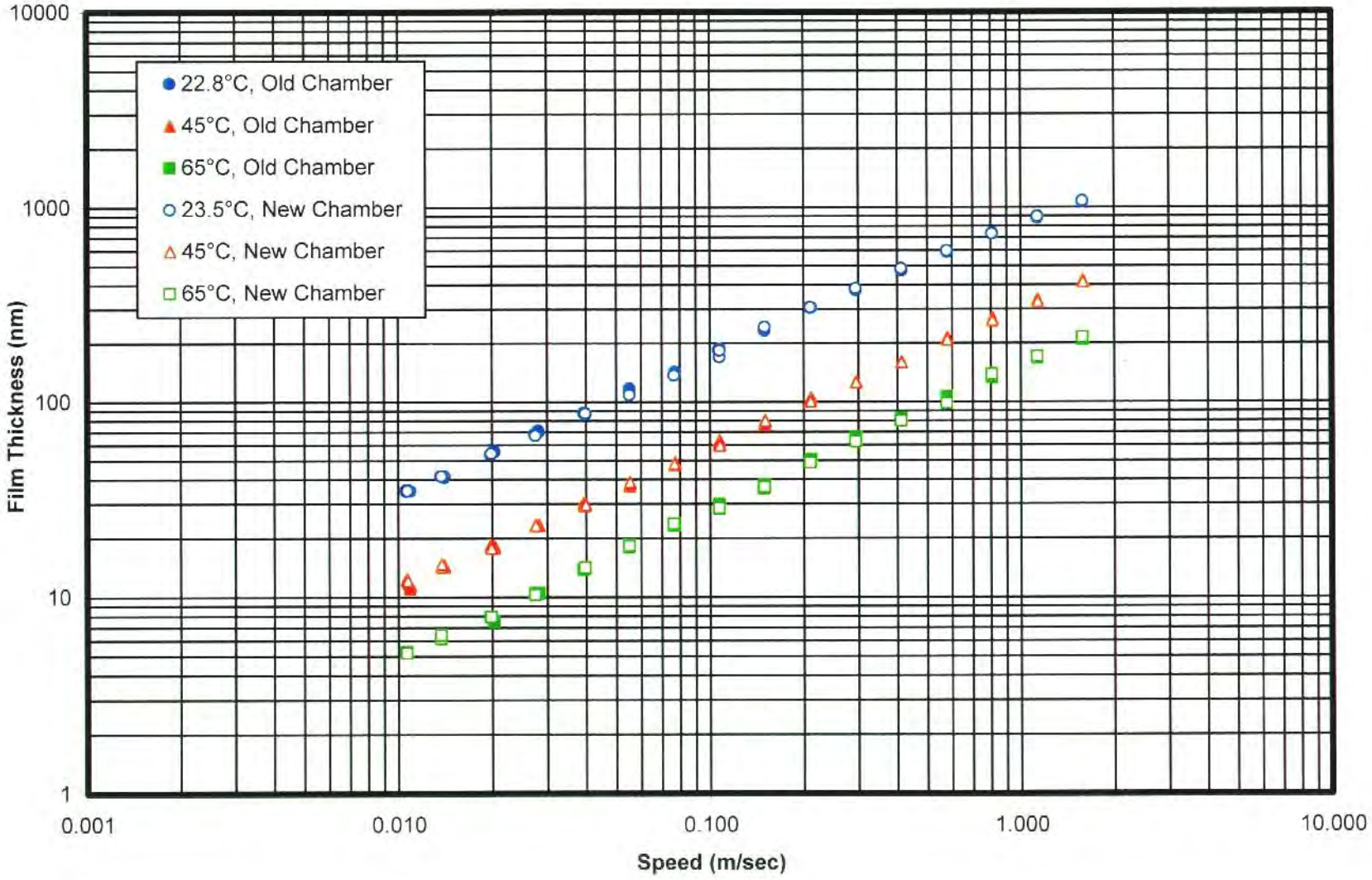

**Figure 20. Film Thickness Data for ISO 32 Polyolester**
**Comparison Between Old and New Test Chamber**

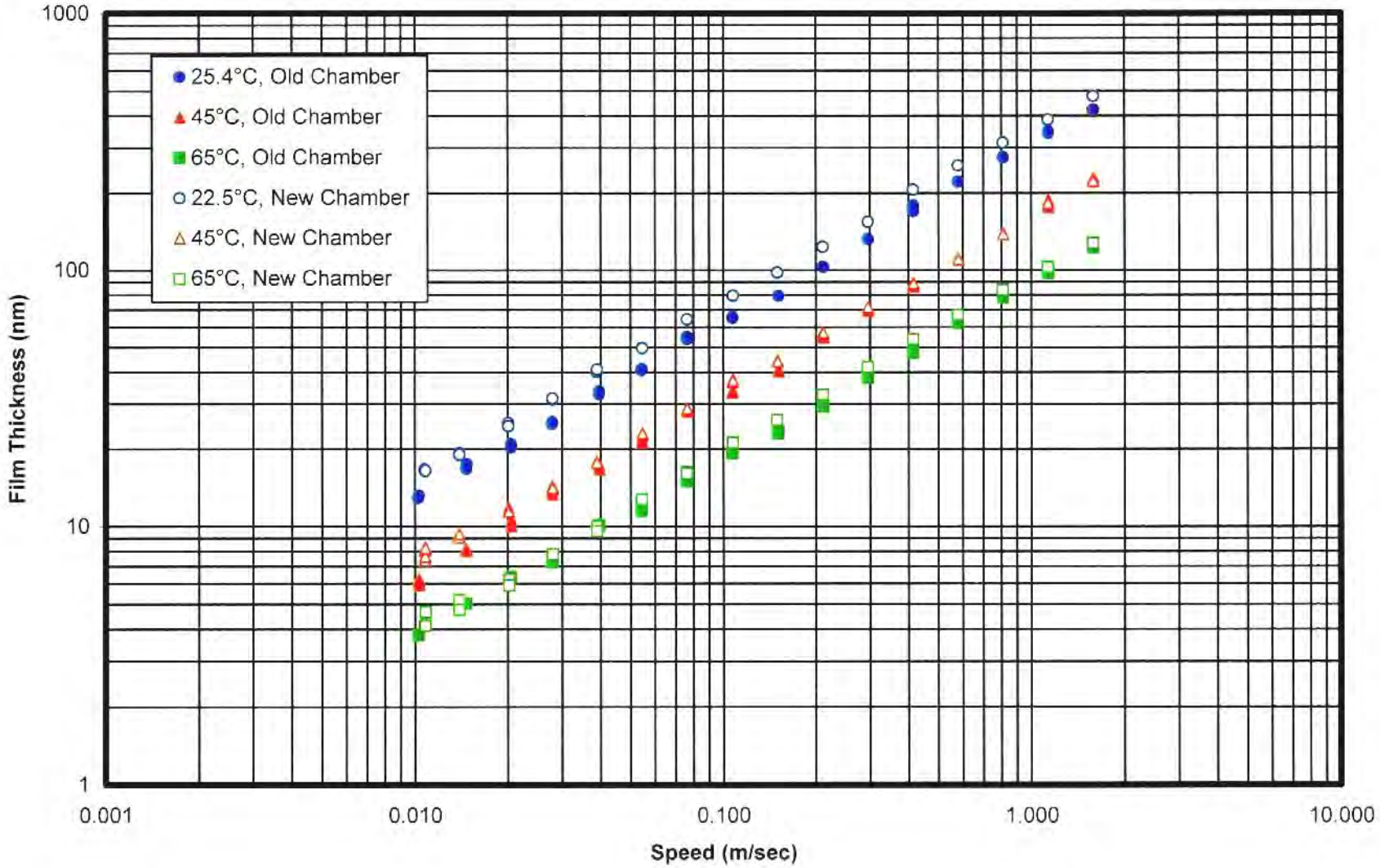

**Figure 21. Film Thickness Data for ISO 68 Polyolester A**
**Comparison Between Old and New Test Chamber**

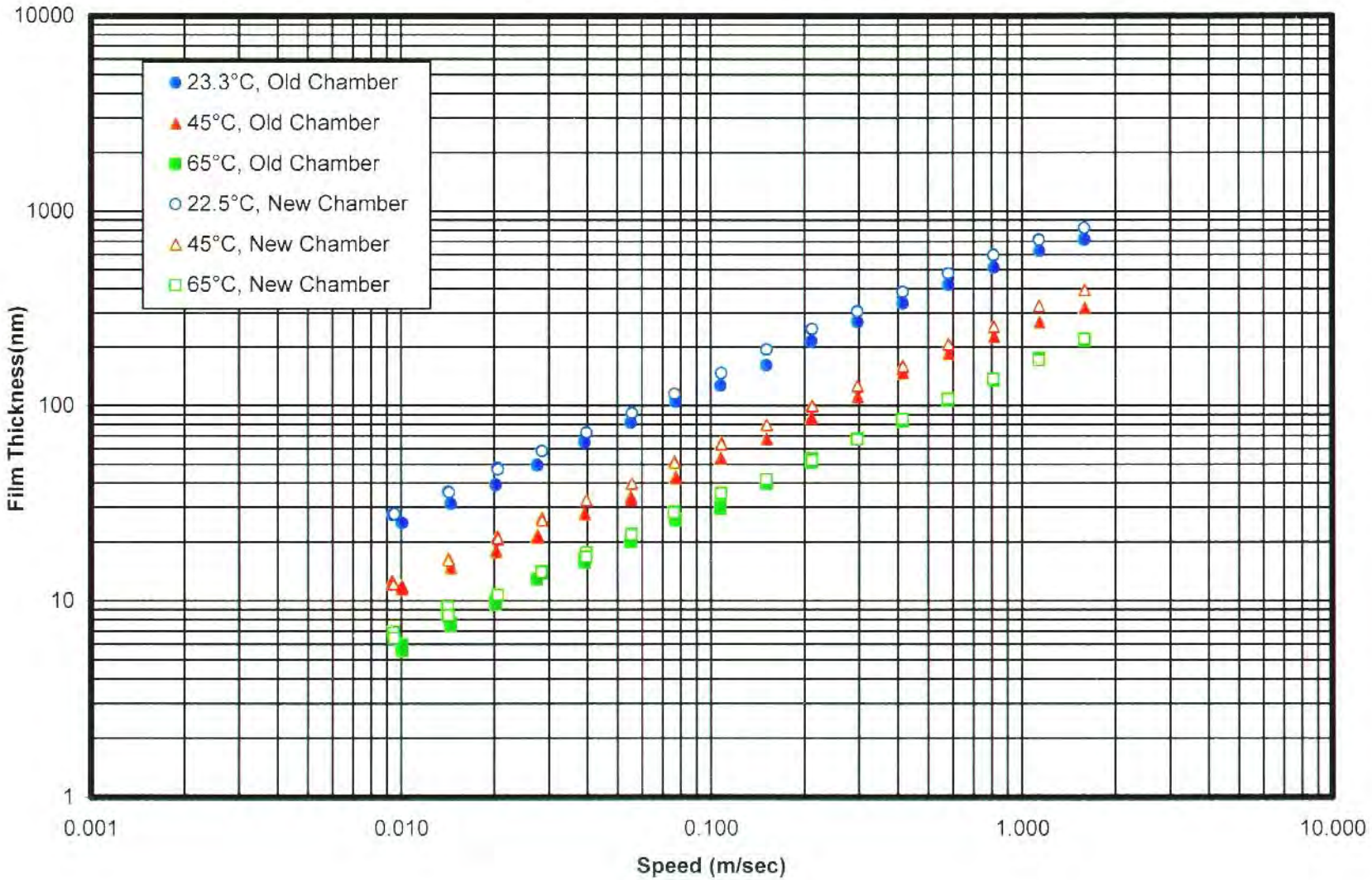

**Figure 22. Film Thickness Data for ISO 68 Polyolester B**
**Comparison of Two Runs**

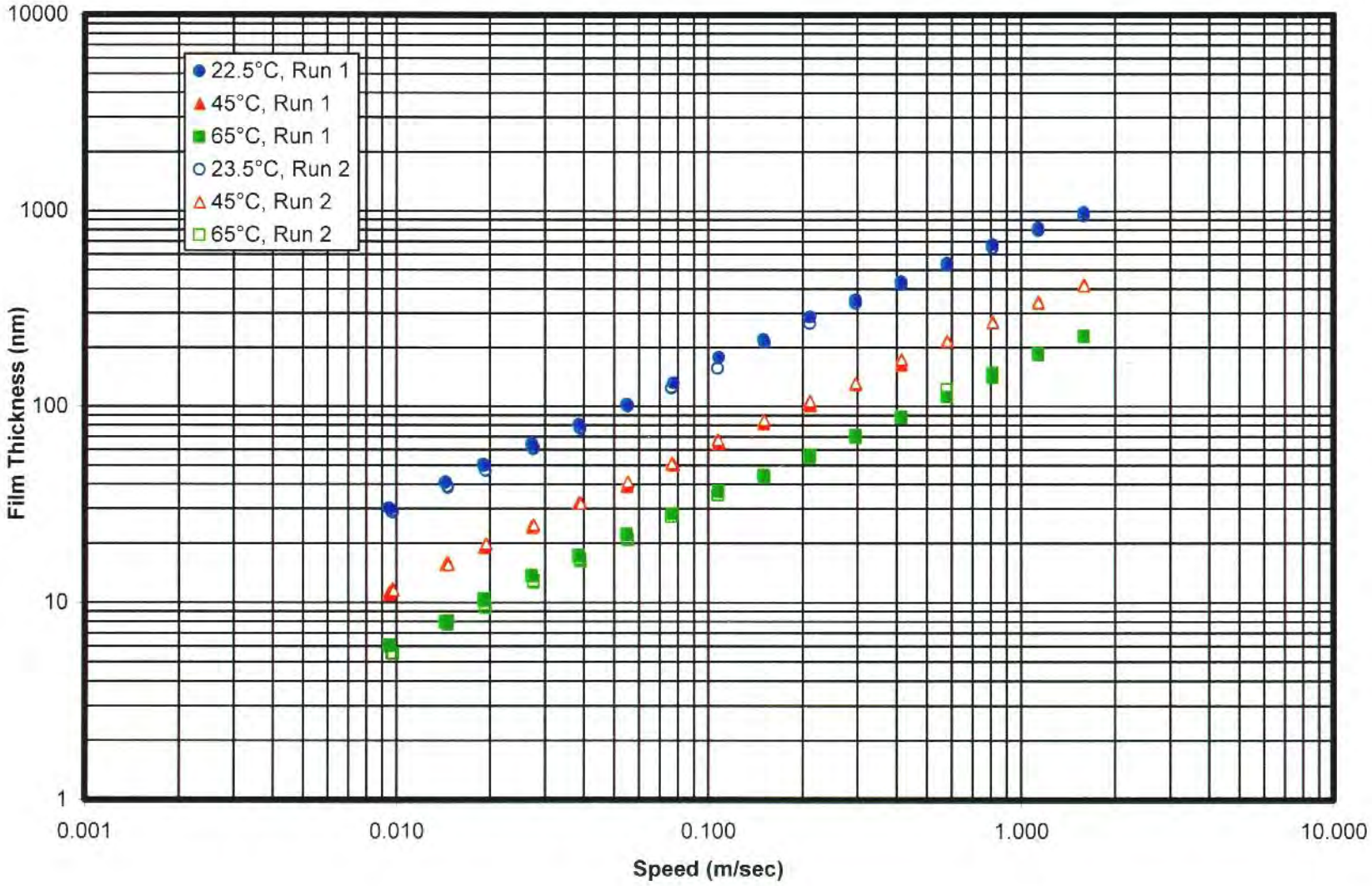

**Figure 23. Film Thickness Data for ISO 68 Polyolester C**
**Comparison of Two Runs**

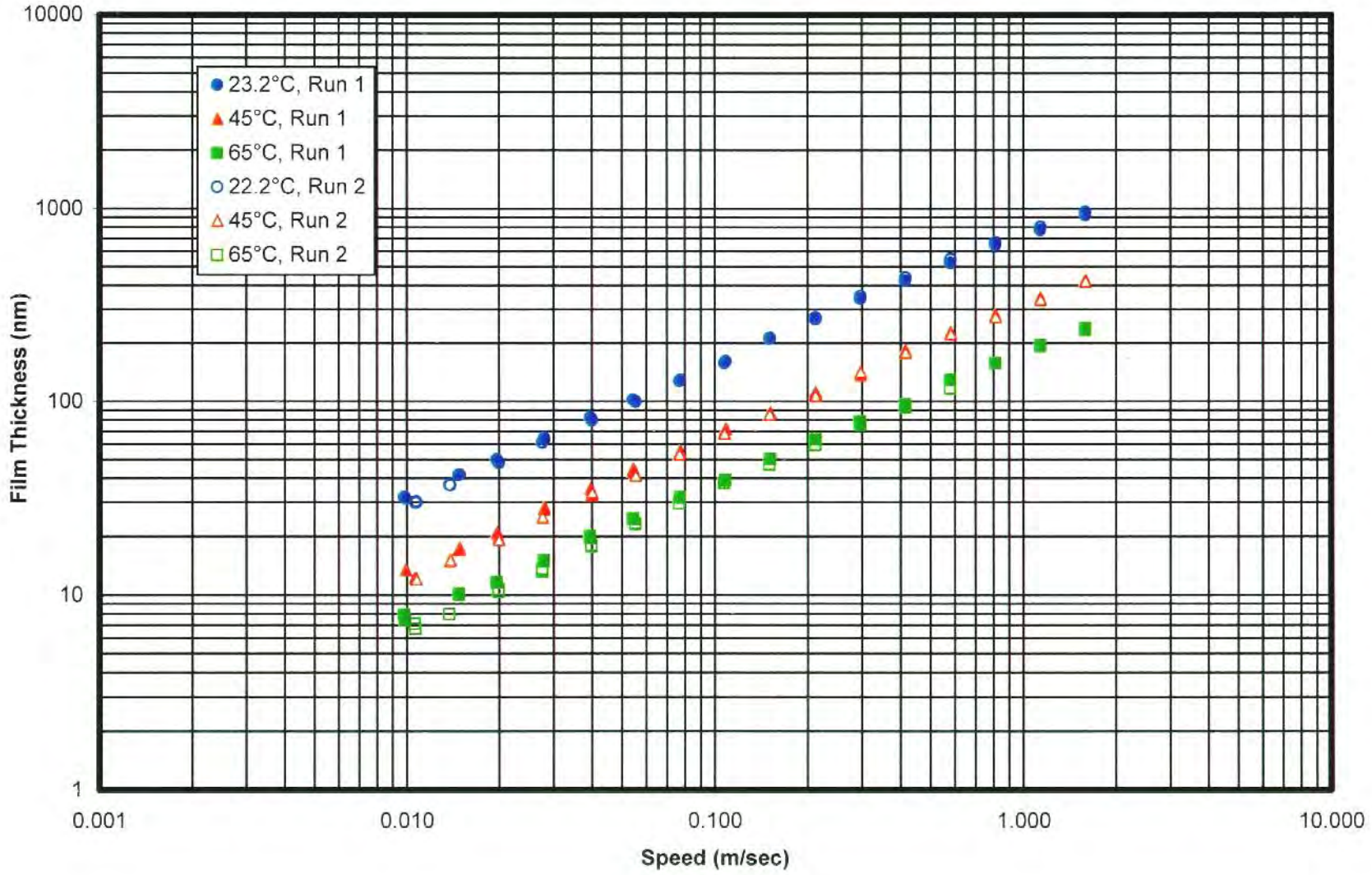

**Figure 24. Film Thickness Data for ISO 32 Polyvinyl Ether**
**Comparison of Two Runs**

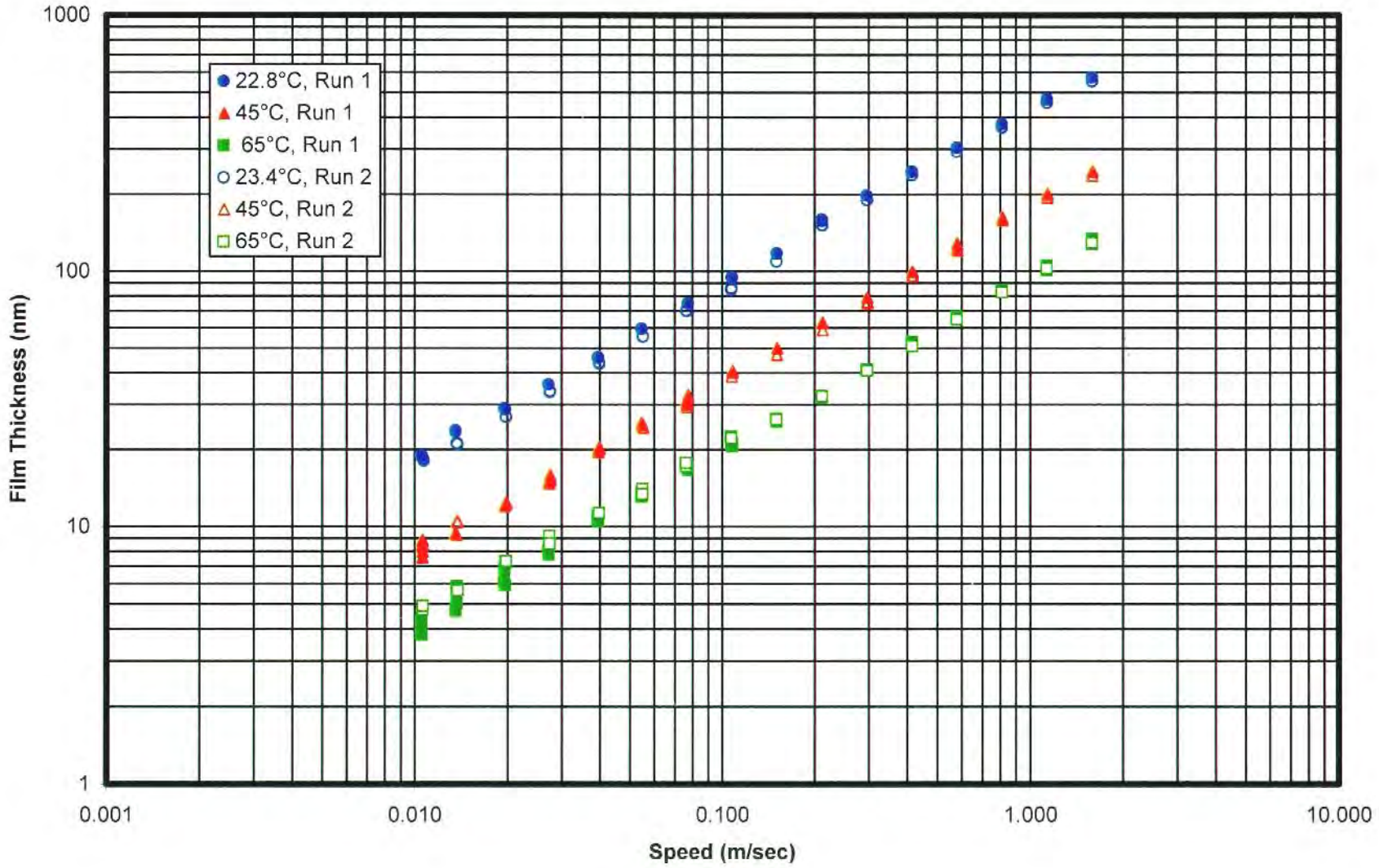

**Figure 25. Film Thickness Data for ISO 68 Polyvinyl Ether**
**Comparison of Two Runs**

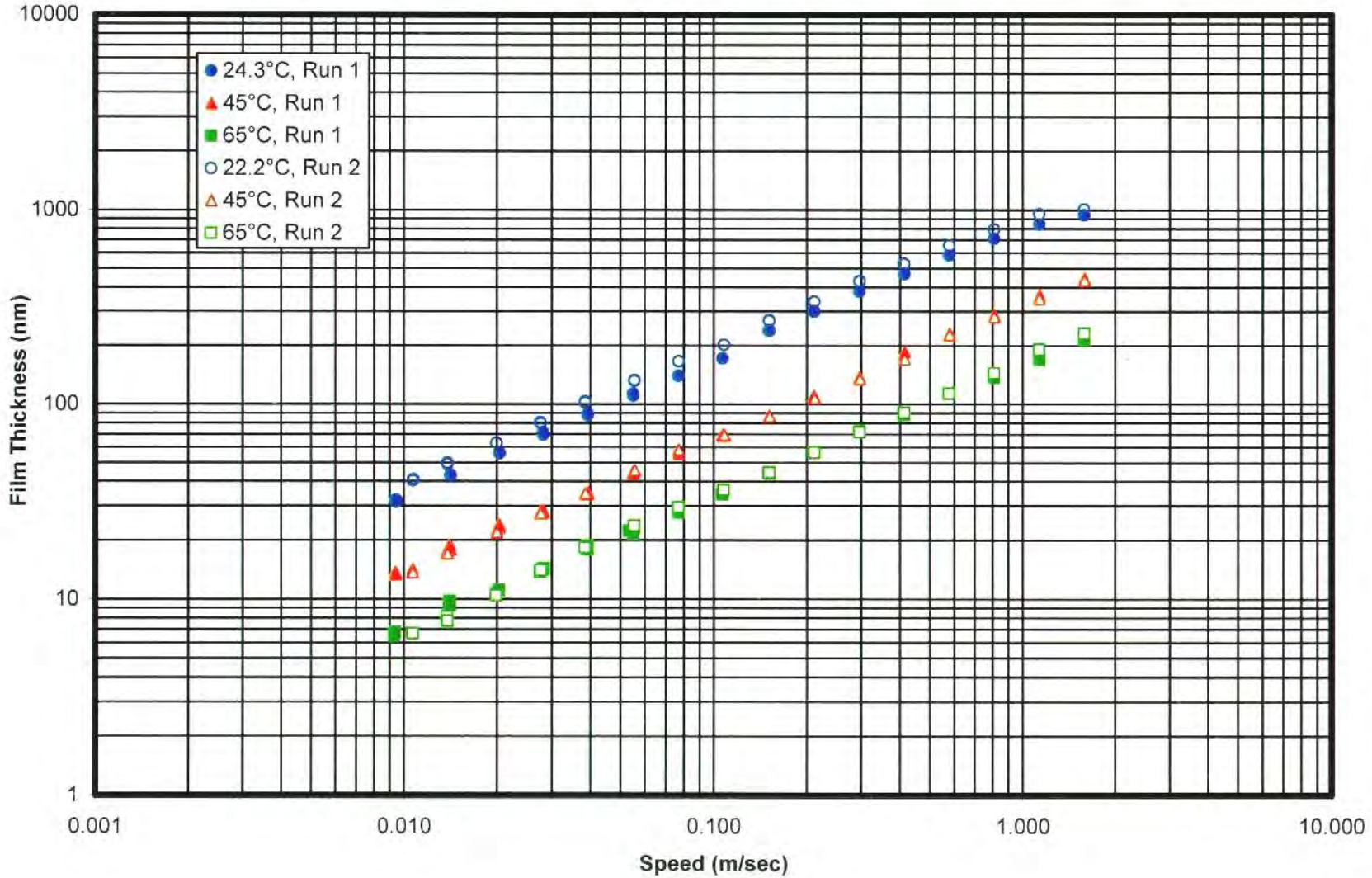

**Figure 26. Effective Pressure-Viscosity Coefficients vs. Temperature for ISO 32 Fluids**

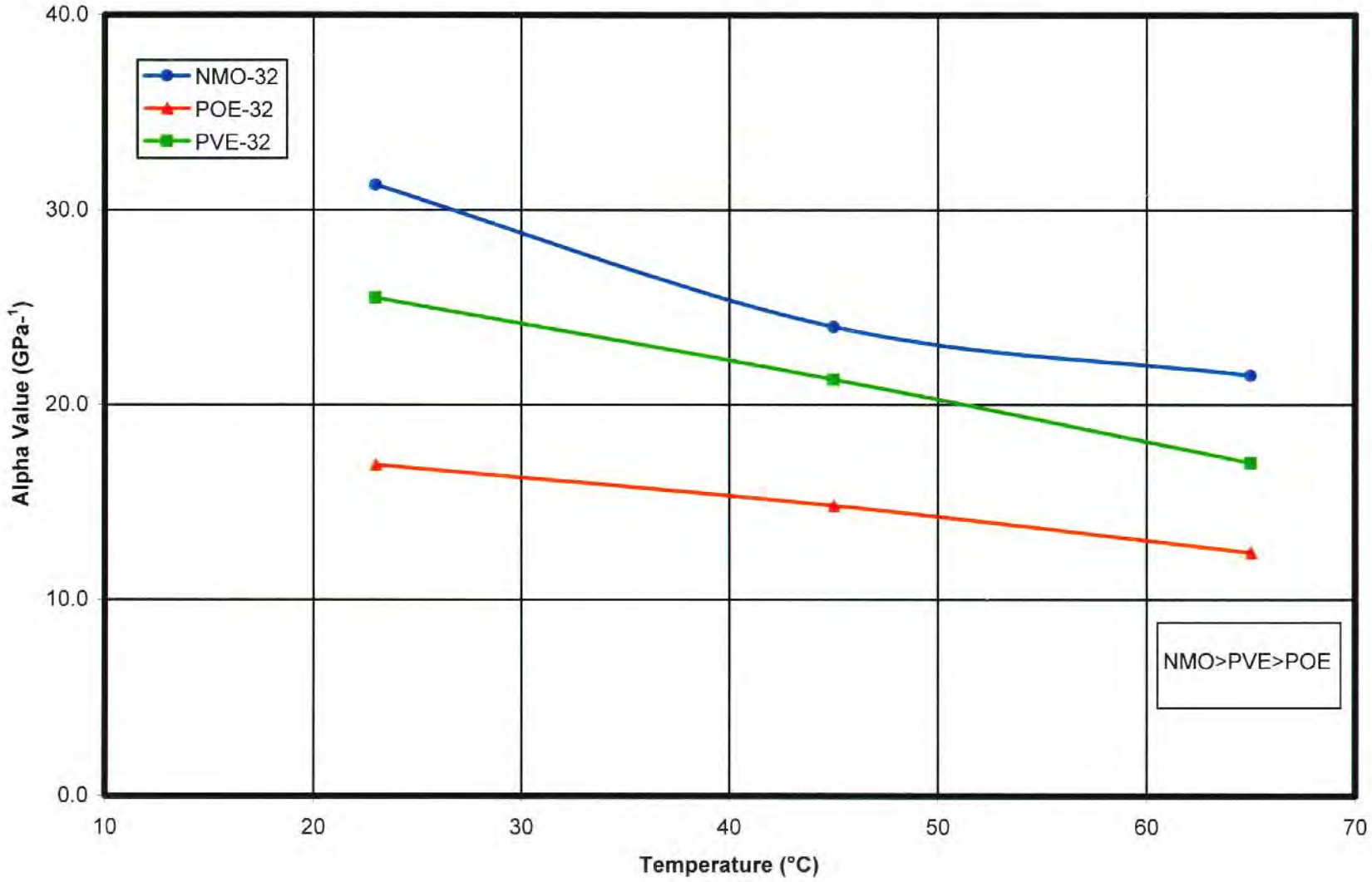

**Figure 27. Effective Pressure-Viscosity Coefficients vs. Temperature for ISO 68 Fluids**

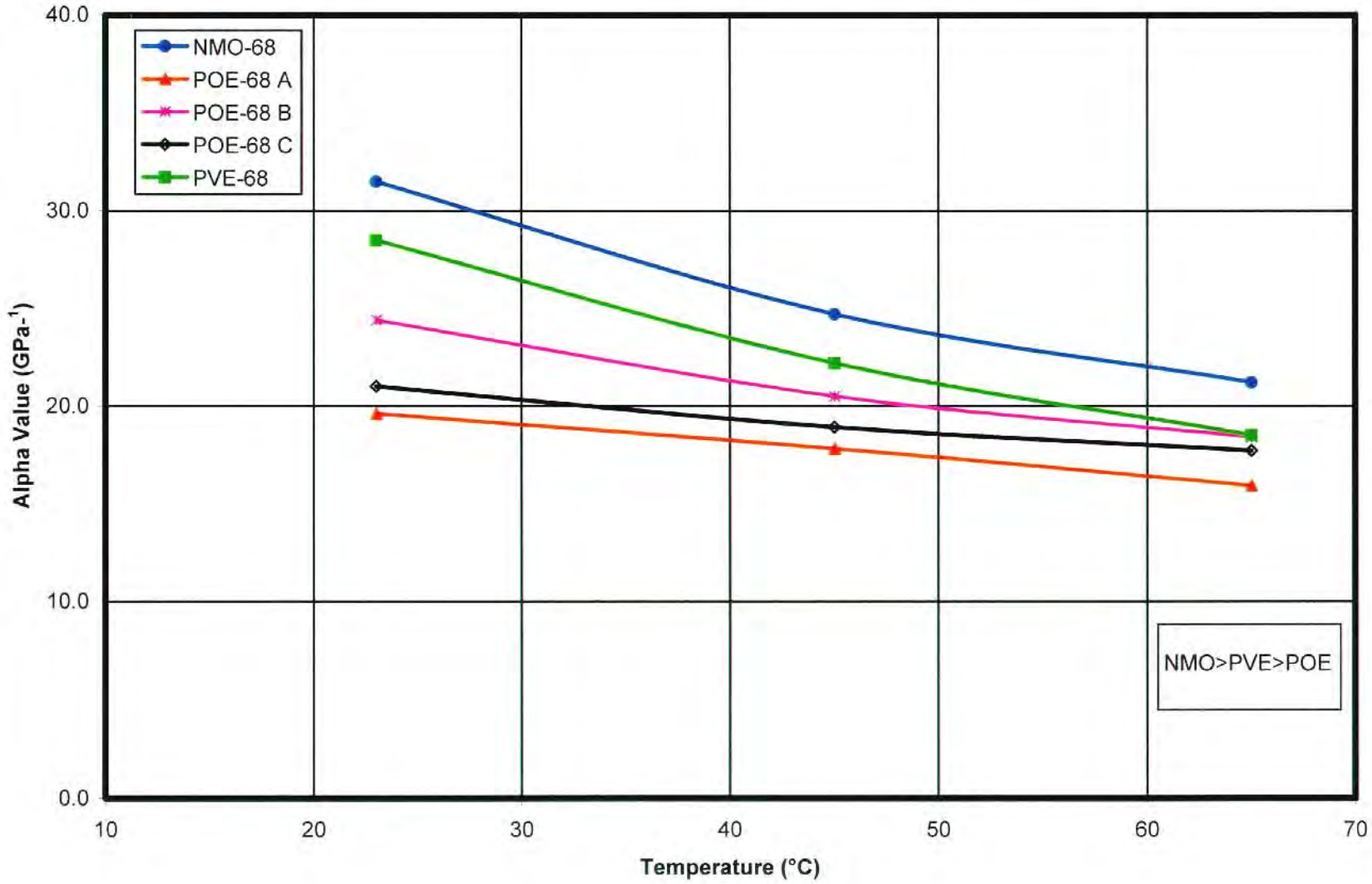

### 6.3.1 ISO 32 Naphthenic Mineral Oil/R-22

Figures 28 through 30 show the film thickness data as a function of rolling speed and refrigerant concentration for mixtures of ISO 32 naphthenic mineral oil and R-22 at 23 °C, 45 °C and 65 °C, respectively. The gradients of the plots, in general, agree with the EHD theoretical slope. However, some deviations are observed at the higher temperatures with high refrigerant concentrations. The R-22 concentrations studied included 0, 10, 20, 40 and 60% by weight. It must be noted that the refrigerant concentrations reported on the plots throughout this report are the percent weight of the refrigerant soluble in the lubricant. At the highest R-22 concentration of 60% by weight, tests were limited up to a temperature of 45 °C due to the formation of extremely thin films (<10 nm) within the speed range studied.

Figure 28 compares the film thickness data of ISO 32 naphthenic mineral oil with various concentrations of R-22 at ambient temperature. Film thickness decreases significantly in the contact as the refrigerant concentration increases. The same trend is observed at the higher test temperatures of 45 and 65 °C, as shown in Figures 29 and 30.

Figure 31 compares the reduction in film thickness with increasing refrigerant concentration at a constant speed of 0.81 m/s at the three test temperatures. It is interesting to note that even at the low refrigerant concentration of 10%, a reduction in film thickness of 45 to 63% was measured. Table 5 compares the percent reduction in film thickness at the different concentration levels of R-22 at the three test temperatures. At each temperature, the film thickness was decreased with increasing refrigerant concentration. However, at a given refrigerant concentration, the percent reduction in film thickness becomes smaller as the temperature is increased.

**Table 5. Percent Reduction in Film Thickness for Mixtures of ISO 32 Naphthenic Mineral Oil and R-22 at a constant rolling speed of 0.8 m/s**

| Refrigerant Concentration, wt % | Temperature, °C | % Reduction in Film Thickness |
|---|---|---|
| 10 | 23 | 63 |
| | 45 | 50 |
| | 65 | 45 |
| 20 | 23 | 85 |
| | 45 | 75 |
| | 65 | 63 |
| 40 | 23 | 94 |
| | 45 | 88 |
| | 65 | 83 |
| 60 | 23 | 98 |
| | 45 | 95 |

### 6.3.2 ISO 68 Naphthenic Mineral Oil/R-22

Figures 32 through 34 show the film thickness data as a function of rolling speed and refrigerant concentration for mixtures of ISO 68 naphthenic mineral oil and R-22 at 23 °C, 45 °C and 65 °C, respectively. The gradients of the plots, in general, agree with the EHD theoretical slope. However, some deviations are observed at high temperatures with high refrigerant concentrations. The R-22 concentrations studied include 0, 10, 15, 30 and 50% by weight. At the highest R-22 concentration of 50% by weight, tests were limited up to a temperature of 45 °C.

Figure 32 compares the film thickness data of ISO 68 naphthenic mineral oil with various concentrations of R-22 at ambient temperature. The data shows similar trends to those observed with the lower viscosity (ISO 32) mineral oil reported above, i.e. film thickness decreases as the refrigerant concentration in the oil increases. The same trend is observed at the higher test temperatures of 45 and 65 °C, as shown in Figures 33 and 34.

Figure 35 compares the reduction in film thickness with increasing refrigerant concentration at a constant speed of 0.81 m/s at the three test temperatures. Table 6 compares the percent reduction in film thickness at the different concentration levels of R-22 at the three test temperatures. The percent reduction in film thickness is similar to that measured with the mixtures of ISO 32 naphthenic mineral oil and R-22, as shown in Table 5. In all cases,

the higher viscosity oil (ISO 68) forms thicker films in the contact than the lower viscosity oil (ISO 32) as expected.

**Table 6. Percent Reduction in Film Thickness for Mixtures of ISO 68 Naphthenic Mineral Oil and R-22 at a constant rolling speed of 0.8 m/s**

| Refrigerant Concentration, wt % | Temperature, °C | % Reduction in Film Thickness |
|---|---|---|
| 10 | 23 | 65 |
| | 45 | 55 |
| | 65 | 48 |
| 15 | 23 | 81 |
| | 45 | 72 |
| | 65 | 64 |
| 30 | 23 | 93 |
| | 45 | 86 |
| | 65 | 79 |
| 50 | 23 | 98 |
| | 45 | 94 |

### 6.3.3 Effect of Refrigerant Concentration (R-22) on Effective Pressure-Viscosity Coefficients of Naphthenic Mineral Oils

Effective pressure-viscosity coefficients of the oil and refrigerant mixtures were calculated as described in Section 3.4. It was assumed that the mixtures obey the theoretical relationship of Hamrock and Dowson (Equations 8-10). The reference oil information was given in Section 6.2. This calculation requires the knowledge of dynamic viscosity (or kinematic viscosity and density) for oil and refrigerant mixtures. This information was obtained from various literature sources including Henderson (70), Cavestri (71) and Van Gaalen (72).

Table 7 shows the dynamic viscosity data obtained from the various references mentioned above for mixtures of ISO 32 naphthenic mineral oil and R-22. As seen in the table, depending on the literature source used, the viscosity values differ significantly by about 13 to 46%. This discrepancy is critical in $\alpha$-value calculations. Depending on the dynamic viscosity used in the calculations, it was found that the $\alpha$-values calculated from the same film thickness data could vary as much as 60%.

**Table 7. Dynamic Viscosity Data on Mixtures of ISO 32 Naphthenic Mineral Oil and R-22 obtained from various references**

| Temp., °C | Dynamic Viscosity, cP R-22 Concentration, Weight Percent | | | | | | | | |
|---|---|---|---|---|---|---|---|---|---|
| | 0% | 10% | | 20% | | 40% | | 60% | |
| | | Ref. 70* | Ref. 71** | Ref. 70* | Ref. 71** | Ref. 71** | Ref. 72*** | Ref. 11**** | Ref. 71** |
| 23 | 60.01 | 21.27 | 18.54 | 8.80 | 6.00 | 1.36 | 1.35 | -- | 0.66 |
| 45 | 21.03 | 8.97 | 6.84 | 4.68 | 2.66 | 0.77 | 0.92 | 1.8 | 0.65 |
| 65 | 9.68 | 5.02 | 3.58 | 3.02 | 1.63 | 0.56 | 0.69 | 1.2 | 0.47 |

* Ref. 70: Henderson, 1994; dynamic viscosity calculated from empirical equations.
** Ref. 71: Cavestri, 1995, kinematic viscosity and density read from graphical data.
*** Ref. 72: Van Gaalen, 1991; dynamic viscosity calculated from empirical equations.
**** Ref. 11: Van Gaalen, 1990; experimental data.

Table 8 shows the effective $\alpha$-values calculated using the dynamic viscosity data from different sources. The $\alpha$-values at 10 and 20 weight percent refrigerant concentration were calculated using the dynamic viscosity data obtained from the regression equations given in Reference 70. Since these equations are valid only up to a refrigerant concentration of 30%, the viscosity data provided in References 71, 72 and 11 were used at the higher R-22 concentrations of 40 and 60%. The numbers in parenthesis show the $\alpha$-values calculated using the kinematic viscosity and density data obtained from Reference 71. As seen in Table 8, there is a big discrepancy in the $\alpha$-values calculated from the same film thickness data using different dynamic viscosities.

Figure 36 shows the effect of refrigerant concentration on effective pressure-viscosity coefficients and dynamic viscosity. In general, both the $\alpha$-value and dynamic viscosity decrease with increasing refrigerant concentration and temperature.

To test for the effect of viscosity on pressure-viscosity coefficient, $\alpha$-values were plotted against dynamic viscosity for the naphthenic mineral oil (NMO-32) alone and its blends with R-22 at all the test temperatures. The data was plotted using a logarithmic viscosity scale as shown in Figure 37. It is known from thermodynamic models that the changes in certain properties are related exponentially to viscosity (62, 66, 67). As can be seen in Figure 37, pressure-viscosity coefficient increases linearly in proportion to dynamic viscosity both for the mineral oil alone and its blends with the refrigerant. This effect has been reported recently for

various lubricant base oils (polyalphaolefins and mineral oils) and polyalphaolefin blends (68, 69).

**Table 8. Effective Pressure-Viscosity Coefficients for Mixtures of ISO 32 Naphthenic Mineral Oil and R-22**

| Temp., °C | Refrigerant Concentration, wt % | | | | |
|---|---|---|---|---|---|
| | 0% | 10%* | 20%* | 40%** | 60%*** |
| | α-values, $GPa^{-1}$ | | | | |
| 23 | 31.3 | 19.7 (23.9)[a] | 12.8 (21.4)[a] | 17.6 | 12.6 |
| 45 | 24.0 | 16.8 (24.6)[a] | 11.1 (25.1)[a] | 14.9 | 6.5 |
| 65 | 21.5 | 14.7 (23.3)[a] | 13.8 (35.6)[a] | 13.4 | -- |

* α-values were based on dynamic viscosity data from Ref. 70.
( )[a] numbers in parenthesis show α-values based on dynamic viscosity data from Ref. 71.
** α-values were based on dynamic viscosity data from Ref. 11 and 72.
*** α-values were based on dynamic viscosity data from Ref. 71.

Effective pressure-viscosity coefficients were also calculated for the mixtures of ISO 68 naphthenic mineral oil and R-22. Dynamic viscosity was calculated from the kinematic viscosity and density data (graphical format) provided by Reference 73 and given in Table 9. Table 10 shows the α-values calculated as a function of refrigerant concentration at the three test temperatures. These were limited to the refrigerant concentrations of up to 30% by weight, since the viscosity data at 50% concentration was not available. Similar to the trends reported above for mixtures of ISO 32 naphthenic mineral oil and R-22, α-values and dynamic viscosities decrease with increasing refrigerant concentration and temperature, Figure 38. This finding agrees with Akei's work (33). Table 11 compares the α-values obtained in this work with those reported by Akei (33) for the same lubricant and refrigerant mixture. As seen in the table, excellent agreement was observed between the two studies. Figure 39 shows the increase in pressure-viscosity coefficient as a function of log (dynamic viscosity).

**Table 9. Dynamic Viscosity Data for Mixtures of ISO 68 Naphthenic Mineral Oil and R-22**

| Temperature, °C | Dynamic Viscosity, cP | | | |
|---|---|---|---|---|
| | R-22 Concentration, wt % | | | |
| | 0% | 10% | 15% | 30% |
| 23 | 128.41 | 33.73 | 20.35 | 5.56 |
| 45 | 37.98 | 14.19 | 7.94 | 3.39 |
| 65 | 15.56 | 6.35 | 4.78 | 2.28 |

**Table 10. Effective Pressure-Viscosity Coefficients for Mixtures of ISO 68 Naphthenic Mineral Oils and R-22**

| Temperature, °C | Refrigerant Concentration, wt % | | | |
|---|---|---|---|---|
| | 0% | 10% | 15% | 30% |
| | $\alpha$-values, $GPa^{-1}$ | | | |
| 23 | 31.5 | 22.3 | 16.8 | 13.6 |
| 45 | 24.7 | 18.2 | 16.7 | 13.2 |
| 65 | 21.2 | 16.6 | 16.3 | 16.4 |

**Table 11. Comparison of Effective Pressure-Viscosity Coefficients for ISO 68 NMO and R-22 Mixtures**

| Temperature, °C | R-22 Concentration, wt % | |
|---|---|---|
| | 0% | 10% |
| | $\alpha$-values, $GPa^{-1}$ | |
| 23<br>20 | 31.5<br>30* | 22.3<br>21.0* |
| 45<br>40 | 24.7<br>26* | 18.2<br>17.0* |
| 65<br>60 | 21.2<br>21.0* | 16.6<br>14.0* |

* reported by M. Akei in Reference 33

**Figure 28. Comparison of Film Thickness Data for ISO 32 Naphthenic Mineral Oil at Ambient Temperature as a Function of R-22 Concentration**

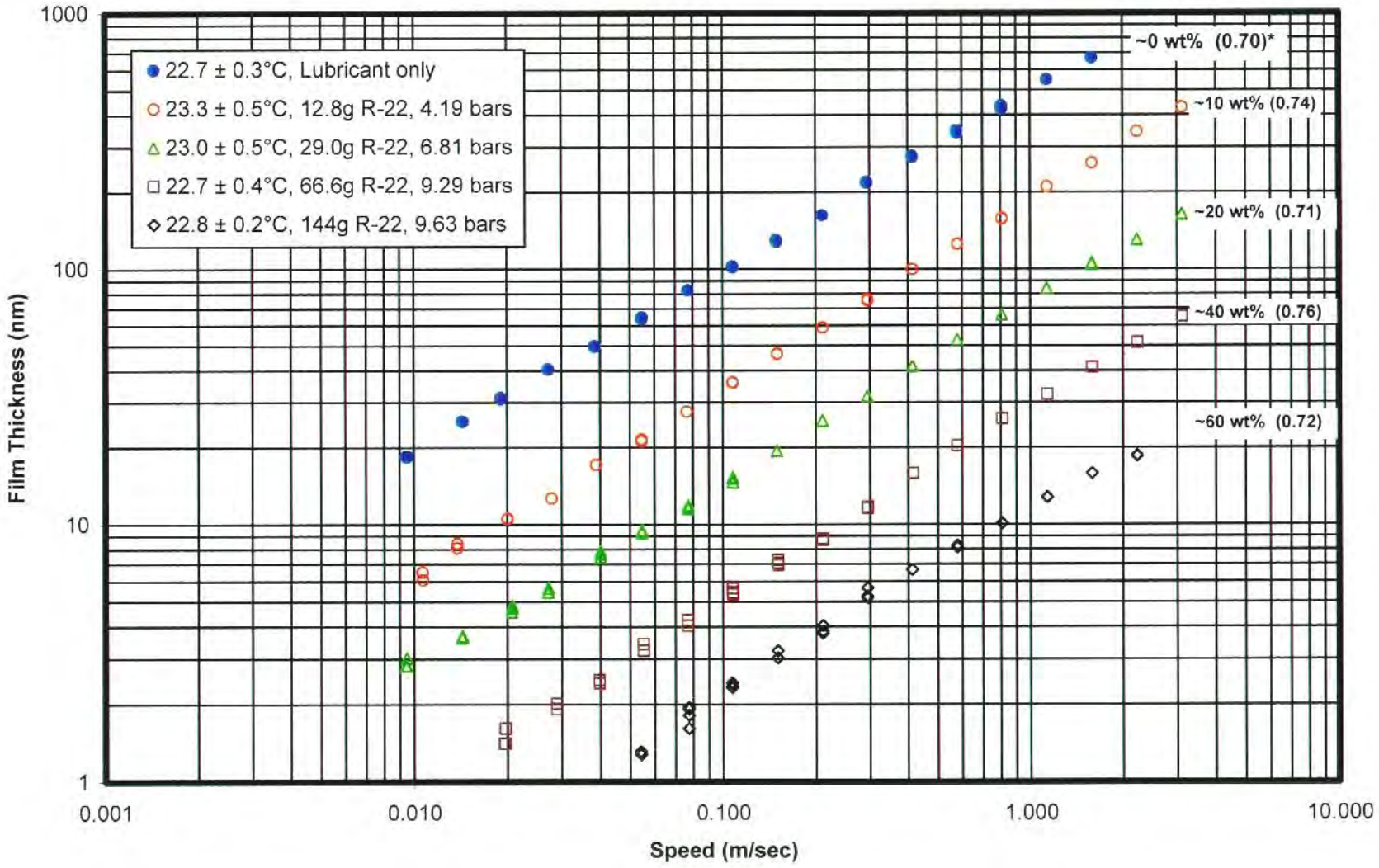


*numbers in parentheses show gradients

**Figure 29. Comparison of Film Thickness Data for ISO 32 Naphthenic Mineral Oil at 45°C as a Function of R-22 Concentration**

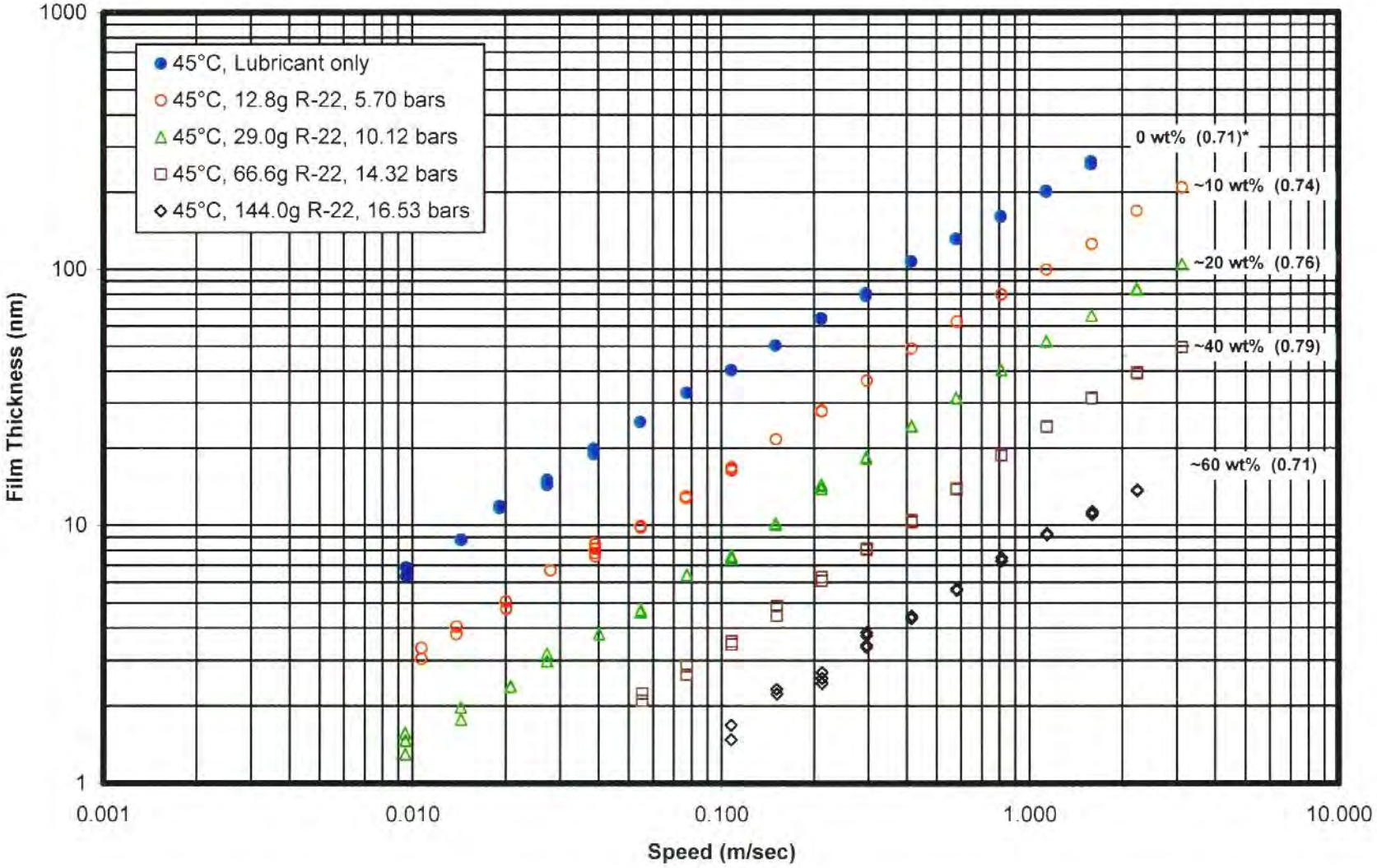


*numbers in parentheses show gradients

**Figure 30. Comparison of Film Thickness Data for ISO 32 Naphthenic Mineral Oil at 65°C as a Function of R-22 Concentration**

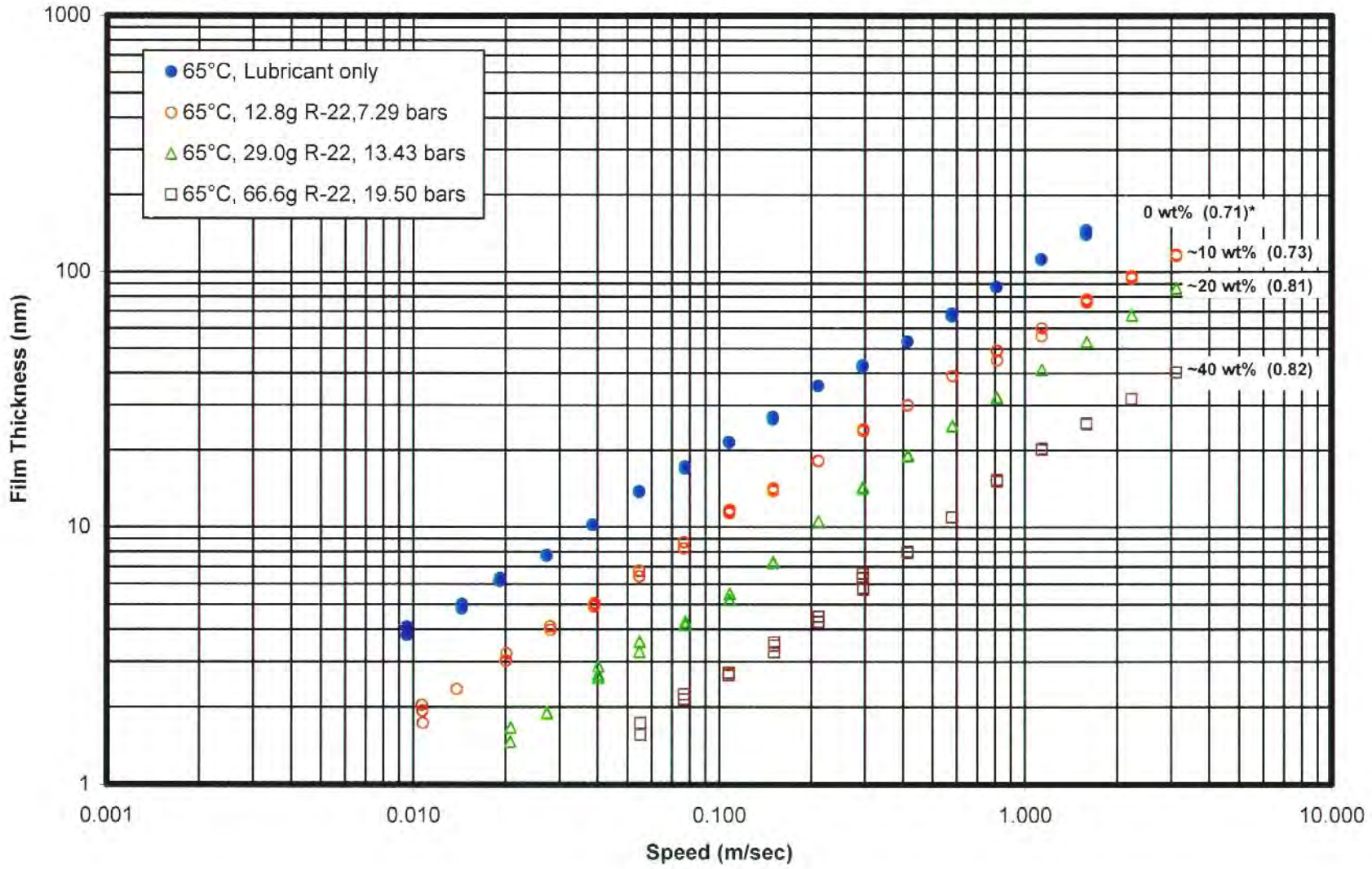


*numbers in parentheses show gradients

**Figure 31. Film Thickness vs. R-22 Concentration for ISO 32 Naphthenic Mineral Oil**

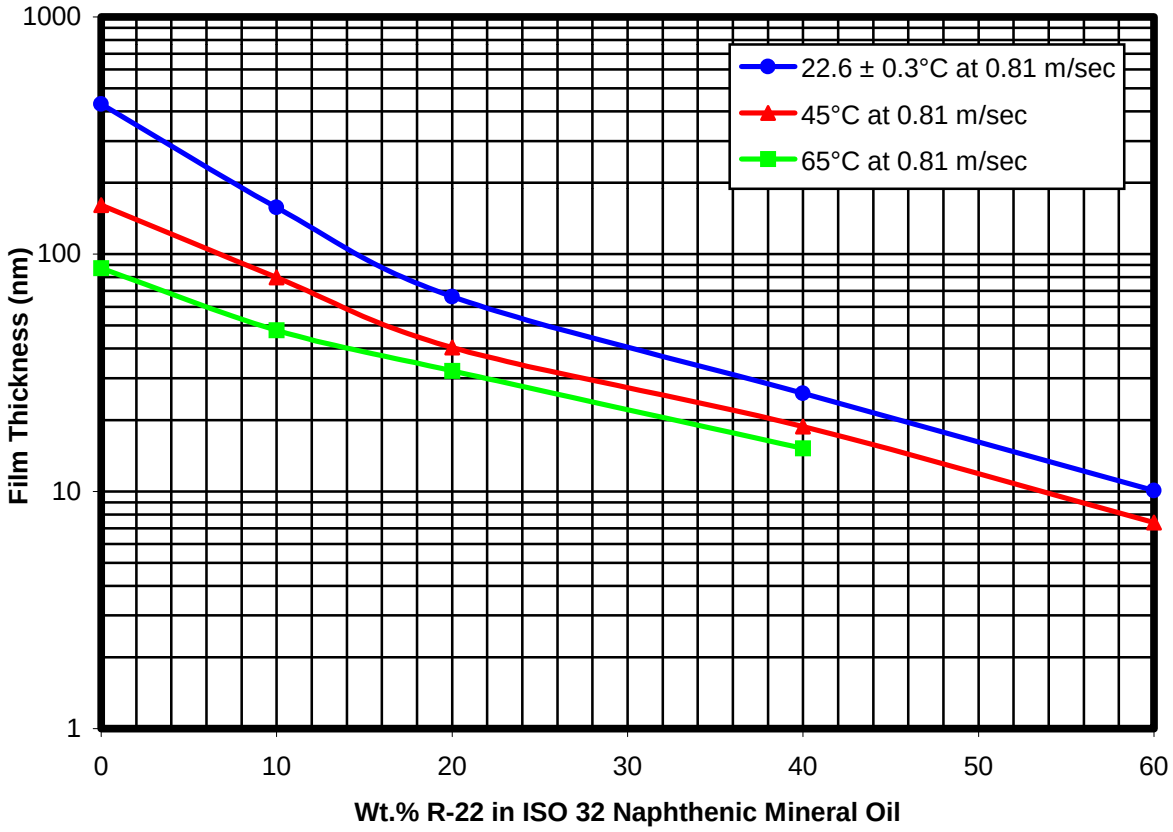

**Figure 32. Comparison of Film Thickness Data for ISO 68 Naphthenic Mineral Oil at Ambient Temperature as a Function of R-22 Concentration**

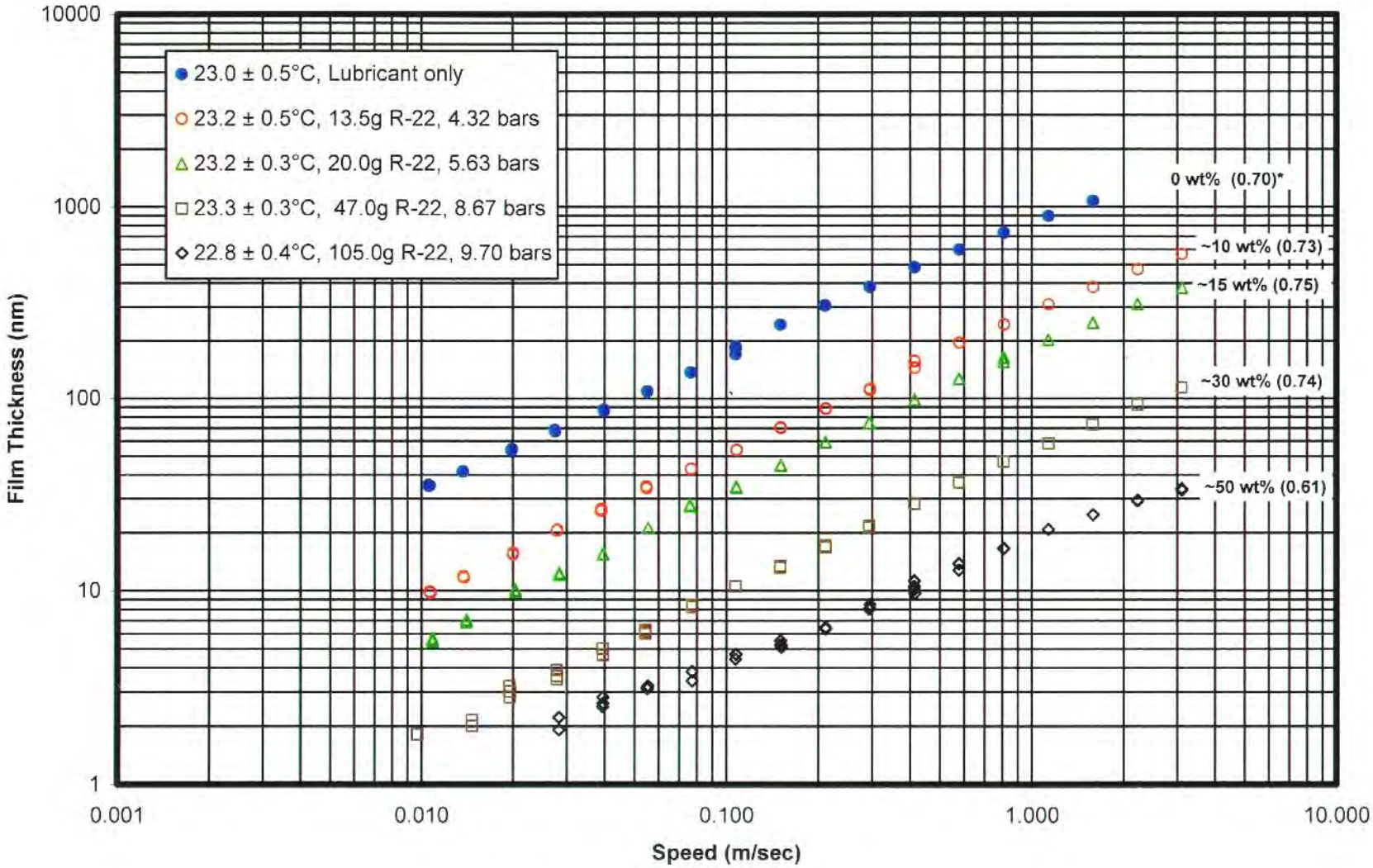


*numbers in parentheses show gradients

**Figure 33. Comparison of Film Thickness Data for ISO 68 Naphthenic Mineral Oil at 45°C as a Function of R-22 Concentration**

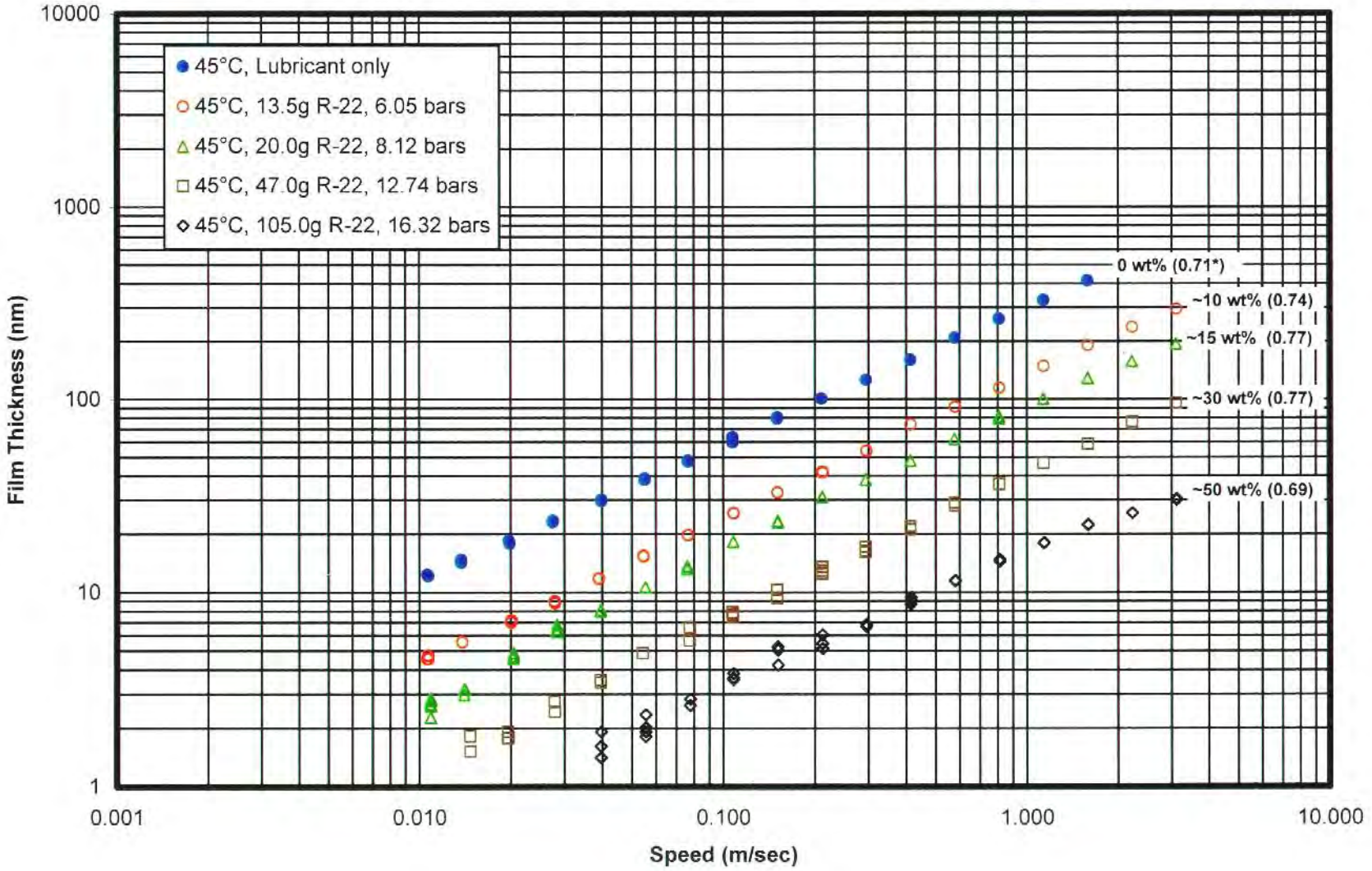


*numbers in parentheses show gradients

**Figure 34. Comparison of Film Thickness Data for ISO 68 Naphthenic Mineral Oil at 65°C as a Function of R-22 Concentration**

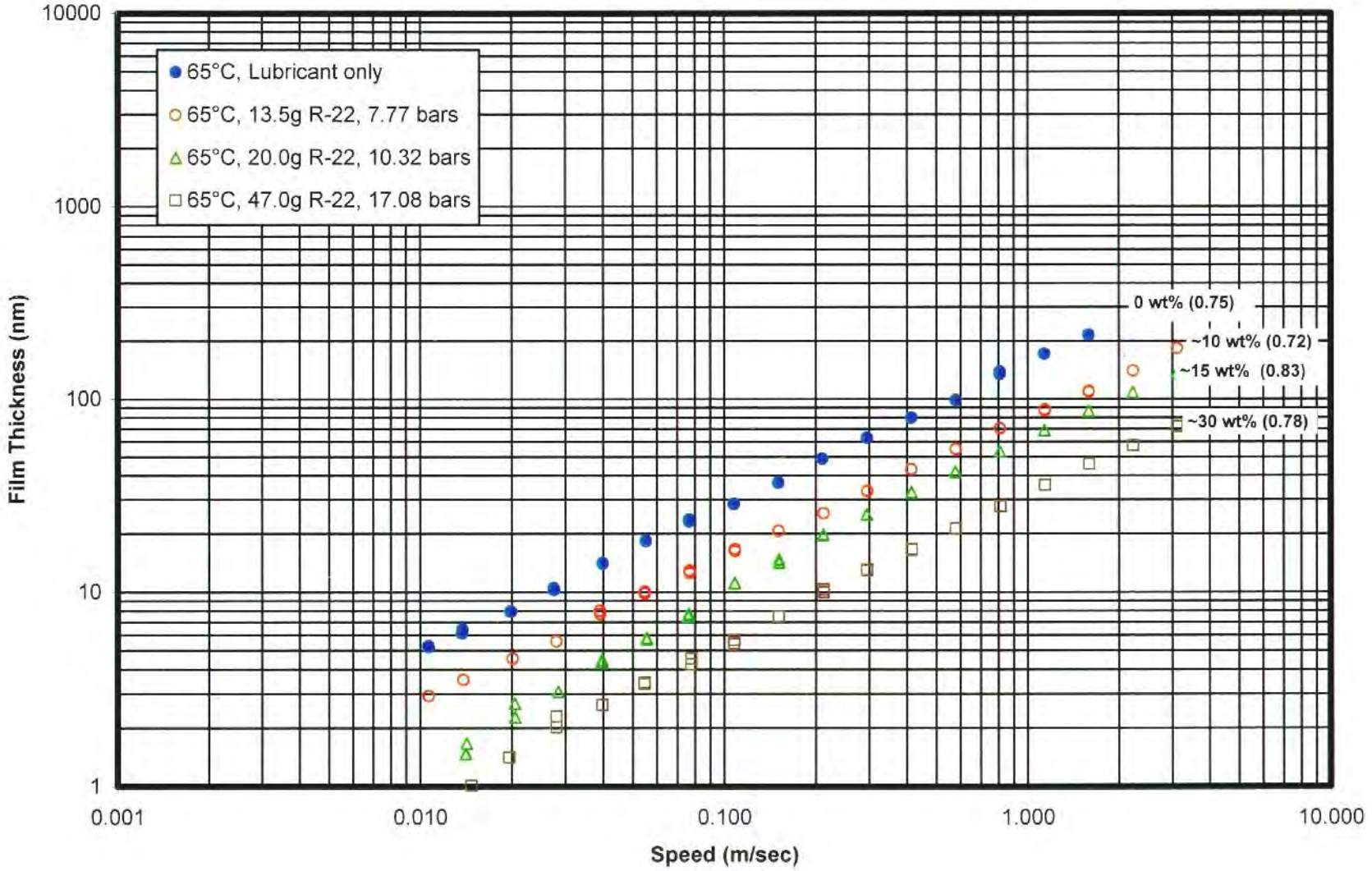


*numbers in parentheses show gradients

**Figure 35. Film Thickness vs. R-22 Concentration for ISO 68 Naphthenic Mineral Oil**

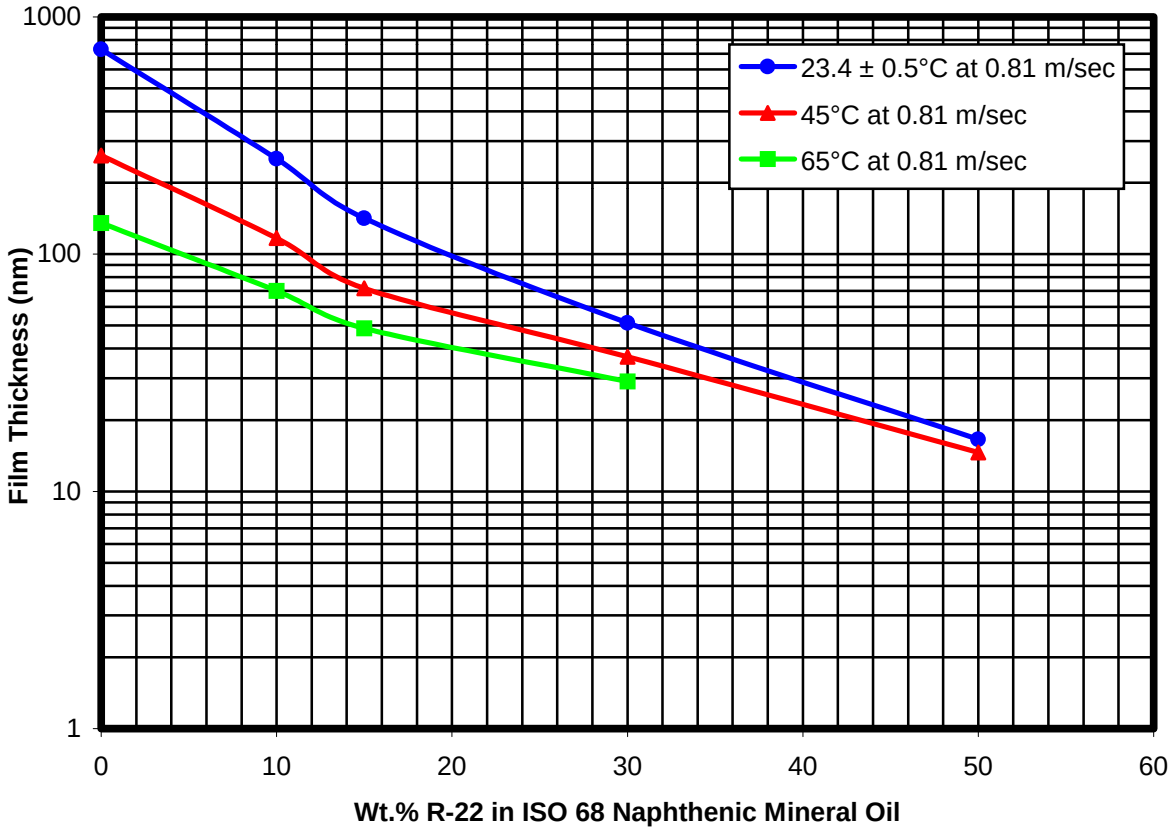

**Figure 36. Effect of Refrigerant Concentration on Effective Pressure-Viscosity Coefficient and Dynamic Viscosity for Mixtures of ISO 32 Naphthenic Mineral Oil and R-22**

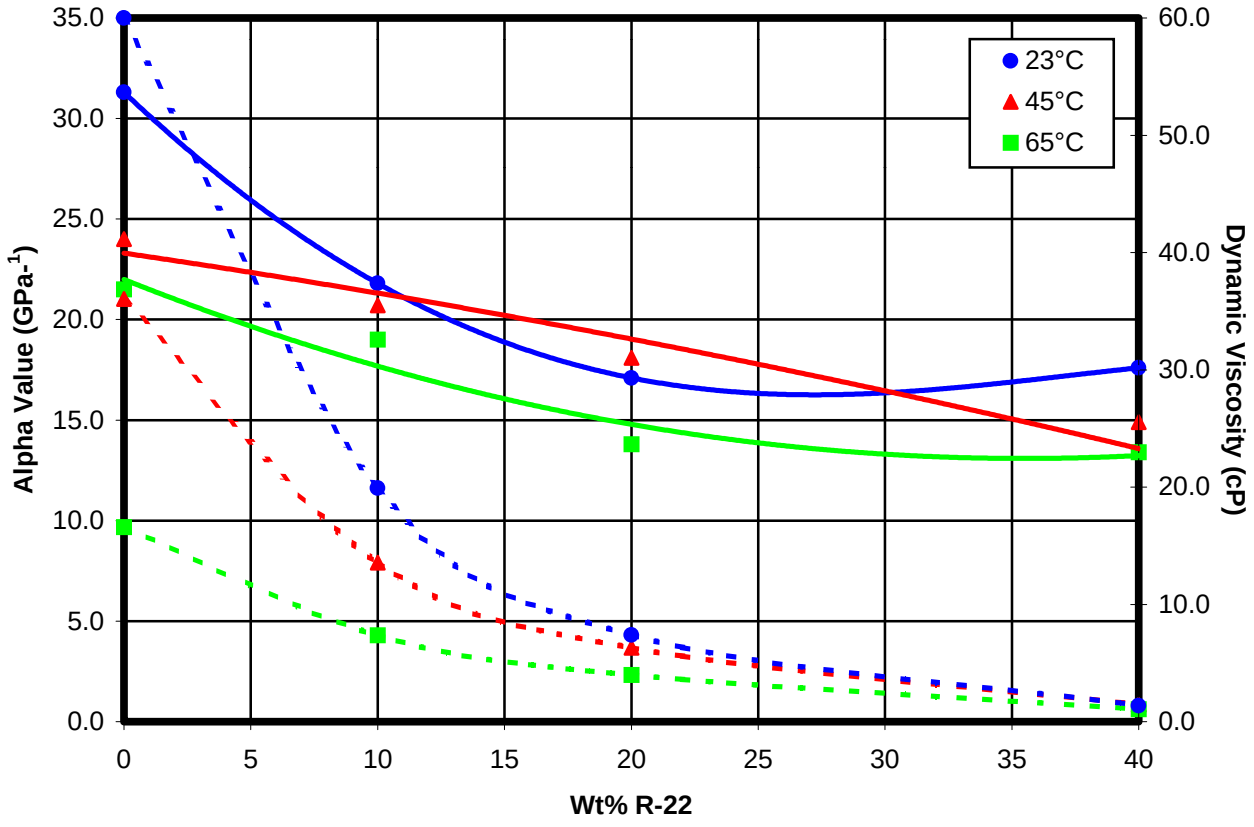


Solid lines represent alpha values
Dashed lines represent dynamic viscosities

**Figure 37. Alpha Value vs. Dynamic Viscosity for ISO 32 Naphthenic Mineral Oil in R-22**

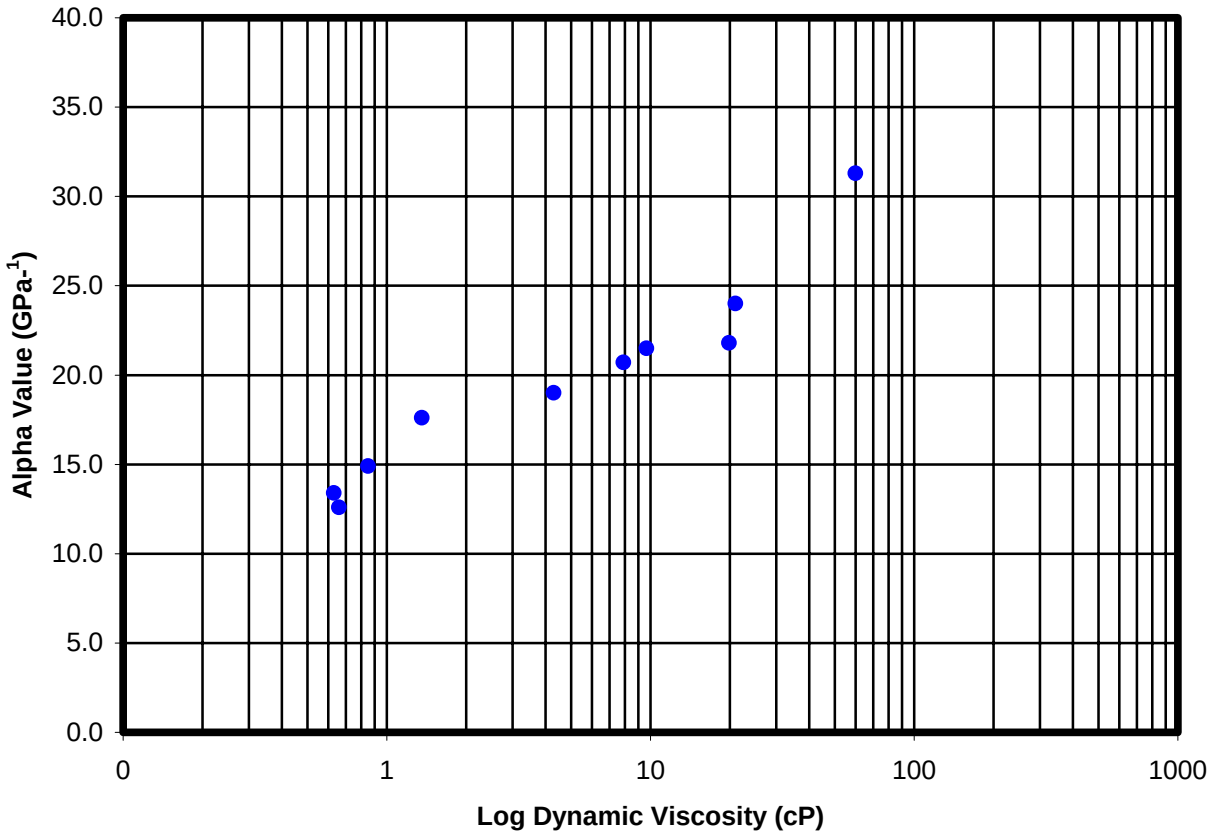

**Figure 38. Effect of Refrigerant Concentration on Effective Pressure-Viscosity Coefficient and Dynamic Viscosity for Mixtures of ISO 68 Naphthenic Mineral Oil and R-22**

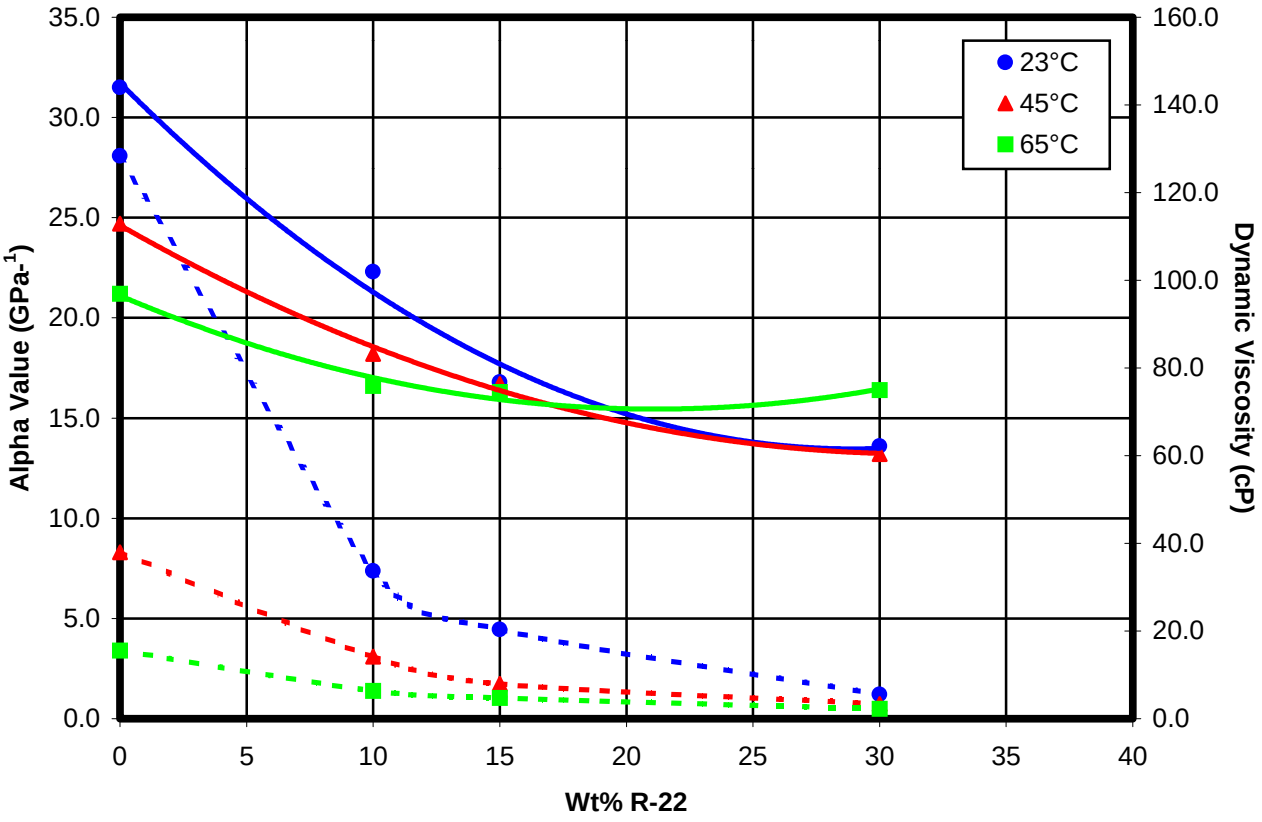


Solid lines represent alpha values
Dashed lines represent dynamic viscosities

**Figure 39. Alpha Value vs. Dynamic Viscosity for ISO 68 Naphthenic Mineral Oil in R-22**

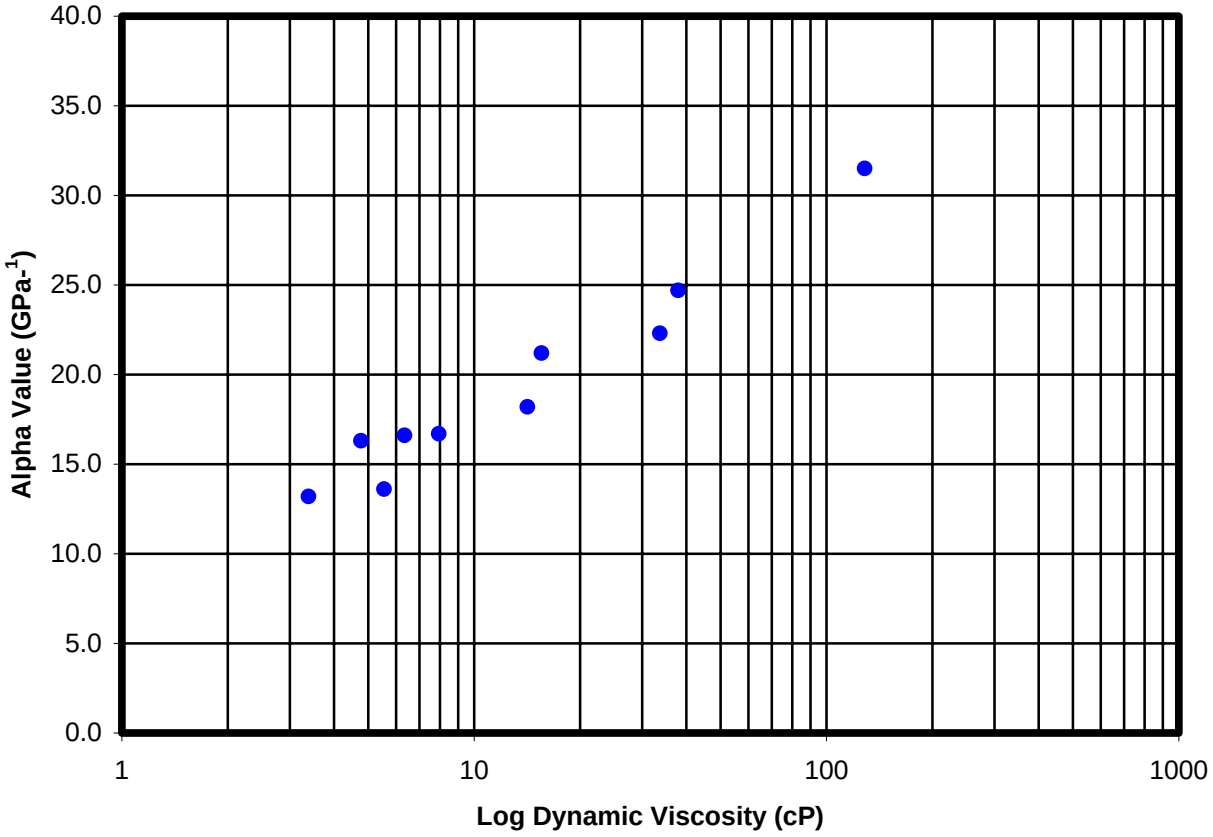

## 6.4 Film Thickness Measurements on Mixtures of Polyolesters and R-134a

Film thickness measurements were conducted on mixtures of R-134a and polyolesters as a function of rolling speed, temperature and refrigerant concentration. One polyolester of ISO 32 viscosity grade (POE-32) and three polyolesters of ISO 68 viscosity grade (POE-68A, POE-68B, POE-68C) were included in this study. The results are reported in the following sections.

### 6.4.1 ISO 32 Polyolester/R-134a

Figures 40 through 42 show the film thickness data as a function of rolling speed and refrigerant concentration for mixtures of ISO 32 polyolester and R-134a at 23 °C, 45 °C and 65 °C, respectively. Overall, the gradients of the plots agree with the EHD theoretical slope. Some deviation from the theoretical slope is observed at the highest refrigerant concentration of 50% at the higher test temperatures. This discrepancy could be related to the miscibility characteristics of the refrigerant/lubricant mixtures under these conditions (i.e., high temperatures, pressures and refrigerant concentrations). It is possible that a two-phase system may occur in the inlet zone of the contact under these test conditions.

The R-134a concentrations studied included 0, 10, 20, 40 and 50% by weight. Similar to the findings reported in the previous sections for naphthenic oils and R-22, film thickness decreases significantly in the contact as the refrigerant concentration in the lubricant increases. Figure 43 compares the reduction in film thickness with increasing refrigerant concentration at a constant speed of 0.81 m/s at the three test temperatures. Percent reduction in film thickness as a function of R-134a concentration is calculated for the data shown in Figure 43 and given in Table 12. Trends observed are similar to those reported in Section 6.3 for the mineral oil and R-22 mixtures.

**Table 12. Percent Reduction in Film Thickness for Mixtures of ISO 32 Polyolester and R-134a at a constant rolling speed of 0.8 m/s**

| Refrigerant Concentration, wt % | Temperature, °C | % Reduction in Film Thickness |
|---|---|---|
| 10 | 23 | 44 |
| | 45 | 43 |
| | 65 | 37 |
| 20 | 23 | 73 |
| | 45 | 63 |
| | 65 | 52 |
| 40 | 23 | 90 |
| | 45 | 79 |
| | 65 | 74 |
| 50 | 23 | 93 |
| | 45 | 87 |
| | 65 | 84 |

### 6.4.2 ISO 68 Polyolesters/R-134a

**Polyolester A/R-134a**

Figures 44 through 46 show the film thickness data as a function of rolling speed and refrigerant concentration for mixtures of ISO 68 polyolester A and R-134a at 23 °C, 45 °C and 65 °C, respectively. The gradients of the plots vary from 0.65 to 0.78 and agree with the EHD theoretical slope. The R-134a concentrations studied include 0, 10, 15, 30 and 50% by weight. Figure 44 compares the film thickness data of ISO 68 polyolester with various concentrations of R-134a at ambient temperature. The data shows similar trends to those observed with the lower viscosity (ISO 32) polyolester reported above, i.e. film thickness decreases as the refrigerant concentration in the oil increases. The same trend is observed at the higher test temperatures of 45 and 65 °C, as shown in Figures 45 and 46.

Figure 47 compares the reduction in film thickness with increasing refrigerant concentration at a constant speed of 0.81 m/s at the three test temperatures. Percent reduction in film thickness as a function of R-134a concentration is calculated from Figure 47 and reported in Table 13. This information is also given in the table for the other polyolesters (POE-68B and POE-68C) tested. The results indicate a similar reduction in film thickness for the three polyolesters studied. Jonsson reported a 55% reduction in film thickness for mixtures of polyolesters and R-134a containing 9% refrigerant at 21 °C (31). This compares favorably

with the 52-57% reduction measured in this study for 10% R-134a concentration at 23 °C (Table 13).

**Polyolester B/R-134a**

Figures 48 through 50 show the film thickness data as a function of rolling speed and refrigerant concentration for mixtures of ISO 68 polyolester B and R-134a at 23 °C, 45 °C and 65 °C, respectively. The gradients of the plots vary from 0.65 to 0.78 and agree with the EHD theoretical slope. Figure 51 compares the reduction in film thickness with increasing refrigerant concentration at a constant speed of 0.81 m/s at the three test temperatures. Trends observed were similar to those reported above for the polyolester A/R-134a mixtures.

**Table 13. Percent Reduction in Film Thickness for Mixtures of ISO 68 Polyolesters and R-134a at a constant rolling speed of 0.8 m/s**

| Refrigerant Concentration, wt % | Temperature, °C | % Reduction in Film Thickness | | |
|---|---|---|---|---|
| | | POE-68A | POE-68B | POE-68C |
| 10 | 23 | 54 | 57 | 52 |
| | 45 | 46 | 50 | 45 |
| | 65 | 37 | 43 | 40 |
| 15 | 23 | 67 | 70 | 66 |
| | 45 | 60 | 65 | 61 |
| | 65 | 46 | 56 | 52 |
| 30 | 23 | 88 | 90 | 89 |
| | 45 | 80 | 83 | 83 |
| | 65 | 71 | 76 | 75 |
| 50 | 23 | 95 | 97 | 96 |
| | 45 | 91 | 95 | 92 |
| | 65 | 88 | 92 | 88 |
| 9* | 21* | 55% | | |

* reported in Reference 31

**Polyolester C/R-134a**

Similar data on ISO 68 polyolester C and R-134a mixtures are given in Figures 52 through 55. Similar trends were observed to those reported above for polyolesters A and B.

**Comparison of Film Thickness Data for Polyolesters A, B and C**

Figures 56 through 58 compare the film thickness data obtained on mixtures of R-134a and polyolesters A, B and C at the test temperatures of 23, 45 and 65 °C, respectively. Overall, the esters produce films of comparable thickness. In some cases, polyolester B produced thinner films in the contact than polyolesters A and C. This could be due to the higher solubility of this ester in the refrigerant due to its more branched structure.

### 6.4.3 Effect of Refrigerant Concentration (R-134a) on Effective Pressure-Viscosity Coefficients of Polyolesters

Effective pressure-viscosity coefficients of the ester and refrigerant mixtures were calculated as described in Section 3.4. It was assumed that the mixtures obey the theoretical relationship of Hamrock and Dowson.

As explained in Section 6.3.3, the calculation of $\alpha$-value requires the knowledge of dynamic viscosity (or kinematic viscosity and density) data for ester and refrigerant mixtures. Dynamic viscosity, given in Table 14 for mixtures of ISO 32 polyolester and R-134a, was calculated from the kinematic viscosity and density data provided by Reference 74. Table 15 shows the effective $\alpha$-values calculated for the mixtures of ISO 32 polyolester and R-134a as a function of refrigerant concentration and temperature. There are some anomalies in the $\alpha$-values at high temperatures (45 and 65 °C) and high refrigerant concentrations (40-50 wt %). There may be several possible reasons for this. First of all, in $\alpha$-calculations, it was assumed that the mixtures of esters and refrigerants obey the theoretical relationship of Hamrock and Dowson, i.e. the EHD film generated in the presence of refrigerants depends on the same viscosity and pressure-viscosity mechanisms as for the lubricants only. This may not be true especially at high refrigerant concentrations. Discrepancies between experiments and theory were also reported by Jonsson (31). There also exists the possibility of the lubricant/refrigerant mixture to form a two-phase system in the inlet region of the contact (31). In this case, the

refrigerant concentration in the lubricant and hence the dynamic viscosity would vary from those reported in Tables 14 and 15. Other reasons may include the use of inaccurate dynamic viscosity in the pressure-viscosity coefficient calculations or the assumption of the same refractive index for the refrigerant/lubricant mixtures as the lubricant only. As discussed in Section 6.3.3, depending on the dynamic viscosity used in the calculations, the pressure-viscosity coefficients calculated from the same film thickness data could vary as much as 60%.

**Table 14. Dynamic Viscosity Data for Mixtures of ISO 32 Polyolester and R-134a**

| Temperature, °C | Dynamic Viscosity, cP<br>R-134a Concentration, wt % | | | | |
|---|---|---|---|---|---|
| | 0% | 10% | 20% | 40% | 50% |
| 23 | 61.36 | 28.76 | 14.88 | 3.20 | 2.07 |
| 45 | 25.12 | 13.68 | 6.99 | 1.88 | 1.25 |
| 65 | 12.64 | 7.30 | 4.32 | 1.43 | 1.04 |

The $\alpha$-value and dynamic viscosity, in general, decrease with increasing refrigerant concentration and temperature as shown in Figure 59. Figure 60 shows the relationship between $\alpha$-values and log (dynamic viscosity).

The $\alpha$-values calculated for the ISO 32 polyolester/R-134a mixtures were compared to those reported in Reference 31 for a series of ISO 32 polyolester/R-134a in Table 15. Considering the differences in the experimental techniques, reasonable agreement was observed between the two studies.

**Table 15. Effective Pressure-Viscosity Coefficients for Mixtures of ISO 32 Polyolester and R-134a**

| Temperature, °C | Refrigerant Concentration, wt % | | | | |
|---|---|---|---|---|---|
| | 0% | 10% | 20% | 40% | 50% |
| | α-values, $GPa^{-1}$ | | | | |
| 23 | 16.9 | 15.6 | 10.9 | 12.3 | 11.8 |
| 45 | 14.8 | 10.8 | 10.8 | 20.6(?) | 19.2(?) |
| 65 | 12.4 | 10.3 | 13.1 | 20.1(?) | 14.9 |
| 40* | 14.2-18 | 13.5-16* | 13-15.5* | ~ 13* | |

* reported in Reference 31 for a series of ISO 32 Polyolesters

Effective pressure-viscosity coefficients were also calculated for the mixtures of ISO 68 polyolesters A, B and C, and R-134a. Dynamic viscosity data, given in Table 16, were calculated from the kinematic viscosity and density data provided by References 74, 75, and 76. Table 17 compares the α-values calculated as a function of refrigerant concentration and temperature for the polyolesters A, B and C. The α-values calculated for these mixtures were compared to those reported by Akei (33) and Jonsson (31) in Table 18. In general, there is a good agreement between the ranges of α-values reported in this study and those reported in the literature. Figures 61 through 63 show the effect of R-134a concentration on dynamic viscosity and α-values. Figure 64 shows α-values plotted against log (dynamic viscosity) for the three polyolesters. The same overall trend as reported above for mineral oil/R-22 mixtures is seen, although there is more apparent overall scatter.

**Table 16. Dynamic Viscosity Data for Mixtures of ISO 68 Polyolester and R-134a**

| Temperature, °C | Polyolester | Dynamic Viscosity, cP | | | |
|---|---|---|---|---|---|
| | | R-134a Concentration, wt % | | | |
| | | 0% | 10% | 15% | 30% |
| 23 | A | 131.15 | 49.75 | 30.57 | 11.47 |
| 45 | | 48.14 | 19.54 | 14.03 | 5.82 |
| 65 | | 22.26 | 12.30 | 8.25 | 3.62 |
| 23 | B | 138.25 | 47.38 | 30.62 | 9.05 |
| 45 | | 47.35 | 19.72 | 14.49 | 4.67 |
| 65 | | 20.96 | 10.17 | 7.35 | 2.84 |
| 23 | C | 143.58 | 60.43 | 44.66 | 13.1 |
| 45 | | 50.18 | 26.12 | 18.62 | 6.73 |
| 65 | | 22.46 | 13.03 | 9.79 | 4.05 |

**Table 17. Effective Pressure-Viscosity Coefficients for Mixtures of ISO 68 Polyolester and R-134a**

| Temperature, °C | Polyolester | Refrigerant Concentration, wt % | | | |
|---|---|---|---|---|---|
| | | 0% | 10% | 15% | 30% |
| | | $\alpha$-values, $GPa^{-1}$ | | | |
| 23 | A | 19.6 | 21.9 | 21.3 | 10.4 |
| 45 | | 17.8 | 20.7 | 18.4 | 14.3 |
| 65 | | 15.9 | 15.9 | 18.0 | 17.1 |
| 23 | B | 24.4 | 24.1 | 16.6 | 13.5 |
| 45 | | 20.5 | 23.3 | 13.4 | 15.3 |
| 65 | | 18.4 | 21.4 | 15.9 | 17.5 |
| 23 | C | 21.0 | 15.2 | 11.8 | 8.8 |
| 45 | | 18.9 | 14.3 | 12.0 | 11.2 |
| 65 | | 17.7 | 12.4 | 13.6 | 13.3 |

**Table 18. Comparison of Effective Pressure-Viscosity Coefficients for ISO 68 Polyolester and R-134a Mixtures**

| Temperature, °C | Lubricant | R-134a Concentration, wt % | | |
|---|---|---|---|---|
| | | 0% | 10% | 30% |
| | | α-values, $GPa^{-1}$ | | |
| 23 | A | 19.6 | 21.9 | 10.4 |
| | | 24.4 | 24.1 | 13.5 |
| | | 21.0 | 15.2 | 8.8 |
| 20 | POE* | 28.0 | 23 | 18 |
| 45 | A | 17.8 | 20.7 | 14.3 |
| | B | 20.5 | 23.3 | 15.3 |
| | C | 18.9 | 14.3 | 11.2 |
| 40 | POE* | 25.0 | 19 | 18 |
| 40 | POE** | ~14-31 | ~14-25 | ~13-19 |
| 65 | A | 15.9 | 15.9 | 17.1 |
| | B | 18.4 | 21.4 | 17.5 |
| | C | 17.7 | 12.4 | 13.3 |
| 60 | POE* | 21.0 | 17 | -- |

* reported in Reference 33 for ISO 68 POE
** reported in Reference 31 for a series of ISO 32 to ISO 370 polyolesters

**Figure 40. Comparison of Film Thickness Data for ISO 32 Polyolester at Ambient Temperature as a Function of R-134a Concentration**

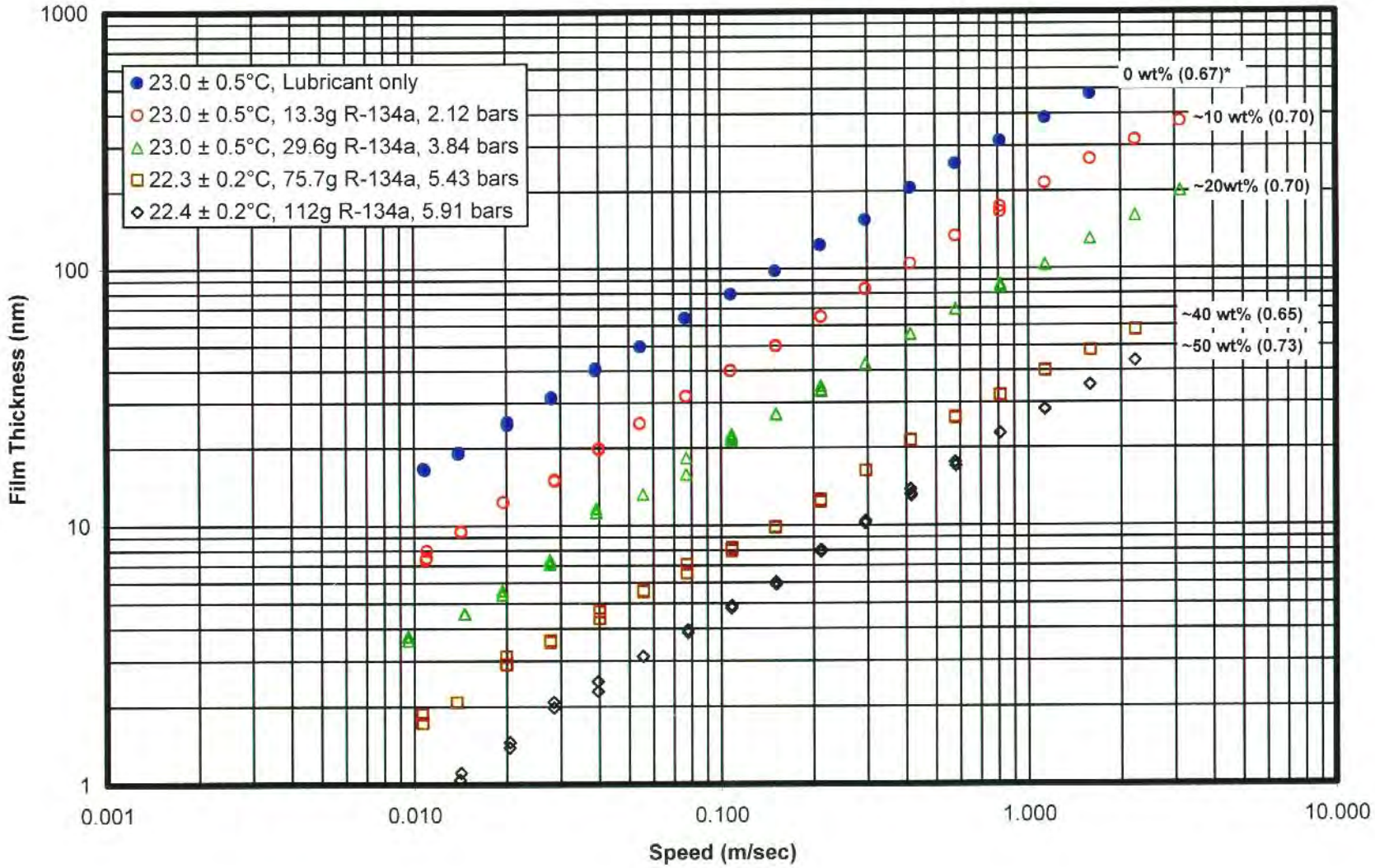


*numbers in parentheses show gradients

**Figure 41. Comparison of Film Thickness Data for ISO 32 Polyolester at 45°C as a Function of R-134a Concentration**

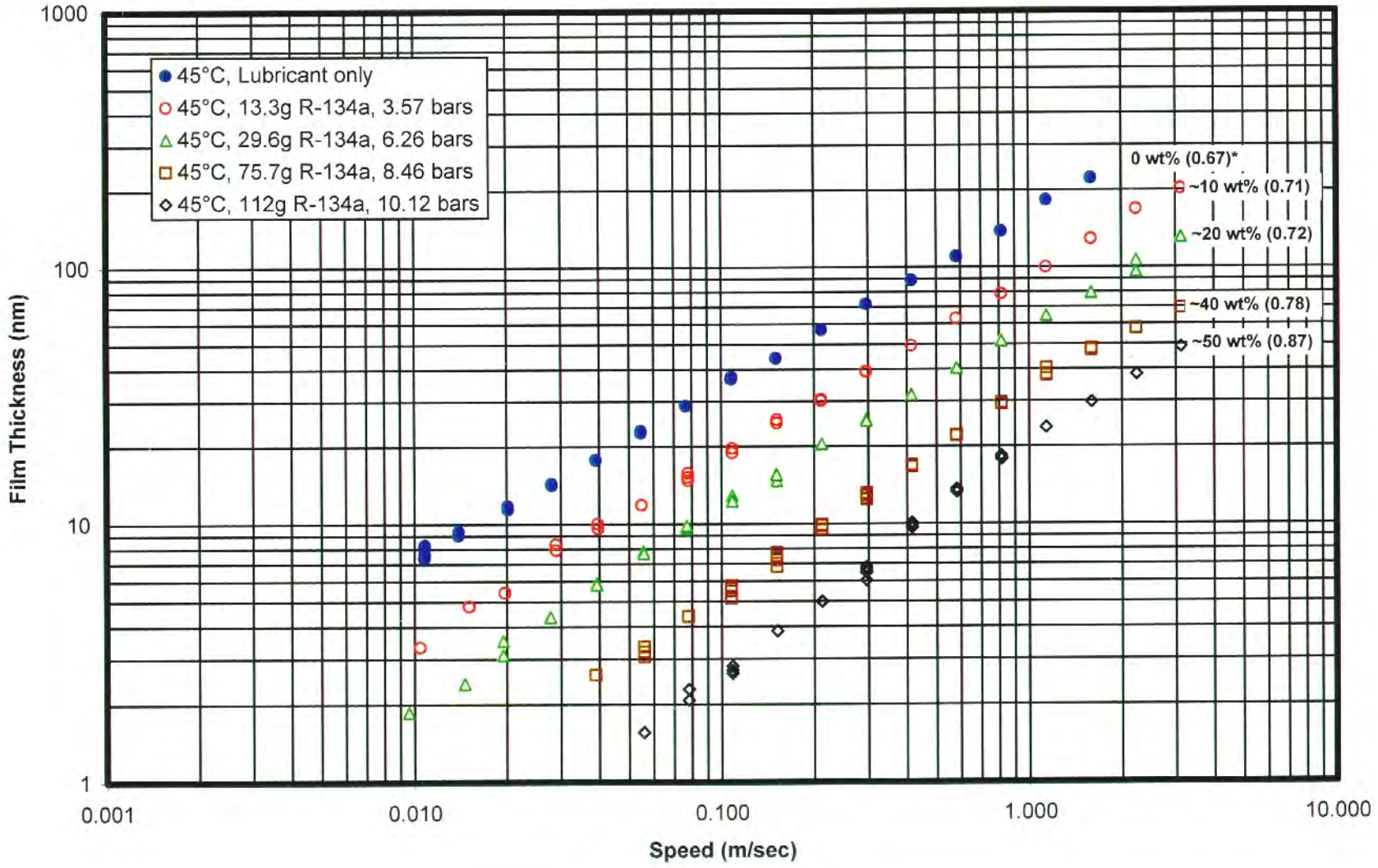


*numbers in parentheses show gradients

**Figure 42. Comparison of Film Thickness Data for ISO 32 Polyolester at 65°C as a Function of R-134a Concentration**

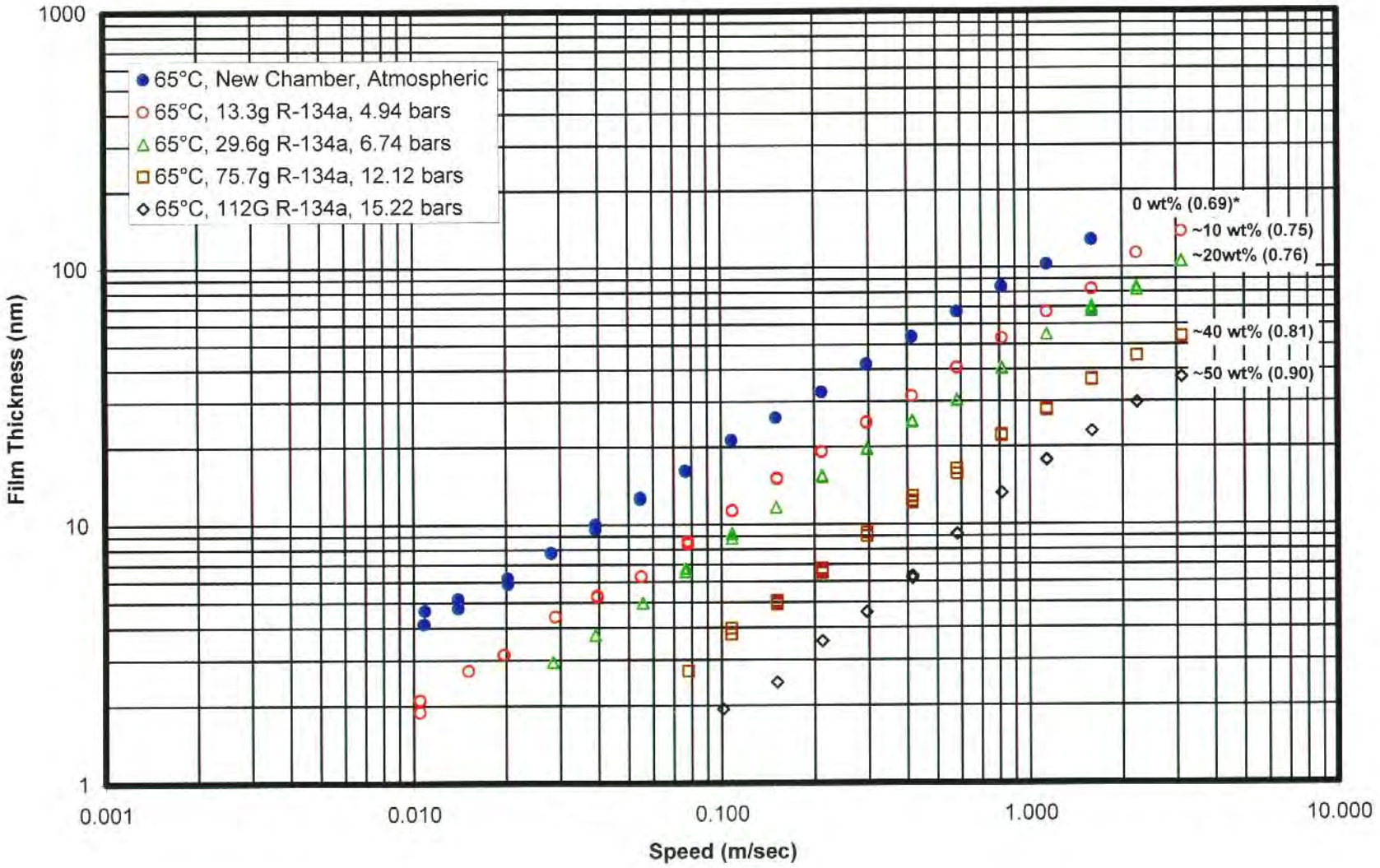


*numbers in parentheses show gradients

**Figure 43. Film Thickness vs. R-134a Concentration for ISO 32 Polyolester**

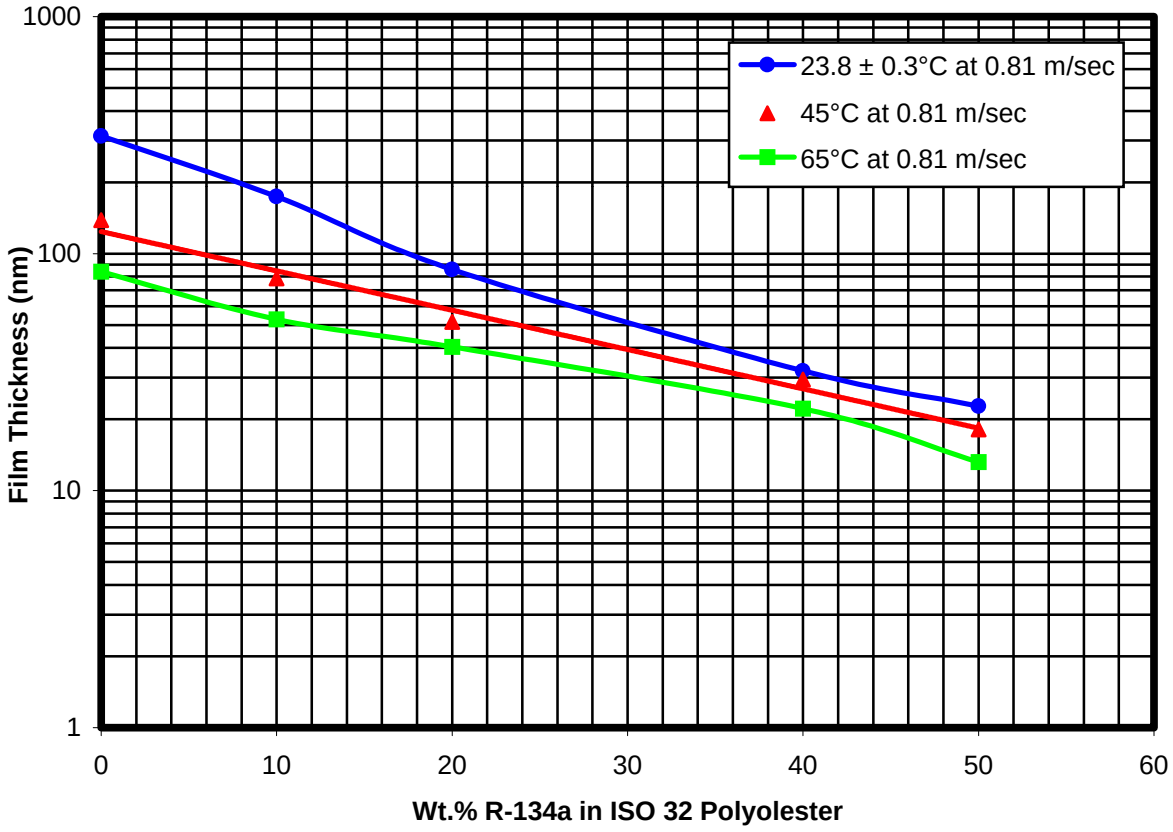

**Figure 44. Comparison of Film Thickness Data for ISO 68 Polyolester A at Ambient Temperature as a Function of R-134a Concentration**

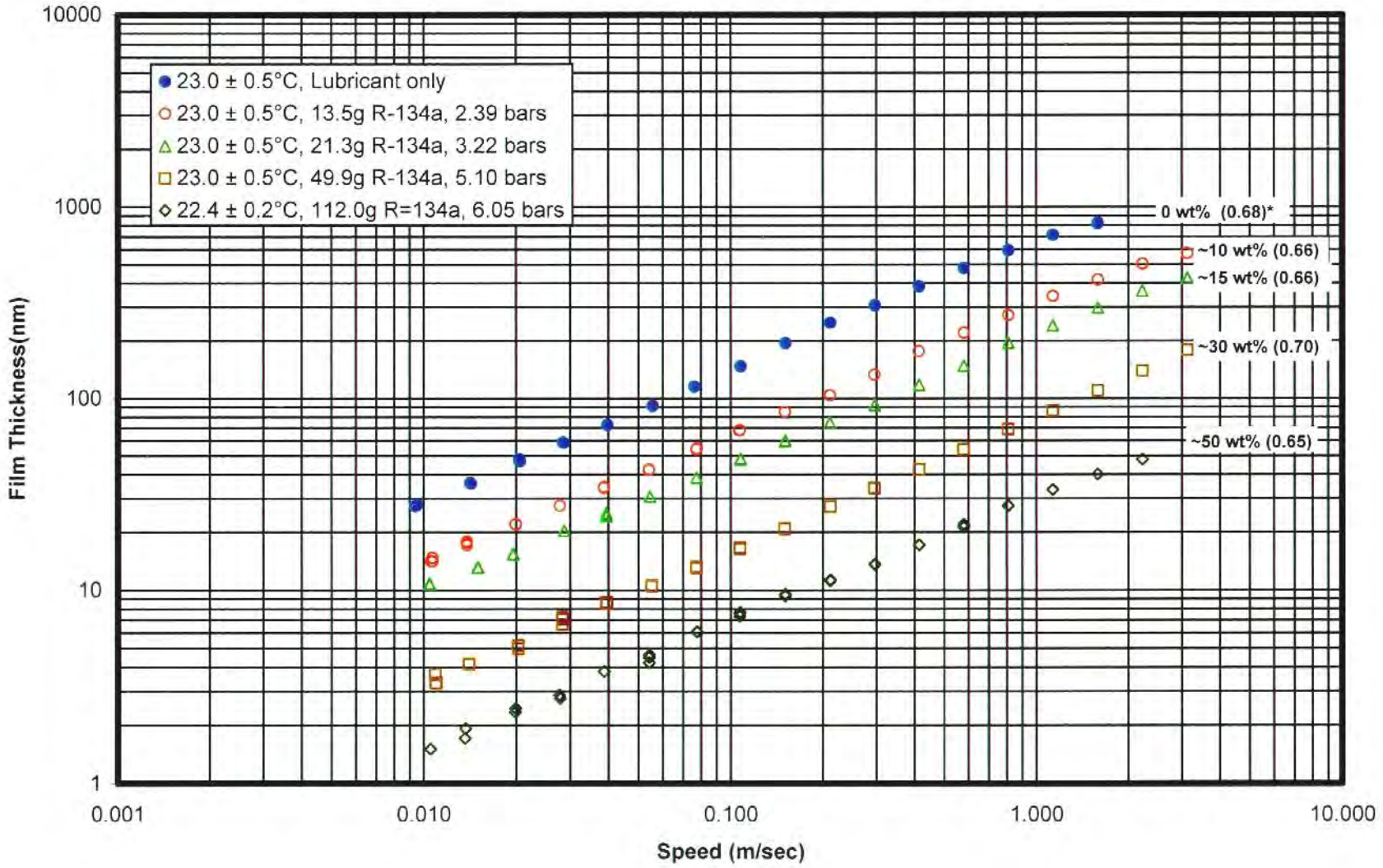


*numbers in parentheses show gradients

**Figure 45. Comparison of Film Thickness Data for ISO 68 Polyolester A at 45°C as a Function of R-134a Concentration**

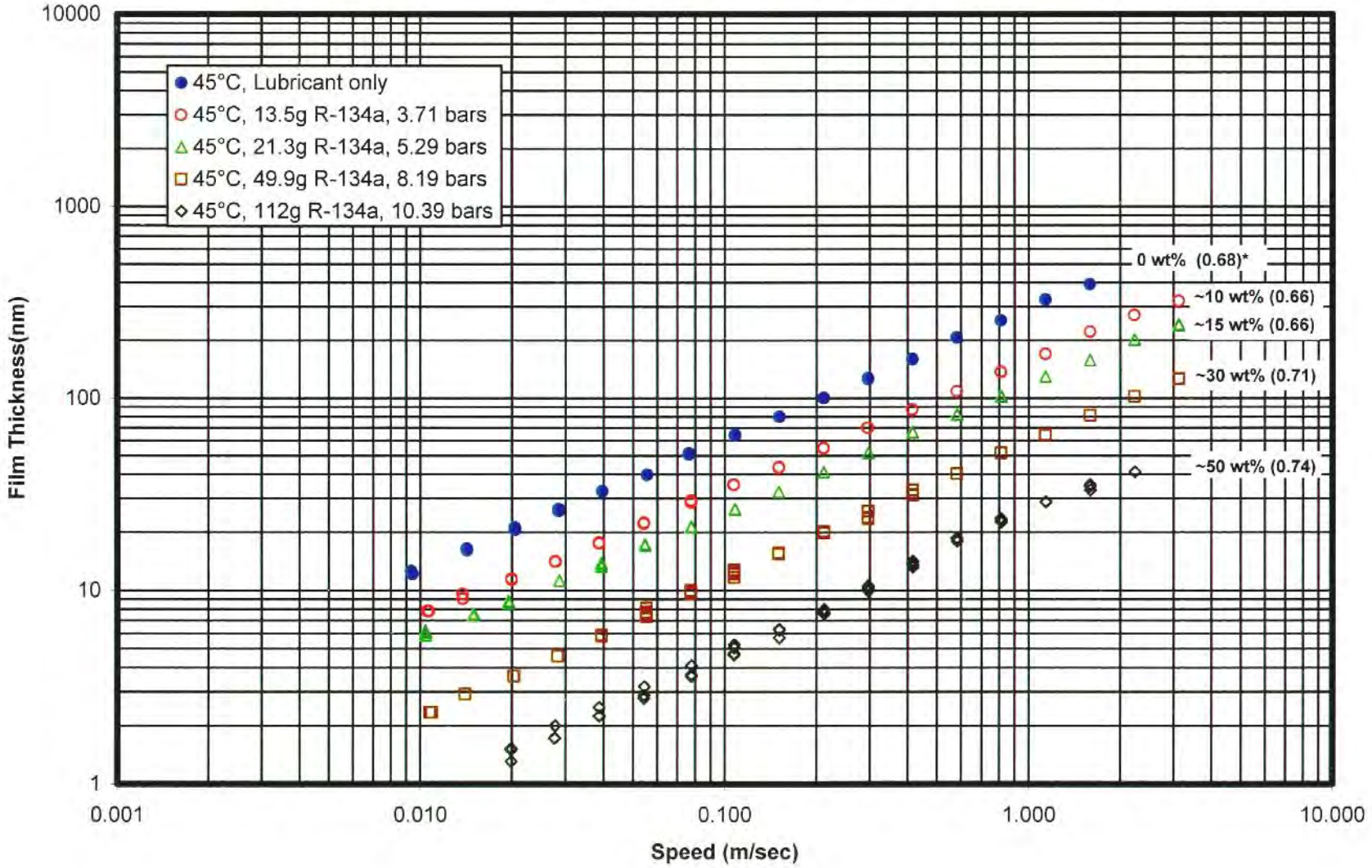


*numbers in parentheses show gradients

**Figure 46. Comparison of Film Thickness Data for ISO 68 Polyolester A at 65°C as a Function of R-134a Concentration**

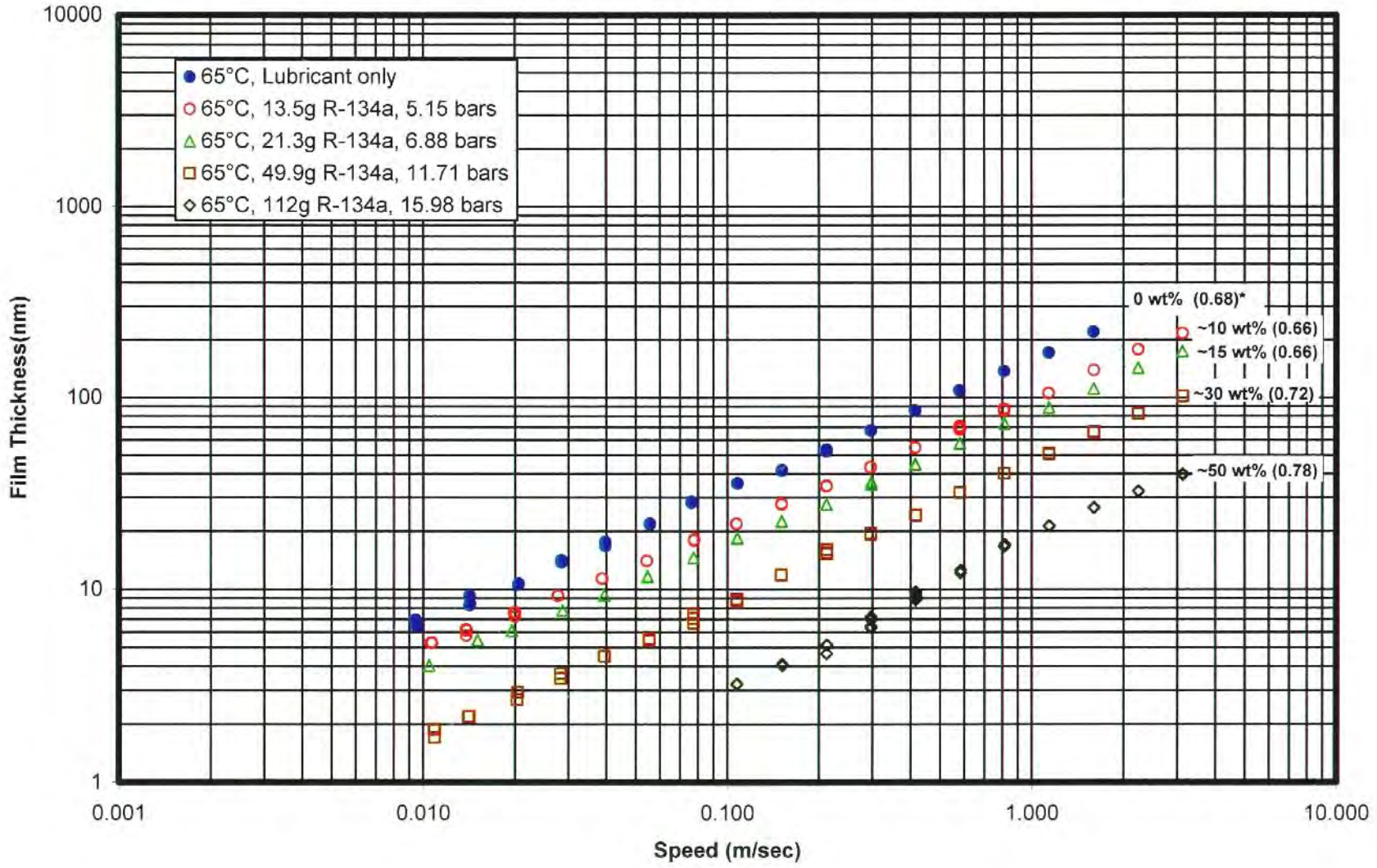


*numbers in parentheses show gradients

**Figure 47. Film Thickness vs. R-134a Concentration for ISO 68 Polyolester A**

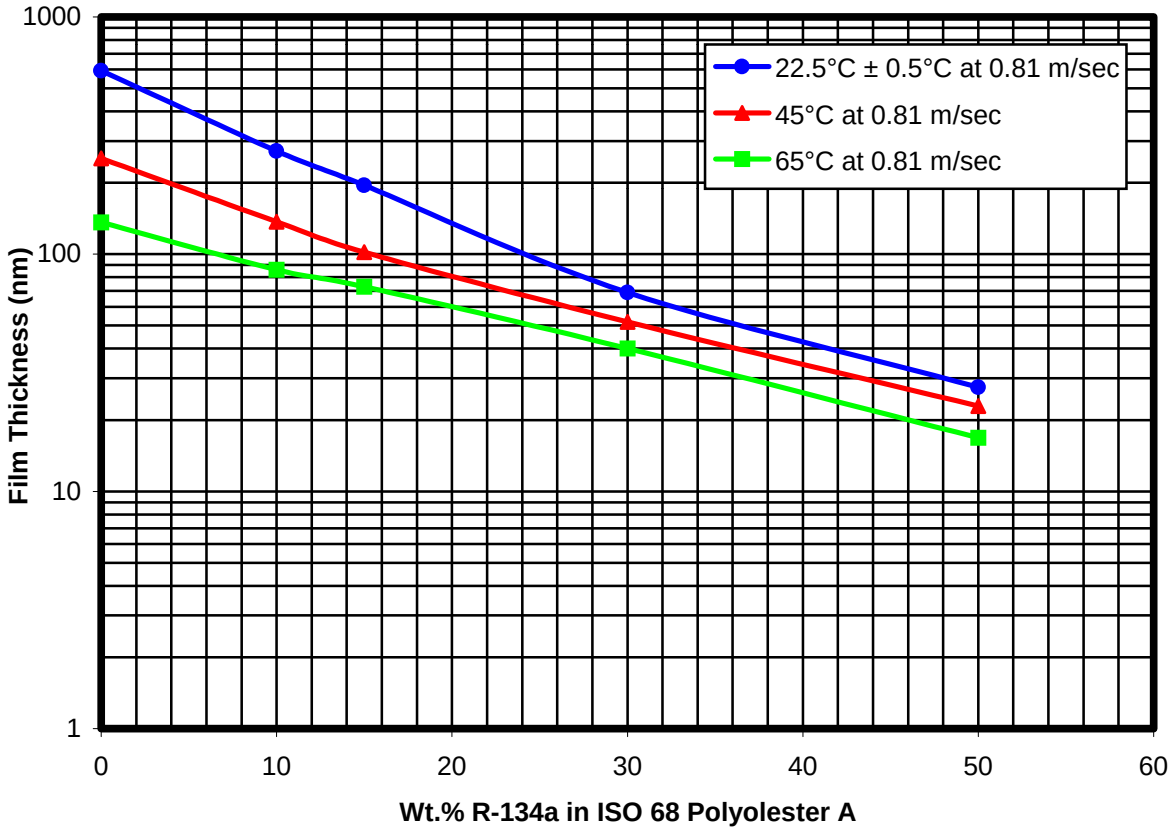

**Figure 48. Comparison of Film Thickness Data for ISO 68 Polyolester B at Ambient Temperature as a Function of R-134a Concentration**

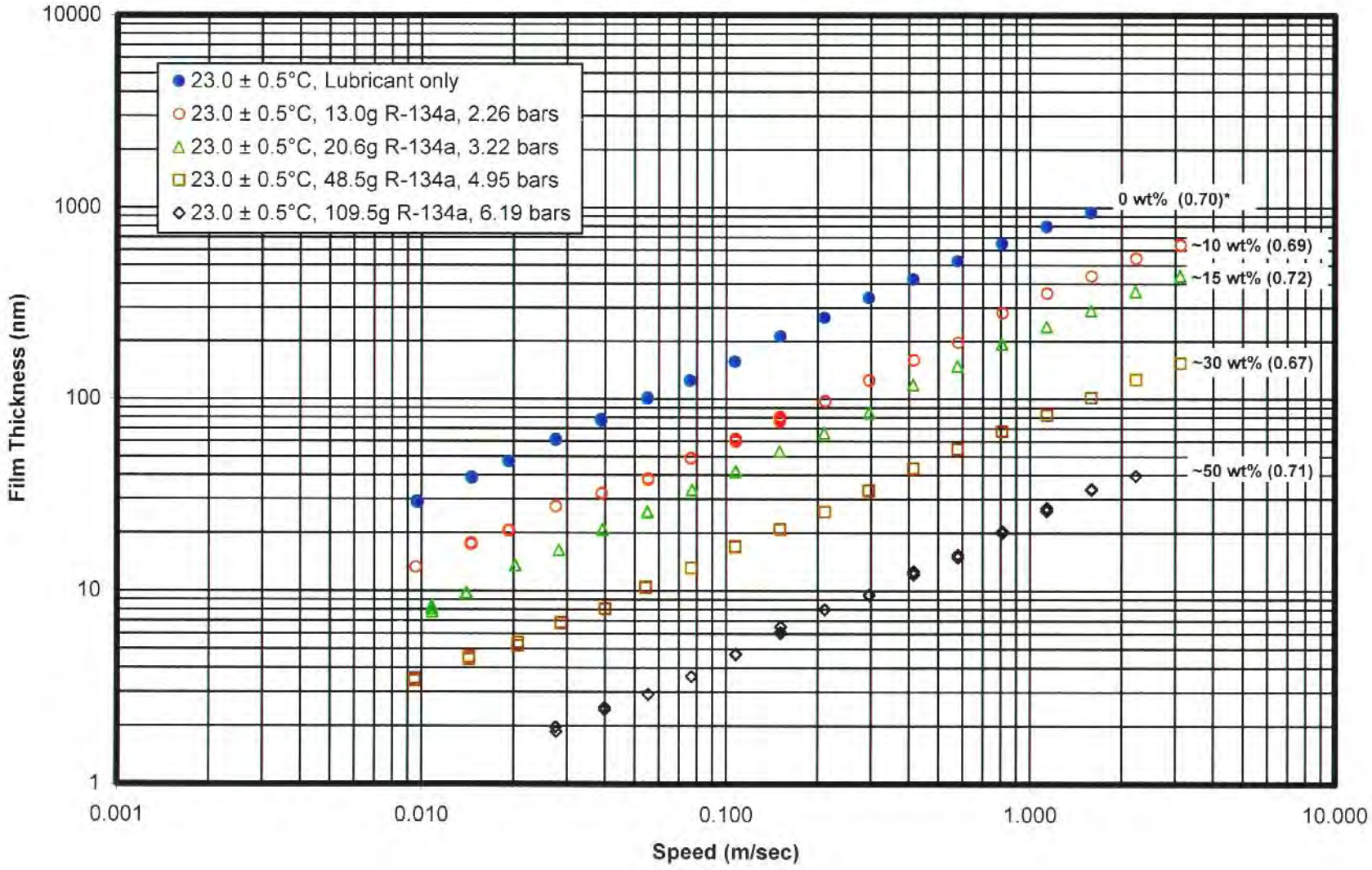


*numbers in parentheses show gradients

**Figure 49. Comparison of Film Thickness Data for ISO 68 Polyolester B at 45°C as a Function of R-134a Concentration**

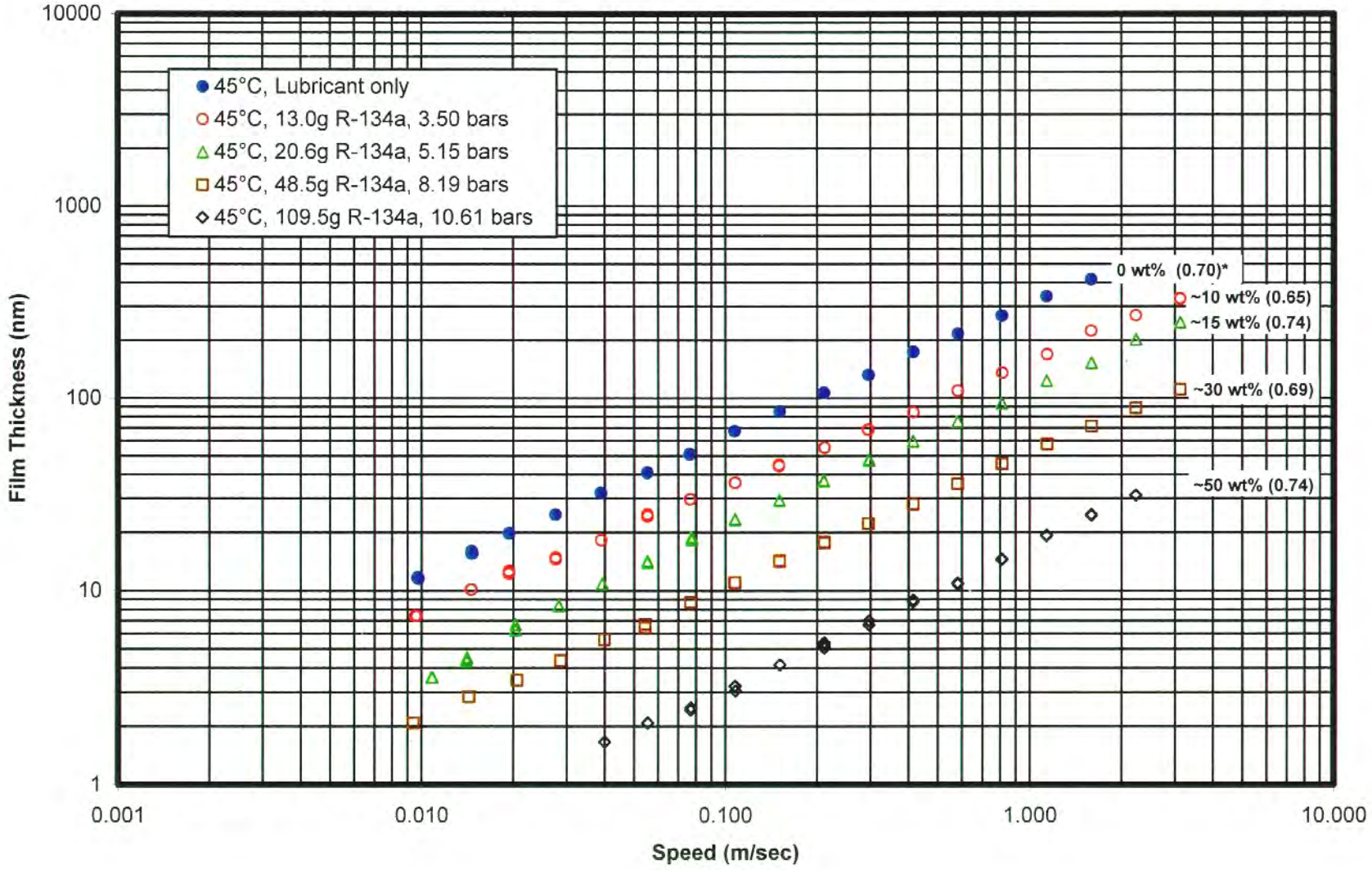


*numbers in parentheses show gradients

**Figure 50. Comparison of Film Thickness Data for ISO 68 Polyolester B at 65°C as a Function of R-134a Concentration**

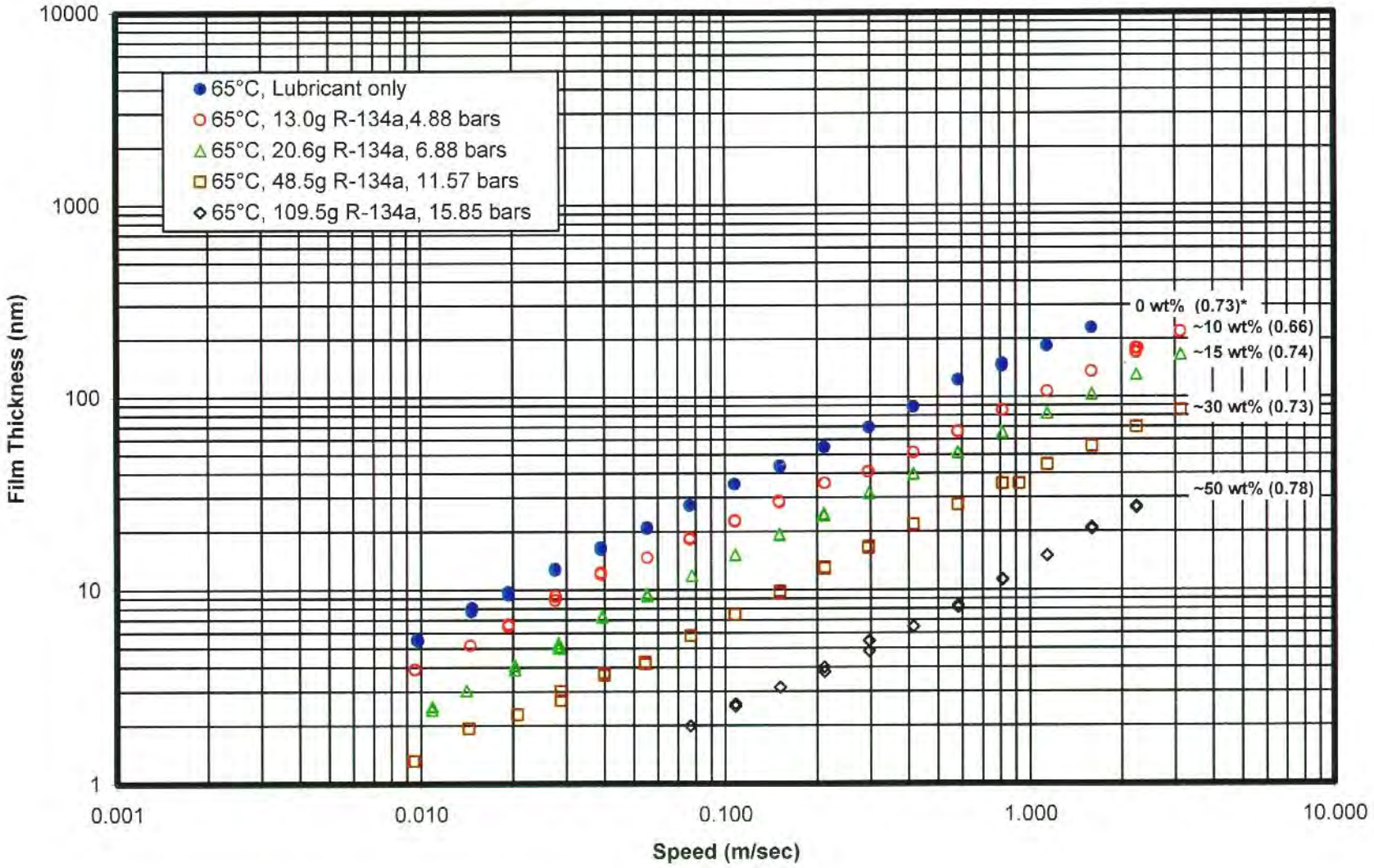


*numbers in parentheses show gradients

**Figure 51. Film Thickness vs. R-134a Concentration for ISO 68 Polyolester B**

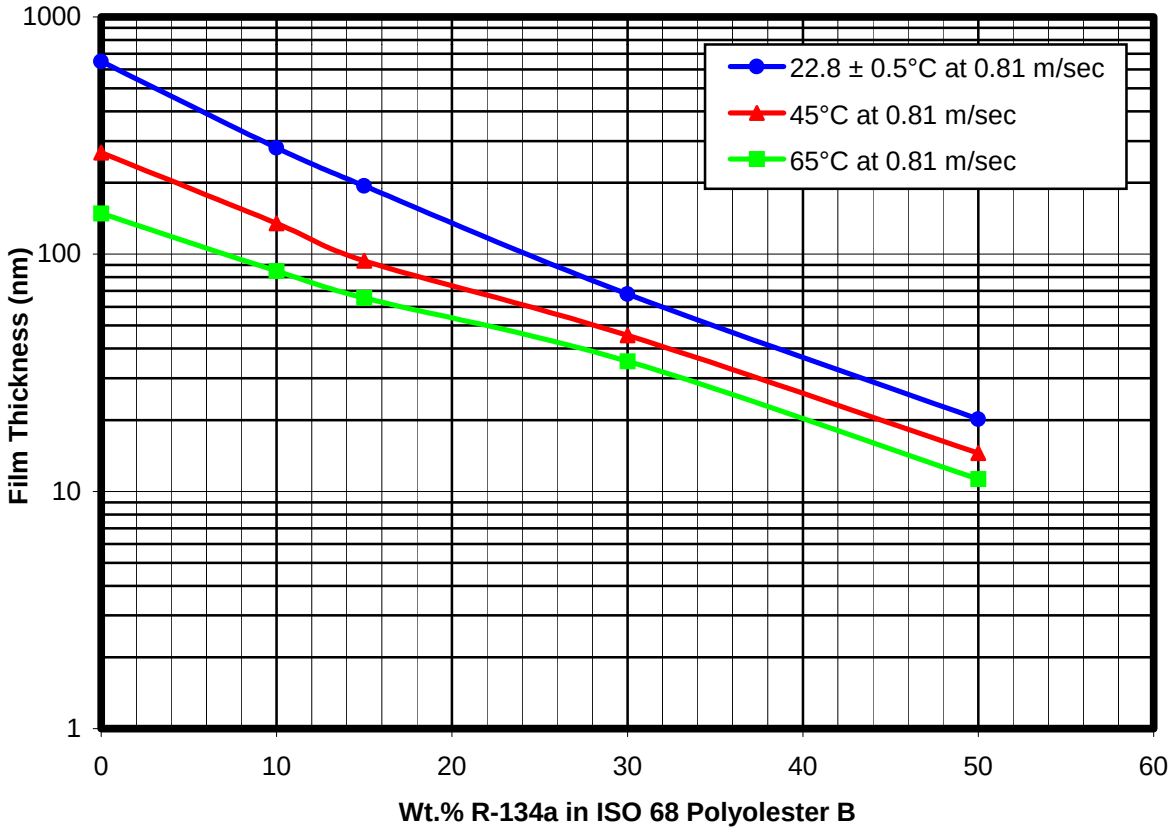

**Figure 52. Comparison of Film Thickness Data for ISO 68 Polyolester C at Ambient Temperature as a Function of R-134a Concentration**

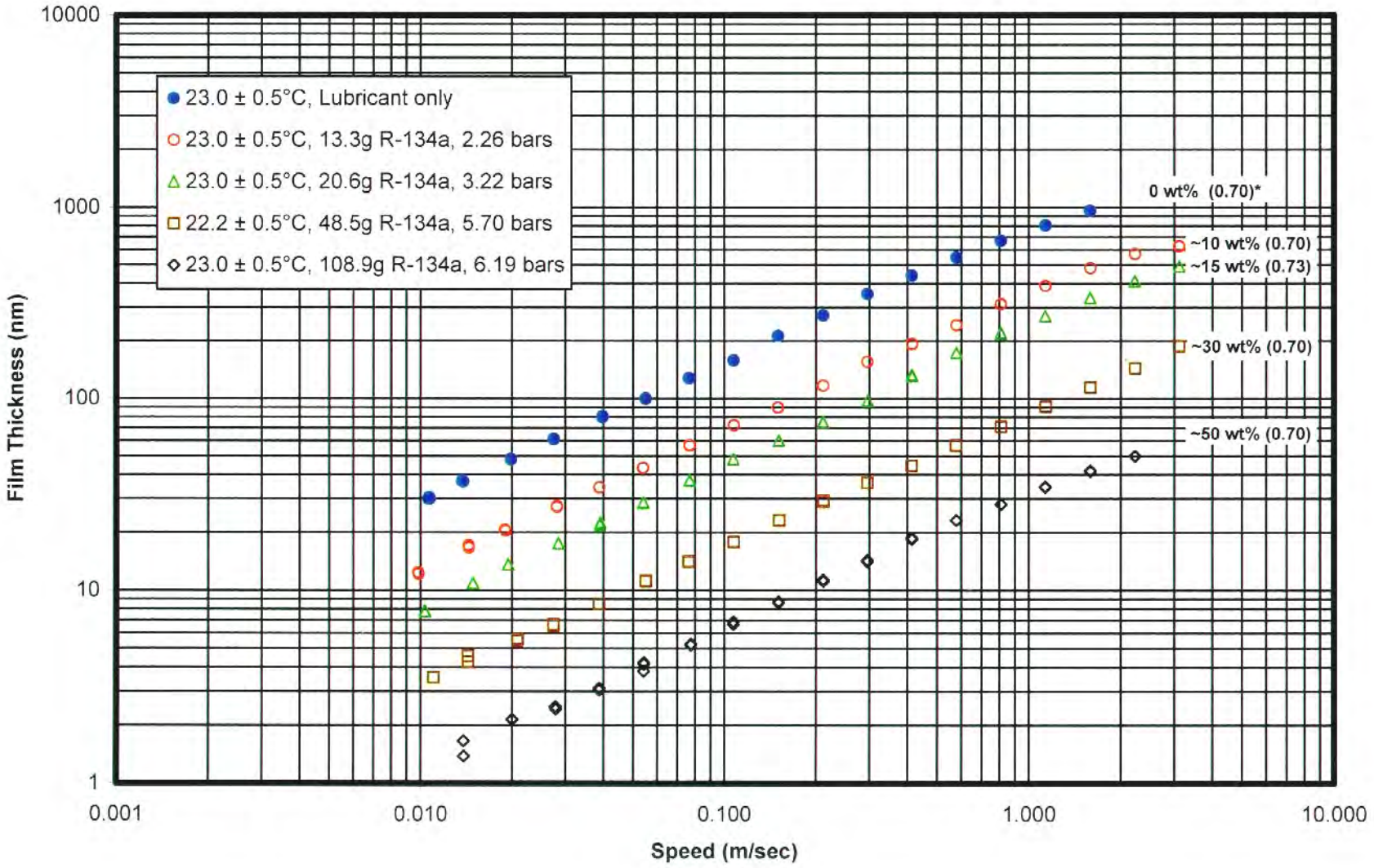


*numbers in parentheses show gradients

**Figure 53. Comparison of Film Thickness Data for ISO 68 Polyolester C at 45°C as a Function of R-134a Concentration**

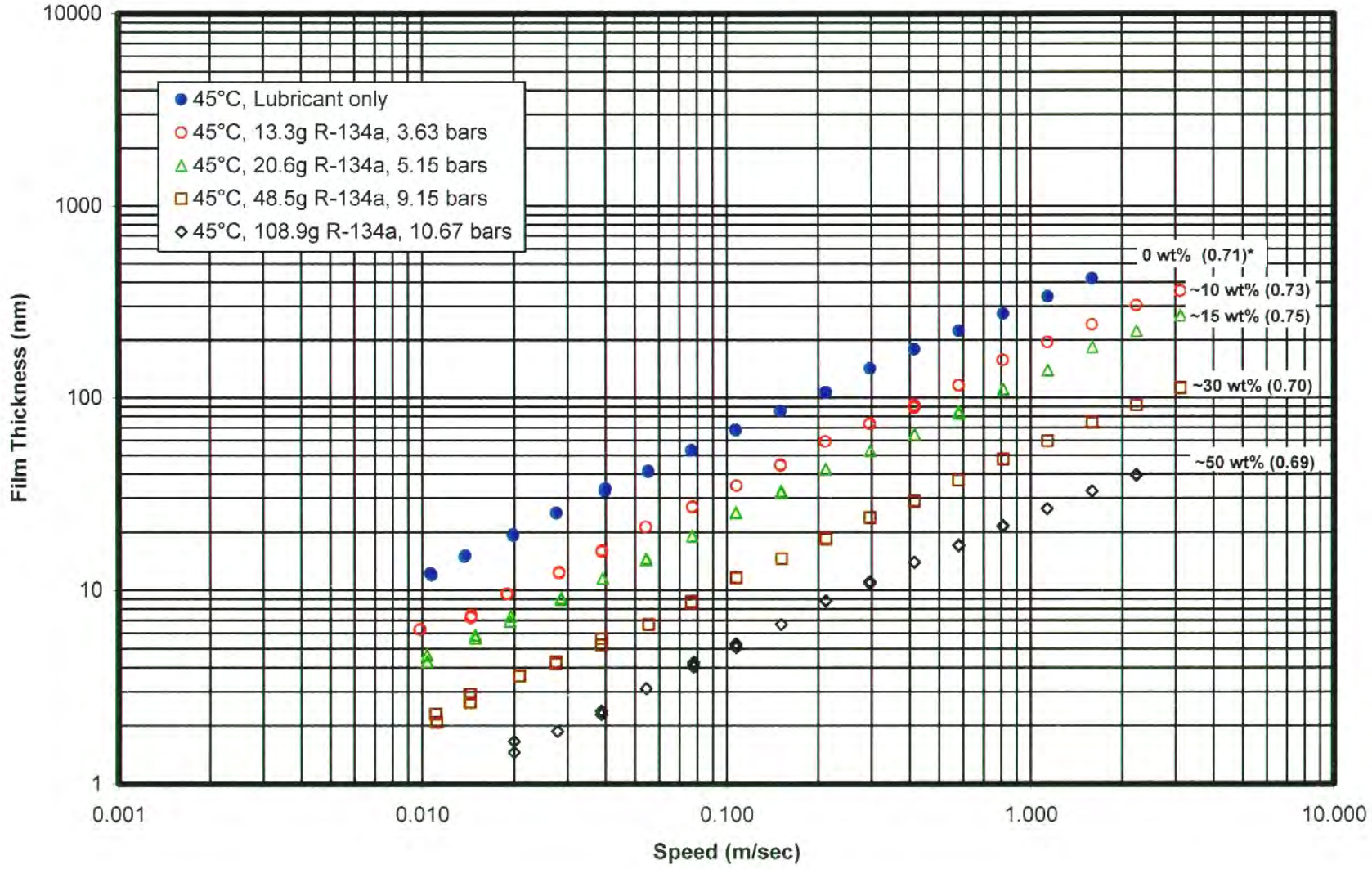


*numbers in parentheses show gradients

**Figure 54. Comparison of Film Thickness Data for ISO 68 Polyolester C at 65°C as a Function of R-134a Concentration**

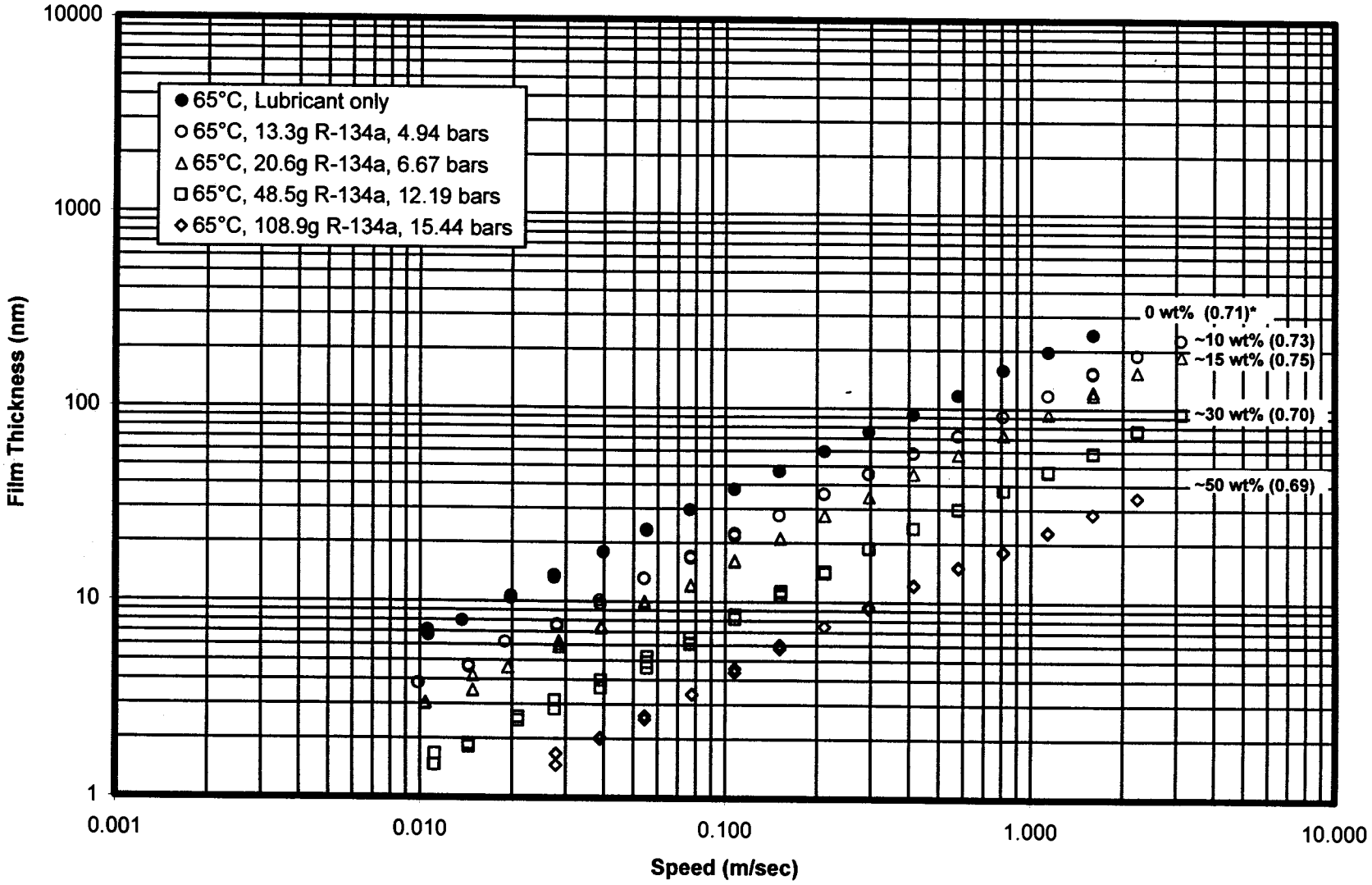


*numbers in parentheses show gradients

**Figure 55. Film Thickness vs. R-134a Concentration for ISO 68 Polyolester C**

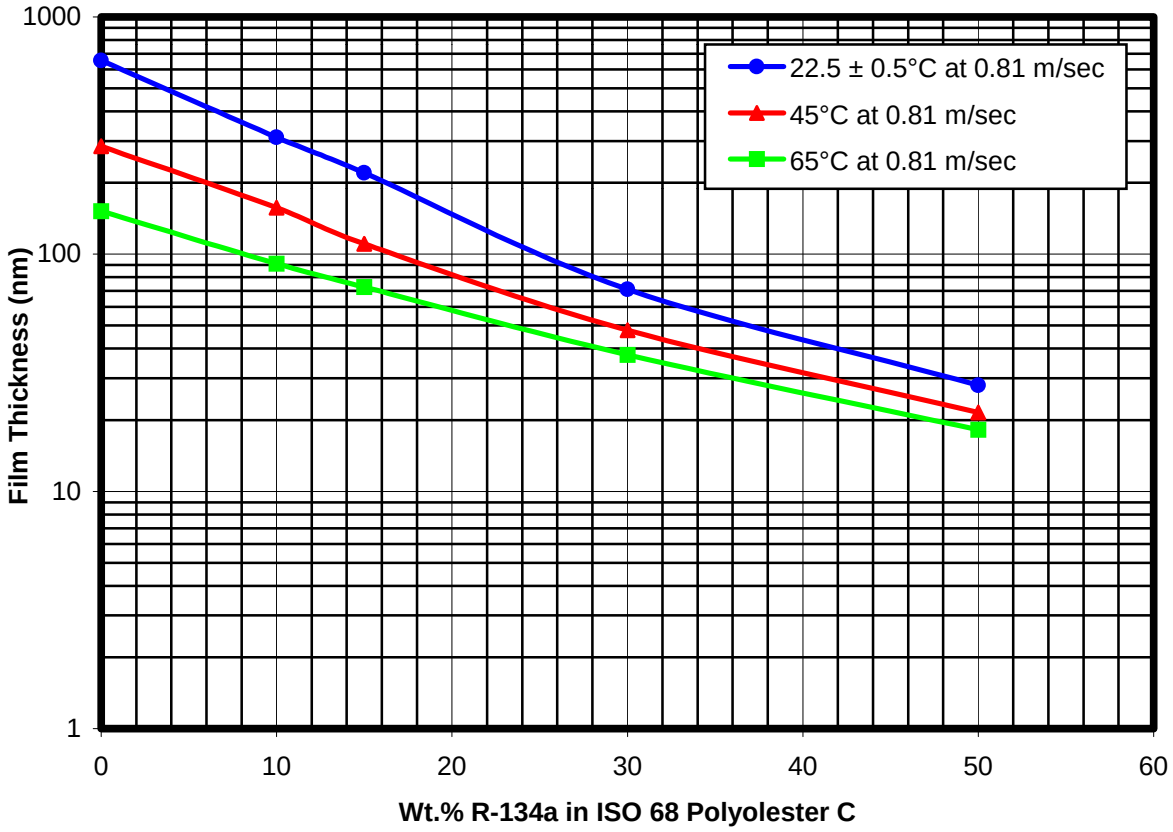

**Figure 56. Comparison of Film Thickness Data for ISO 68 Polyolesters A, B and C at 23°C as a Function of R-134a Concentration**

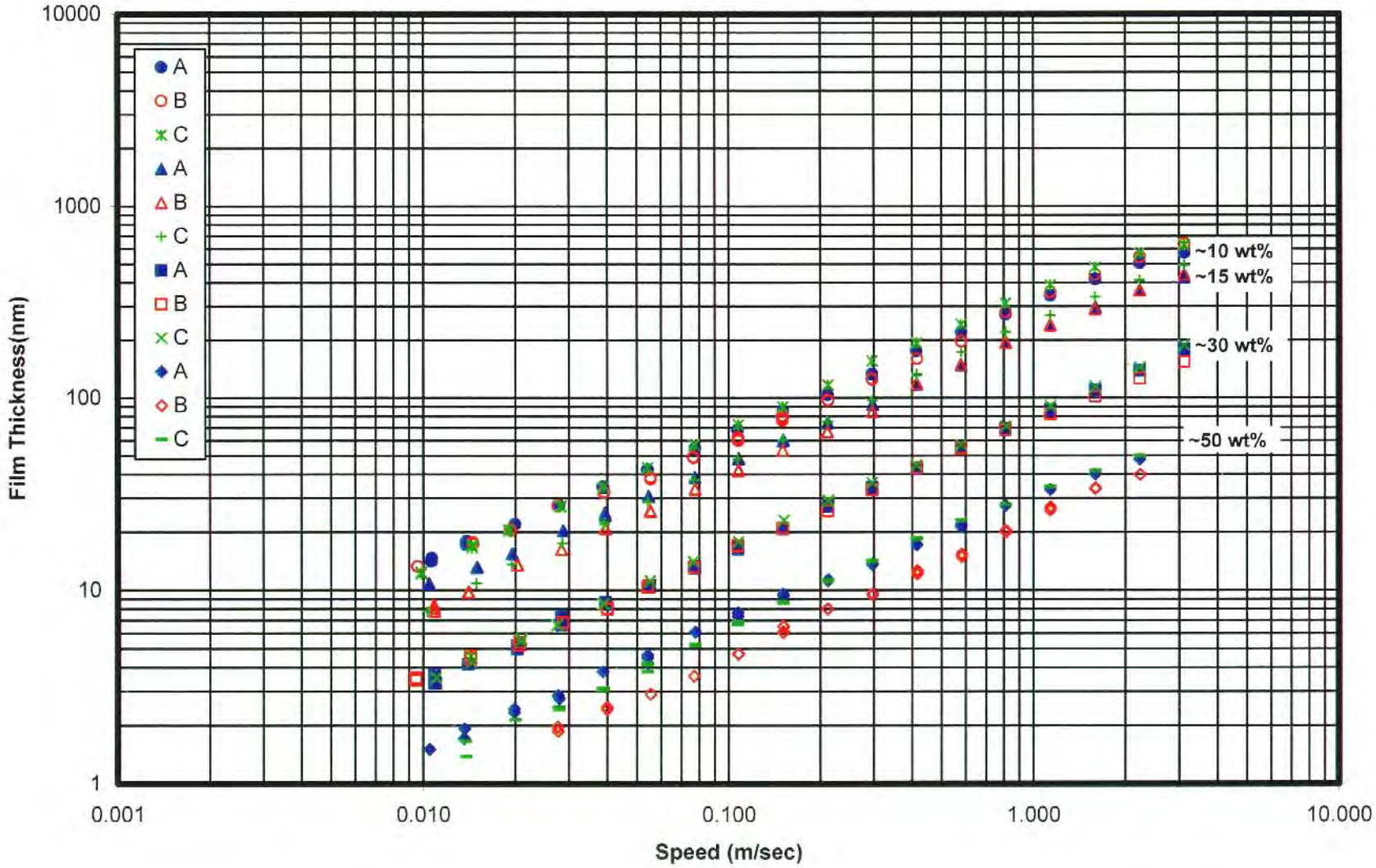

**Figure 57. Comparison of Film Thickness Data for ISO 68 Polyolesters A, B and C at 45°C as a Function of R-134a Concentration**

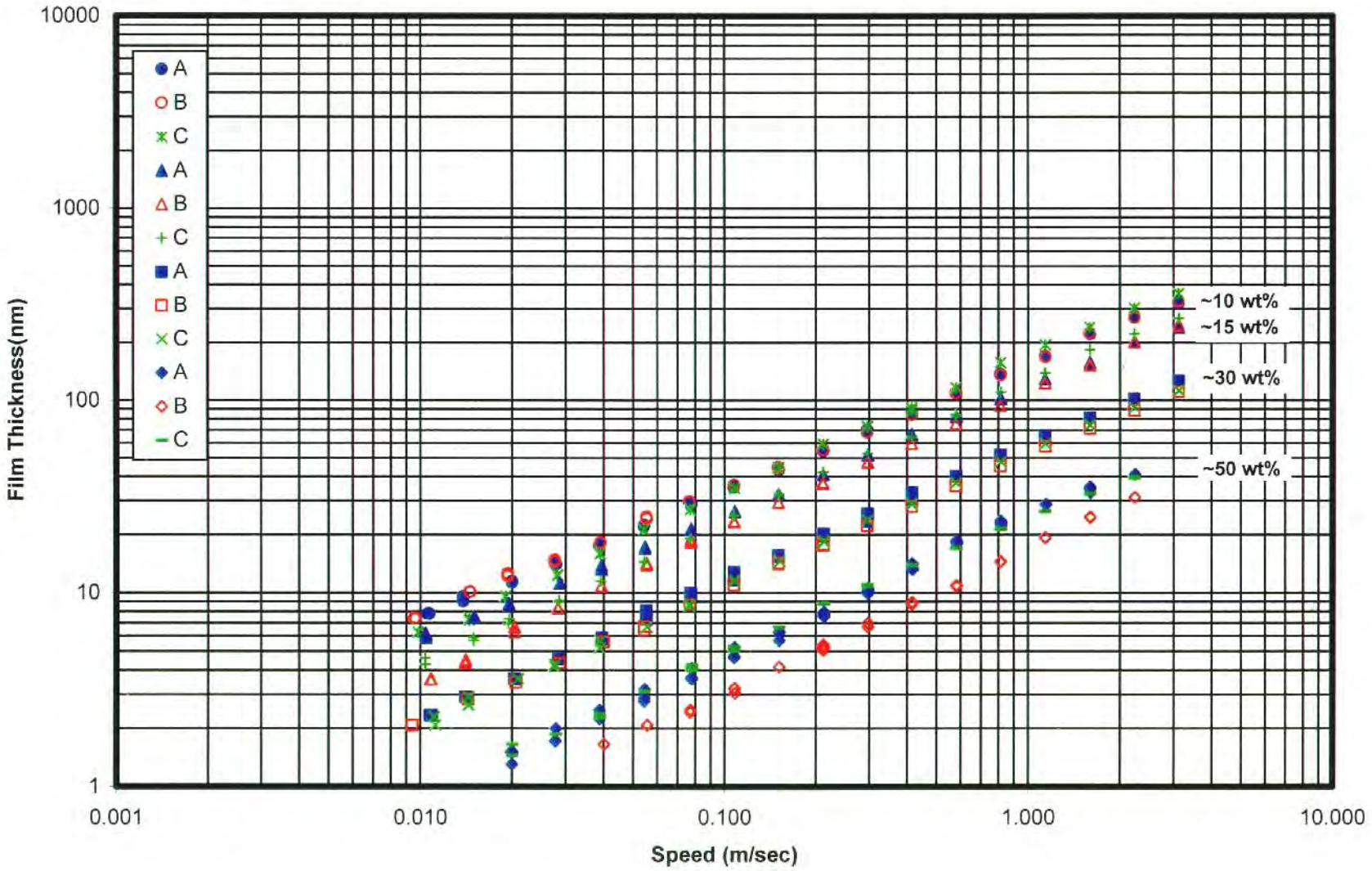

**Figure 58. Comparison of Film Thickness Data for ISO 68 Polyolesters A, B and C at 65°C as a Function of R-134a Concentration**

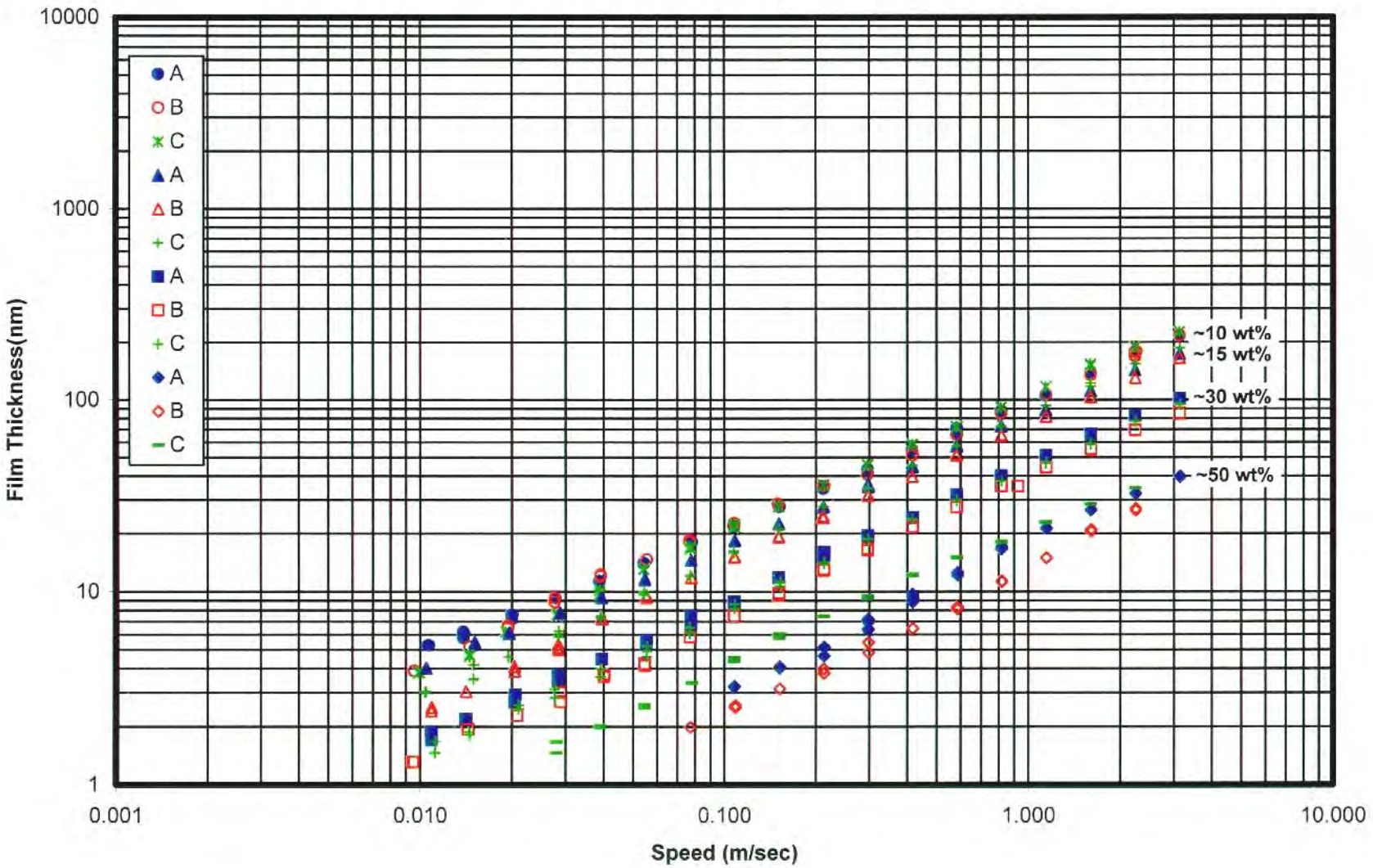

**Figure 59. Effect of Refrigerant Concentration on Effective Pressure-Viscosity Coefficient and Dynamic Viscosity for Mixtures of ISO 32 Polyolester and R-134a**

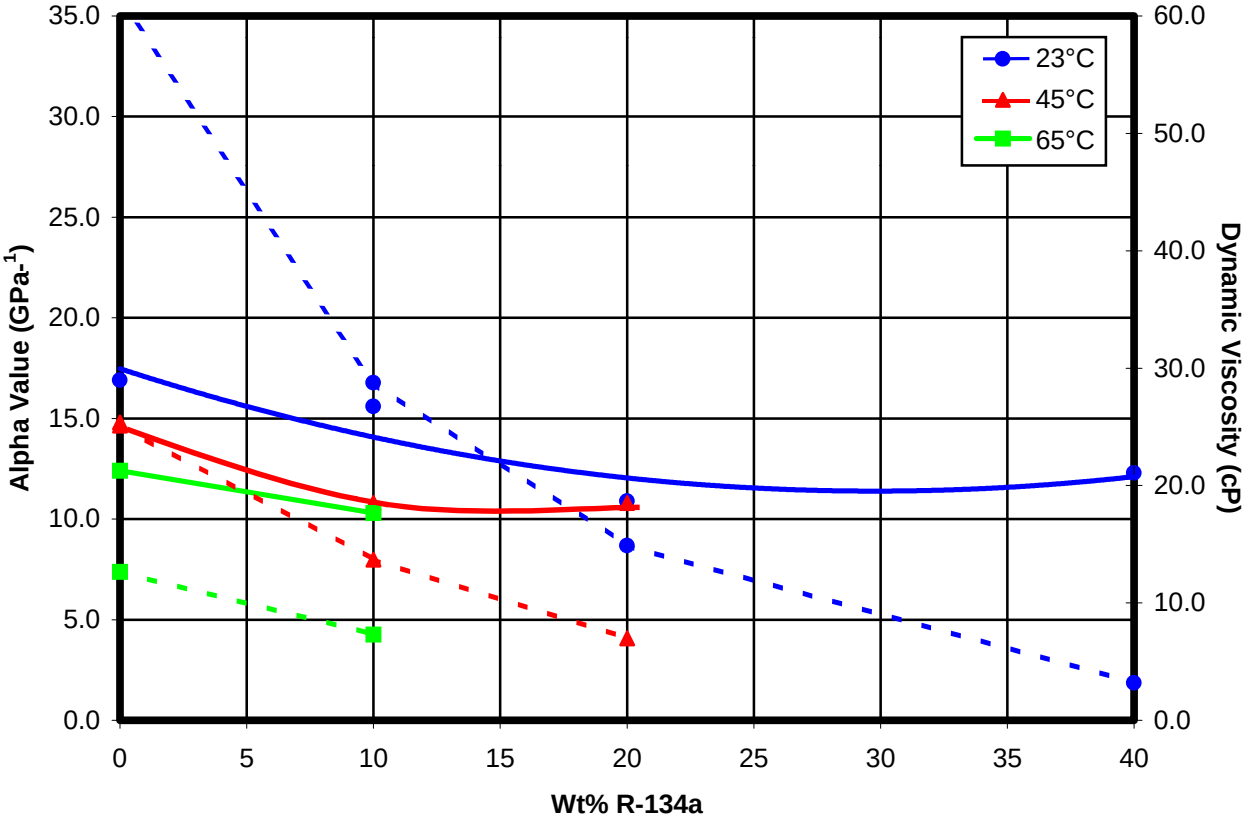


Solid lines represent alpha values
Dashed lines represent dynamic viscosities

**Figure 60. Alpha Value vs. Dynamic Viscosity for ISO 32 Polyolester in R-134a**

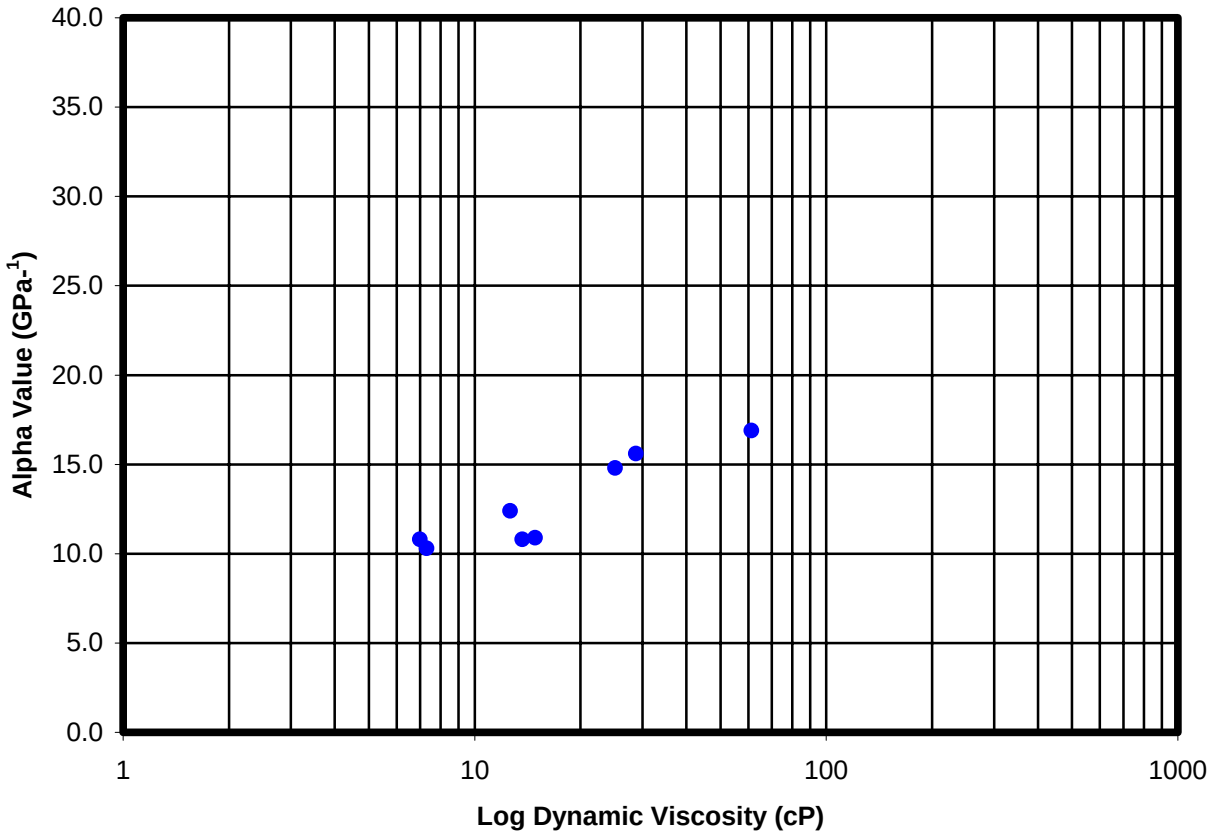

**Figure 61. Effect of Refrigerant Concentration on Effective Pressure-Viscosity Coefficient and Dynamic Viscosity for Mixtures of ISO 68 Polyolester A and R-134a**

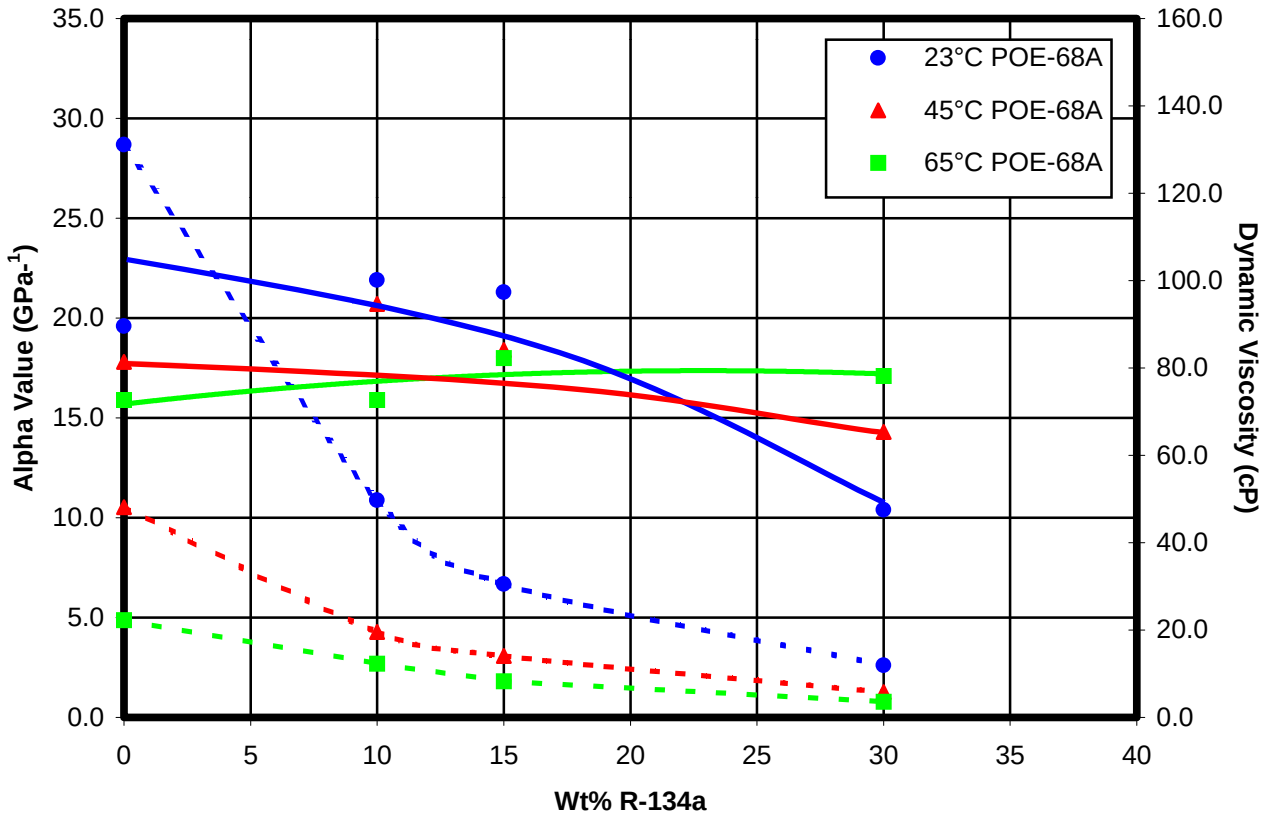


Solid lines represent alpha values
Dashed lines represent dynamic viscosities

**Figure 62. Effect of Refrigerant Concentration on Effective Pressure-Viscosity Coefficient and Dynamic Viscosity for Mixtures of ISO 68 Polyolester B and R-134a**

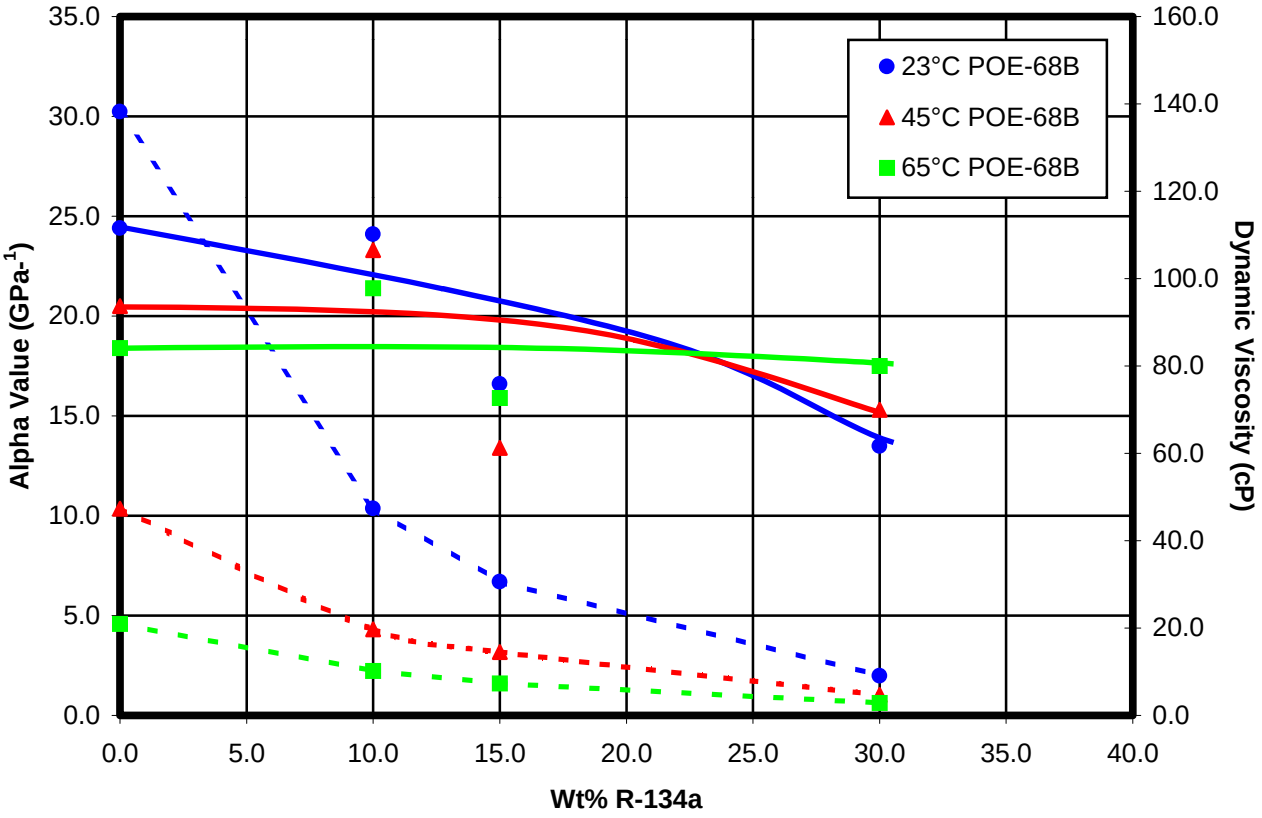


Solid lines represent alpha values
Dashed lines represent dynamic viscosities

**Figure 63. Effect of Refrigerant Concentration on Effective Pressure-Viscosity Coefficient and Dynamic Viscosity for Mixtures of ISO 68 Polyolester C and R-134a**

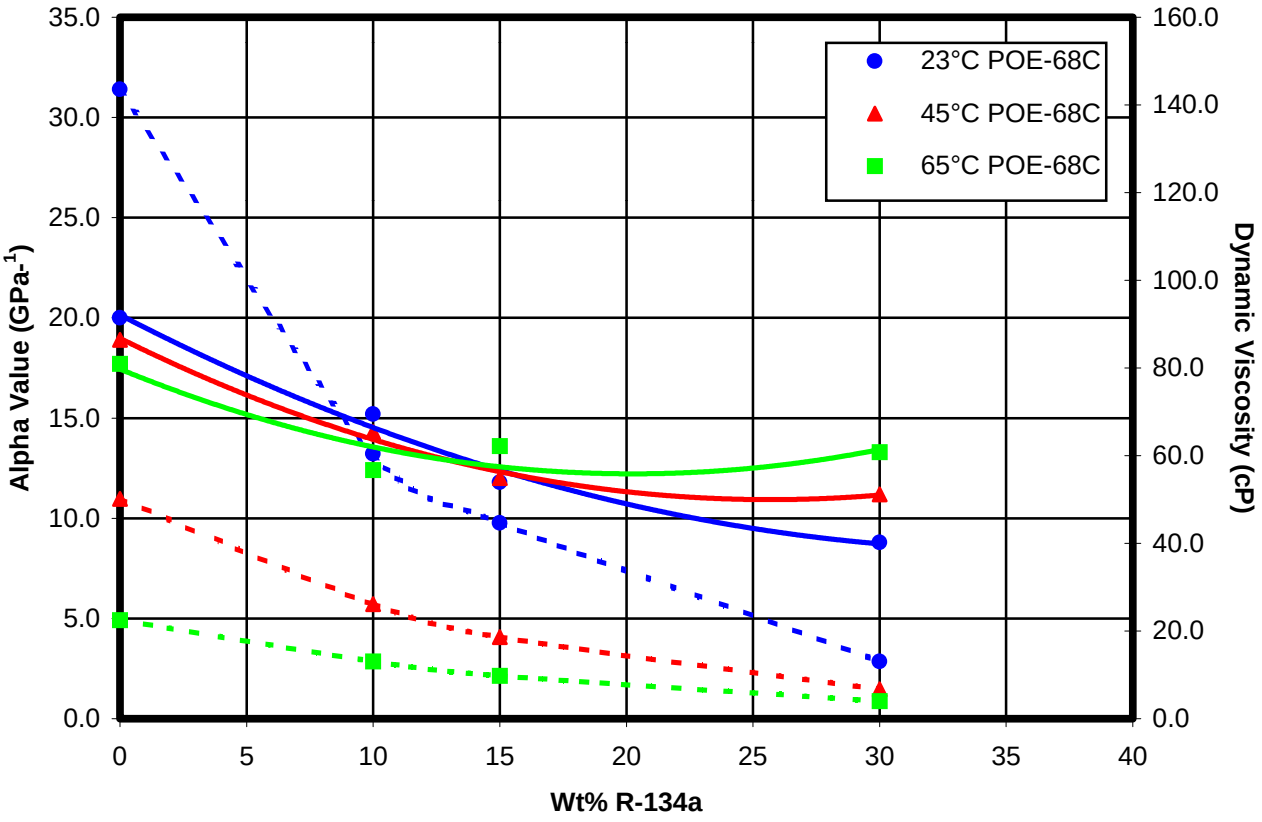


Solid lines represent alpha values
Dashed lines represent dynamic viscosities

**Figure 64. Alpha Value vs. Dynamic Viscosity for ISO 68 Polyolesters A, B and C in R-134a**

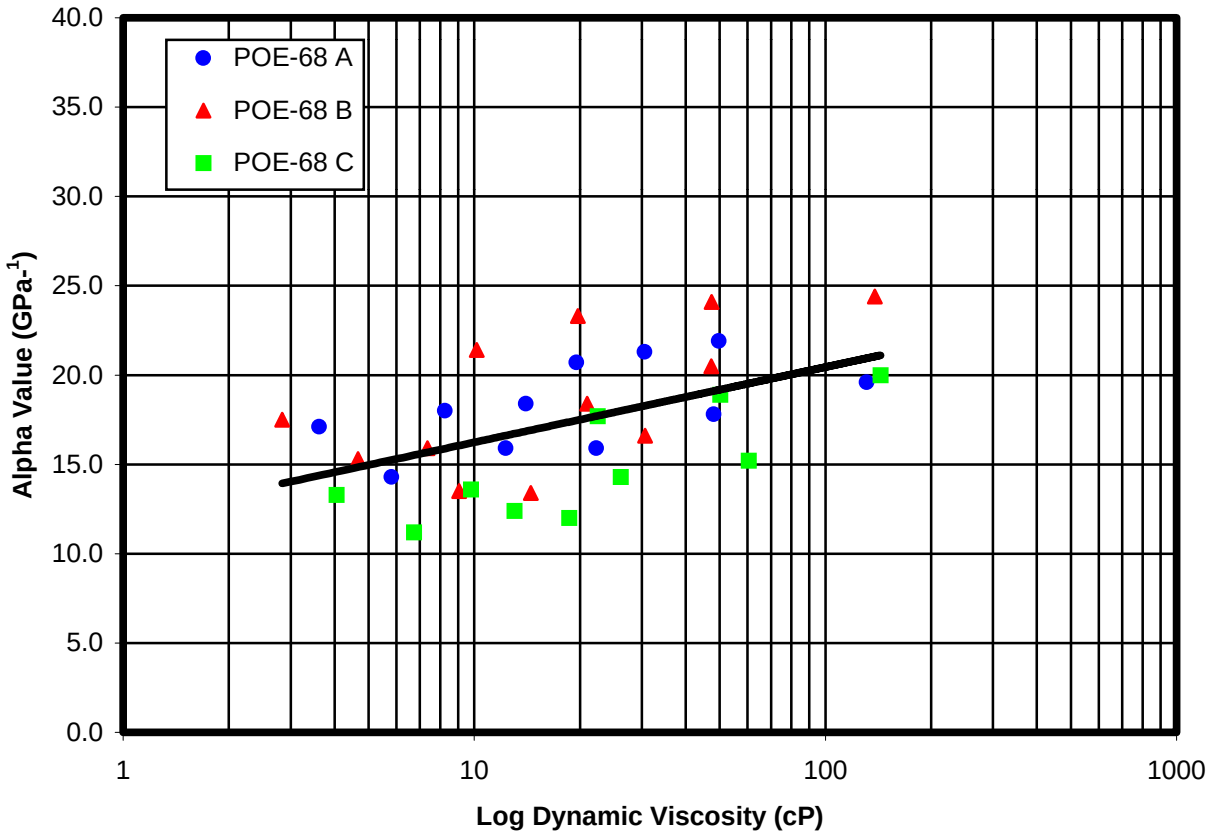

### 6.5 Film Thickness Measurements on Mixtures of Polyvinyl Ethers and R-134a

Film thickness measurements were conducted on mixtures of ISO 32 and ISO 68 polyvinyl ethers as a function of rolling speed, temperature and refrigerant concentration. The results are reported in the following sections.

#### 6.5.1 ISO 32 Polyvinyl Ether/R-134a

Figures 65 through 67 show the film thickness data as a function of rolling speed and refrigerant concentration for mixtures of ISO 32 polyvinyl ether (PVE) and R-134a at 23 °C, 45 °C and 65 °C, respectively. The gradients of the plots, in general, agree with the EHD theoretical slope. However, deviations are observed at the higher refrigerant concentrations and temperatures. The R-134a concentrations studied included 0, 10, 20 and 40% by weight. Similar to the trends observed with the polyolesters, Section 6.4, film thickness decreases significantly in the contact as the refrigerant concentration and temperature increase.

Figure 68 compares the reduction in film thickness with increasing refrigerant concentration as a function of temperature at a constant speed of 0.81 m/s. At each temperature, the film thickness decreases with increasing refrigerant concentration. Table 19 compares the percent reduction in film thickness as a function of refrigerant concentration and temperature. At a constant refrigerant concentration, the reduction in film thickness becomes smaller as the temperature increases.

**Table 19. Percent Reduction in Film Thickness for Mixtures of ISO 32 Polyvinyl Ether and R-134a at a constant rolling speed of 0.8 m/s**

| Refrigerant Concentration, wt % | Temperature, °C | % Reduction in Film Thickness |
|---|---|---|
| 10 | 23 | 43 |
| | 45 | 45 |
| | 65 | 31 |
| 20 | 23 | 71 |
| | 45 | 64 |
| | 65 | 48 |
| 40 | 23 | 90 |
| | 45 | 80 |
| | 65 | 73 |

### 6.5.2 ISO 68 Polyvinyl Ether/R-134a

Figures 69 through 71 show the film thickness data as a function of rolling speed and refrigerant concentration for mixtures of ISO 68 polyvinyl ether (PVE) and R-134a at 23 °C, 45 °C and 65 °C, respectively. The gradients of the plots vary from 0.67 to 0.74 and agree with the EHD theoretical slope. The R-134a concentrations studied include 0, 10, 15, 30 and 50% by weight. The data shows similar trends to those observed with the lower viscosity (ISO 32) PVE reported above, i.e. film thickness decreases as the refrigerant concentration in the lubricant increases.

Figure 72 compares the reduction in film thickness with increasing refrigerant concentration at a constant speed of 0.81 m/s at the three test temperatures. Percent reduction in film thickness is given in Table 20.

### 6.5.3 Effect of Refrigerant Concentration (R-134a) on Effective Pressure-Viscosity Coefficients of Polyvinyl Ethers

Effective pressure-viscosity coefficients of the PVE and R-134a mixtures were calculated as described in Section 3.4. It was assumed that the mixtures obey the theoretical relationship of Hamrock and Dowson.

Dynamic viscosity data for mixtures of ISO 32 PVE and R-134a, given in Table 21, were obtained from Reference 77. The effective $\alpha$-values calculated for these mixtures are given in

Table 22 as a function of refrigerant concentration and temperature. In general, the α-value and dynamic viscosity decrease with increasing refrigerant concentration and temperature as shown in Figure 73. Figure 74 shows the increase in α-values as a function of log (dynamic viscosity).

Effective pressure-viscosity coefficients were also calculated for the mixtures of ISO 68 PVE and R-134a. Dynamic viscosity data obtained from Reference 77 is given in Table 23. The α-values and dynamic viscosity as a function of refrigerant concentration and temperature are given in Table 24 and Figure 75. The α-values reported for 30% refrigerant concentration at high temperatures (45 and 65 °C) show some anomalies, i.e. they increase with increasing temperature. This was also observed for mixtures of R-134a and polyolesters. Possible reasons for this finding were discussed in Section 6.4.3.

Figure 76 shows the increase in α-values as a function of log (dynamic viscosity).

**Table 20. Percent Reduction in Film Thickness for Mixtures of ISO 68 Polyvinyl Ether and R-134a at a constant rolling speed of 0.8 m/s**

| Refrigerant Concentration, wt % | Temperature, °C | % Reduction in Film Thickness |
|---|---|---|
| 10 | 23 | 54 |
| | 45 | 41 |
| | 65 | 39 |
| 15 | 23 | 69 |
| | 45 | 61 |
| | 65 | 48 |
| 30 | 23 | 90 |
| | 45 | 83 |
| | 65 | 72 |
| 50 | 23 | 96 |
| | 45 | 91 |
| | 65 | 86 |

**Table 21. Dynamic Viscosity Data for Mixtures of ISO 32 Polyvinyl Ether and R-134a**

| Temperature, °C | Dynamic Viscosity, cP R-134a Concentration, wt % | | | |
|---|---|---|---|---|
| | 0% | 10% | 20% | 40% |
| 23 | 60.21 | 25.5 | 12.8 | 3.6 |
| 45 | 22.53 | 11.0 | 6.5 | 2.4 |
| 65 | 10.75 | 6.2 | 3.8 | 1.8 |

**Table 22. Effective Pressure-Viscosity Coefficient for Mixtures of ISO 32 Polyvinyl Ether and R-134a**

| Temperature, °C | Refrigerant Concentration, wt % | | | |
|---|---|---|---|---|
| | 0% | 10% | 20% | 40% |
| | $\alpha$-values, $GPa^{-1}$ | | | |
| 23 | 25.5 | 23.1 | 19.7 | 13.1 |
| 45 | 21.3 | 16.8 | 14.7 | 15.6 |
| 65 | 17.0 | 13.3 | 13.5 | 13.7 |

**Table 23. Dynamic Viscosity Data for Mixtures of ISO 68 Polyvinyl Ether and R-134a**

| Temperature, °C | Dynamic Viscosity, cP | | | | |
|---|---|---|---|---|---|
| | R-134a Concentration, wt % | | | | |
| | 0% | 10% | 15% | 30% | 50% |
| 23 | 161.32 | 77.22 | 45.00 | 15.00 | 3.65 |
| 45 | 51.59 | 25.39 | 17.50 | 7.50 | N/A |
| 65 | 21.83 | 11.60 | 9.30 | 4.50 | N/A |

**Table 24. Effective Pressure-Viscosity Coefficients for Mixtures of ISO 68 Polyvinyl Ether and R-134a**

| Temp., °C | Refrigerant Concentration, wt % | | | | |
|---|---|---|---|---|---|
| | 0% | 10% | 15% | 30% | 50% |
| | $\alpha$-values, $GPa^{-1}$ | | | | |
| 23 | 28.5 | 21.9 | 19.9 | 11.4 | 8.2 |
| 45 | 22.2 | 20.9 | 16.2 | 18.8 (?) | -- |
| 65 | 18.5 | 16.4 | 14.3 | 24.2 (?) | -- |

### 6.6 Film Thickness Measurements on Mixtures of Polyolesters and R-410A

Film thickness measurements were conducted on mixtures of R-410A and polyolesters, POE-32 and POE-68A, as a function of rolling speed, temperature and refrigerant concentration. The results are reported in the following sections.

#### 6.6.1 ISO 32 Polyolester/R-410A

Figures 77 through 79 show the film thickness data as a function of rolling speed and refrigerant concentration for mixtures of ISO 32 polyolester and R-410A at 23 °C, 45 °C and 65 °C, respectively. Overall, the gradients of the plots agree with the EHD theoretical slope.

The R-410A concentrations studied were limited to 10 and 20% by weight due to the high vapor pressure of this refrigerant. The data shows similar trends to those observed with the other lubricant and refrigerant mixtures reported in the previous sections, i.e. the film thickness decreases as the refrigerant concentration in the lubricant increases. Figure 80

compares the reduction in film thickness with increasing refrigerant concentration at a constant speed of 0.81 m/s at the three test temperatures. The percent reduction in film thickness at this speed is given in Table 25.

**Table 25. Percent Reduction in Film Thickness for Mixtures of ISO 32 Polyolester and R-410A at a constant rolling speed of 0.8 m/s**

| Refrigerant Concentration, wt % | Temperature, °C | % Reduction in Film Thickness |
|---|---|---|
| 10 | 23 | 57 |
| | 45 | 45 |
| | 65 | 40 |
| 20 | 23 | 82 |
| | 45 | 70 |
| | 65 | 59 |

### 6.6.2 ISO 68 Polyolester A/R-410A

Similar data on ISO 68 polyolester A and R-410A mixtures are given in Figures 81 through 84 and Table 26. The data shows similar trends to those reported above in Section 6.6.1 for the ISO 32 polyolester. As expected, the film thicknesses measured for POE-68A/R-410A were greater than those measured for POE-32/R-410A.

**Table 26. Percent Reduction in Film Thickness for Mixtures of ISO 68 Polyolester A and R-410A at a constant rolling speed of 0.8 m/s**

| Refrigerant Concentration, wt % | Temperature, °C | % Reduction in Film Thickness |
|---|---|---|
| 10 | 23 | 61 |
| | 45 | 51 |
| | 65 | 39 |
| 15 | 23 | 75 |
| | 45 | 65 |
| | 65 | 56 |
| 20 | 23 | 86 |
| | 45 | 77 |
| | 65 | 61 |
| 30 | 23 | 93 |
| | 45 | 83 |
| | 65 | -- |

**Figure 65. Comparison of Film Thickness Data for ISO 32 Polyvinyl Ether at Ambient Temperature as a Function of R-134a Concentration**

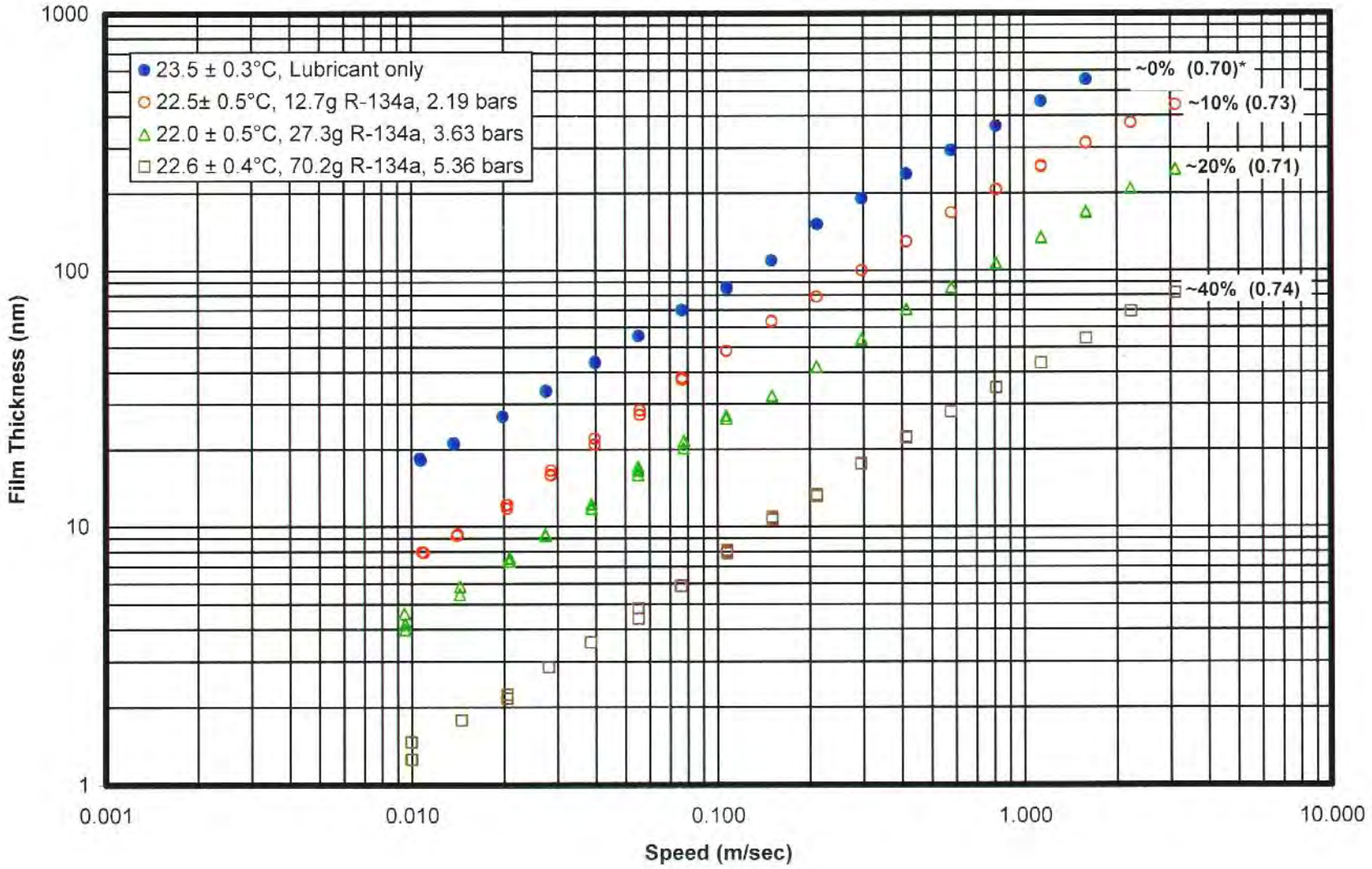


*numbers in parentheses show gradients

**Figure 66. Comparison of Film Thickness Data for ISO 32 Polyvinyl Ether at 45°C as a Function of R-134a Concentration**

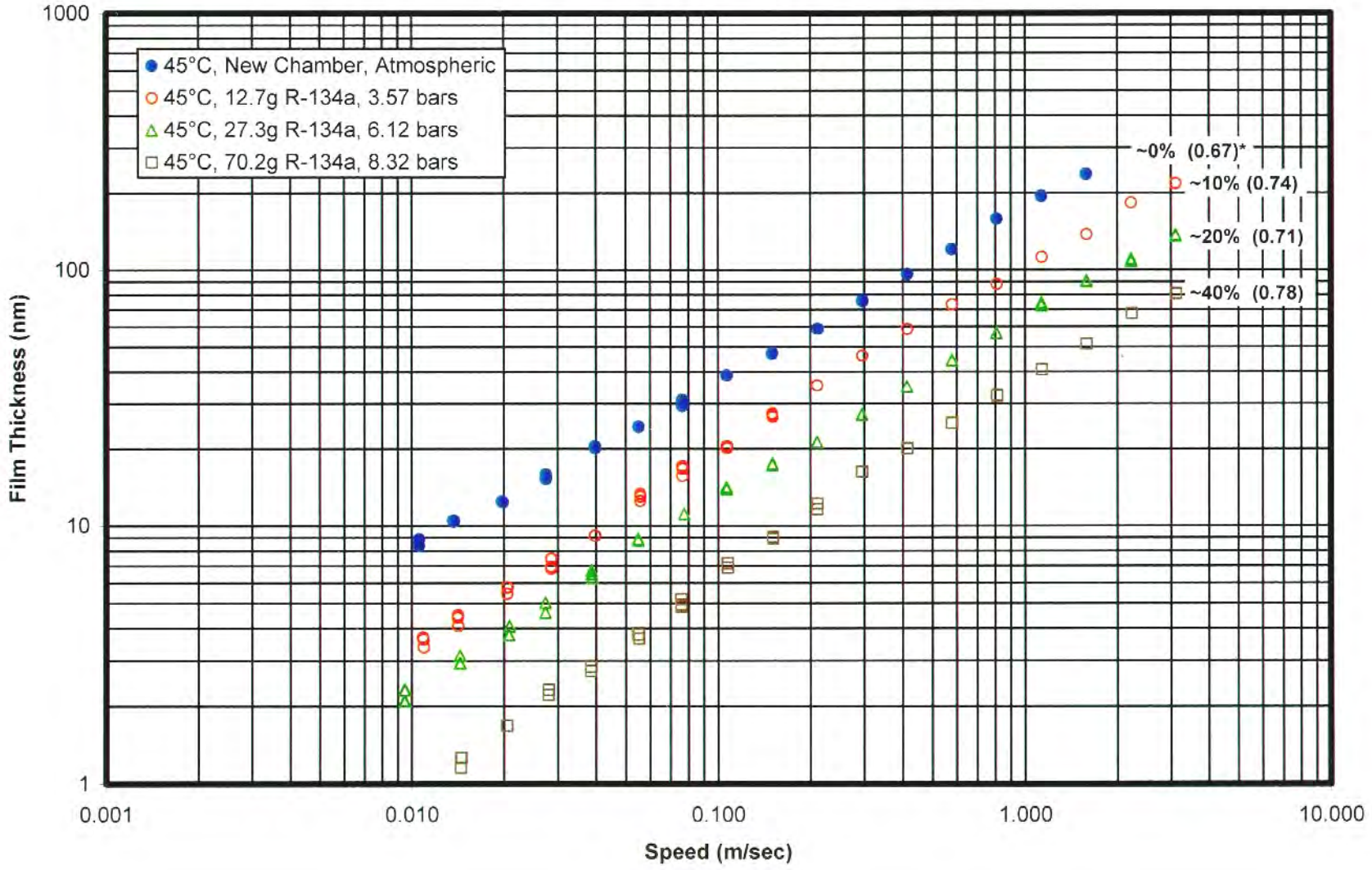


*numbers in parentheses show gradients

**Figure 67. Comparison of Film Thickness Data for ISO 32 Polyvinyl Ether at 65°C as a Function of R-134a Concentration**

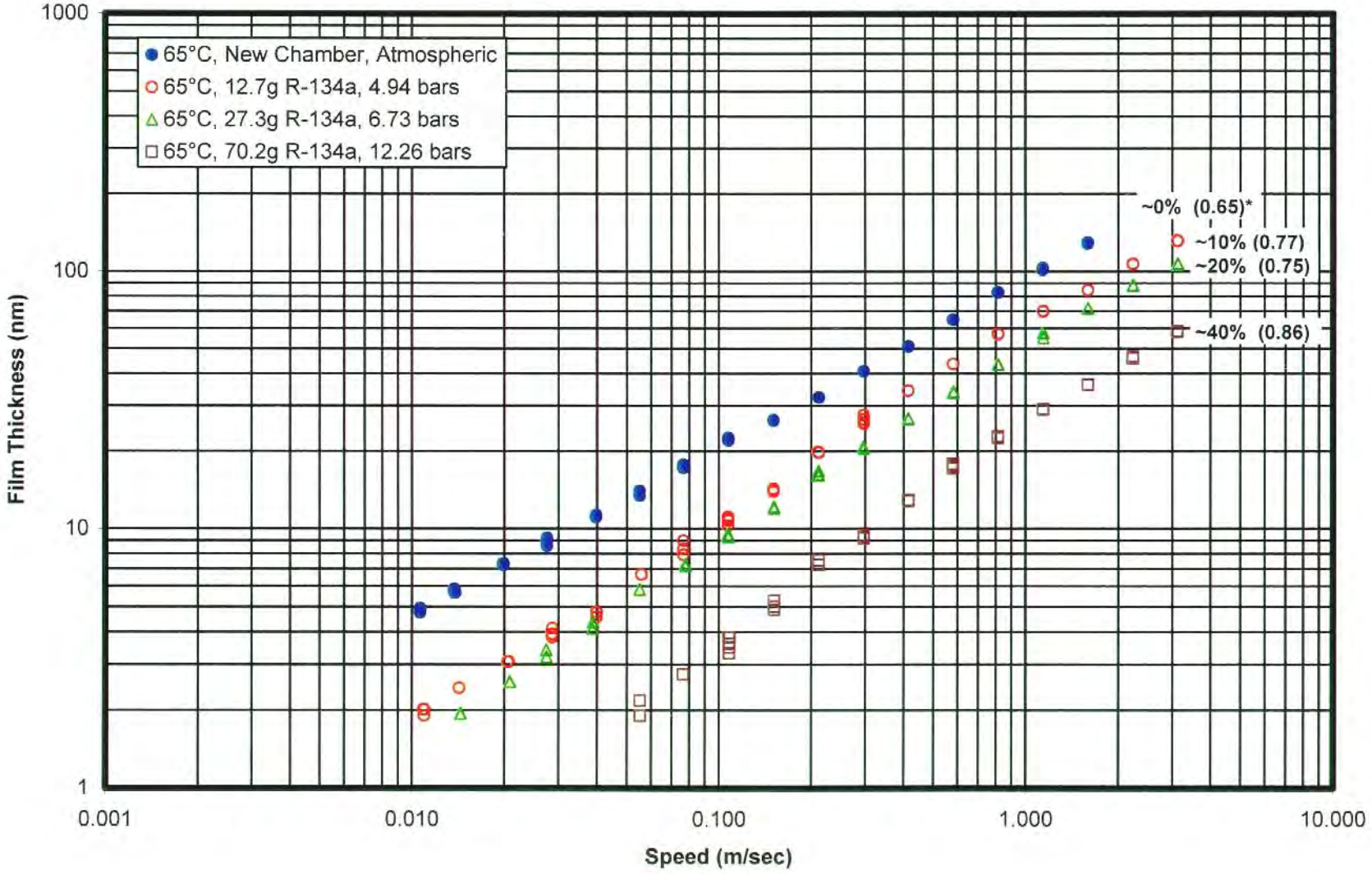


*numbers in parentheses show gradients

**Figure 68. Film Thickness vs. R-134a Concentration for ISO 32 Polyvinyl Ether**

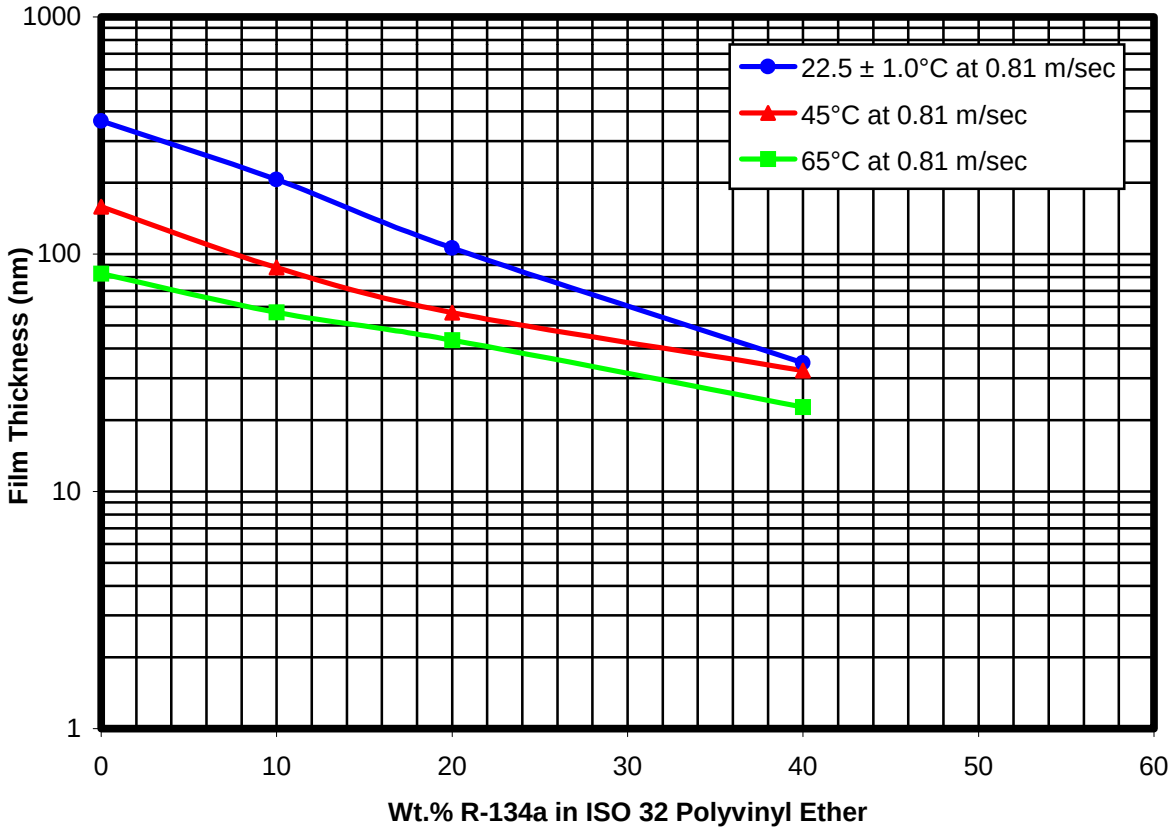

**Figure 69. Comparison of Film Thickness Data for ISO 68 Polyvinyl Ether at Ambient Temperature as a Function of R-134a Concentration**

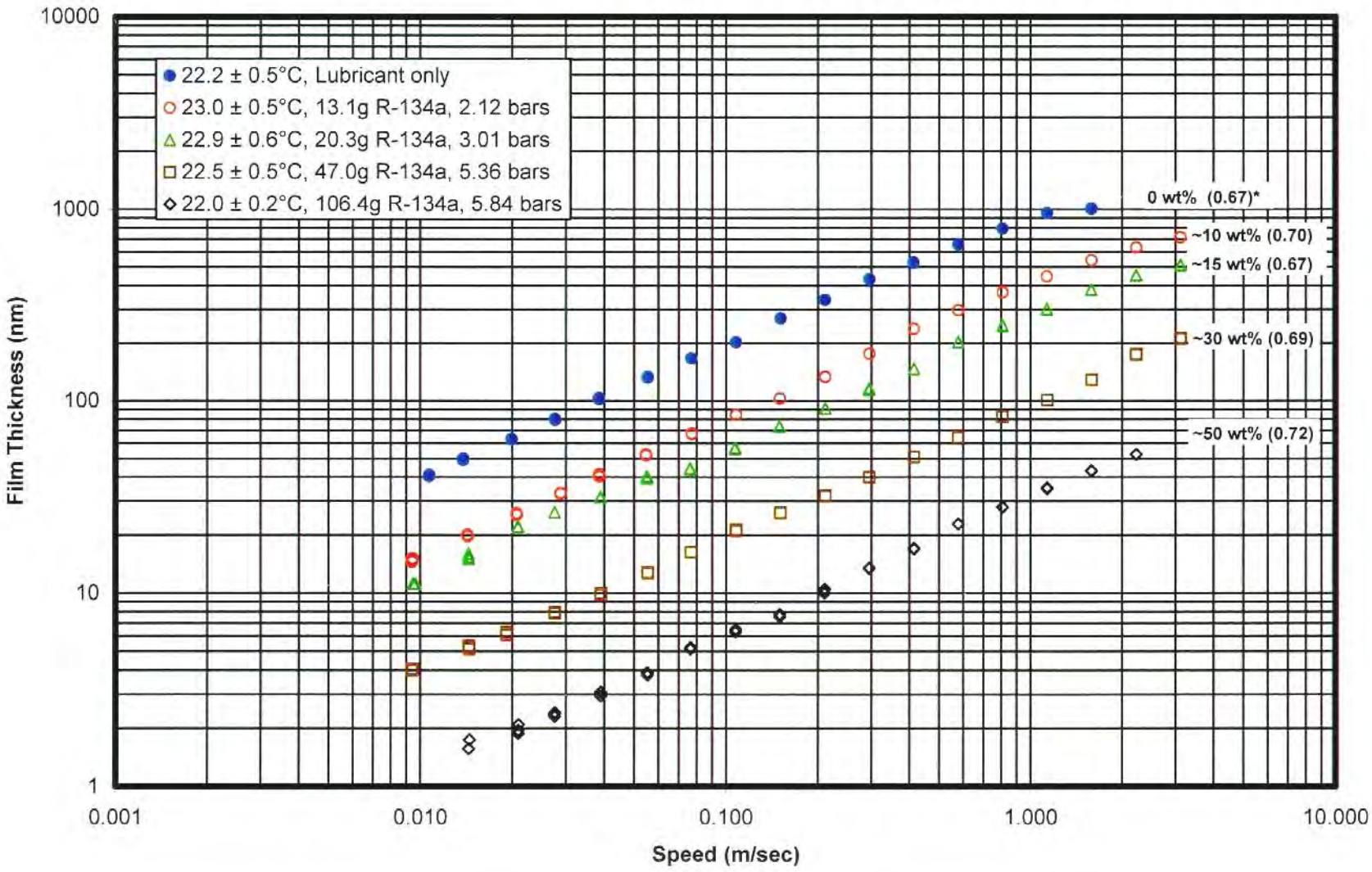

**Figure 70. Comparison of Film Thickness Data for ISO 68 Polyvinyl Ether at 45°C as a Function of R-134a Concentration**

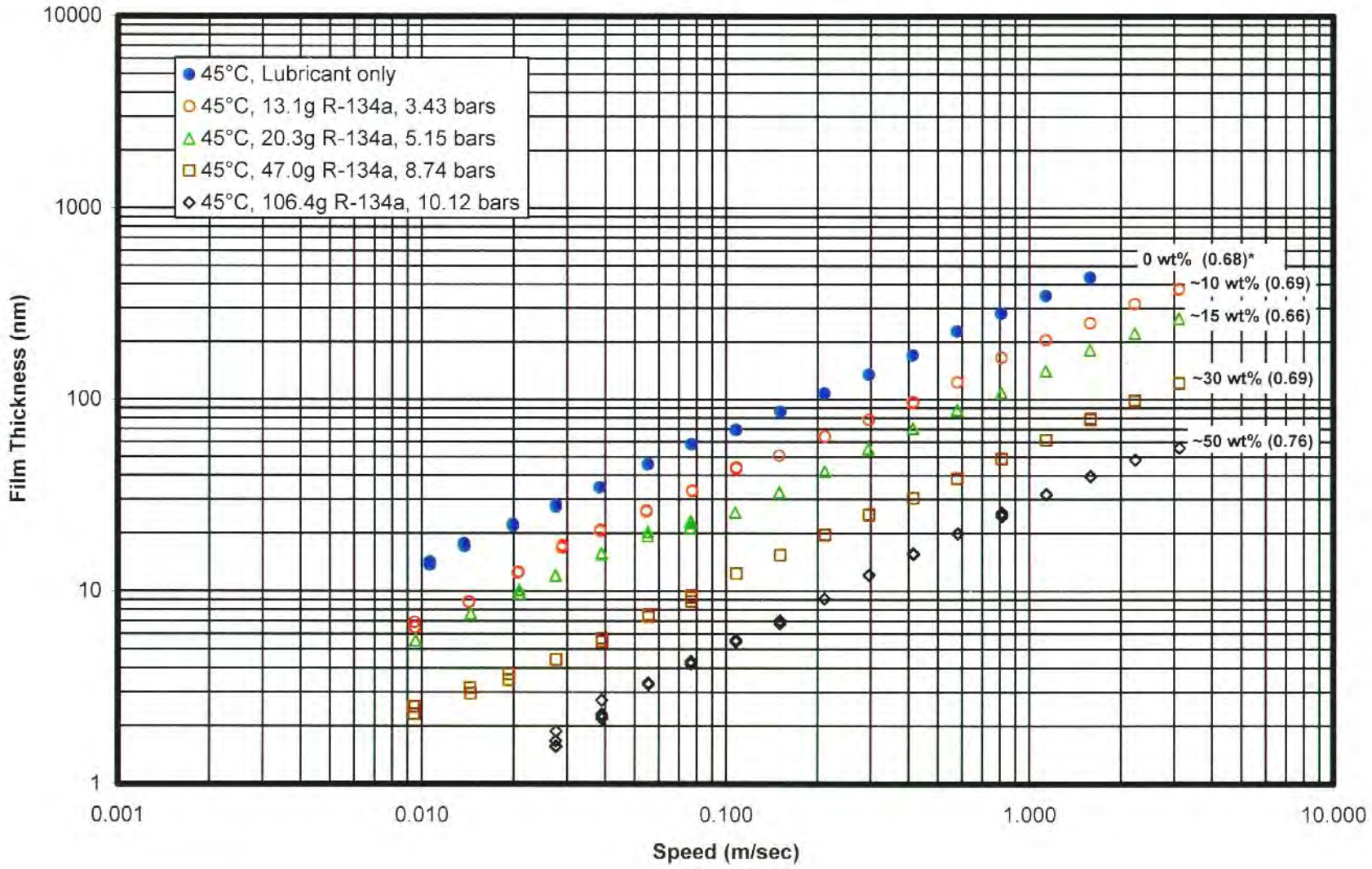

**Figure 71. Comparison of Film Thickness Data for ISO 68 Polyvinyl Ether at 65°C as a Function of R-134a Concentration**

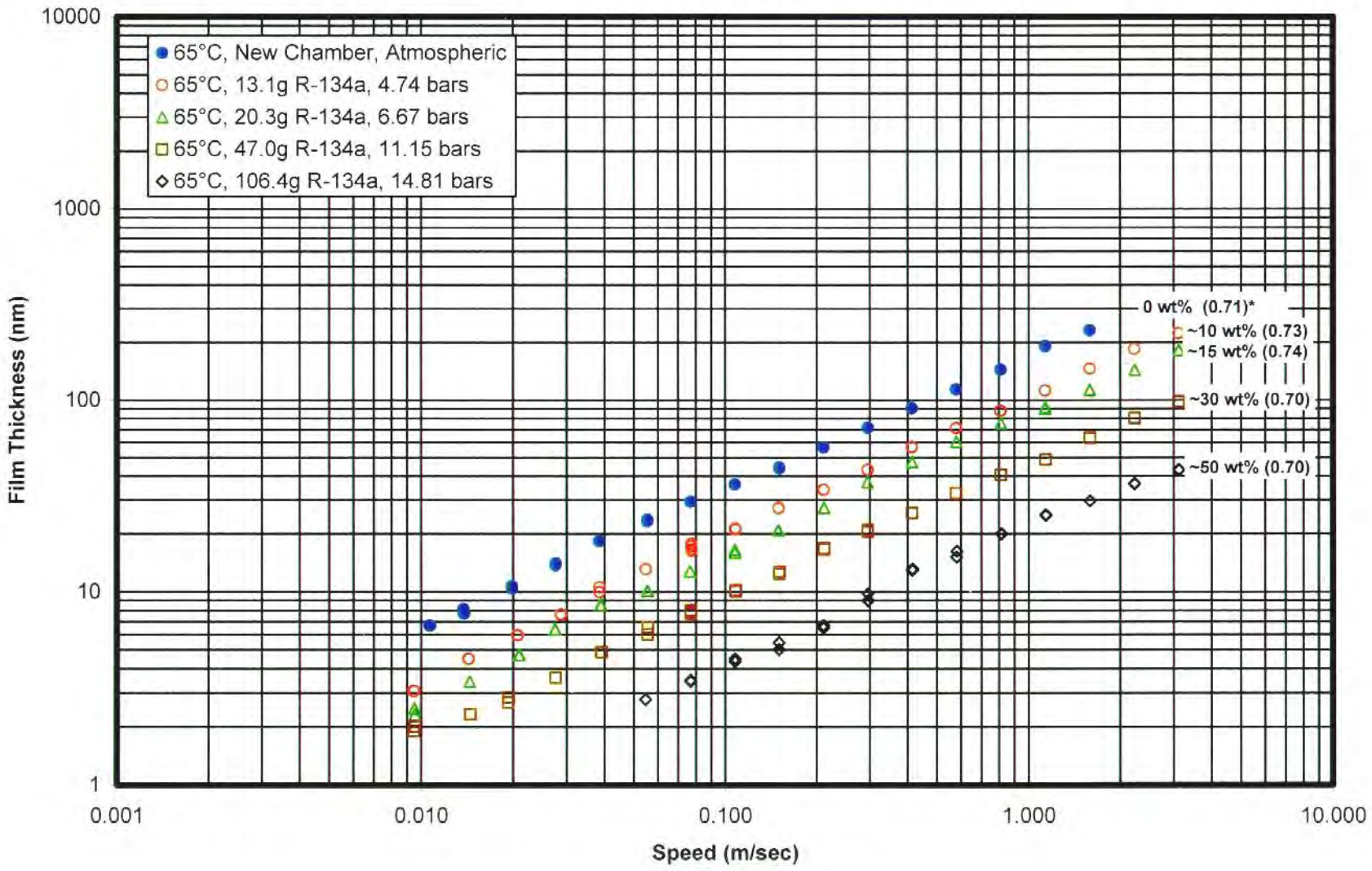

**Figure 72. Film Thickness vs. R-134a Concentration for ISO 68 Polyvinyl Ether**

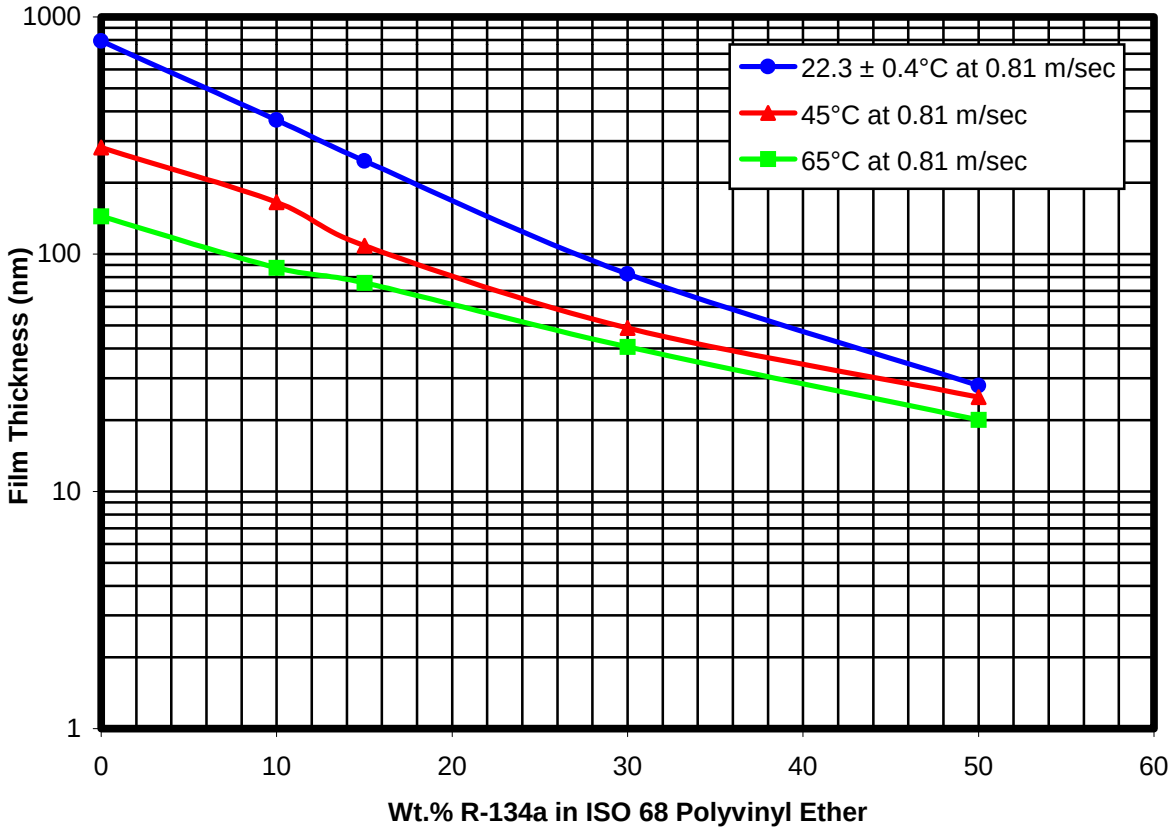

**Figure 73. Effect of Refrigerant Concentration on Effective Pressure-Viscosity Coefficient and Dynamic Viscosity for Mixtures of ISO 32 Polyvinyl Ether and R-134a**

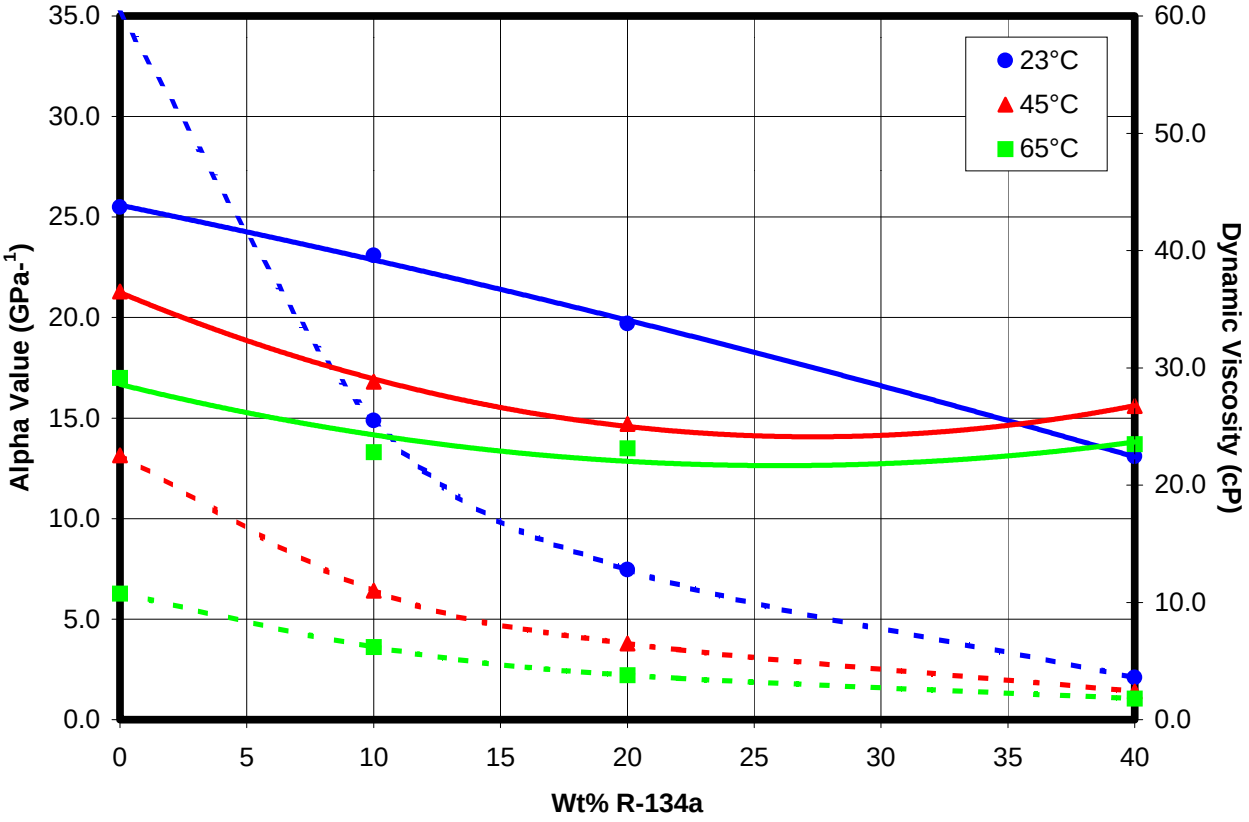


Solid lines represent alpha values
Dashed lines represent dynamic viscosities

**Figure 74. Alpha Value vs. Dynamic Viscosity for ISO 32 Polyvinyl Ether in R-134a**

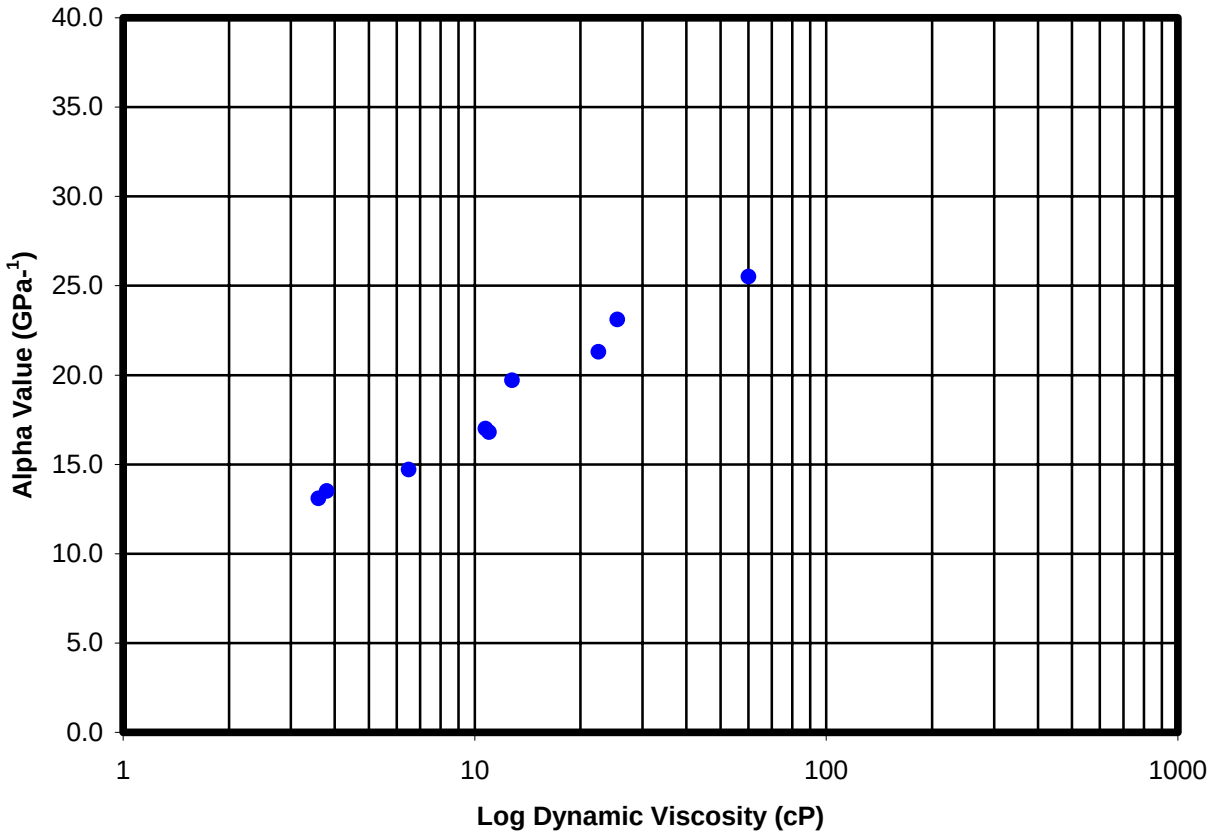


Solid lines represent alpha values
Dashed lines represent dynamic viscosities

**Figure 75. Effect of Refrigerant Concentration on Effective Pressure-Viscosity Coefficient and Dynamic Viscosity for Mixtures of ISO 68 Polyvinyl Ether and R-134a**

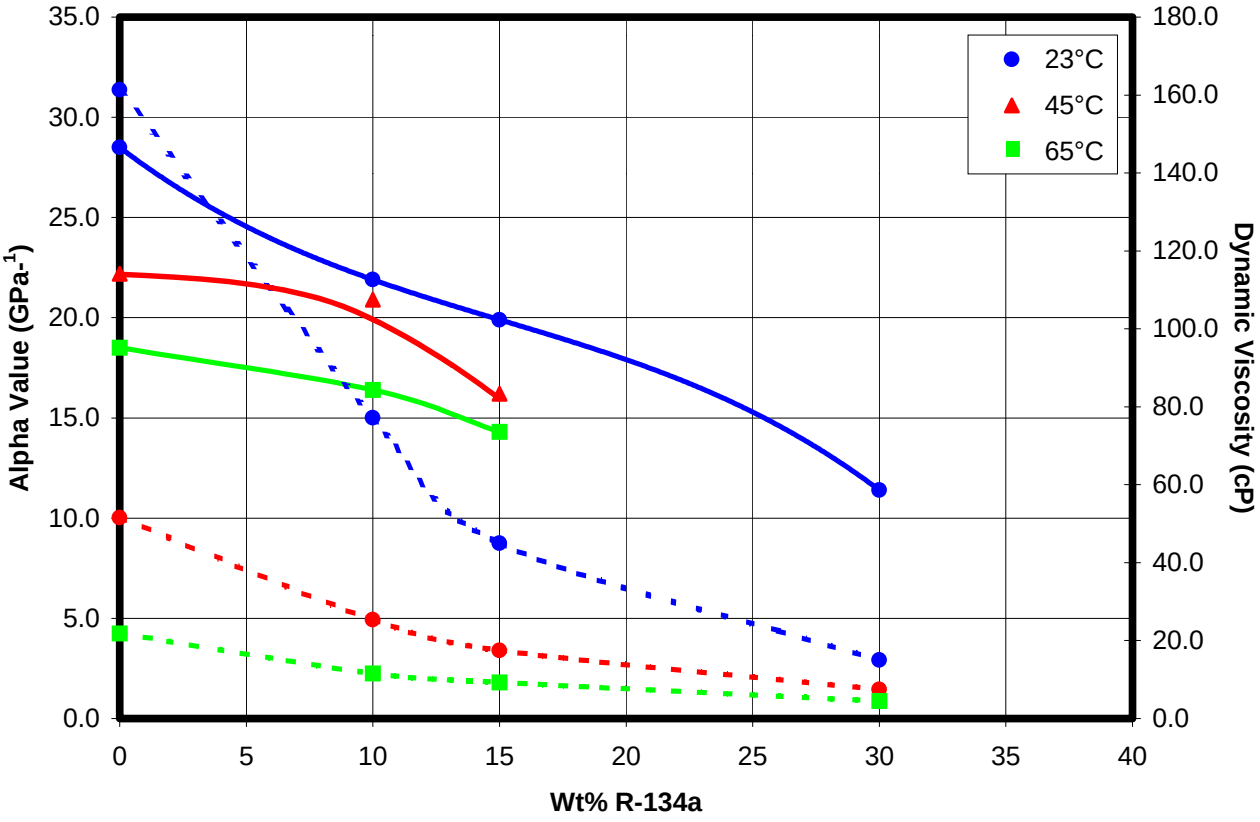


Solid lines represent alpha values
Dashed lines represent dynamic viscosities

**Figure 76. Alpha Value vs. Dynamic Viscosity for ISO 68 Polyvinyl Ether in R-134a**

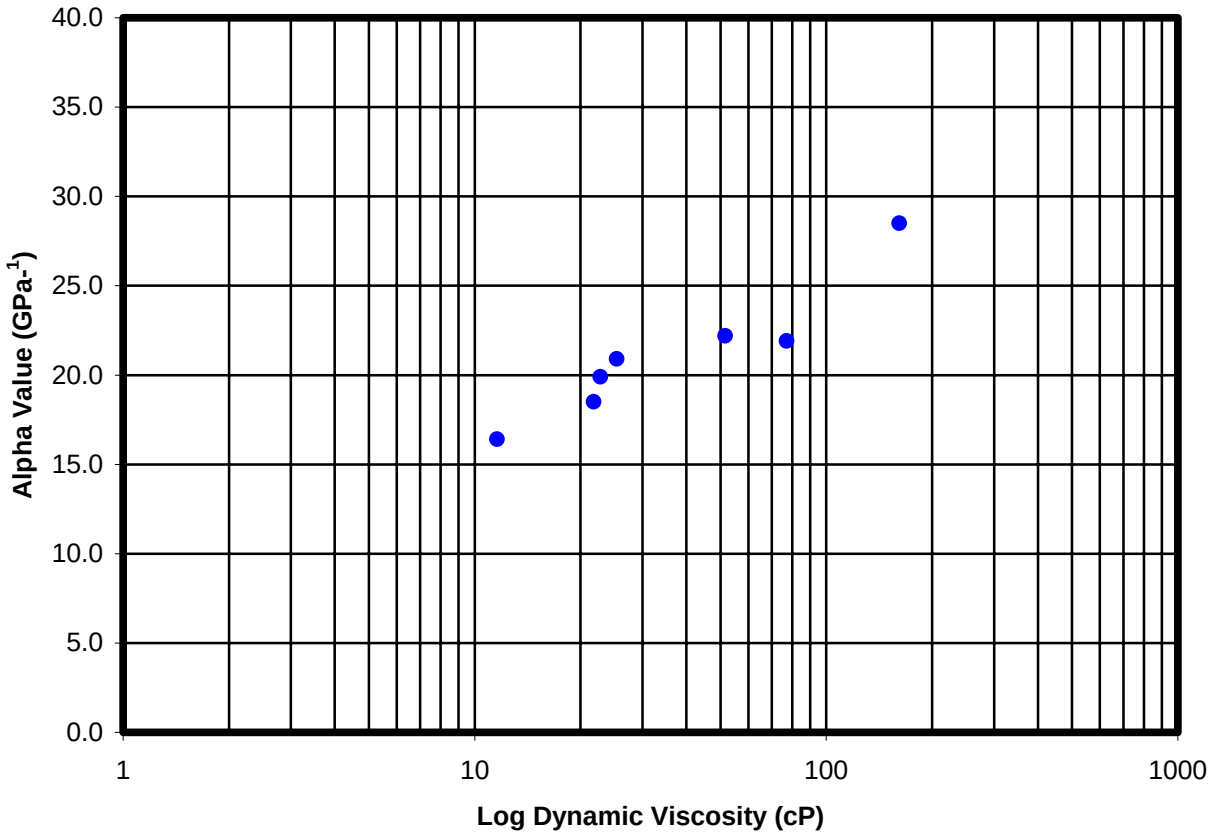

**Figure 77. Comparison of Film Thickness Data for ISO 32 Polyolester at Ambient Temperature as a Function of R-410A Concentration**

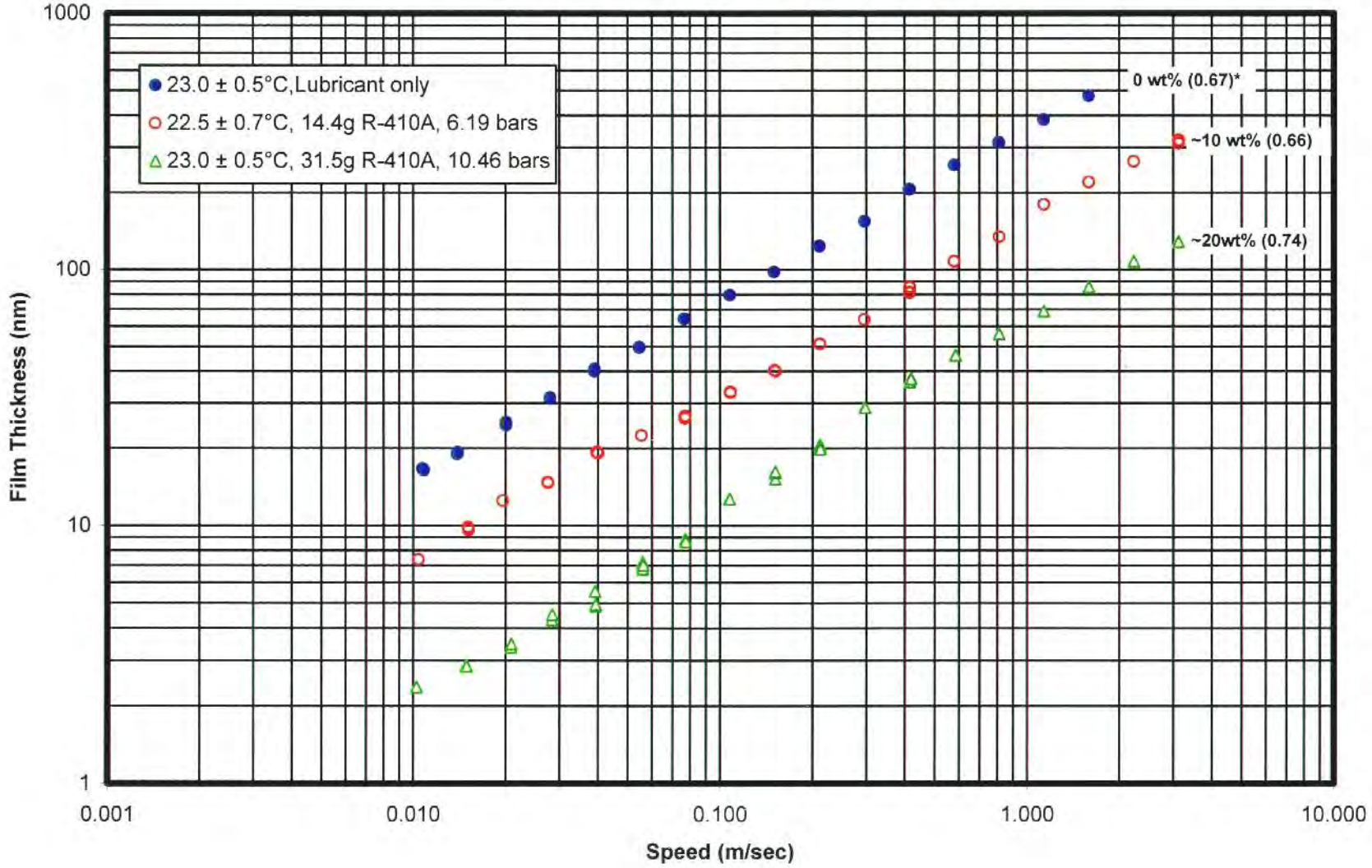


*numbers in parentheses show gradients

**Figure 78. Comparison of Film Thickness Data for ISO 32 Polyolester at 45°C as a Function of R-410A Concentration**

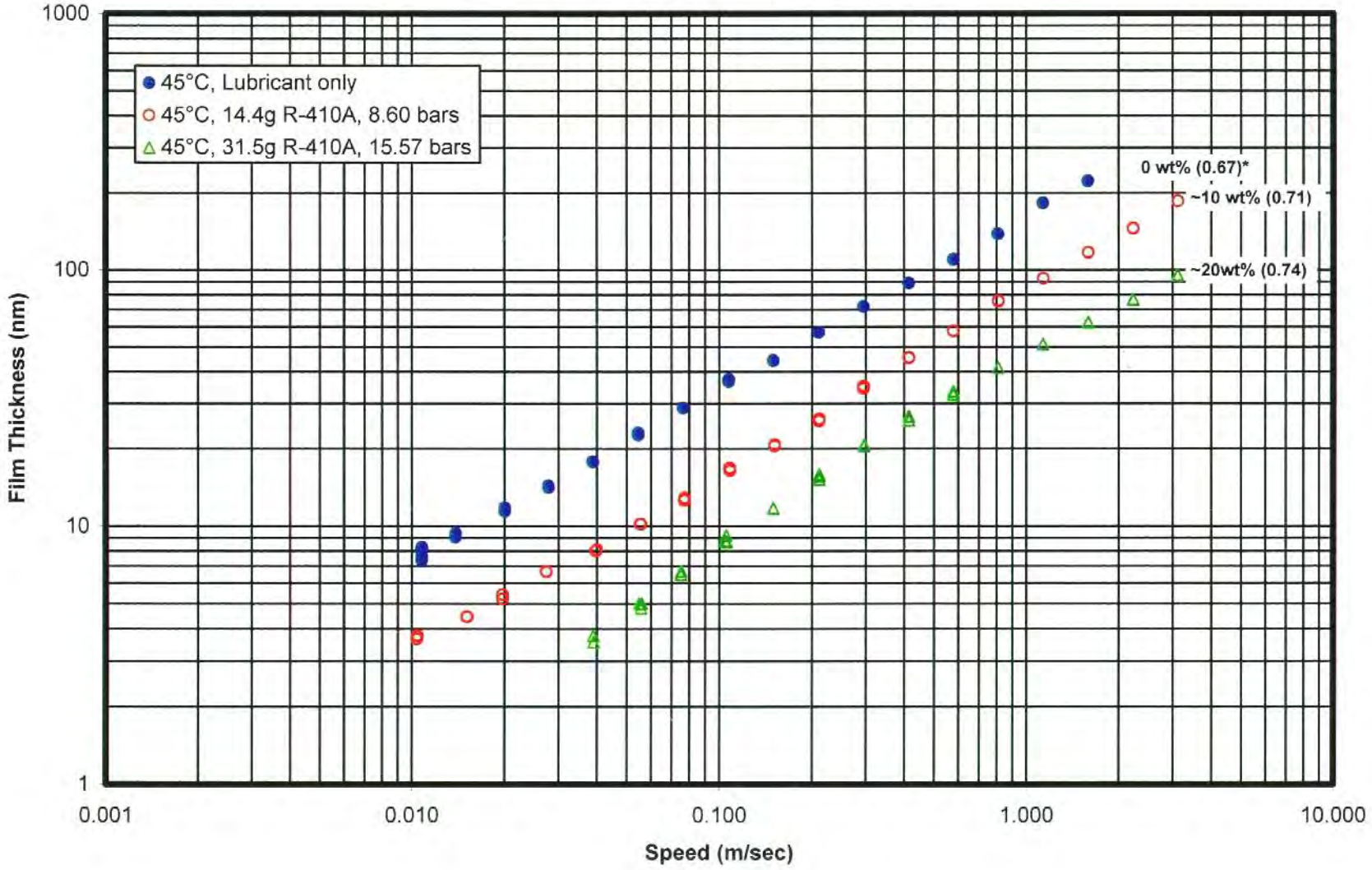


*numbers in parentheses show gradients

**Figure 79. Comparison of Film Thickness Data for ISO 32 Polyolester at 65°C as a Function of R-410A Concentration**

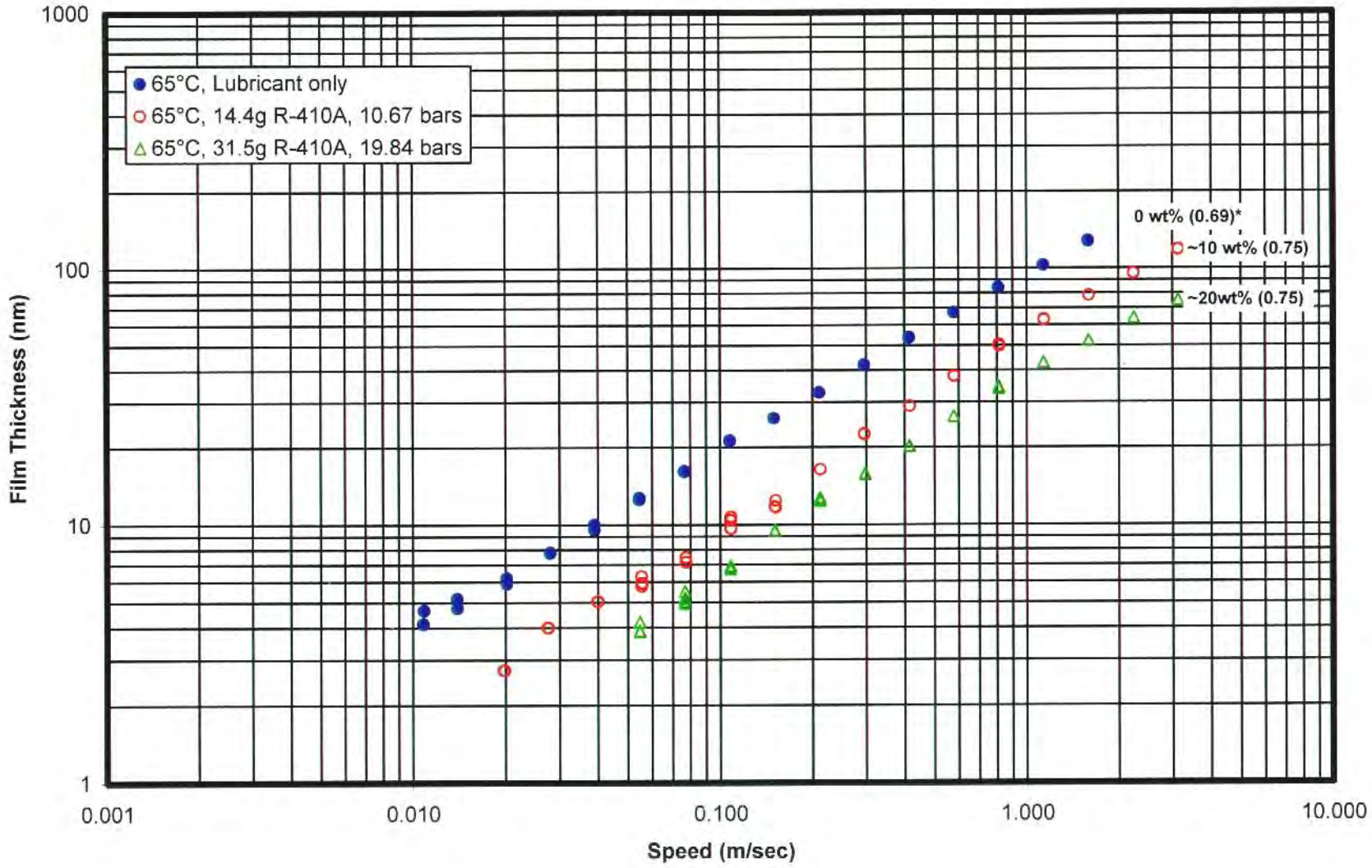


*numbers in parentheses show gradients

**Figure 80. Film Thickness vs. R-410A Concentration for ISO 32 Polyolester**

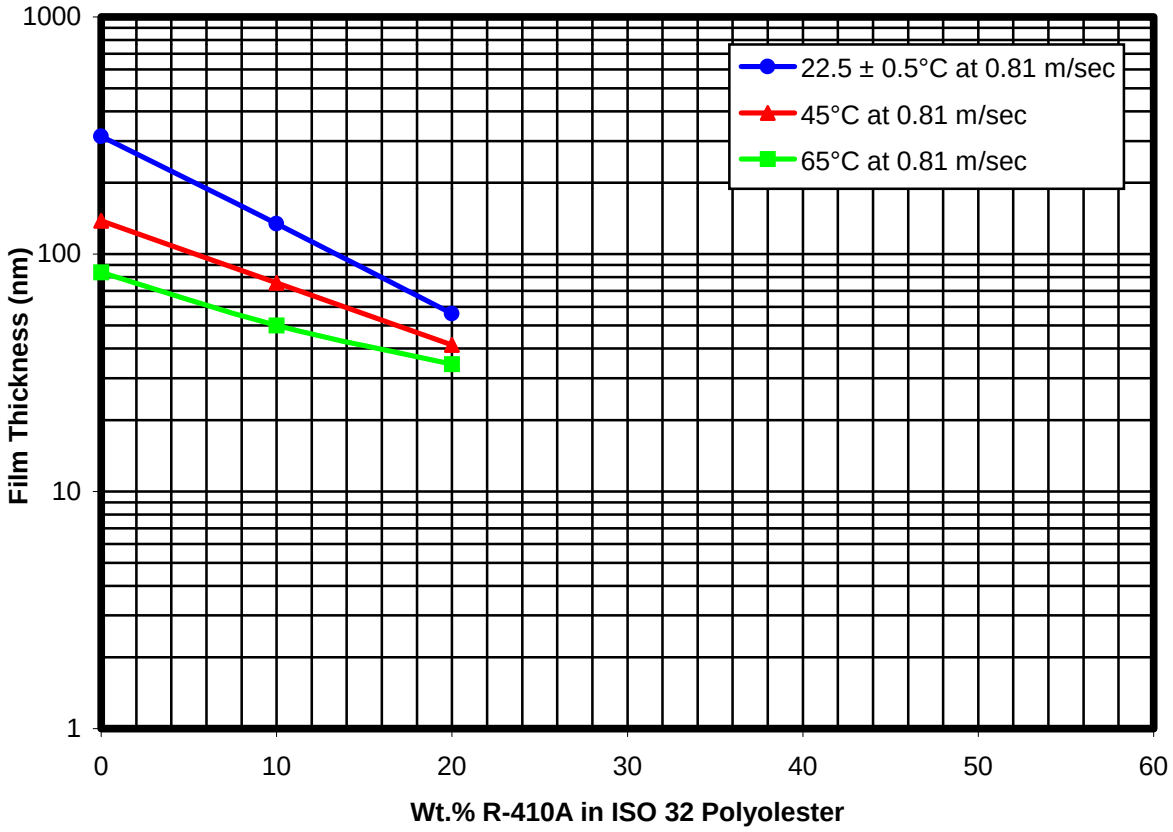

**Figure 81. Comparison of Film Thickness Data for ISO 68 Polyolester A at Ambient Temperature as a Function of R-410A Concentration**

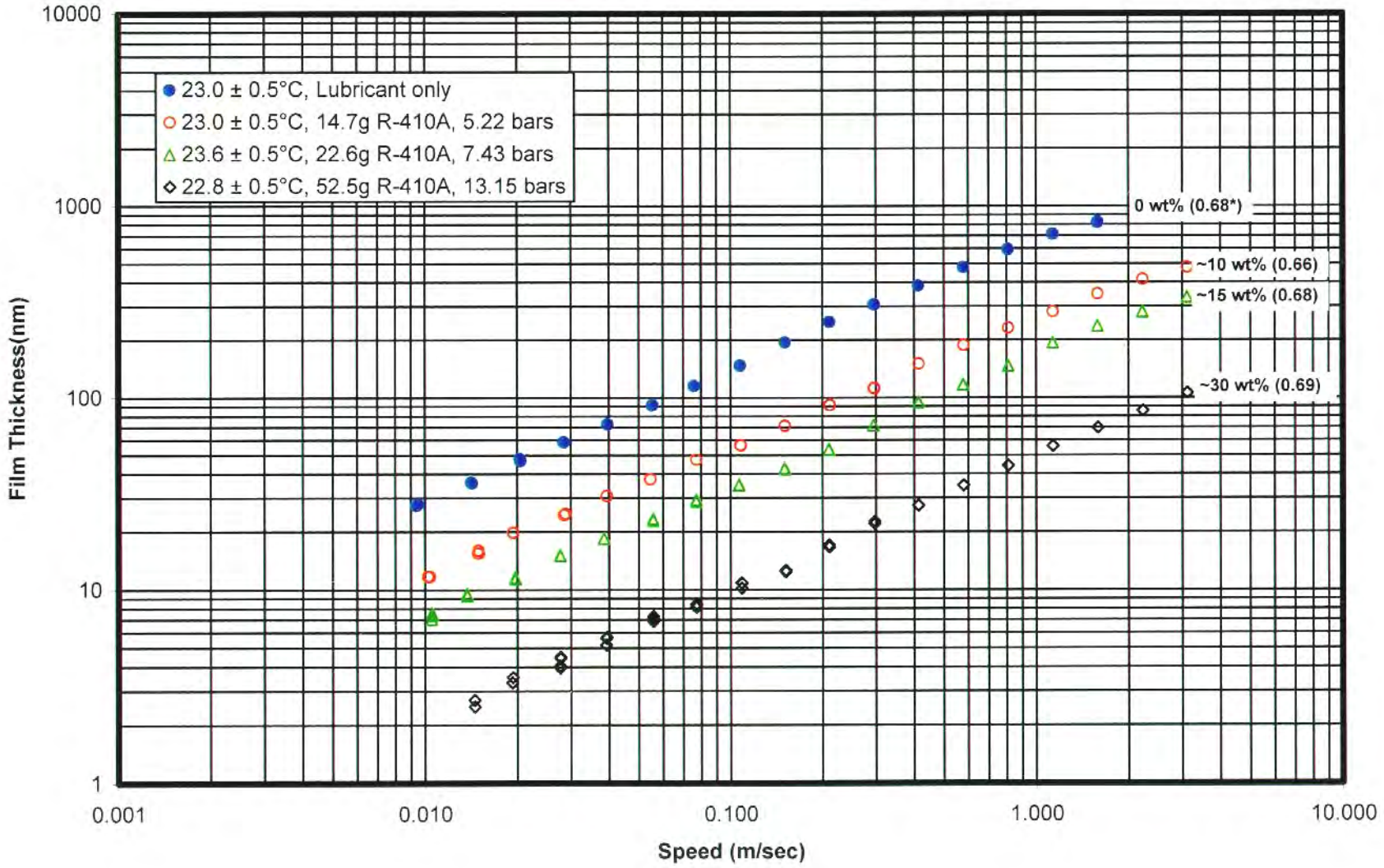


*numbers in parentheses show gradients

**Figure 82. Comparison of Film Thickness Data for ISO 68 Polyolester A at 45°C as a Function of R-410A Concentration**

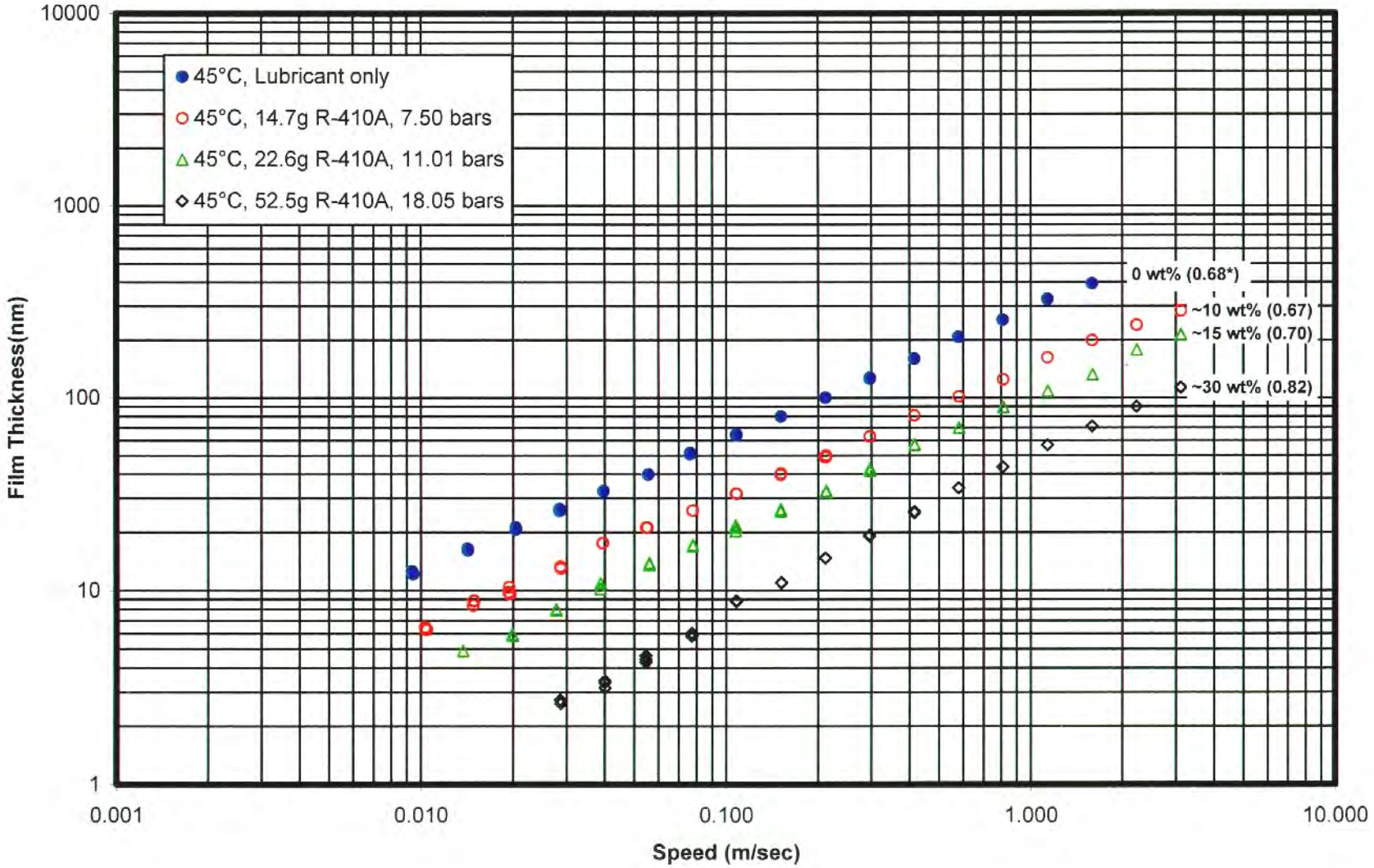


*numbers in parentheses show gradients

**Figure 83. Comparison of Film Thickness Data for ISO 68 Polyolester A at 65°C as a Function of R-410A Concentration**

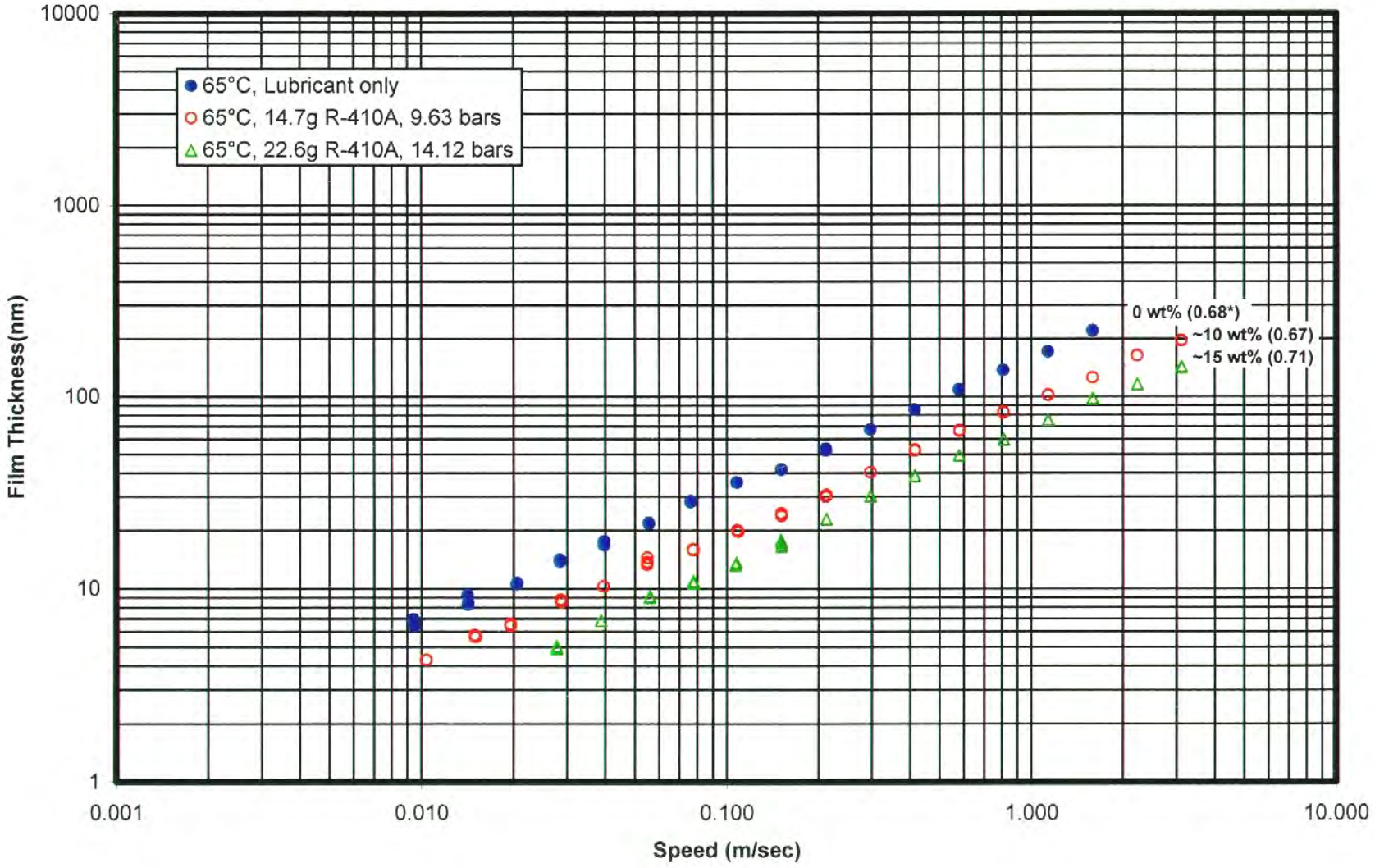


*numbers in parentheses show gradients

**Figure 84. Film Thickness vs. R-410A Concentration for ISO 68 Polyolester A**

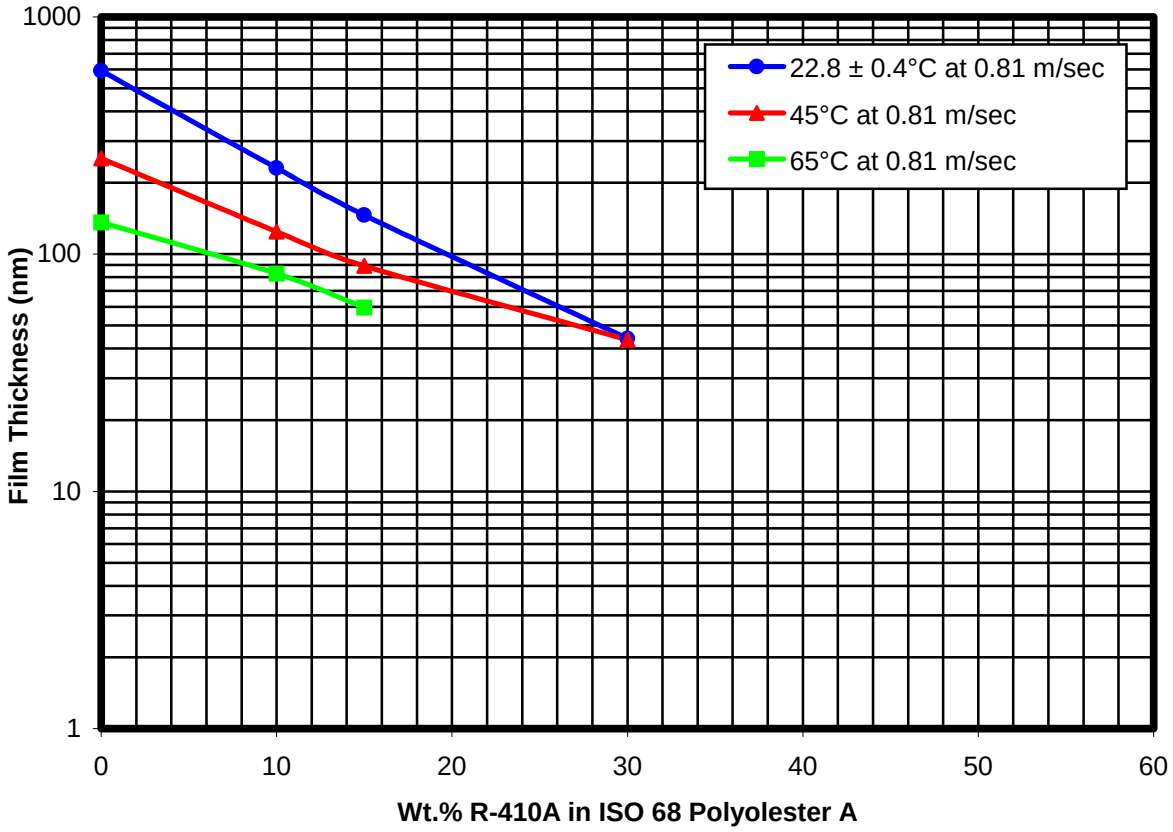

### 6.6.3 Effect of Refrigerant (R-410A) Concentration on Effective Pressure-Viscosity Coefficients of Polyolesters

Effective pressure-viscosity coefficients of the ester and refrigerant mixtures were calculated as described in Section 3.4. It was assumed that the mixtures obey the theoretical relationship of Hamrock and Dowson.

Dynamic viscosity data for mixtures of POE-32 and R-410A were calculated from the kinematic viscosity and density data provided by Reference 74 and given in Table 27. The effective $\alpha$-values calculated for these mixtures are given in Table 28. Figure 85 shows the variation of $\alpha$-value and dynamic viscosity as a function of refrigerant concentration and temperature. Figure 86 shows the variation of $\alpha$-values with the logarithm of dynamic viscosity.

**Table 27. Dynamic Viscosity Data for Mixtures of ISO 32 Polyolester and R-410A**

| Temperature, °C | Dynamic Viscosity, cP | | |
|---|---|---|---|
| | R-410A Concentration, wt % | | |
| | 0% | 10% | 20% |
| 23 | 61.36 | 26.46 | 11.47 |
| 45 | 25.12 | 12.18 | 5.84 |
| 65 | 12.64 | 6.66 | 3.36 |

**Table 28. Effective Pressure-Viscosity Coefficients for Mixtures of ISO 32 Polyolester and R-410A**

| Temperature, °C | R-410A Concentration, wt % | | |
|---|---|---|---|
| | 0% | 10% | 20% |
| | $\alpha$-values, $GPa^{-1}$ | | |
| 23 | 16.9 | 13.6 | 6.0 |
| 45 | 14.8 | 10.1 | 8.5 |
| 65 | 12.4 | 9.7 | 12.4 (?) |

Effective pressure-viscosity coefficients were also calculated for the mixtures of POE-68A and R-410A. Table 29 shows the dynamic viscosity data calculated from the kinematic viscosity and density data provided by Reference 74. The $\alpha$-values calculated as a function of refrigerant concentration and temperature are given in Table 30 and Figure 87. Figure 88 shows the variation of pressure-viscosity coefficient with log (dynamic viscosity).

The data reported in Tables 28 and 30 show that $\alpha$-values increase with temperature at high R-410A concentrations. This was also observed for the mixtures of R-134a and

polyolesters, and R-134a and polyvinyl ethers. Possible reasons for this observation were discussed in Section 6.4.3.

**Table 29. Dynamic Viscosity Data for Mixtures of ISO 68 Polyolester A and R-410A**

| Temperature, °C | Dynamic Viscosity, cP | | | |
|---|---|---|---|---|
| | R-410A Concentration, wt % | | | |
| | 0% | 10% | 15% | 30% |
| 23 | 131.15 | 45.77 | 28.53 | 7.30 |
| 45 | 48.14 | 19.54 | 12.25 | 4.08 |
| 65 | 22.26 | 10.09 | 7.28 | N/A |

**Table 30. Effective Pressure-Viscosity Coefficients for Mixtures of ISO 68 Polyolester A and R-410A**

| Temperature, °C | R-410A Concentration, wt % | | | |
|---|---|---|---|---|
| | 0% | 10% | 15% | 30% |
| | $\alpha$-values, $GPa^{-1}$ | | | |
| 23 | 19.6 | 18.1 | 13.4 | 7.8 |
| 45 | 17.8 | 17.1 | 14.6 | 15.6 (?) |
| 65 | 15.9 | 17.3 | 13.9 | -- |

### 6.7 Film Thickness Measurements on Mixtures of Polyvinyl Ethers and R-410A

Film thickness measurements were conducted on mixtures of ISO 32 and ISO 68 polyvinyl ethers and R-410A as a function of rolling speed, temperature and refrigerant concentration. The results are reported in the following sections.

#### 6.7.1 ISO 32 Polyvinyl Ether/R-410A

Figures 89 through 91 show the film thickness data as a function of rolling speed and refrigerant concentration for mixtures of ISO 32 polyvinyl ether (PVE) and R-410A at 23 °C, 45 °C and 65 °C, respectively. The gradients of the plots vary from 0.65 to 0.71 and agree with the EHD theoretical slope. The R-410A concentrations studied included 0, 20, and 40% by weight. Similar to the trends observed with the other lubricant and refrigerant system investigated in this study, film thickness decreases significantly in the contact as the refrigerant concentration and temperature increase.

Figure 92 compares the reduction in film thickness with increasing refrigerant concentration at a constant speed of 0.81 m/s as a function of temperature. At each temperature, the film thickness decreases with increasing refrigerant concentration. Table 31 compares the percent reduction in film thickness as a function of refrigerant concentration and temperature. At a constant refrigerant concentration, the reduction in film thickness becomes smaller as the temperature increases.

**Table 31. Percent Reduction in Film Thickness for Mixtures of ISO 32 Polyvinyl Ether and R-410A at a constant rolling speed of 0.8 m/s**

| Refrigerant Concentration, wt % | Temperature, °C | % Reduction in Film Thickness |
|---|---|---|
| 10 | 23 | 62 |
| | 45 | 51 |
| | 65 | 36 |
| 20 | 23 | 79 |
| | 45 | 70 |
| | 65 | 54 |
| 40 | 23 | 93 |
| | 45 | 87 |
| | 65 | -- |

### 6.7.2 ISO 68 Polyvinyl Ether/R-410A

Figures 93 through 95 show the film thickness data as a function of rolling speed and refrigerant concentration for mixtures of ISO 68 polyvinyl ether (PVE) and R-410A at 23 °C, 45 °C and 65 °C, respectively. The gradients of the plots vary from 0.67 to 0.78 and agree with the EHD theoretical slope. The R-410A concentrations studied include 0, 10, 15, 20, 30 and 50% by weight. The data shows similar trends to those observed with the lower viscosity (ISO 32) PVE reported above, i.e. film thickness decreases as the refrigerant concentration in the lubricant increases. As expected, the film thicknesses measured for PVE-68A/R-410A were greater than those measured for PVE-32/R-410A.

Figure 96 compares the reduction in film thickness with increasing refrigerant concentration at a constant speed of 0.81 m/s at the three test temperatures. The same data is also given in Table 32.

### 6.7.3 Effect of Refrigerant Concentration (R-410A) on Effective Pressure-Viscosity Coefficients of Polyvinyl Ethers

Effective pressure-viscosity coefficients of the PVE and R-410A mixtures were calculated as described in Section 3.4.

Dynamic viscosity data for mixtures of ISO 32 PVE and R-410A, given in Table 33, were obtained from Reference 77. The effective $\alpha$-values calculated for these mixtures are given in Table 34 as a function of refrigerant concentration and temperature. Dynamic viscosity and $\alpha$-value decrease with increasing refrigerant concentration and temperature as shown in Figure 97. Figure 98 shows the increase in $\alpha$-values as a function of log (dynamic viscosity).

Effective pressure-viscosity coefficients were also calculated for the mixtures of ISO 68 PVE and R-410A. Dynamic viscosity data obtained from Reference 77 is given in Table 35. The $\alpha$-values calculated as a function of refrigerant concentration and temperature are given in Table 36 and Figure 99. Figure 100 shows the increase in $\alpha$-values as a function of log (dynamic viscosity).

**Table 32. Percent Reduction in Film Thickness for Mixtures of ISO 68 Polyvinyl Ether and R-410A at a constant rolling speed of 0.8 m/s**

| Refrigerant Concentration, wt % | Temperature, °C | % Reduction in Film Thickness |
|---|---|---|
| 10 | 23 | 50 |
| | 45 | 35 |
| | 65 | 31 |
| 15 | 23 | 76 |
| | 45 | 66 |
| | 65 | 61 |
| 20 | 23 | 87 |
| | 45 | 78 |
| | 65 | 67 |
| 30 | 23 | 94 |
| | 45 | 87 |
| | 65 | -- |
| 50 | 23 | 97 |
| | 45 | 94 |
| | 65 | -- |

**Table 33. Dynamic Viscosity Data for Mixtures of ISO 32 Polyvinyl Ether and R-410A**

| Temperature, °C | Dynamic Viscosity, cP | | | |
|---|---|---|---|---|
| | R-410 Concentration, wt % | | | |
| | 0% | 10% | 20% | 40% |
| 23 | 60.21 | 20.0 | 9.2 | 2.6 |
| 45 | 22.53 | 9.0 | 4.9 | 1.9 |
| 65 | 10.75 | 6.7 | 3.4 | N/A |

**Table 34. Effective Pressure-Viscosity Coefficients for Mixtures of ISO 32 Polyvinyl Ether and R-410A**

| Temperature, °C | R-410A Concentration, wt % | | | |
|---|---|---|---|---|
| | 0% | 10% | 20% | 40% |
| | $\alpha$-values, $GPa^{-1}$ | | | |
| 23 | 25.5 | 16.6 | 15.4 | 10.5 |
| 45 | 21.3 | 14.4 | 11.3 | 10.3 |
| 65 | 17.0 | 16.3 | 17.0 | -- |

**Table 35. Dynamic Viscosity Data for Mixtures of ISO 68 Polyvinyl Ether and R-410A**

| Temperature, °C | Dynamic Viscosity, cP | | | |
|---|---|---|---|---|
| | R-410 Concentration, wt % | | | |
| | 0% | 15% | 20% | 30% |
| 23 | 161.32 | 27.0 | 18.0 | 7.8 |
| 45 | 51.59 | 12.0 | 8.0 | 4.4 |
| 65 | 21.83 | 6.5 | 4.8 | 2.9 |

**Table 36. Effective Pressure-Viscosity Coefficients for Mixtures of ISO 68 Polyvinyl Ether and R-410A**

| Temperature, °C | R-410A Concentration, wt % | | | |
|---|---|---|---|---|
| | 0% | 15% | 20% | 30% |
| | $\alpha$-values, $GPa^{-1}$ | | | |
| 23 | 28.5 | 17.9 | 12.7 | 9.6 |
| 45 | 22.2 | 16.6 | 13.7 | 10.8 |
| 65 | 18.5 | 14.6 | 13.3 | -- |

**Figure 85. Effect of Refrigerant Concentration on Effective Pressure-Viscosity Coefficient and Dynamic Viscosity for Mixtures of ISO 32 Polyolester and R-410A**

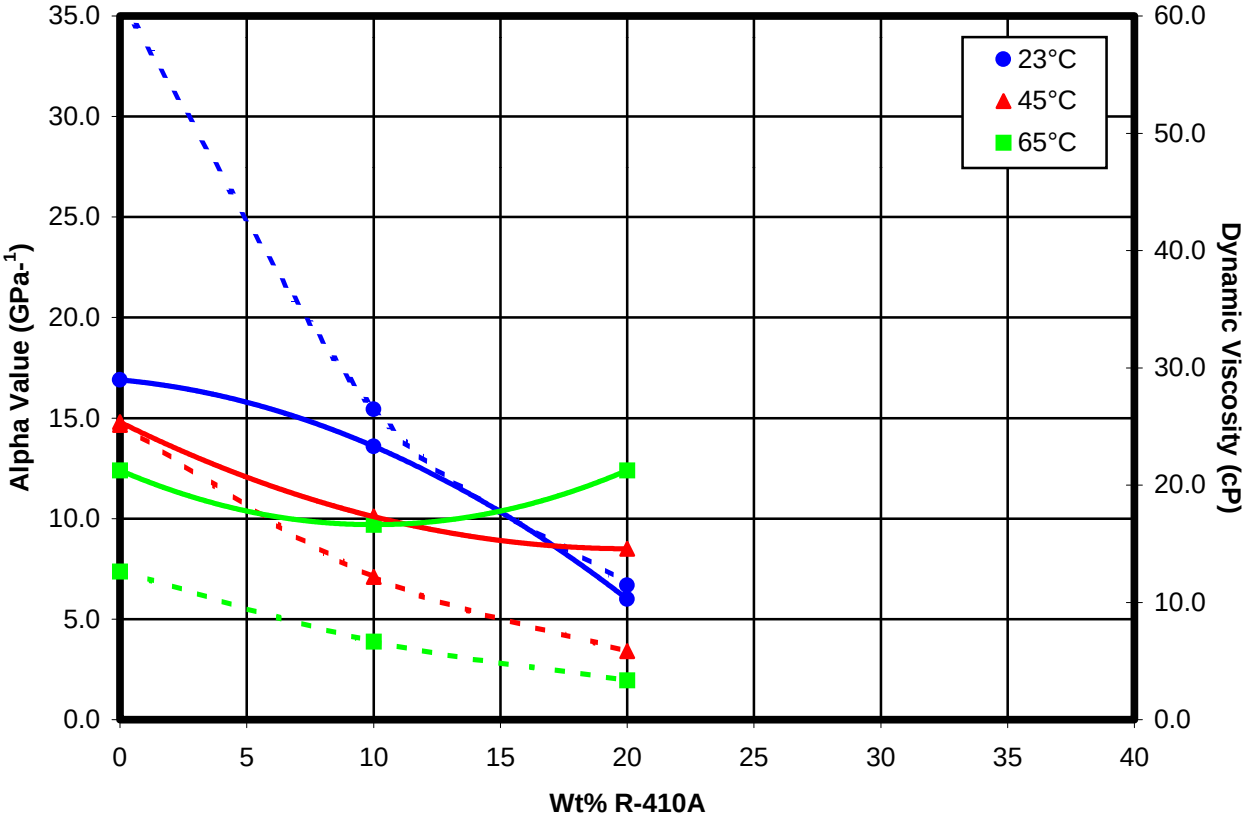


Solid lines represent alpha values
Dashed lines represent dynamic viscosities

**Figure 86. Alpha Value vs. Dynamic Viscosity for ISO 32 Polyolester in R-410A**

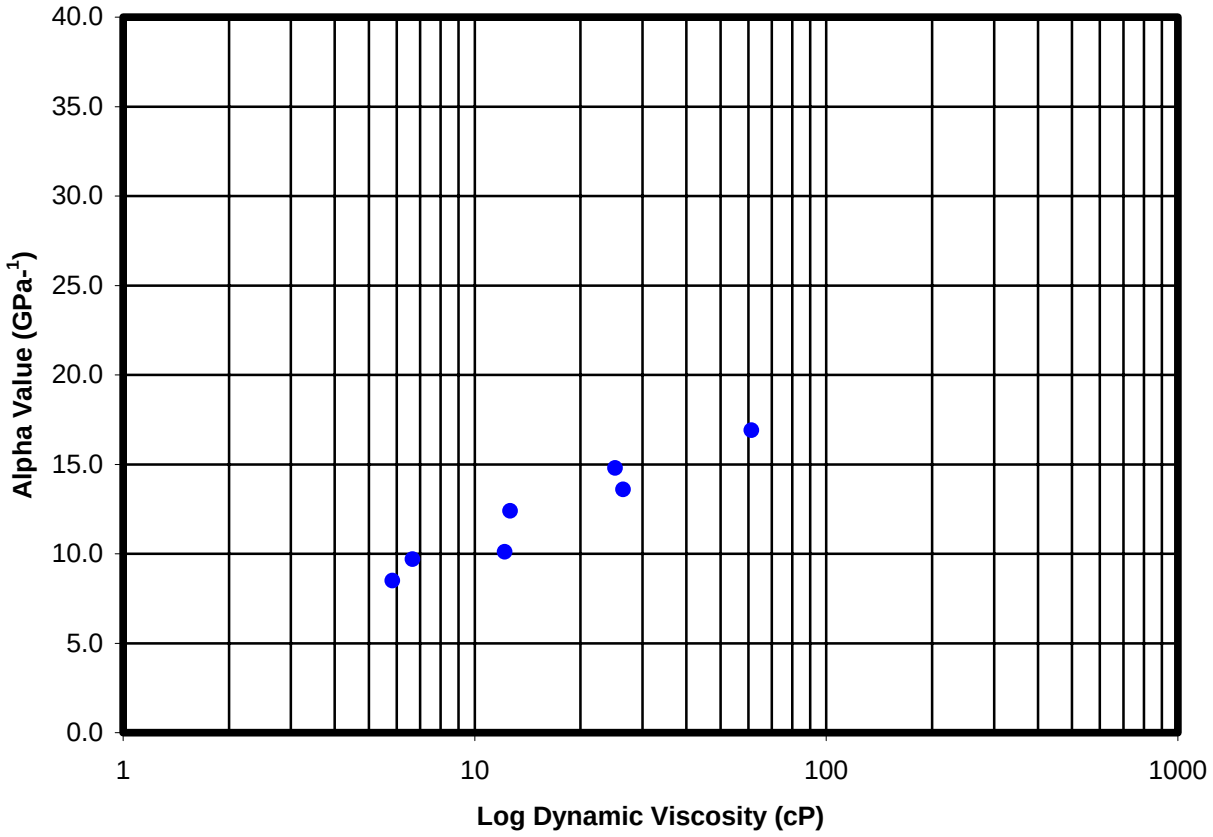

**Figure 87. Effect of Refrigerant Concentration on Effective Pressure-Viscosity Coefficient and Dynamic Viscosity for Mixtures of ISO 68 Polyolester A and R-410A**

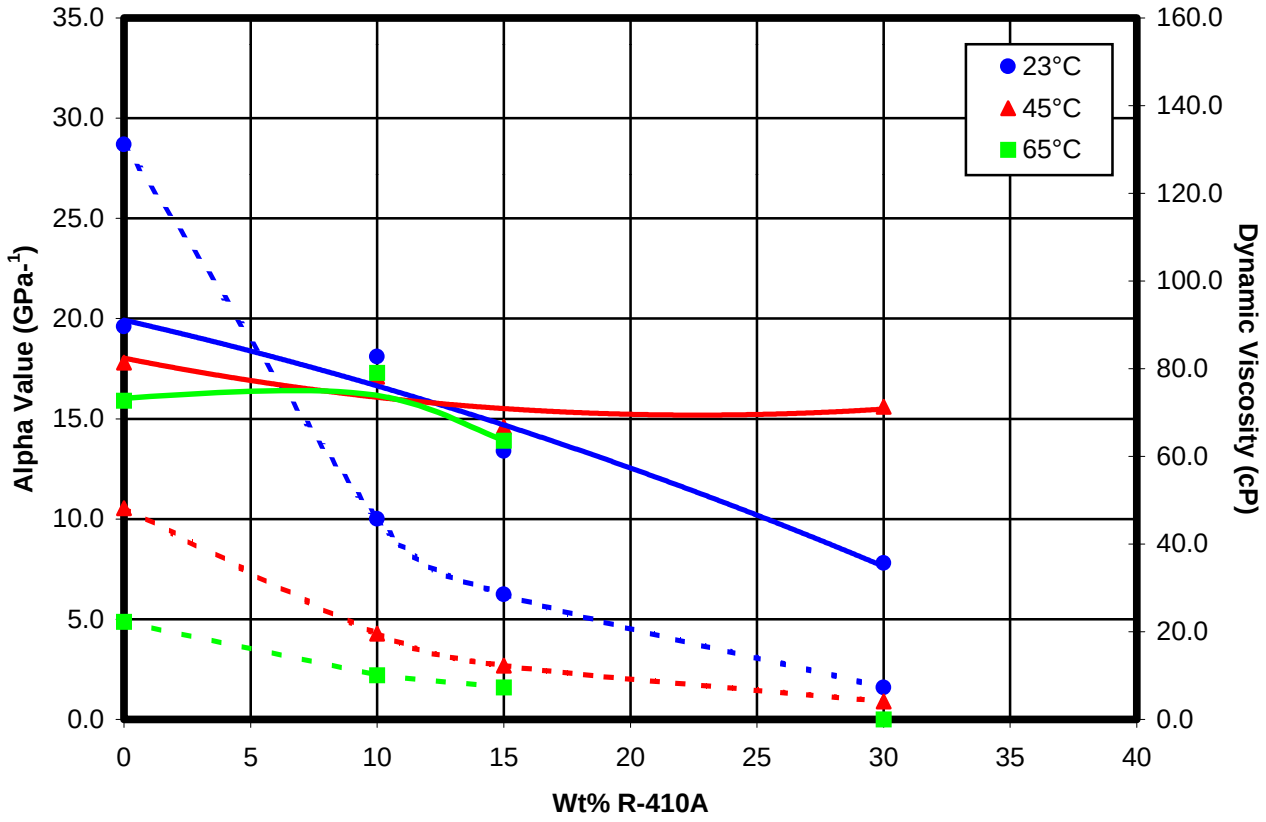


Solid lines represent alpha values
Dashed lines represent dynamic viscosities

**Figure 88. Alpha Value vs. Dynamic Viscosity for ISO 68 Polyolester A in R-410A**

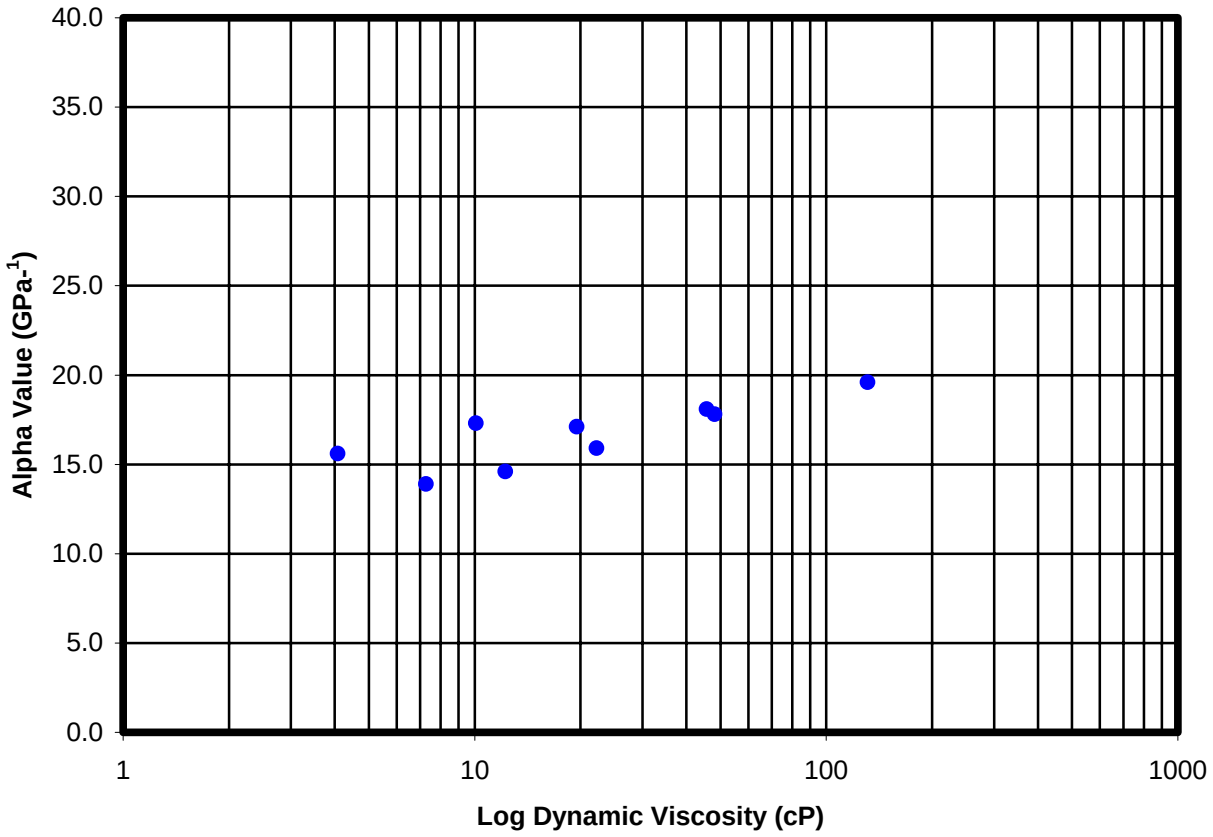

**Figure 89. Comparison of Film Thickness Data for ISO 32 Polyvinyl Ether at Ambient Temperature as a Function of R-410A Concentration**

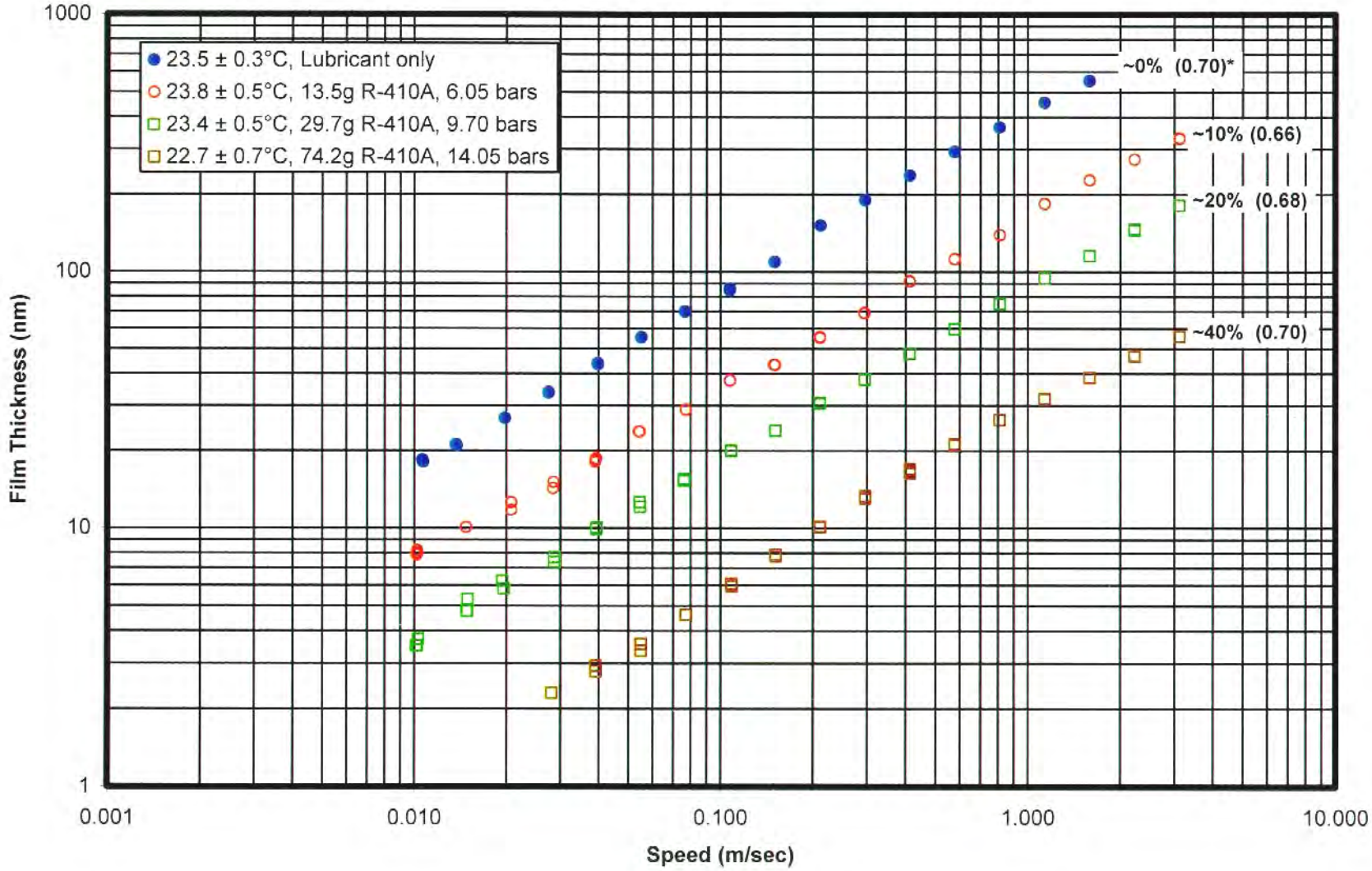


*numbers in parentheses show gradients

**Figure 90. Comparison of Film Thickness Data for ISO 32 Polyvinyl Ether at 45°C as a Function of R-410A Concentration**

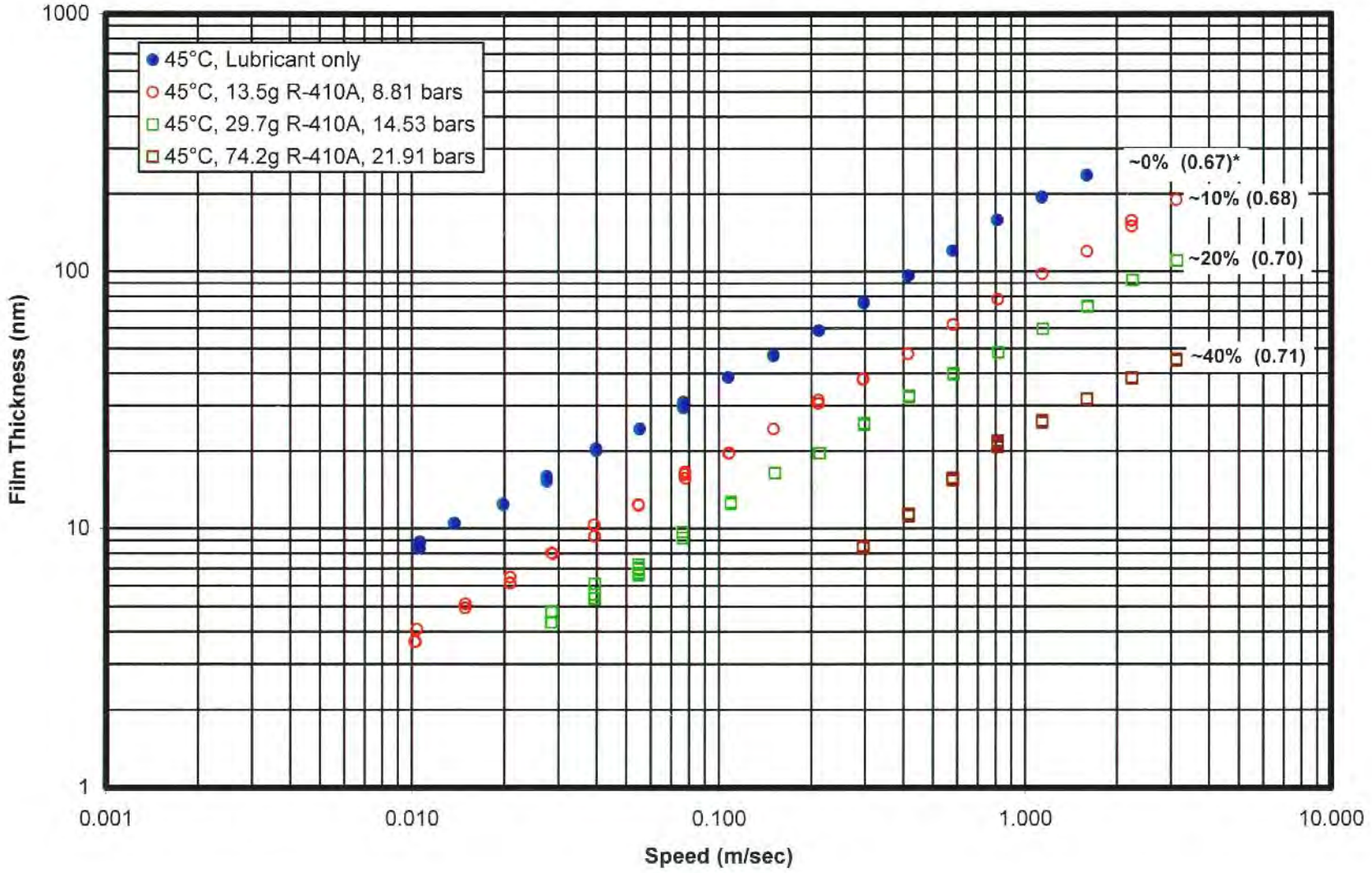


*numbers in parentheses show gradients

**Figure 91. Comparison of Film Thickness Data for ISO 32 Polyvinyl Ether at 65°C as a Function of R-410A Concentration**

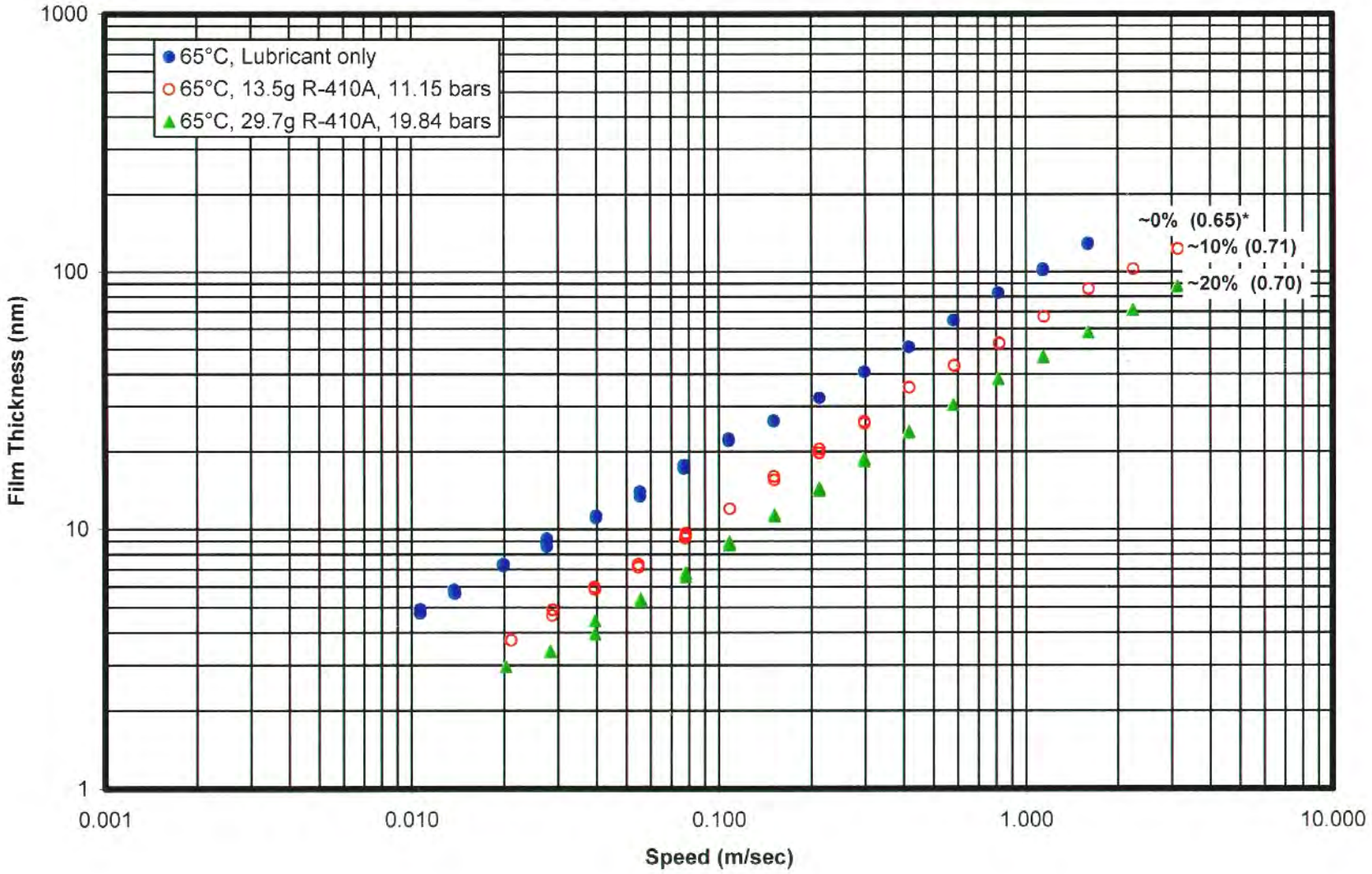


*numbers in parentheses show gradients

**Figure 92. Film Thickness vs. R-410A Concentration for ISO 32 Polyvinyl Ether**

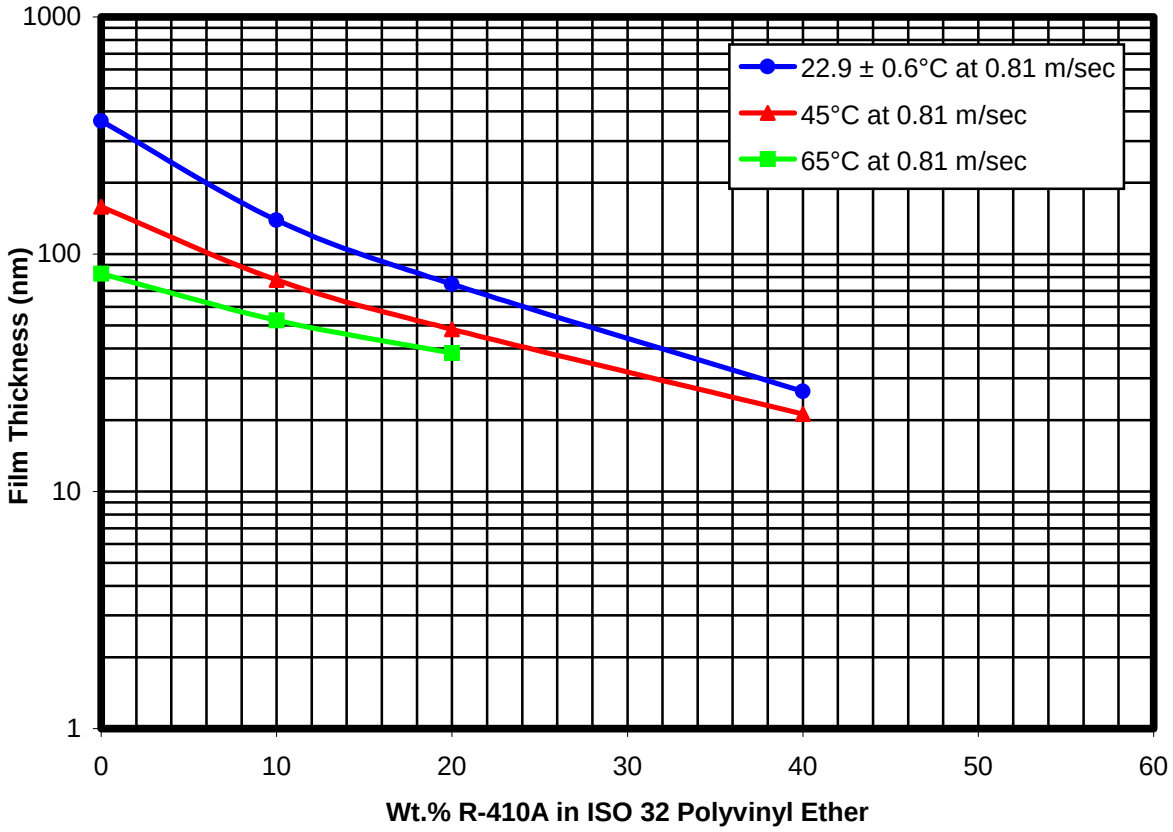

**Figure 93. Comparison of Film Thickness Data for ISO 68 Polyvinyl Ether at Ambient Temperature as a Function of R-410A Concentration**

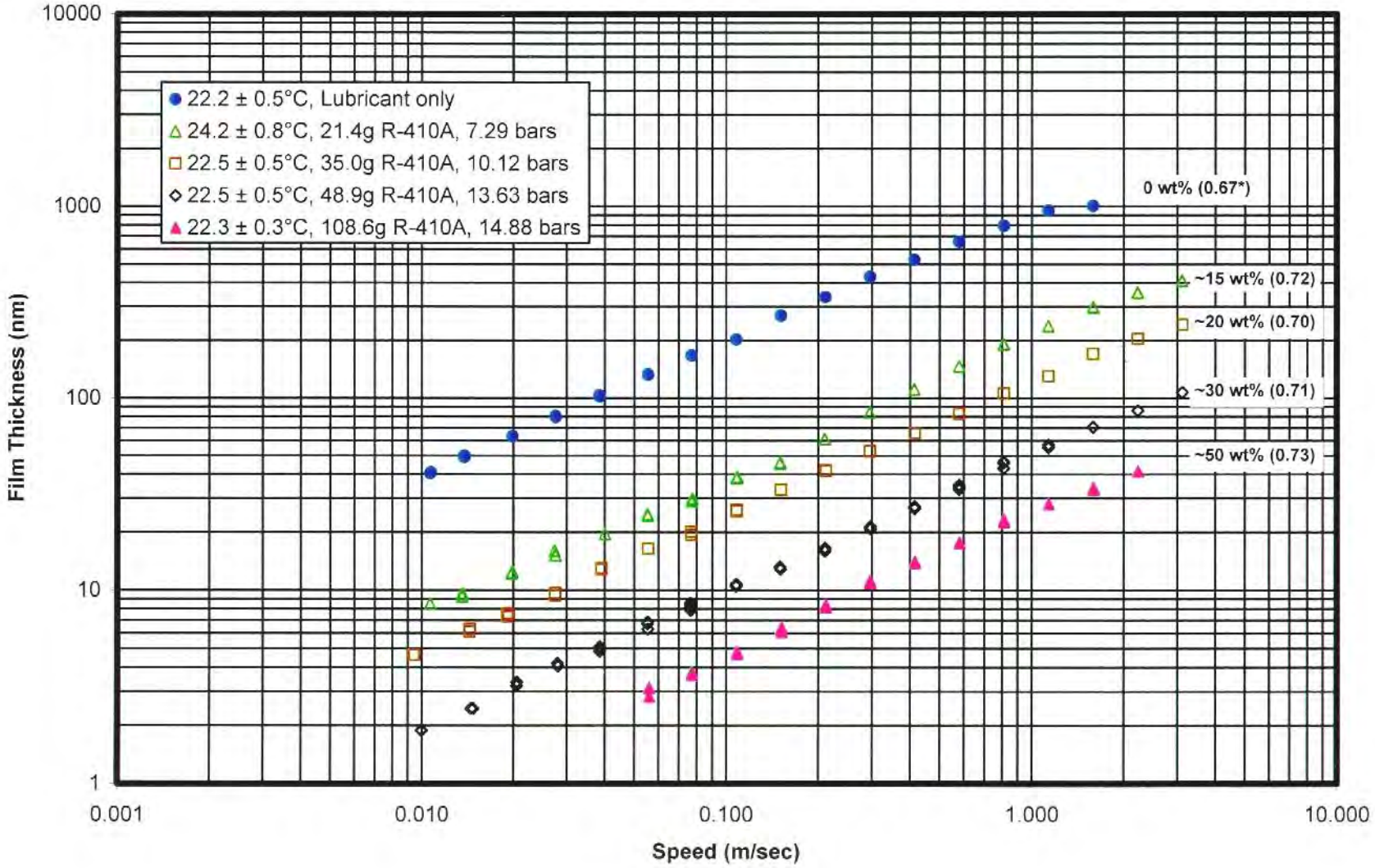


*numbers in parentheses show gradients

**Figure 94. Comparison of Film Thickness Data for ISO 68 Polyvinyl Ether at 45°C as a Function of R-410A Concentration**

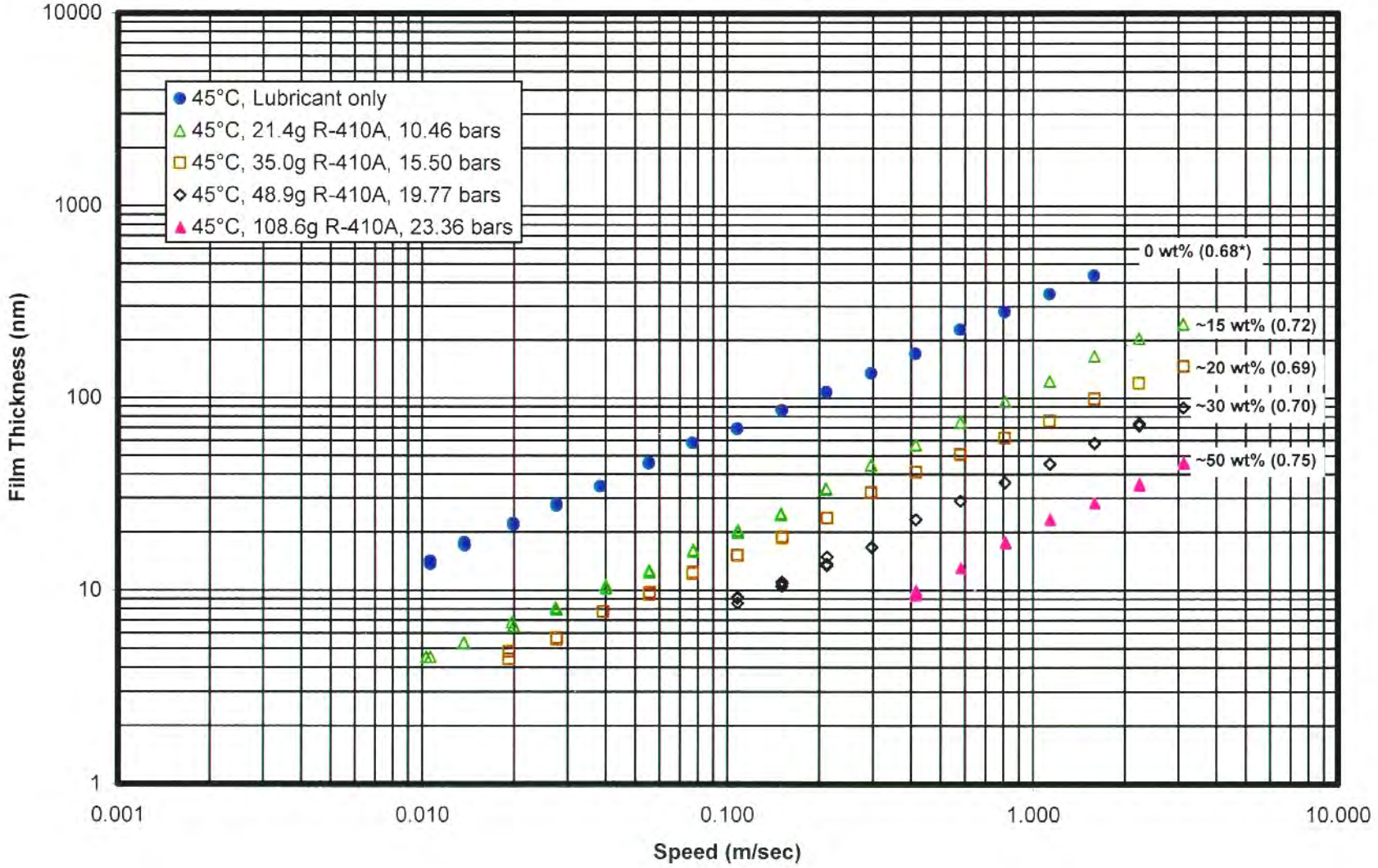


*numbers in parentheses show gradients

**Figure 95. Comparison of Film Thickness Data for ISO 68 Polyvinyl Ether at 65°C as a Function of R-410A Concentration**

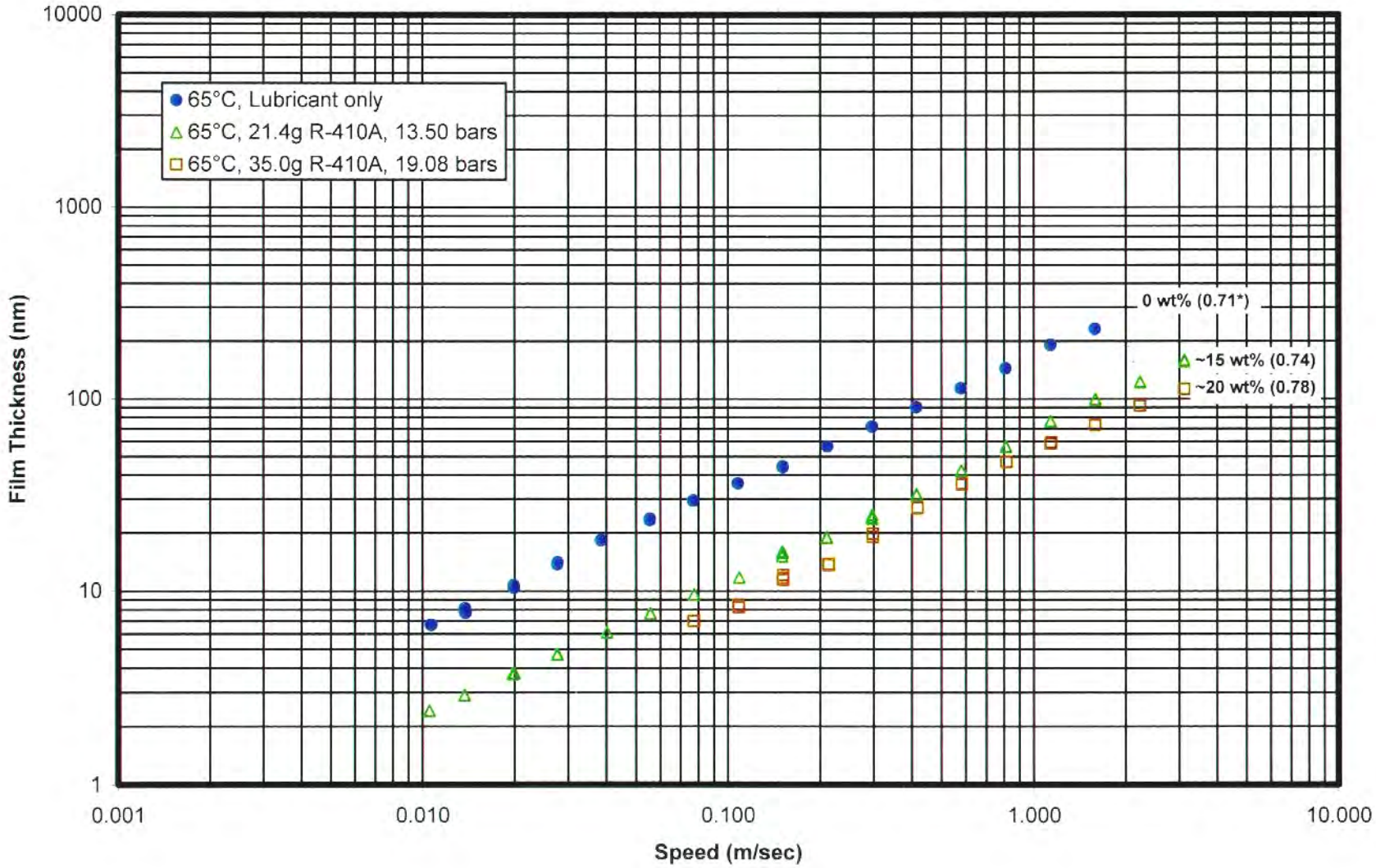


*numbers in parentheses show gradients

**Figure 96. Film Thickness vs. R-410A Concentration for ISO 68 Polyvinyl Ether**

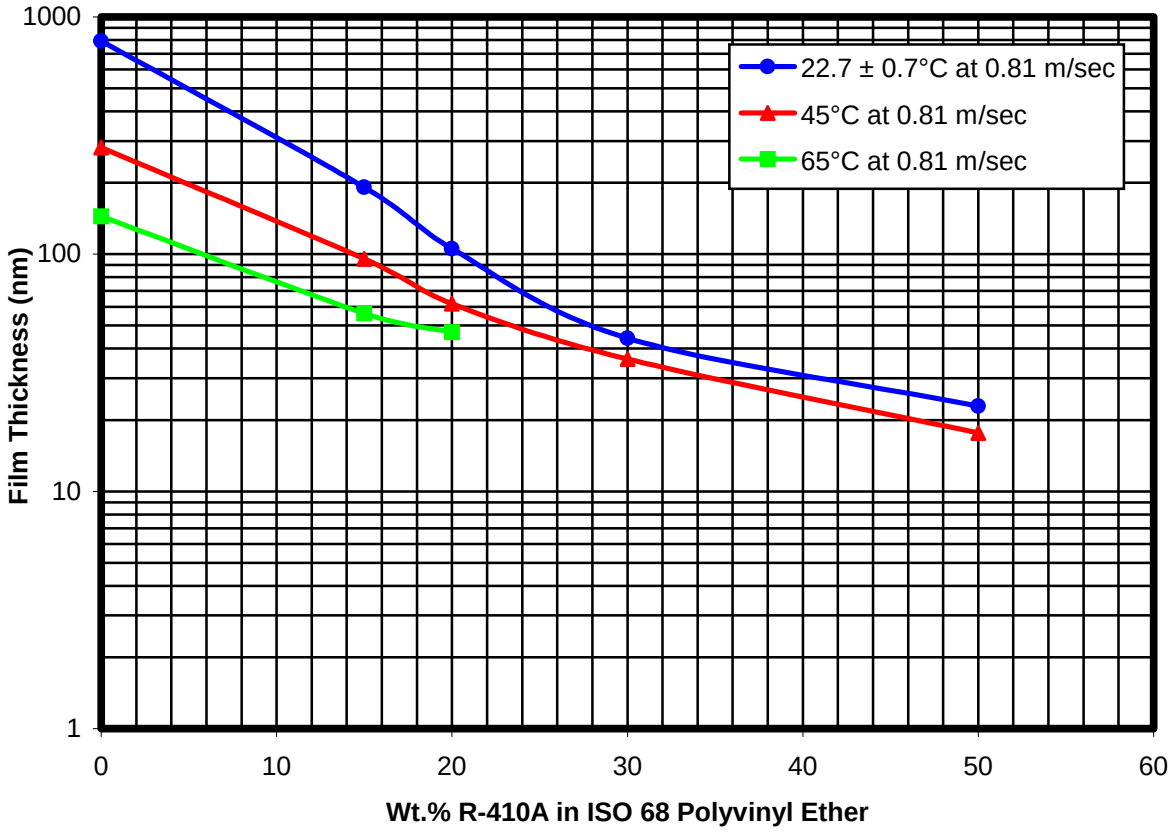

**Figure 97. Effect of Refrigerant Concentration on Effective Pressure-Viscosity Coefficient and Dynamic Viscosity for Mixtures of ISO 32 Polyvinyl Ether and R-410A**

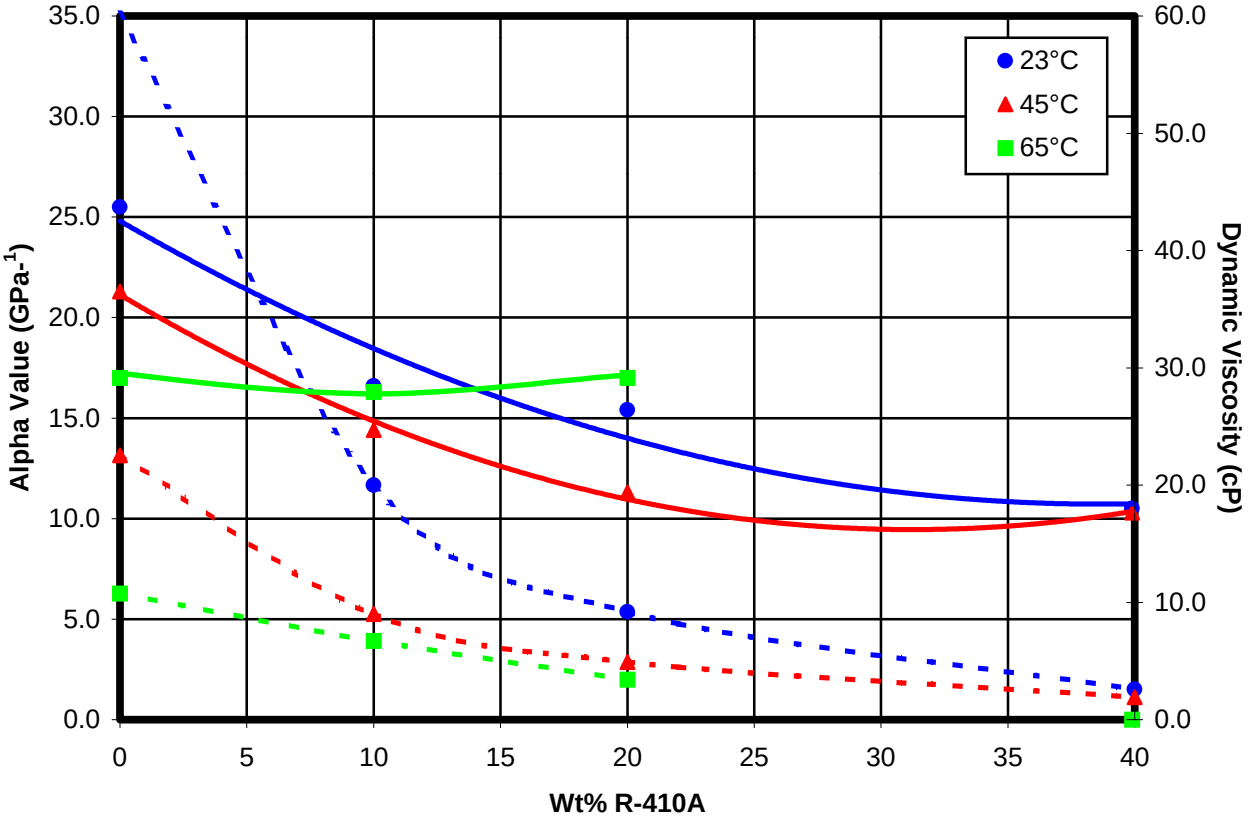


Solid lines represent alpha values
Dashed lines represent dynamic viscosities

**Figure 98. Alpha Value vs. Dynamic Viscosity for ISO 32 Polyvinyl Ether in R-410A**

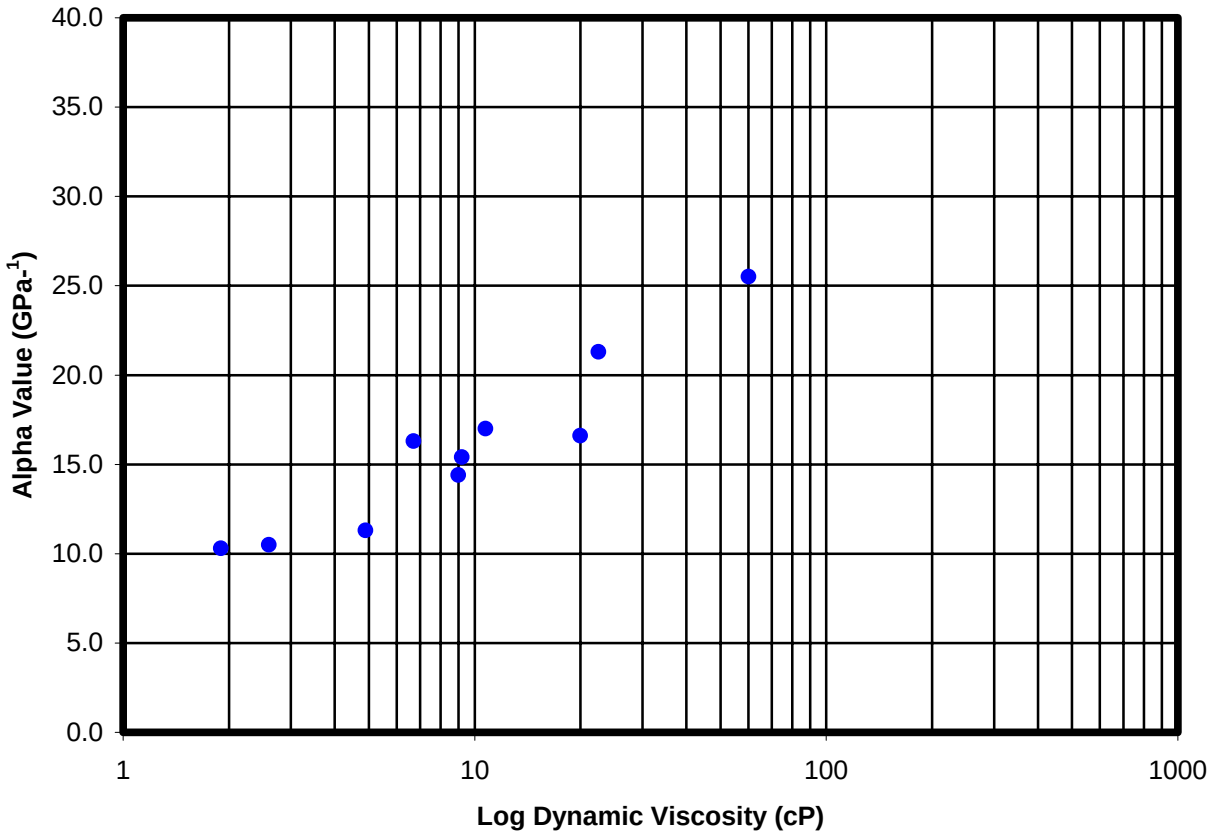

**Figure 99. Effect of Refrigerant Concentration on Effective Pressure-Viscosity Coefficient and Dynamic Viscosity for Mixtures of ISO 68 Polyvinyl Ether and R-410A**

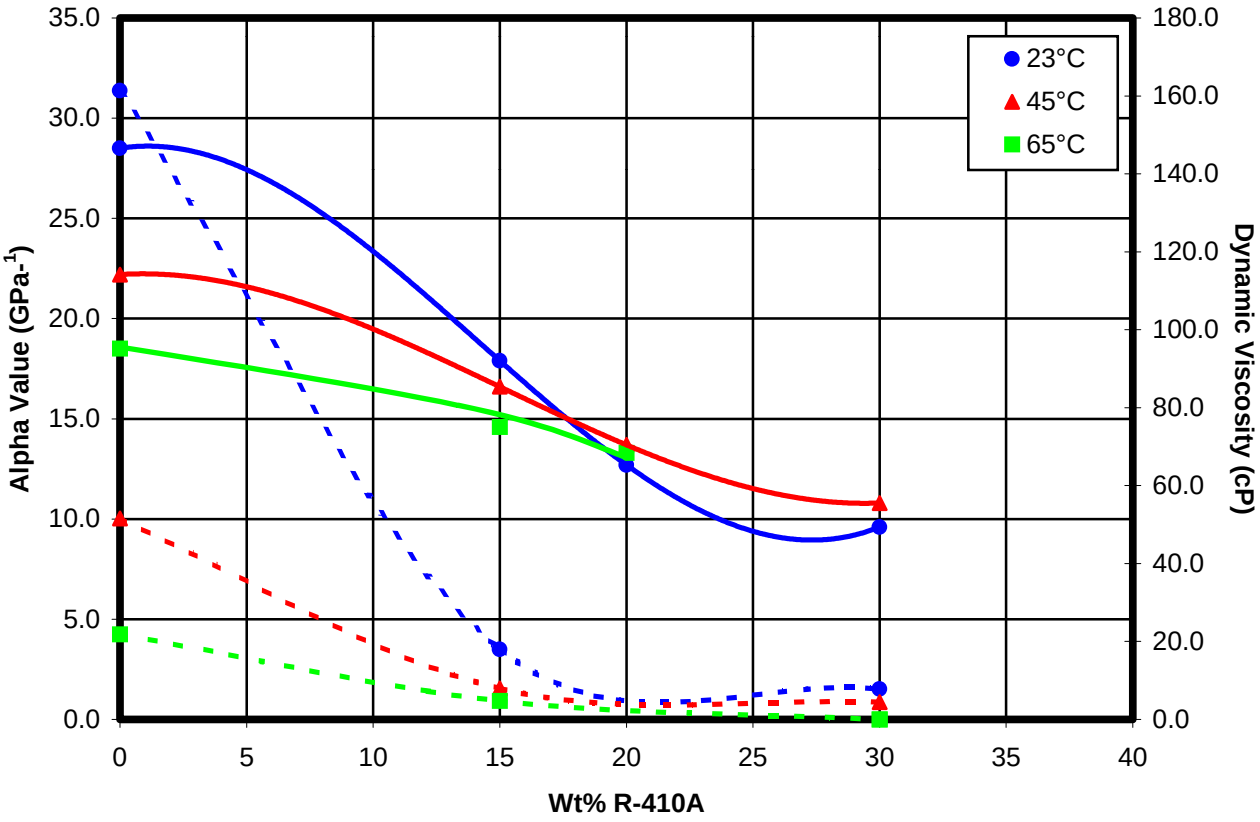


Solid lines represent alpha values
Dashed lines represent dynamic viscosities

**Figure 100. Alpha Value vs. Dynamic Viscosity for ISO 68 Polyvinyl Ether in R-410A**

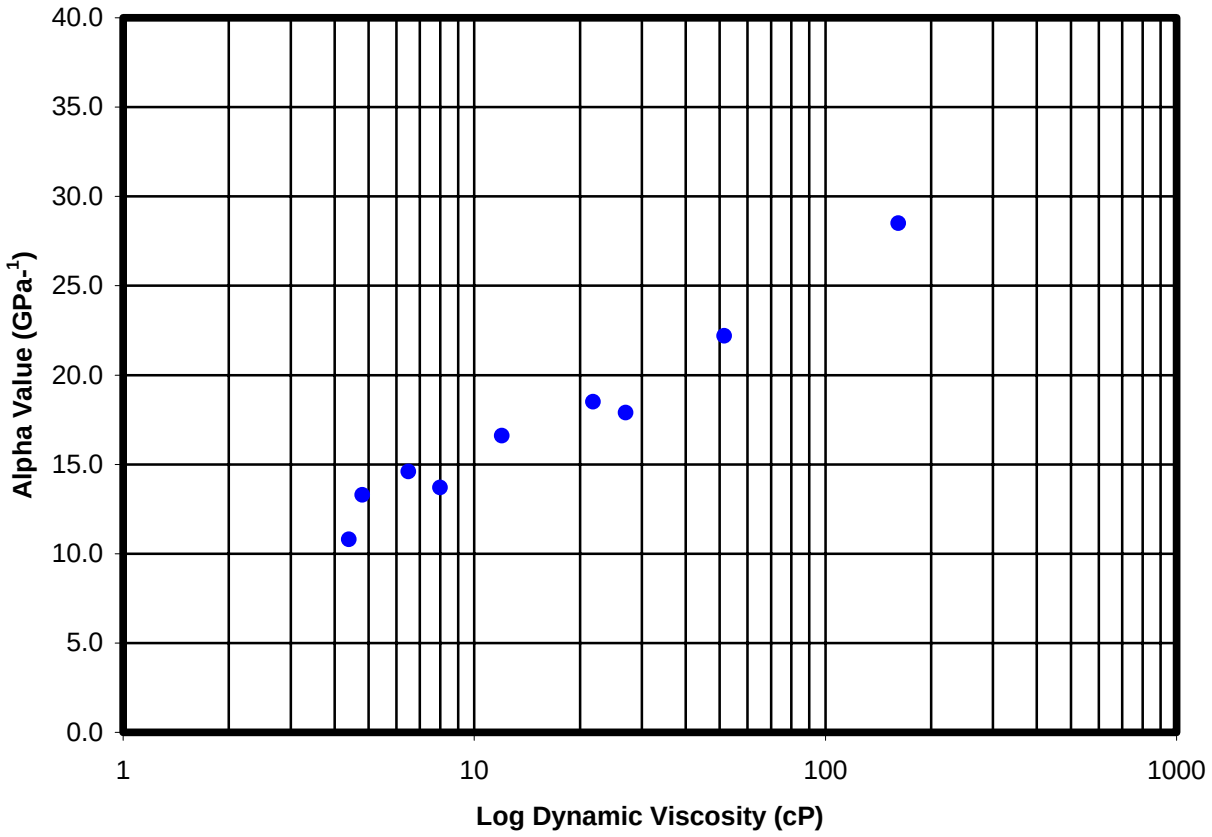

## 6.8 Comparison of Different Lubricant/Refrigerant Systems

### 6.8.1 Polyolesters/R-134a vs. Mineral Oils/R-22

Figures 101 through 106 compare the film thickness measured for polyolester/R-134a mixtures with those measured with mineral oil/R-22 mixtures. Figures 101 through 103 compare the data for ISO 32 fluids, whereas Figures 104 through 106 compare the data for ISO 68 fluids at the three test temperatures. It is interesting to note that when there is no refrigerant in the lubricant, mineral oils produce thicker EHD films in the contact than the esters, particularly at low temperatures. The difference becomes smaller as the temperature increases due to the higher viscosity index of the ester fluids. In the presence of refrigerants, the mineral oil/R-22 system produces thinner films in the contact as compared to the polyolester/R-134a system. The difference is more significant as the refrigerant concentration in the lubricant increases. The differences observed can be related to the dynamic viscosity of the lubricant/refrigerant mixtures. As discussed in Section 3.2, the thickness of the lubricant film formed in EHD contacts is determined by the rheology of the lubricant in the contact inlet region and depends on two fluid properties: dynamic viscosity and pressure-viscosity coefficient. As shown in Tables 14, 16, 21 and 23, the dynamic viscosity of the naphthenic mineral oil/R-22 mixtures is lower than that of the polyolester/R-134a mixtures.

### 6.8.2 Polyvinyl Ethers/R134a vs. Polyolesters/R-134a and Mineral Oils/R-22

Figures 107 through 112 compare the film thickness measured for polyvinyl ether/R-134a mixtures with those measured with polyolester/R-134a and mineral oil/R-22 mixtures. Figures 107 through 109 compare the data for ISO 32 fluids, whereas Figures 110 through 112 compare the data for ISO 68 fluids at the three test temperatures. Overall, PVE/R-134a mixtures give comparable films in thickness to POE/R-134a mixtures. At the low refrigerant concentrations (10 and 20 wt %), some differences were observed between the film formation capability of polyvinyl ethers and polyolesters in that polyvinyl ethers formed thicker films in the contact than polyolesters.

**Figure 101. ISO 32 Polyolester/R-134a vs. ISO 32 Naphthenic Mineral Oil/R-22 Mixtures**
**Film Thickness as a Function of Refrigerant Concentration at 23°C**

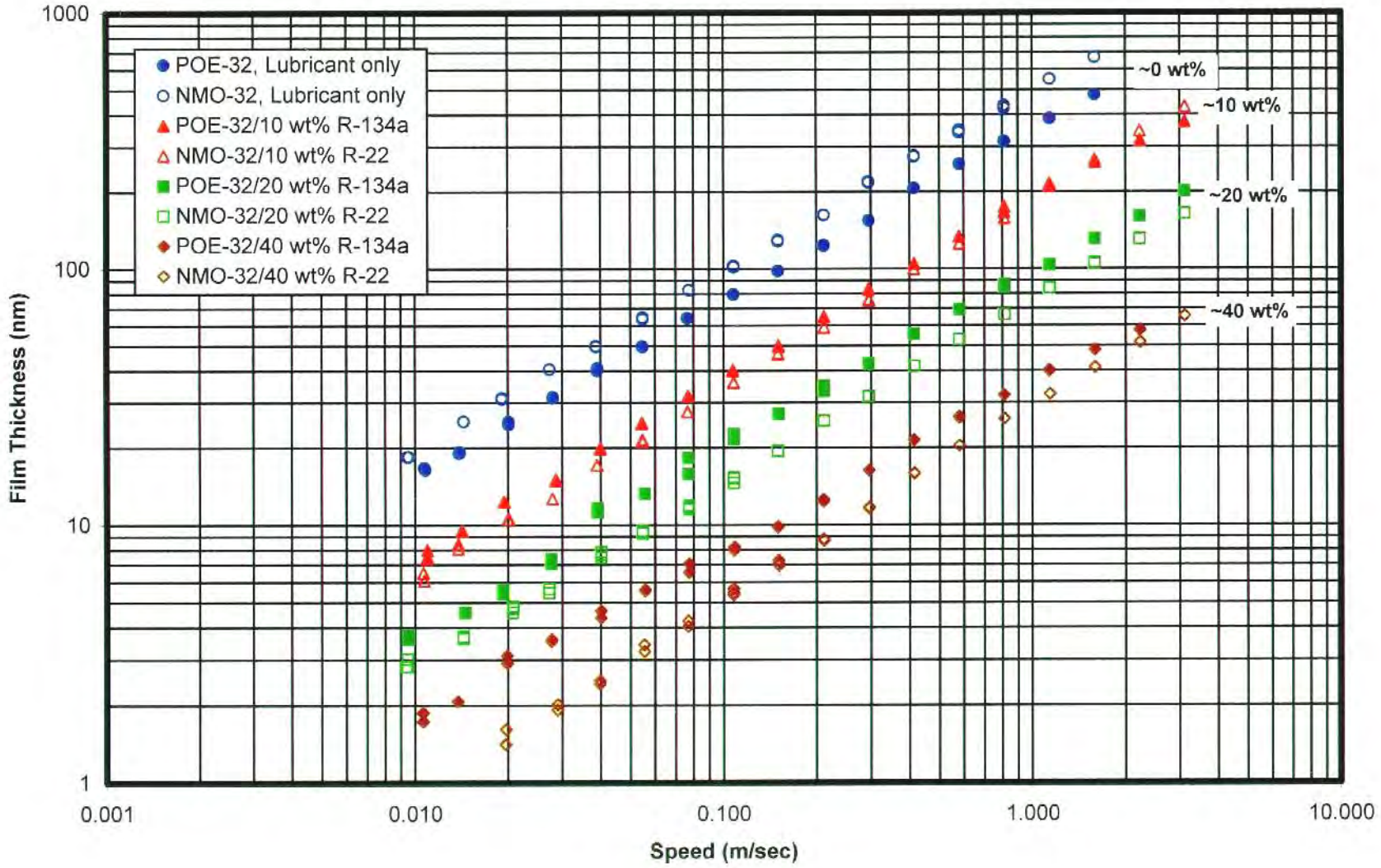

**Figure 102. ISO 32 Polyolester/R-134a vs. ISO 32 Naphthenic Mineral Oil/R-22 Mixtures**
**Film Thickness as a Function of Refrigerant Concentration at 45°C**

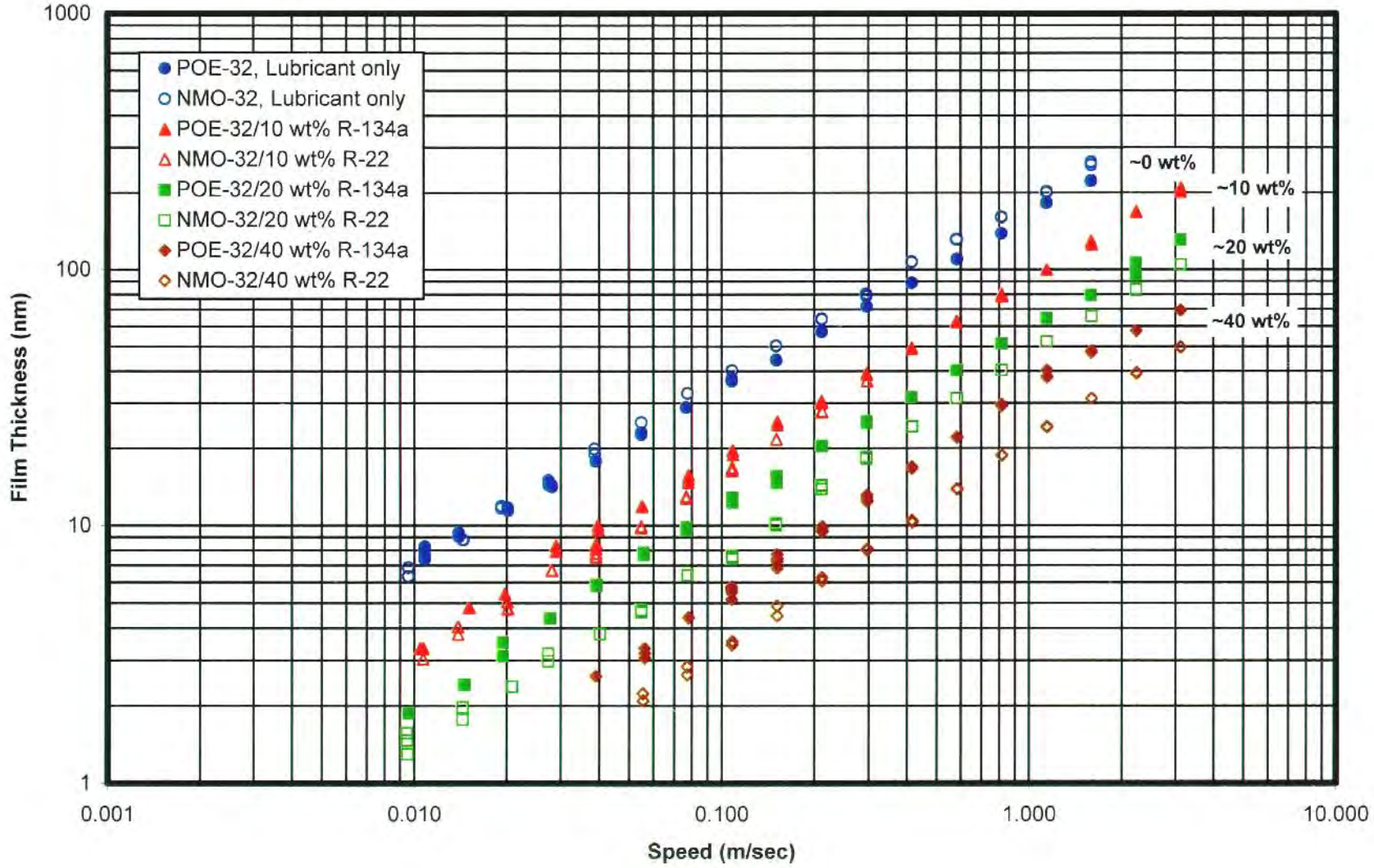

**Figure 103. ISO 32 Polyolester/R-134a vs. ISO 32 Naphthenic Mineral Oil/R-22 Mixtures**
**Film Thickness as a Function of Refrigerant Concentration at 65°C**

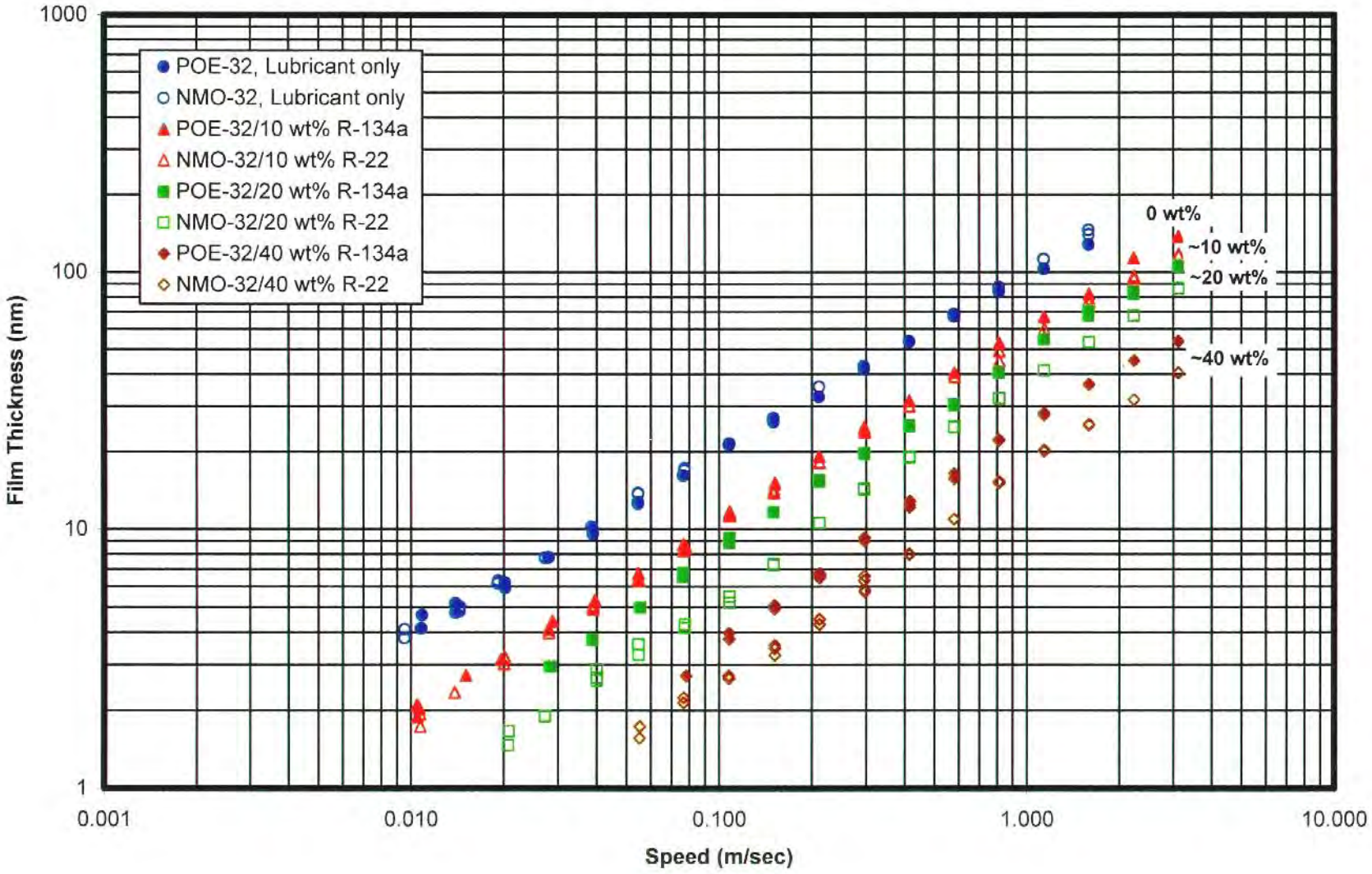

**Figure 104. ISO 68 Polyolester A/R-134a vs. ISO 68 Naphthenic Mineral Oil/R-22 Mixtures**
**Film Thickness as a Function of Refrigerant Concentration at 23°C**

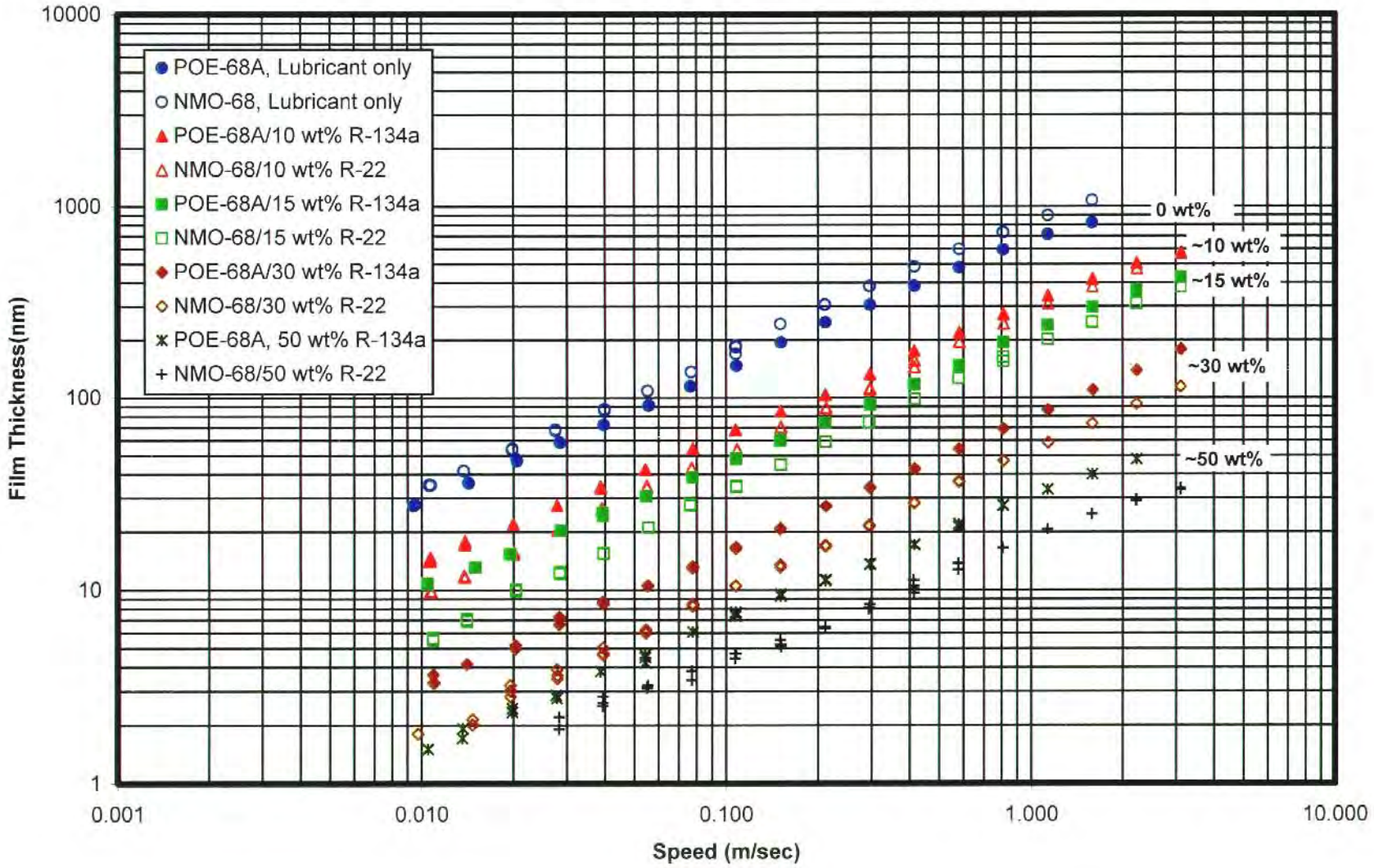

**Figure 105. ISO 68 Polyolester A/R-134a vs. ISO 68 Naphthenic Mineral Oil/R-22 Mixtures**
**Film Thickness as a Function of Refrigerant Concentration at 45°C**

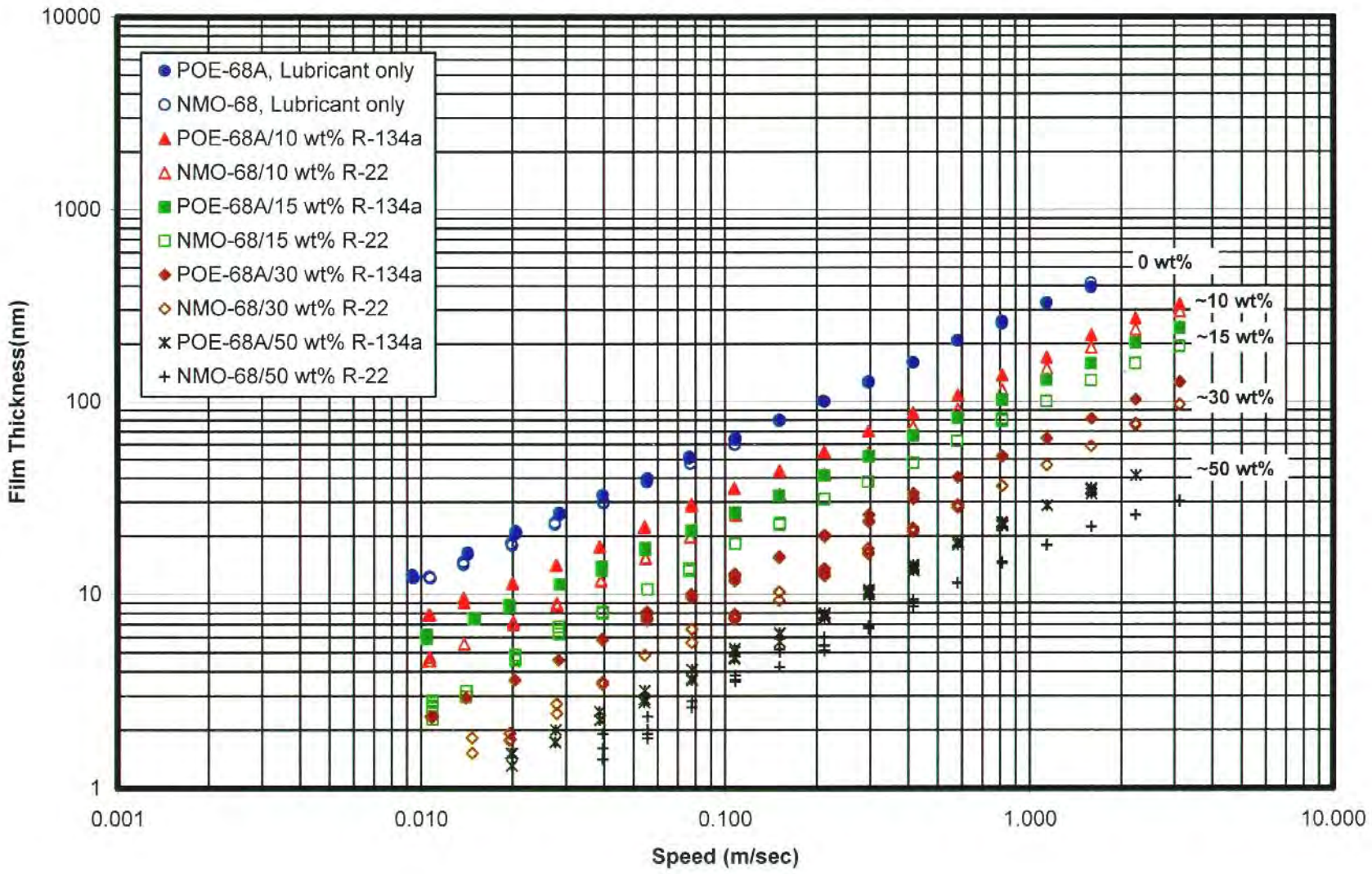

**Figure 106. ISO 68 Polyolester A/R-134a vs. ISO 68 Naphthenic Mineral Oil/R-22 Mixtures**
**Film Thickness as a Function of Refrigerant Concentration at 65°C**

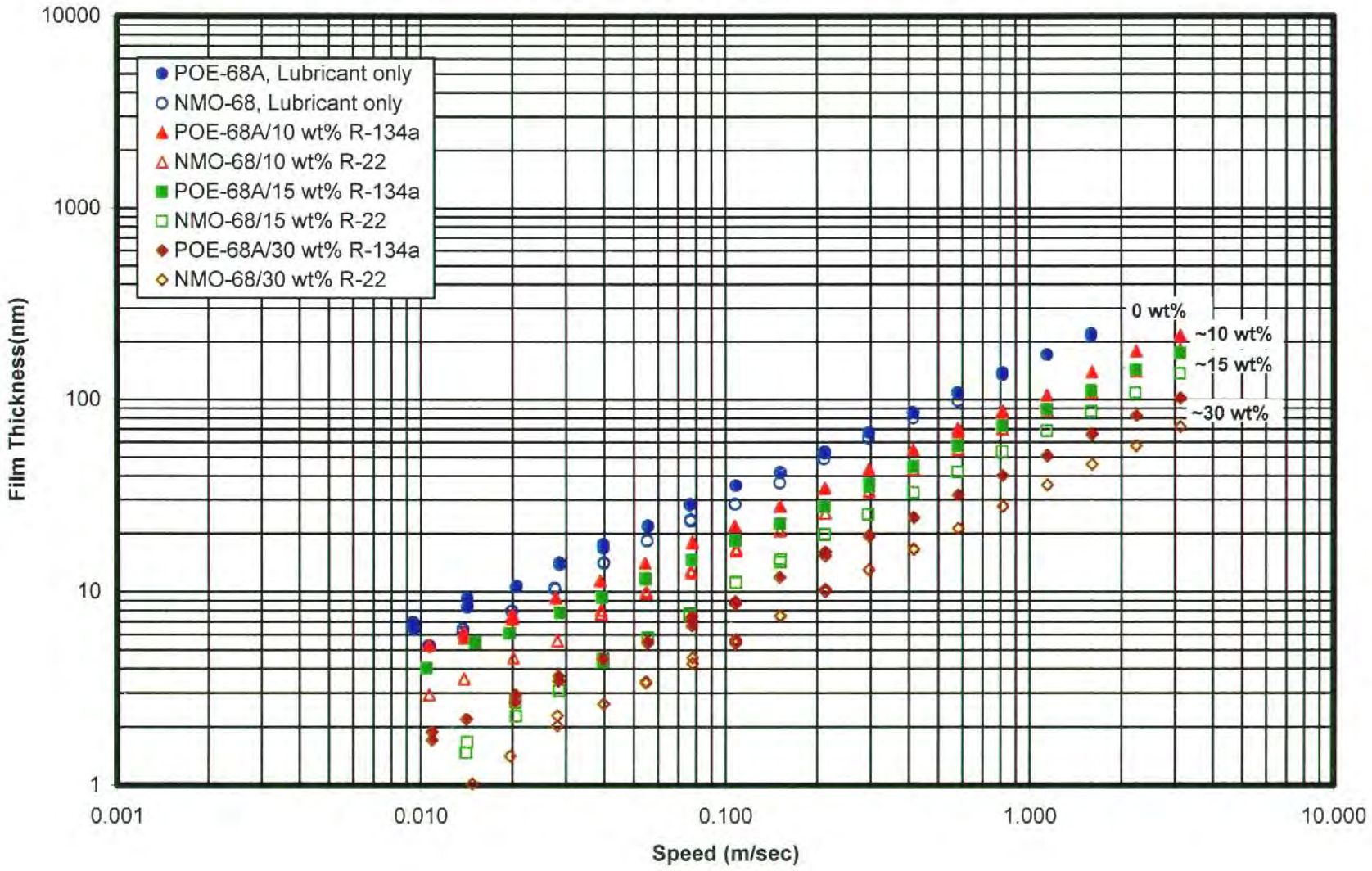

**Figure 107. ISO 32 Polyolester/R-134a, ISO 32 Polyvinyl Ether/R-134a and ISO 32 Naphthenic Mineral Oil/R-22 Mixtures - Film Thickness as a Function of Refrigerant Concentration at 23°C**

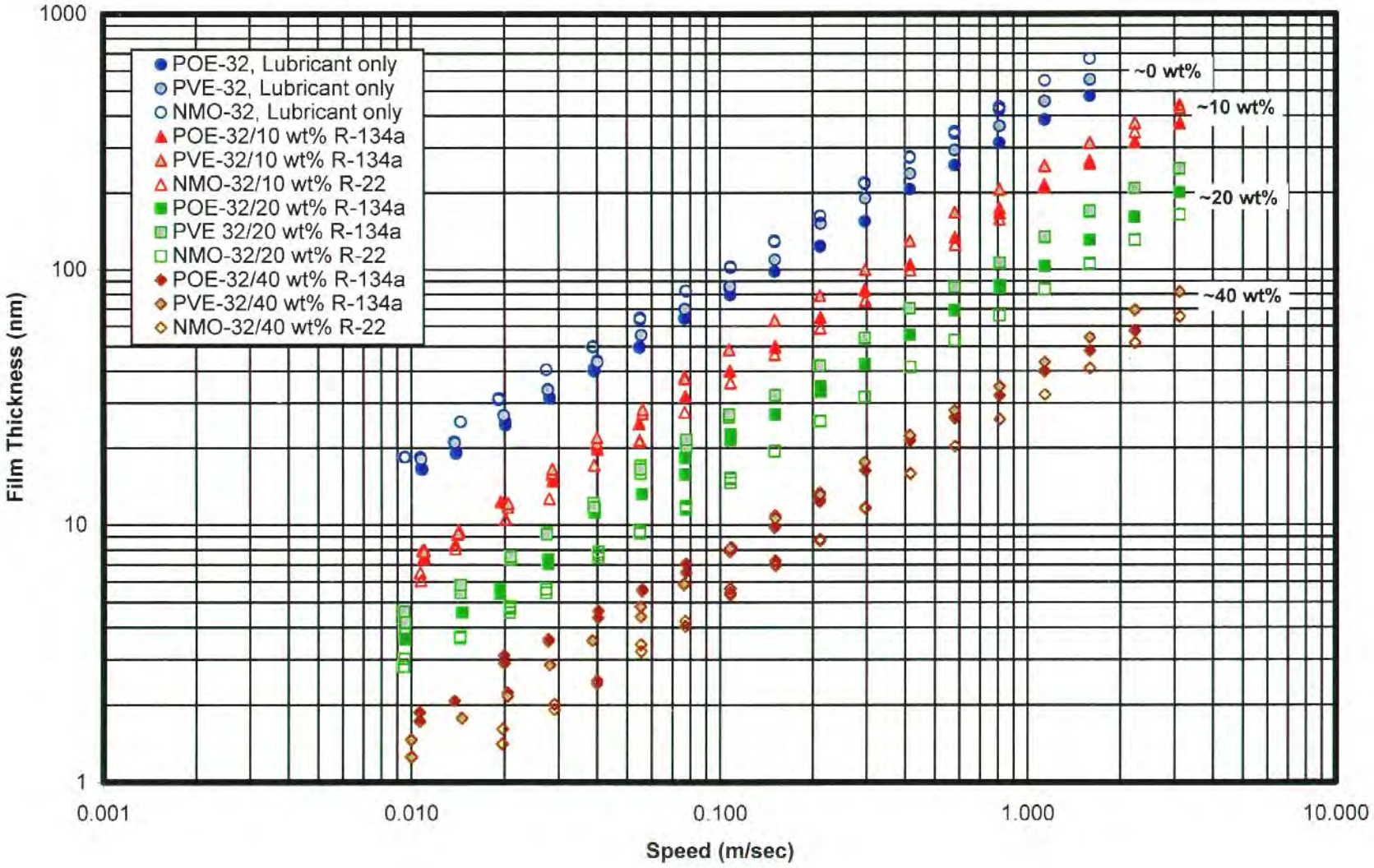

**Figure 108. ISO 32 Polyolester/R-134a, ISO 32 Polyvinyl Ether/R-134a and ISO 32 Naphthenic Mineral Oil/R-22 Mixtures - Film Thickness as a Function of Refrigerant Concentration at 45°C**

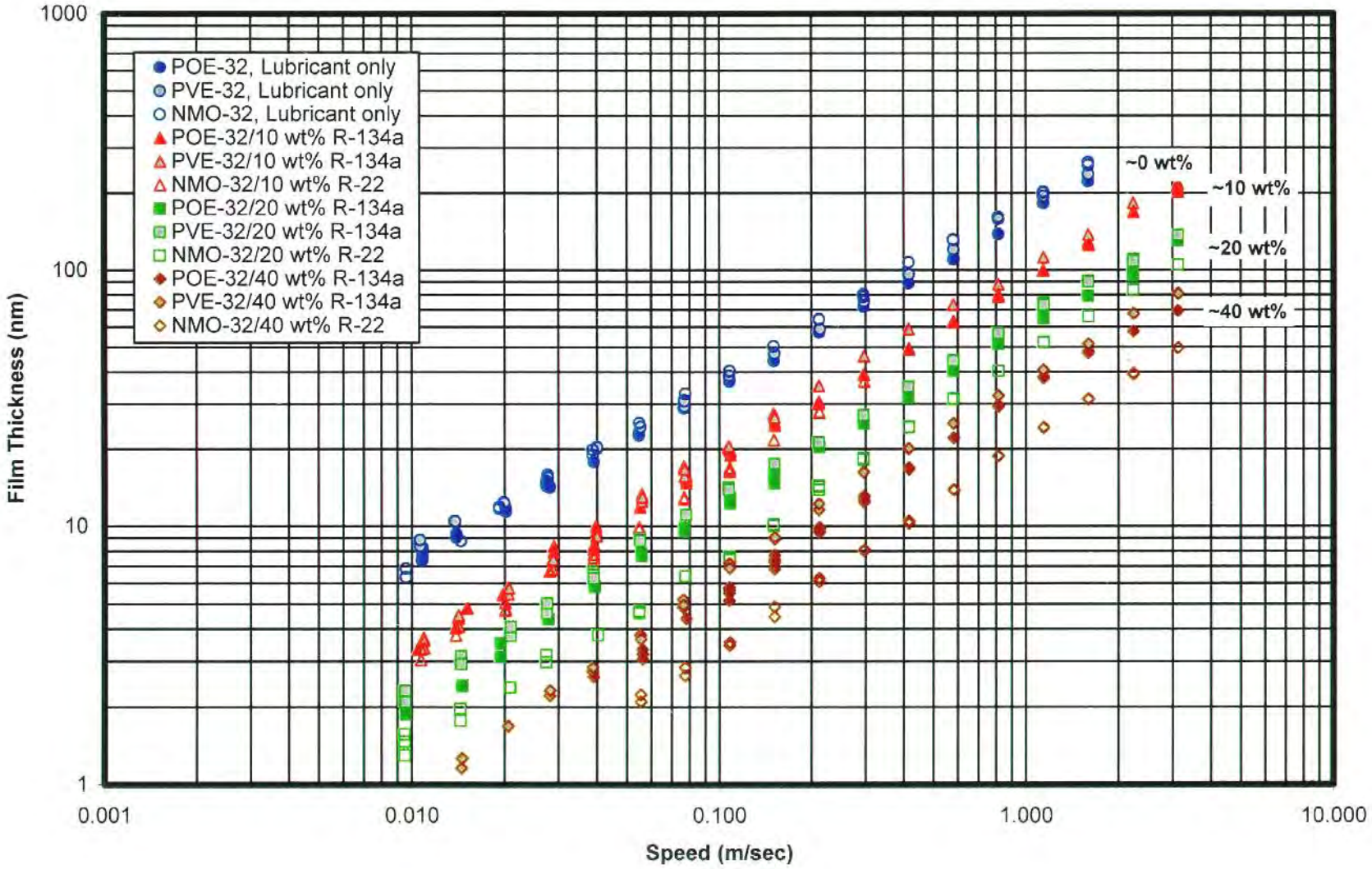

**Figure 109. ISO 32 Polyolester/R-134a, ISO 32 Polyvinyl Ether/R-134a and ISO 32 Naphthenic Mineral Oil/R-22 Mixtures - Film Thickness as a Function of Refrigerant Concentration at 65°C**

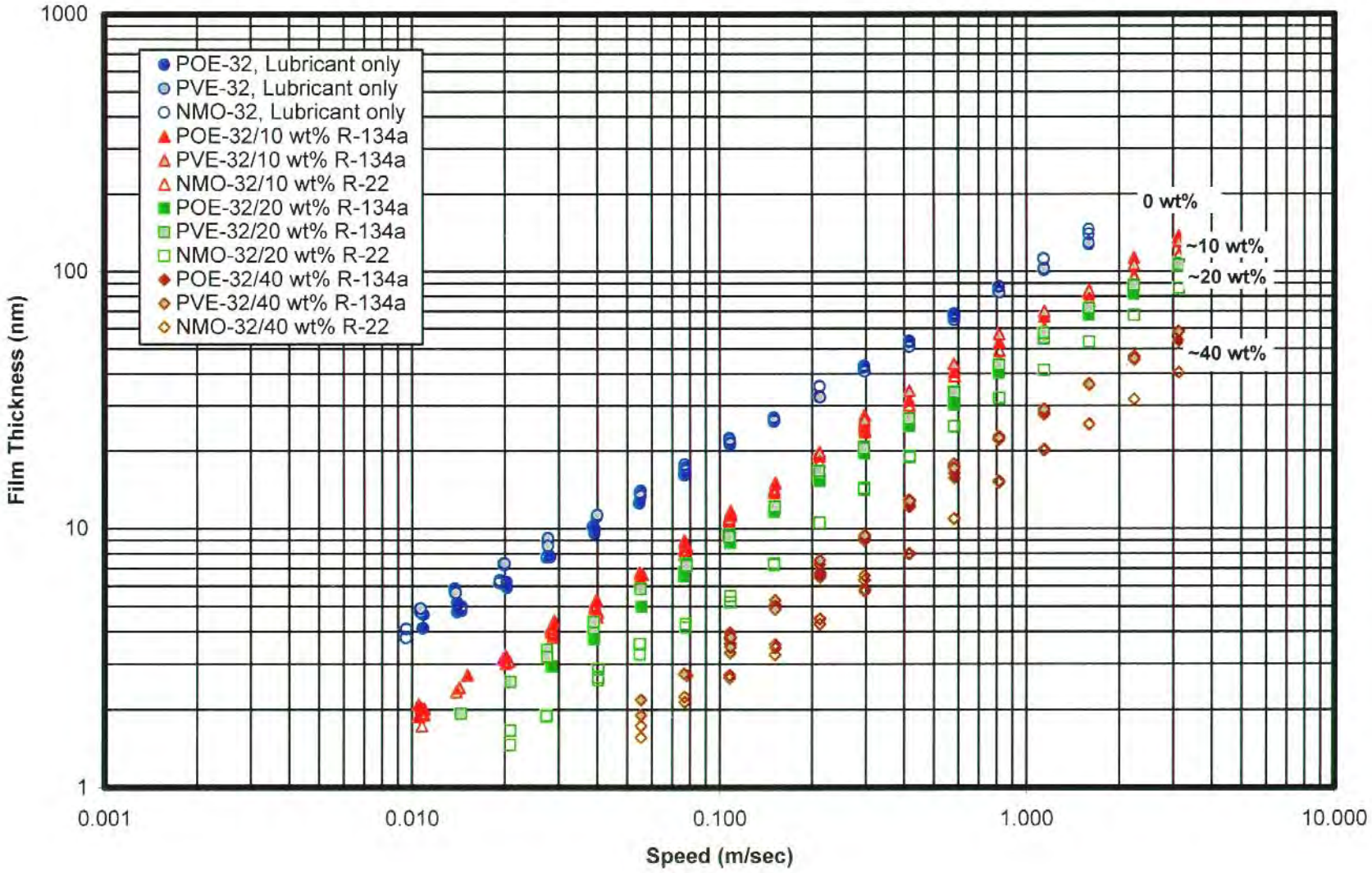

**Figure 110. ISO 68 Polyolester A/R-134a, ISO 68 Polyvinyl Ether/R-134a and ISO 68 Naphthenic Mineral Oil/R-22 Mixtures - Film Thickness as a Function of Refrigerant Concentration at 23°C**

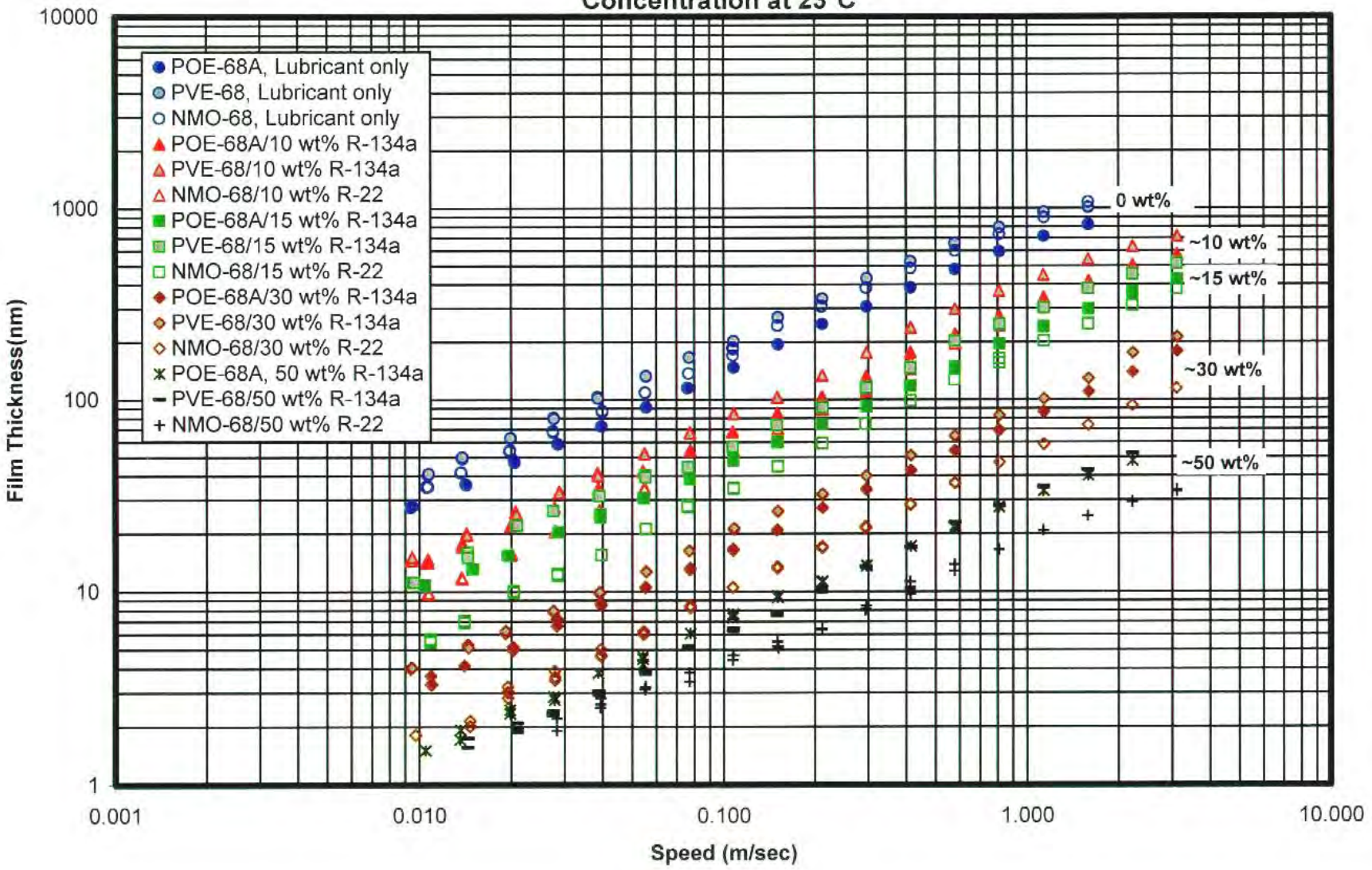

**Figure 111. ISO 68 Polyolester A/R-134a, ISO 68 Polyvinyl Ether/R-134a and ISO 68 Naphthenic Mineral Oil/R-22 Mixtures - Film Thickness as a Function of Refrigerant Concentration at 45°C**

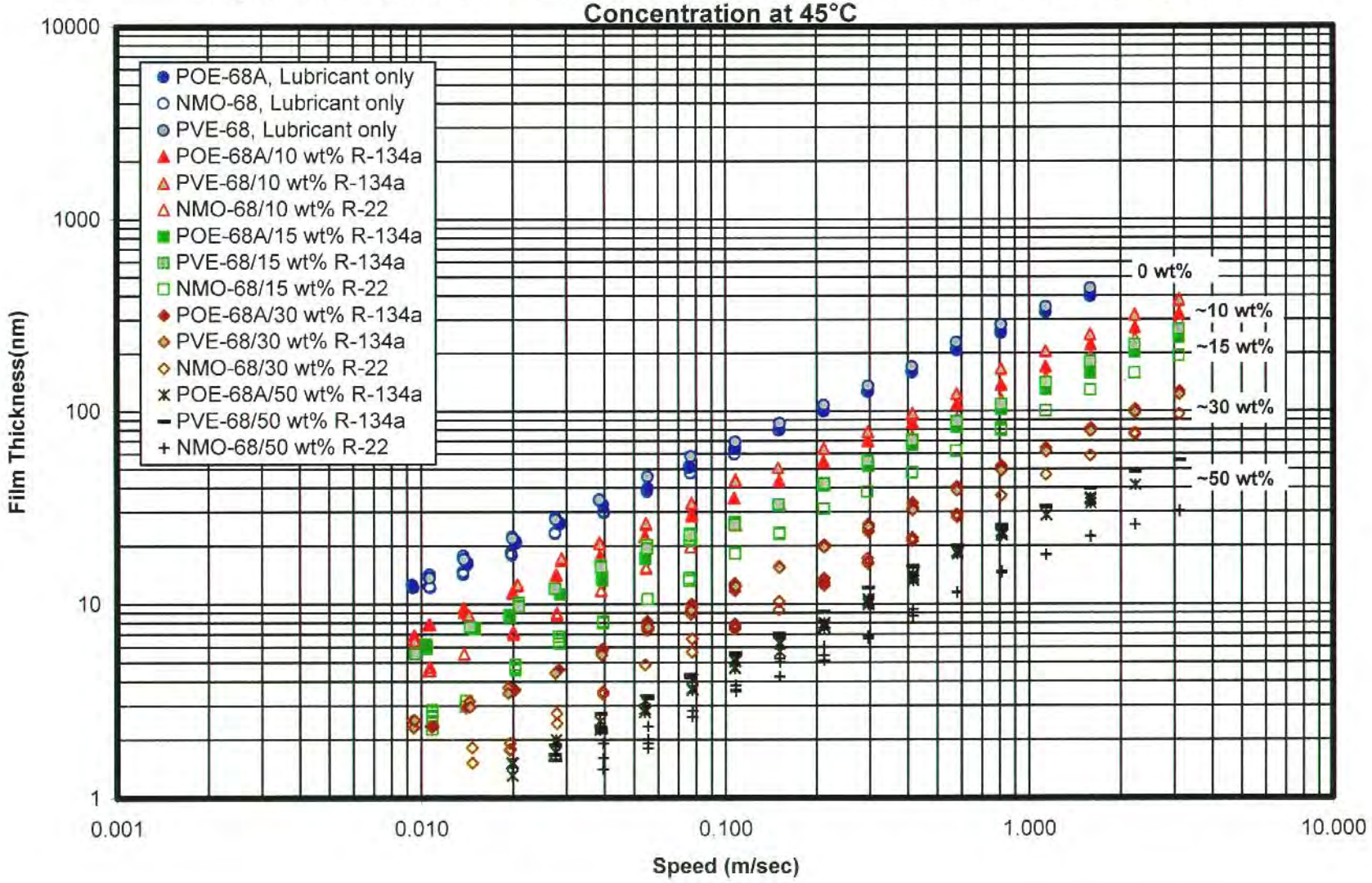

**Figure 112. ISO 68 Polyolester A/R-134a, ISO 68 Polyvinyl Ether/R-134a and ISO 68 Naphthenic Mineral Oil/R-22 Mixtures - Film Thickness as a Function of Refrigerant Concentration at 65°C**

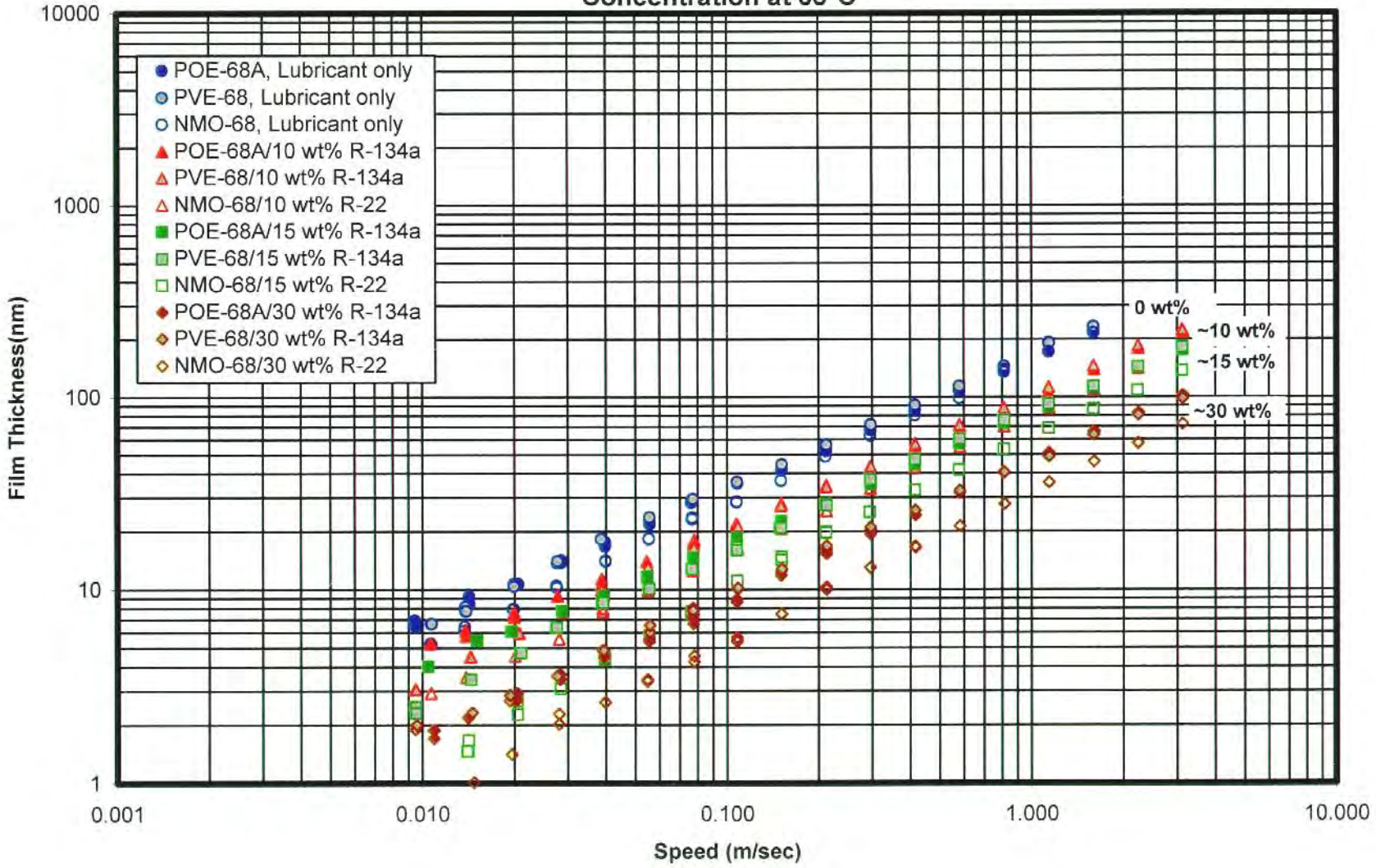

### 6.8.3 Polyolesters/R410A vs. Mineral Oils/R-22

Figures 113 through 118 compare the film thickness measured for polyolesters/R-410A mixtures with those measured with mineral oil/R-22 mixtures. Figures 113 through 115 compare the data for ISO 32 fluids, whereas Figures 116 through 118 compare the data for ISO 68 fluids at the three test temperatures. Overall, polyolester/R-410A mixtures give comparable films in thickness to mineral oil/R-22 mixtures.

### 6.8.4 Polyvinyl Ethers/R-410A vs. Polyolesters/R-410A and Mineral Oil/R-22

Figures 119 through 124 compare the film thickness measured for polyvinyl ether/R-410A mixtures with those measured with polyolester/R-410A and mineral oil/R-22 mixtures. Figures 119 through 121 compare the data for ISO 32 fluids, whereas Figures 122 through 124 compare the data for ISO 68 fluids at the three test temperatures. Overall, PVE/R-410A mixtures give comparable films in thickness to POE/R-410A mixtures. With the lower viscosity fluids (ISO 32), polyvinyl ether/R-410A mixtures appear to form thicker films in the contact than polyolester/R-410A and mineral oil/R-22 mixtures.

### 6.8.5 R-410A vs. R-134a

Figures 125 through 130 compare the film thickness measured for polyolester/R-134a mixtures with those measured with polyolester/R-410A mixtures. The data indicates that mixtures of polyolester/R-410A produce thinner films in the contact than those of the same lubricant and R-134a. The same result was observed for polyvinyl ethers, as shown in Figures 131 through 136, i.e. the presence of R-410A in the lubricant results in thinner films in the contact than that of R-134a.

### 6.8.6 Effective Pressure-Viscosity Coefficients

Figures 137 through 142 compare the pressure-viscosity coefficients of the various lubricant and refrigerant mixtures tested. The comparisons were shown for ISO 32 fluids.

However, the same trends were also observed for the ISO 68 fluids. The results are summarized as follows:

- POE/R-410A vs. PVE/R-410A: Mixtures with PVE have higher $\alpha$-values than those with polyolesters at all test temperatures.
- POE/R-134a vs. PVE/R-134a: Mixtures with PVE have higher $\alpha$-values than those with polyolesters at all test temperatures.
- PVE/R-134a vs. NMO/R-22: Mixtures with NMO/R-22 have higher $\alpha$-values than those with PVE/R-134a. However, the differences become smaller as the temperature and refrigerant concentration increase.
- POE/R-134a vs. NMO/R-22: NMO/R-22 mixtures have higher $\alpha$-values than POE/R-134a.
- PVE/R-410A vs. NMO/R-22: Mixtures with NMO/R-22 have higher $\alpha$-values than those with PVE/R-410A. However, the differences become smaller as the temperature and refrigerant concentration increase.
- POE/R-410A vs. NMO/R-22: NMO/R-22 mixtures have higher $\alpha$-values than POE/R-410A.

A graphical ranking of all the tested lubricant/refrigerant combinations is shown in Figures 143 through 145. The film thickness data reported in these figures were obtained under the same conditions of temperature (22.5 °C) and speed (0.8 m/s).

**Figure 113. ISO 32 Polyolester/R-410A vs. ISO 32 Naphthenic Mineral Oil/R-22 Mixtures**
**Film Thickness as a Function of Refrigerant Concentration at 23°C**

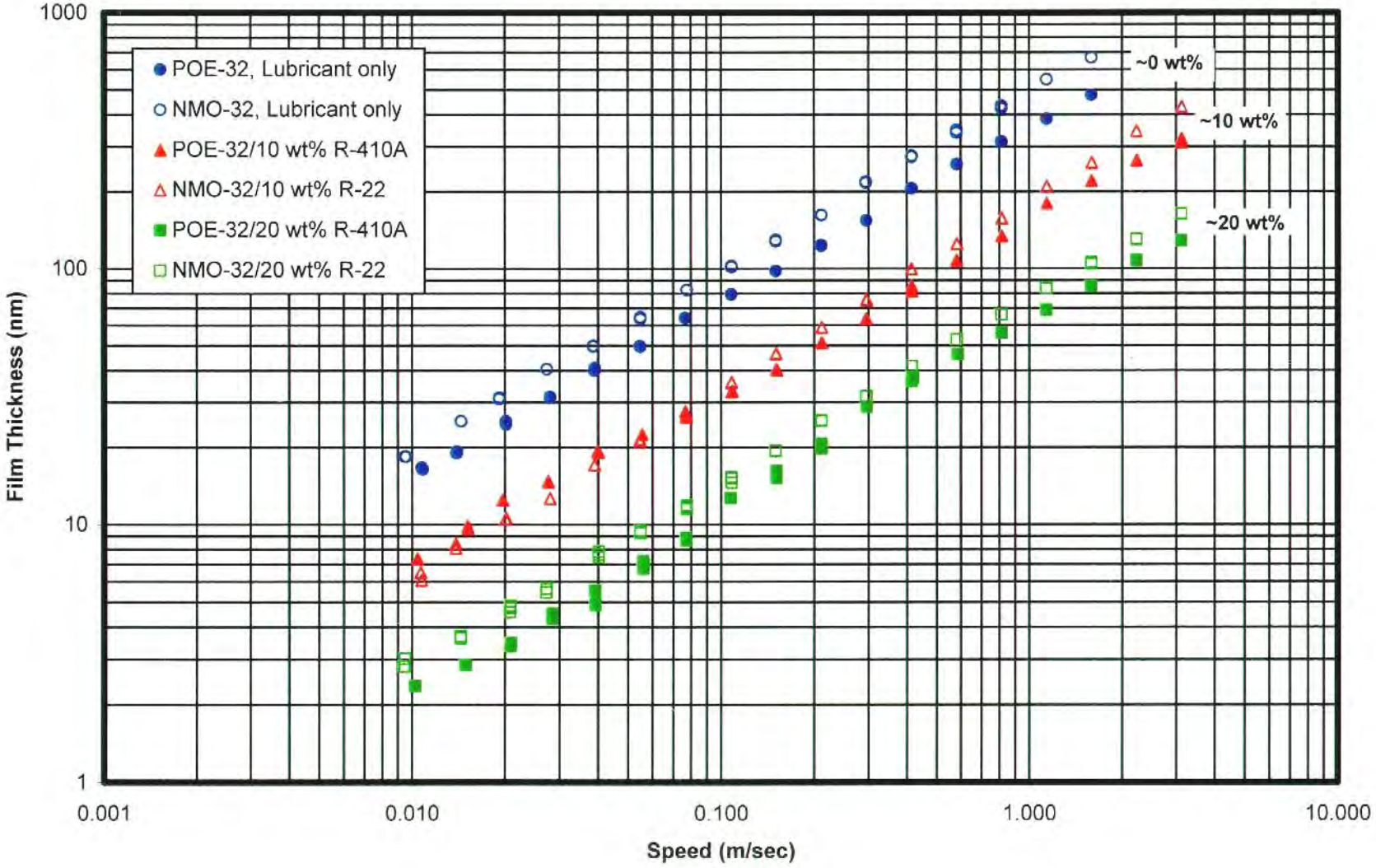

**Figure 114. ISO 32 Polyolester/R-410A vs. ISO 32 Naphthenic Mineral Oil/R-22 Mixtures**
**Film Thickness as a Function of Refrigerant Concentration at 45°C**

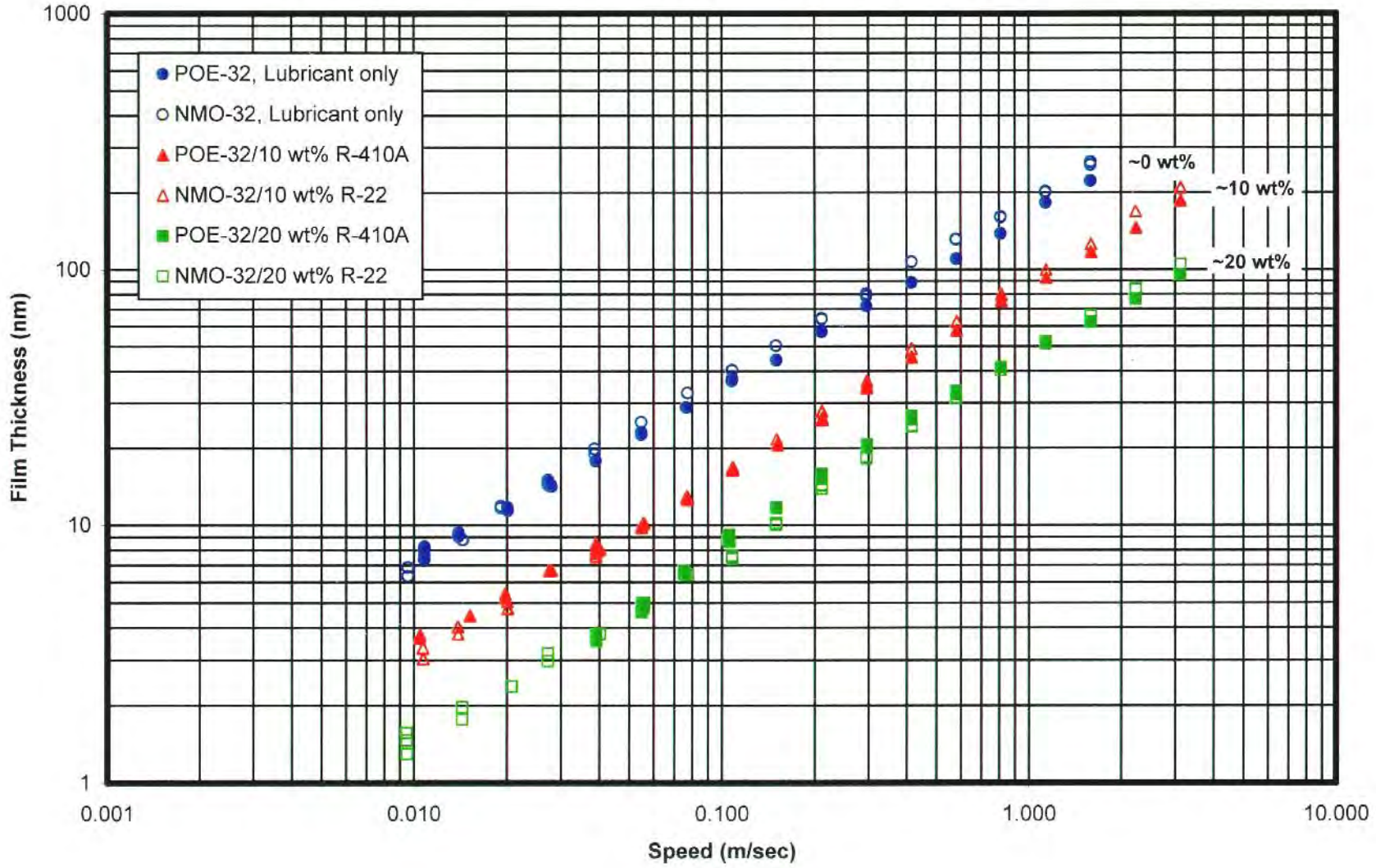

**Figure 115. ISO 32 Polyolester/R-410A vs. ISO 32 Naphthenic Mineral Oil/R-22 Mixtures**
**Film Thickness as a Function of Refrigerant Concentration at 65°C**

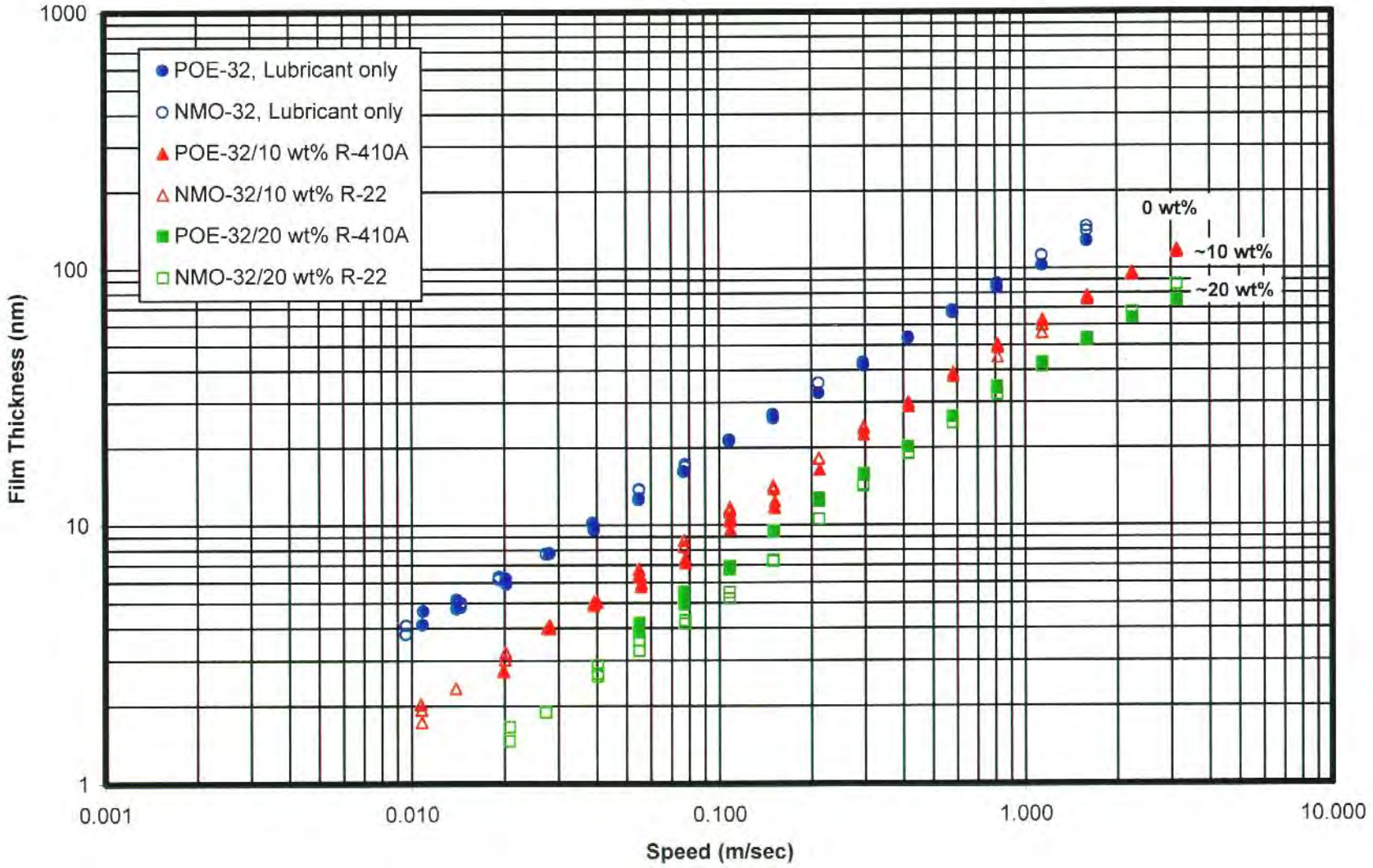

**Figure 116. ISO 68 Polyolester A/R-410A vs. ISO 68 Naphthenic Mineral Oil/R-22 Mixtures - Film Thickness as a Function of Refrigerant Concentration at 23°C**

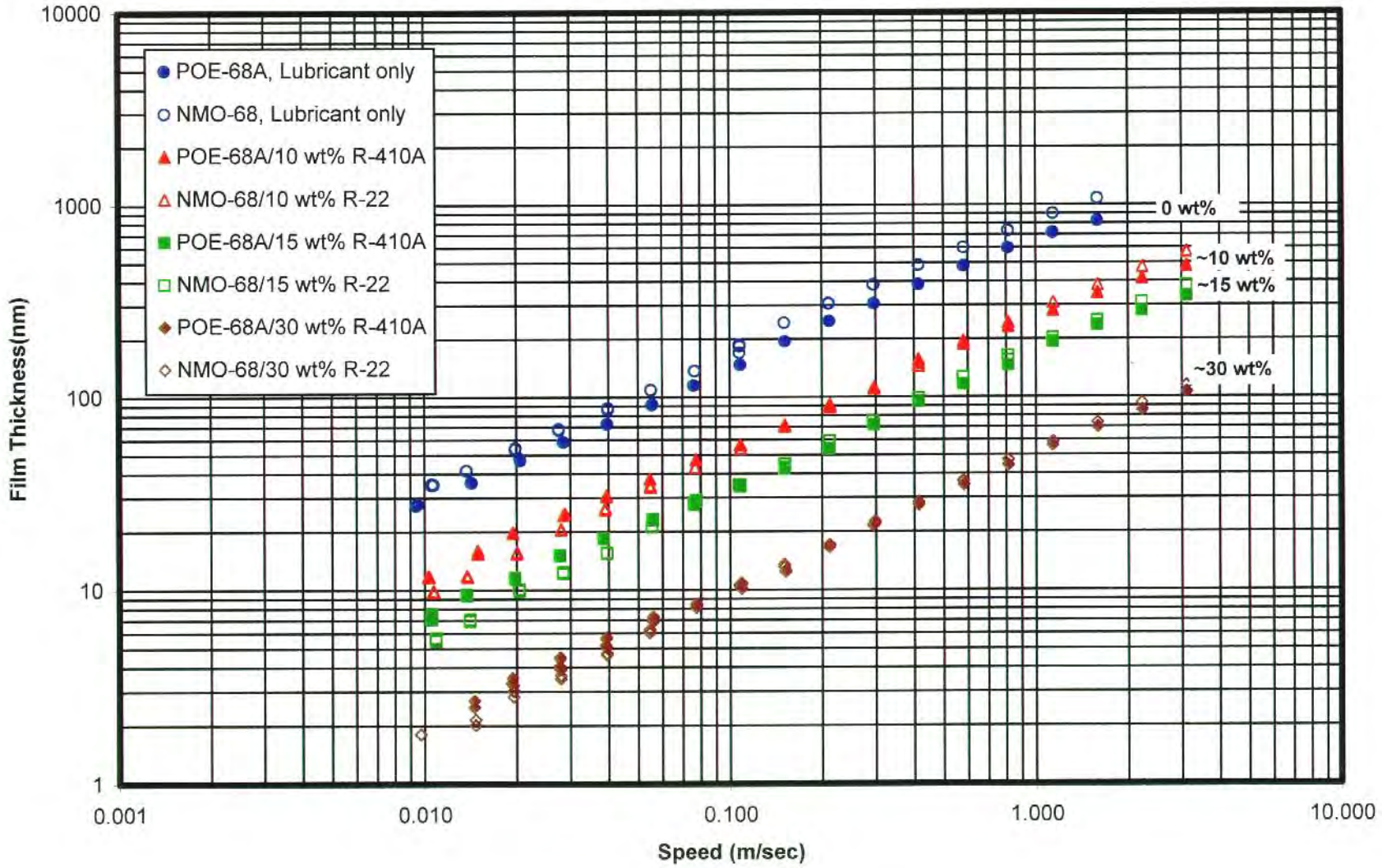

**Figure 117. ISO 68 Polyolester A/R-410A vs. ISO 68 Naphthenic Mineral Oil/R-22 Mixtures - Film Thickness as a Function of Refrigerant Concentration at 45°C**

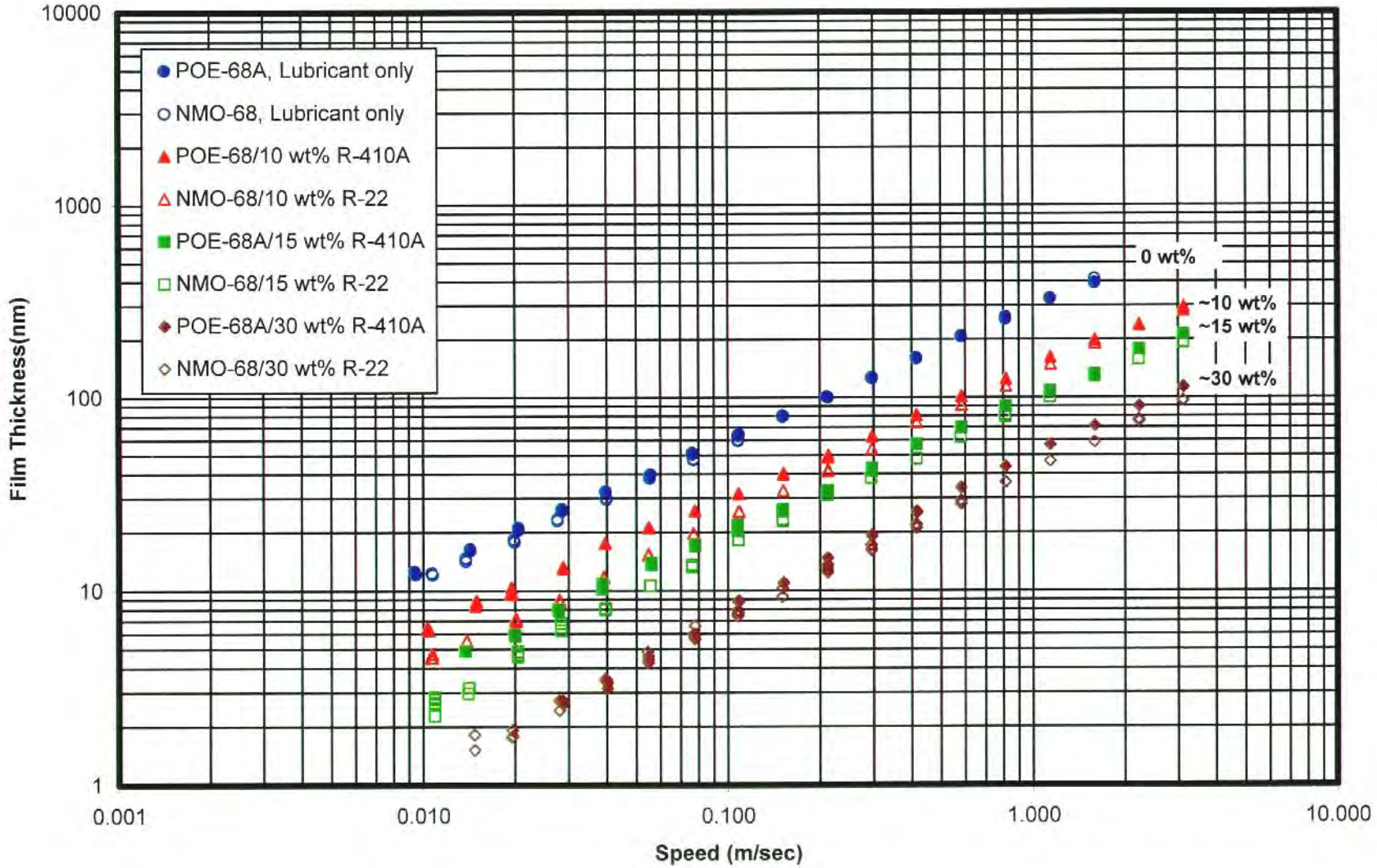

**Figure 118. ISO 68 Polyolester A/R-410A vs. ISO 68 Naphthenic Mineral Oil/R-22 Mixtures - Film Thickness as a Function of Refrigerant Concentration at 65°C**

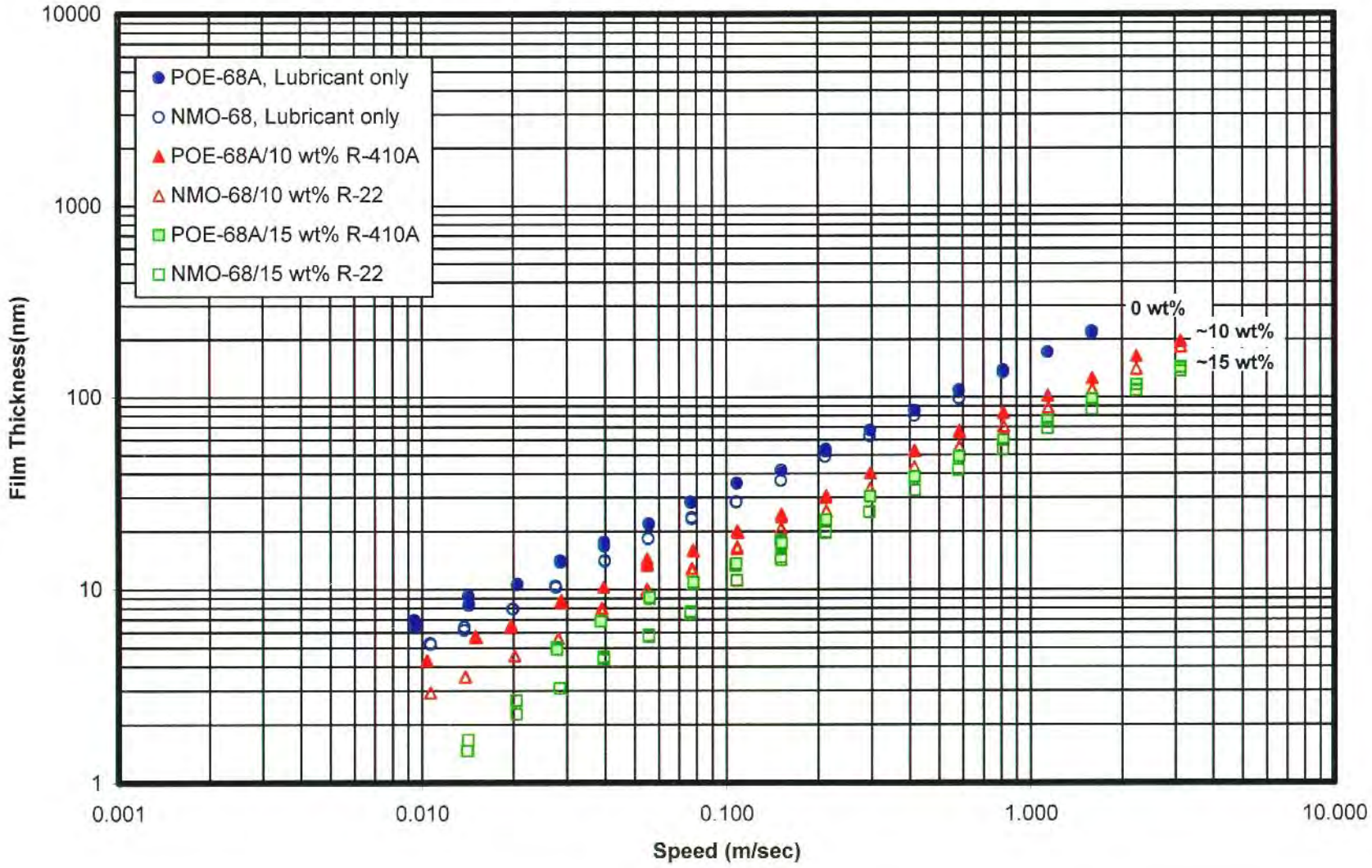

**Figure 119. ISO 32 Polyolester/R-410A, ISO 32 Polyvinyl Ether/R-410A and ISO 32 Naphthenic Mineral Oil/R-22 Mixtures - Film Thickness as a Function of Refrigerant Concentration at 23°C**

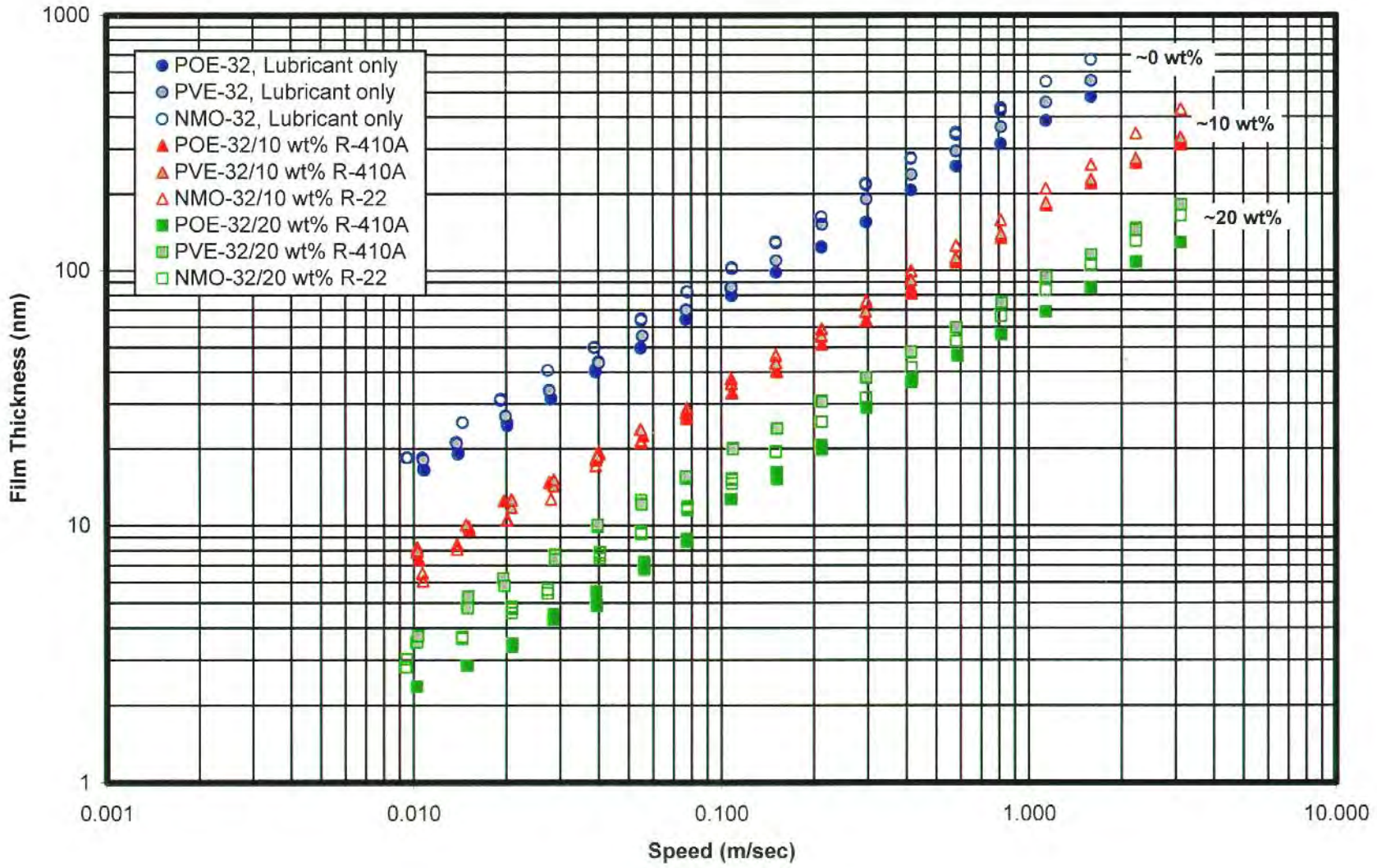

**Figure 120. ISO 32 Polyolester/R-410A, ISO 32 Polyvinyl Ether/R-410A and ISO 32 Naphthenic Mineral Oil/R-22 Mixtures - Film Thickness as a Function of Refrigerant Concentration at 45°C**

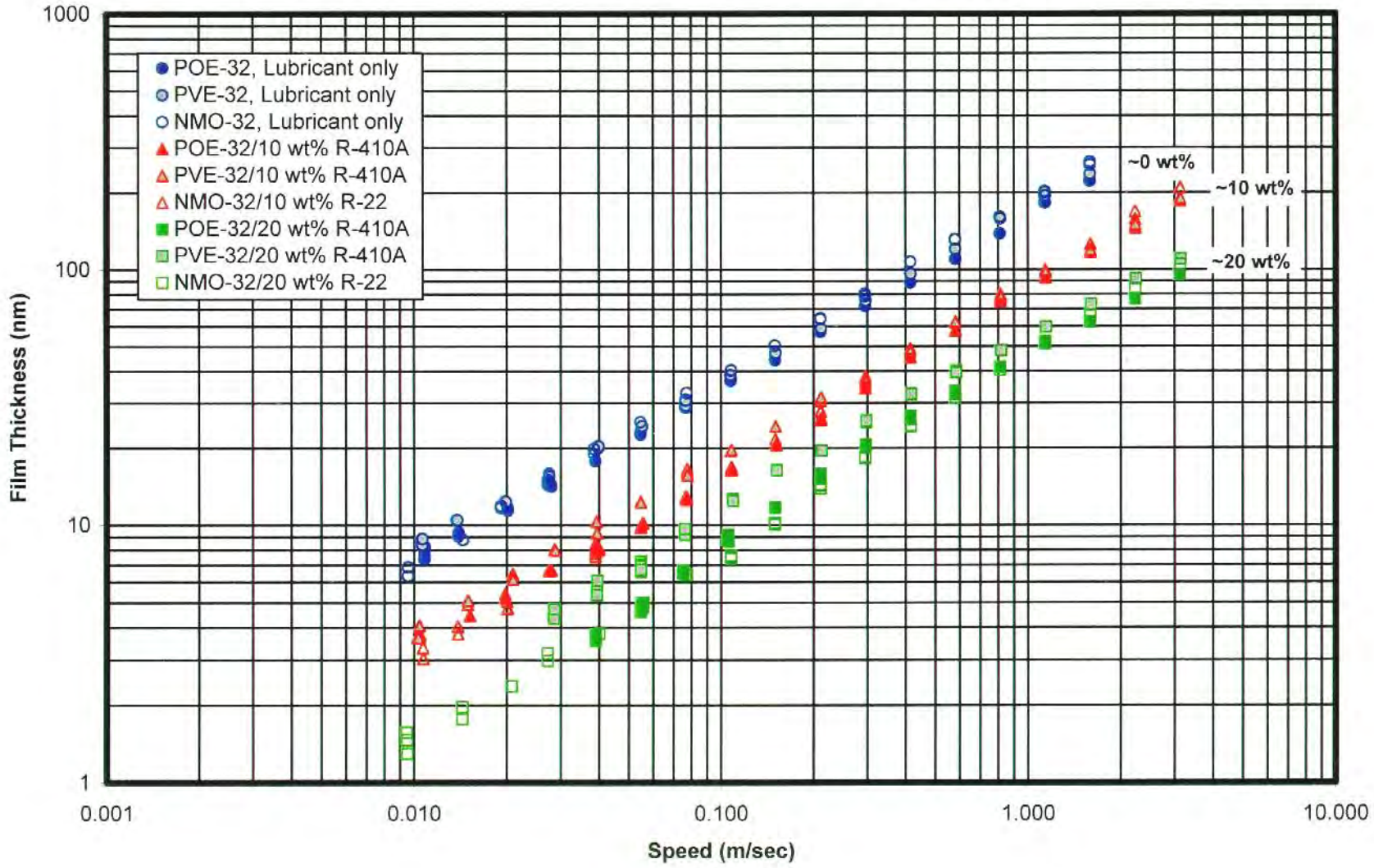

**Figure 121. ISO 32 Polyolester/R-410A, ISO 32 Polyvinyl Ether/R-410A and ISO 32 Naphthenic Mineral Oil/R-22 Mixtures - Film Thickness as a Function of Refrigerant Concentration at 65°C**

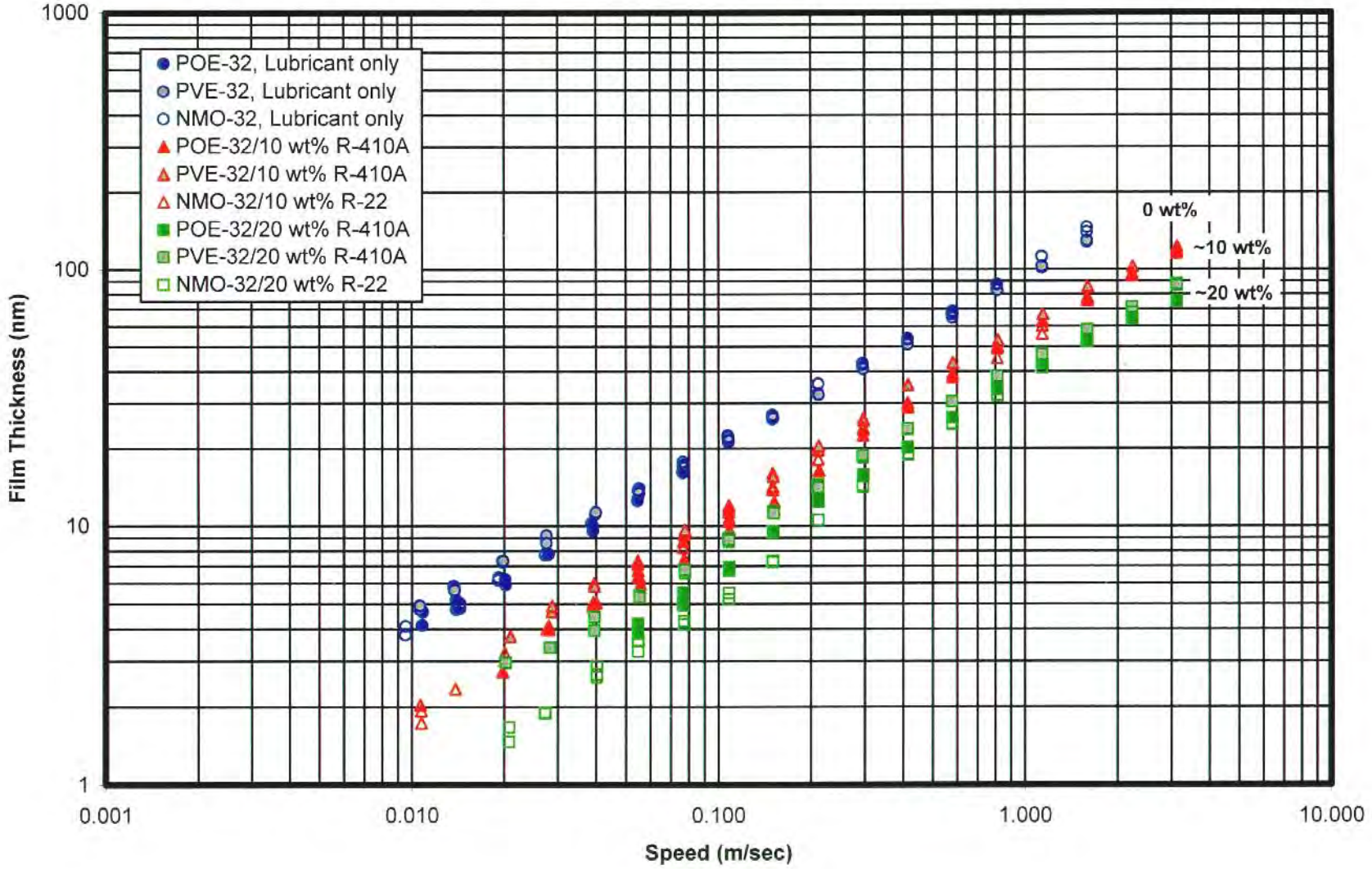

**Figure 122. ISO 68 Polyolester/R-410A, ISO 68 Polyvinyl Ether/R-410A and ISO 68 Naphthenic Mineral Oil/R-22 Mixtures - Film Thickness as a Function of Refrigerant Concentration at 23°C**

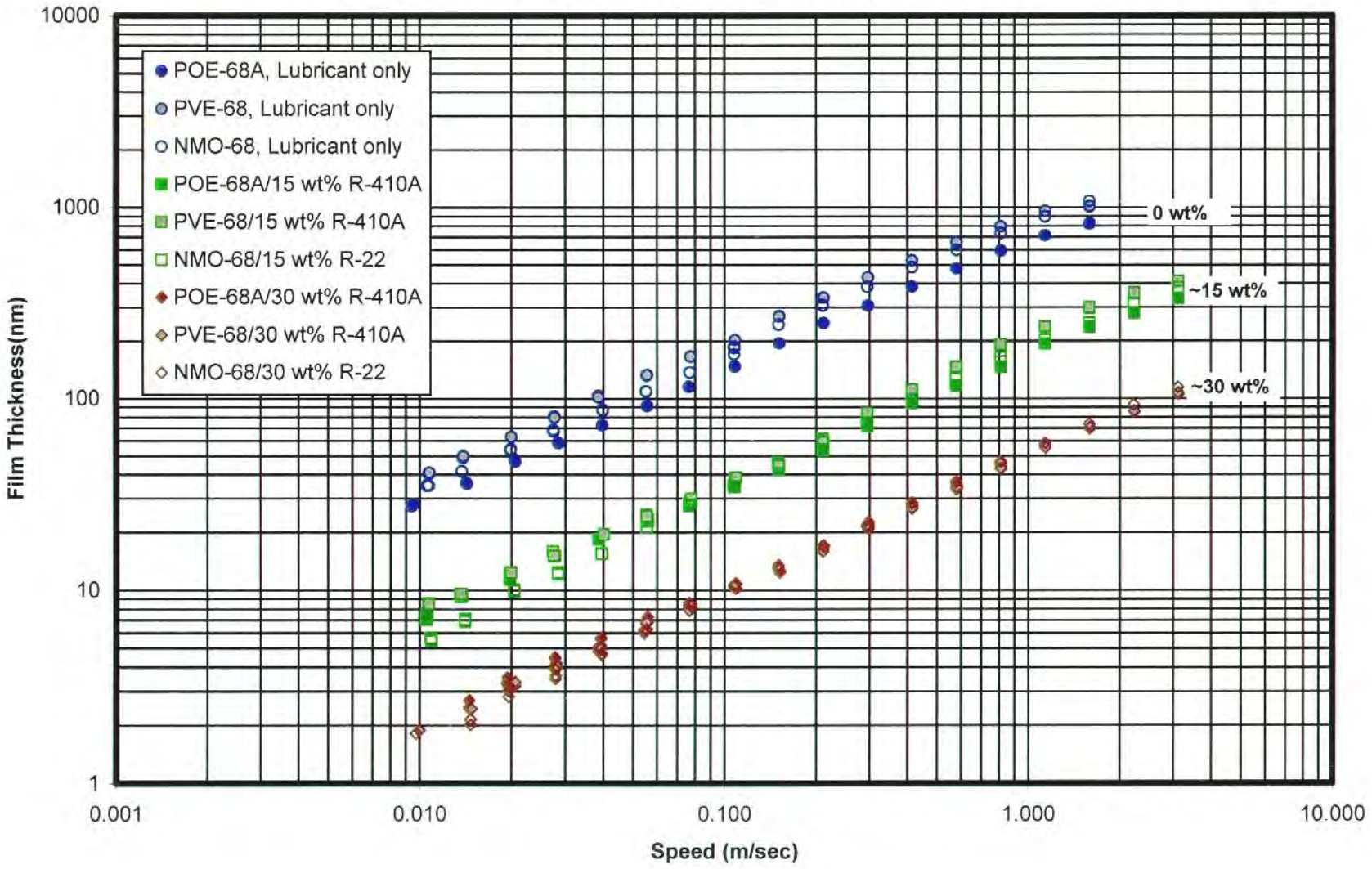

**Figure 123. ISO 68 Polyolester A/R-410A, ISO 68 Polyvinyl Ether/R-410A and ISO 68 Naphthenic Mineral Oil/R-22 Mixtures - Film Thickness as a Function of Refrigerant Concentration at 45°C**

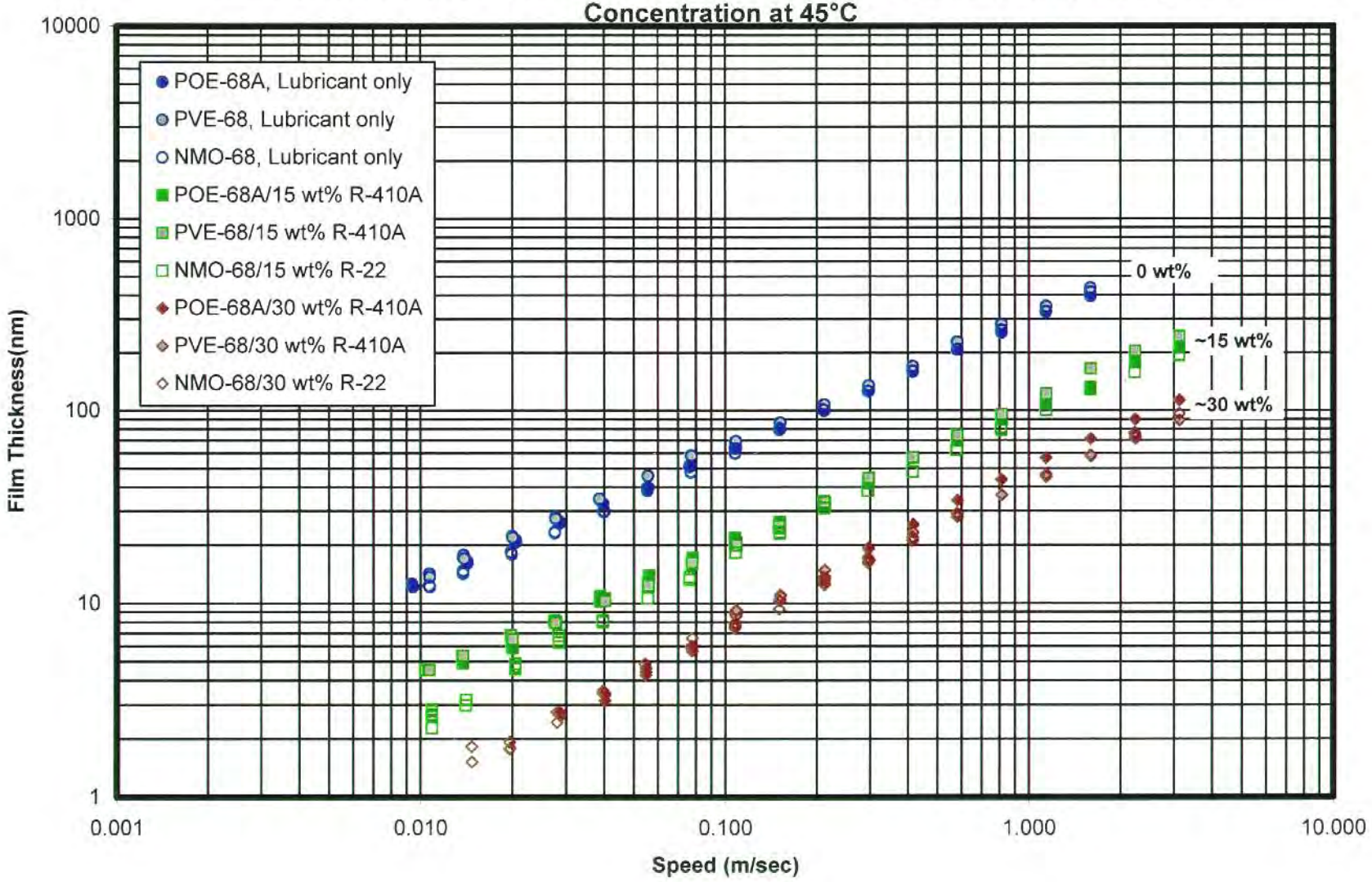

**Figure 124. ISO 68 Polyolester A/R-410A, ISO 68 Polyvinyl Ether/R-410A and ISO 68 Naphthenic Mineral Oil/R-22 Mixtures - Film Thickness as a Function of Refrigerant Concentration at 65°C**

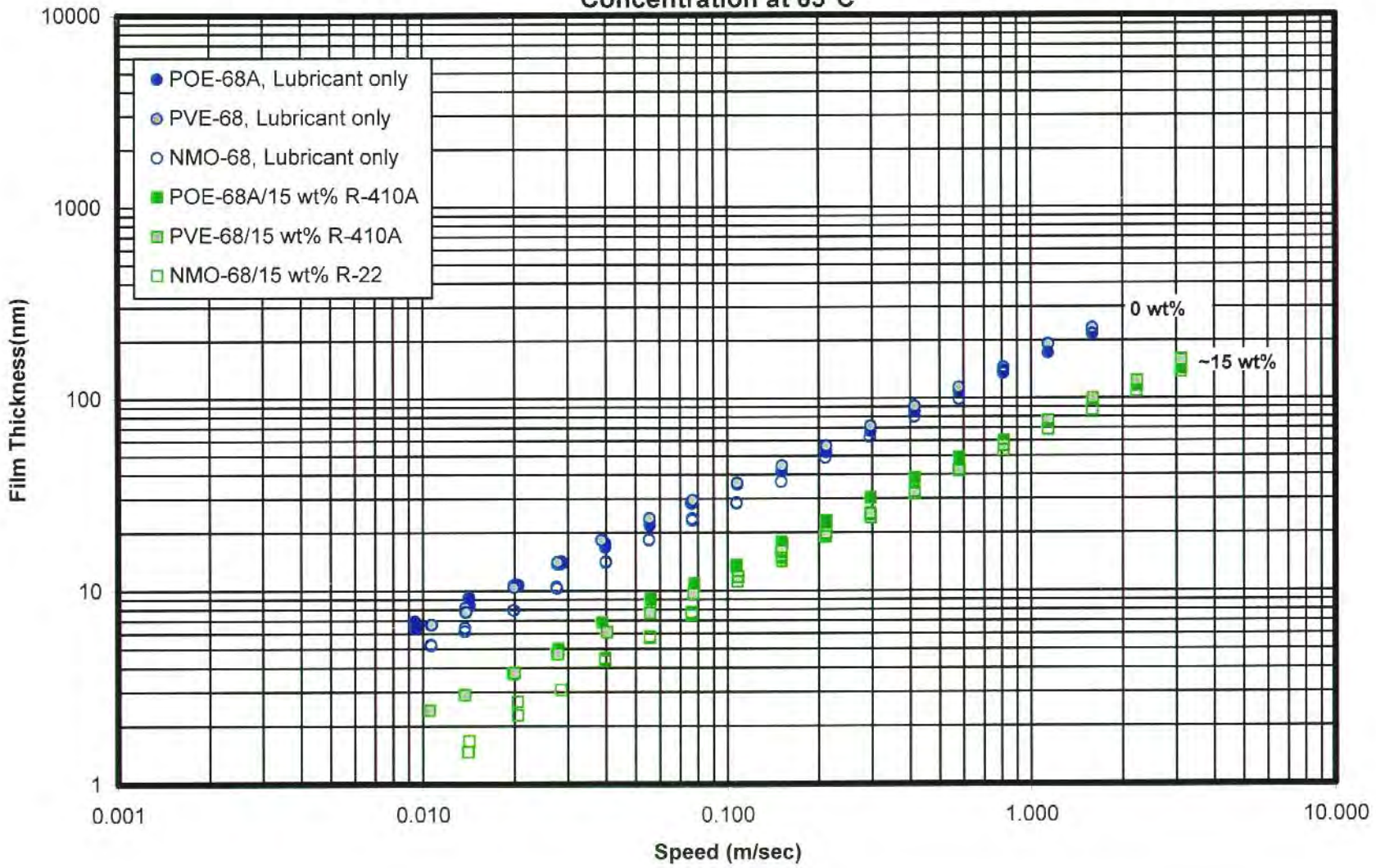

**Figure 125. ISO 32 Polyolester/R-134a vs. ISO 32 Polyolester/R-410A Mixtures**
**Film Thickness as a Function of Refrigerant Concentration at 23°C**

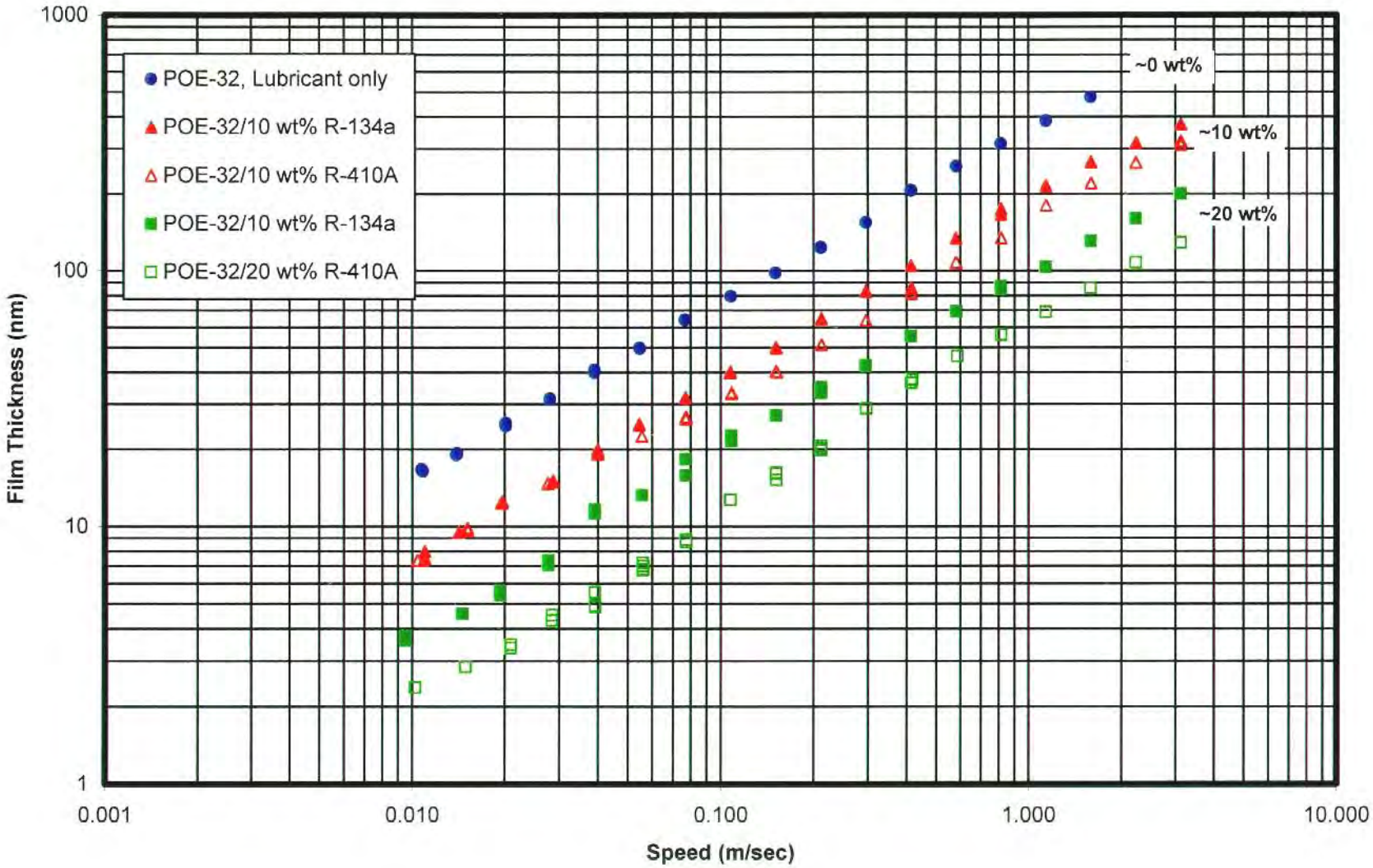

**Figure 126. ISO 32 Polyolester/R-134a vs. ISO 32 Polyolester/R-410A Mixtures**
**Film Thickness as a Function of Refrigerant Concentration at 45°C**

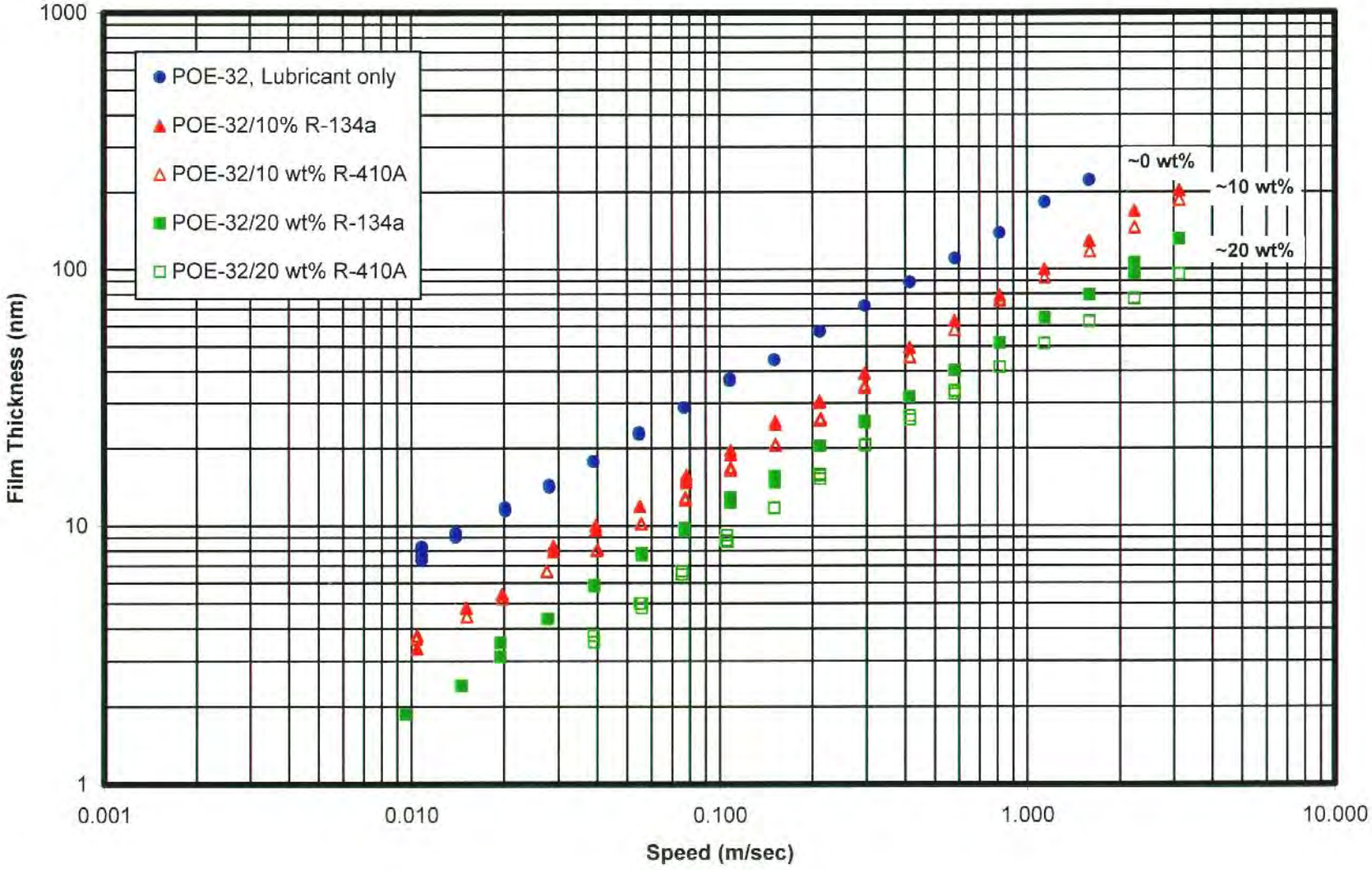

**Figure 127. ISO 32 Polyolester/R-134a vs. ISO 32 Polyolester/R-410A Mixtures**
**Film Thickness as a Function of Refrigerant Concentration at 65°C**

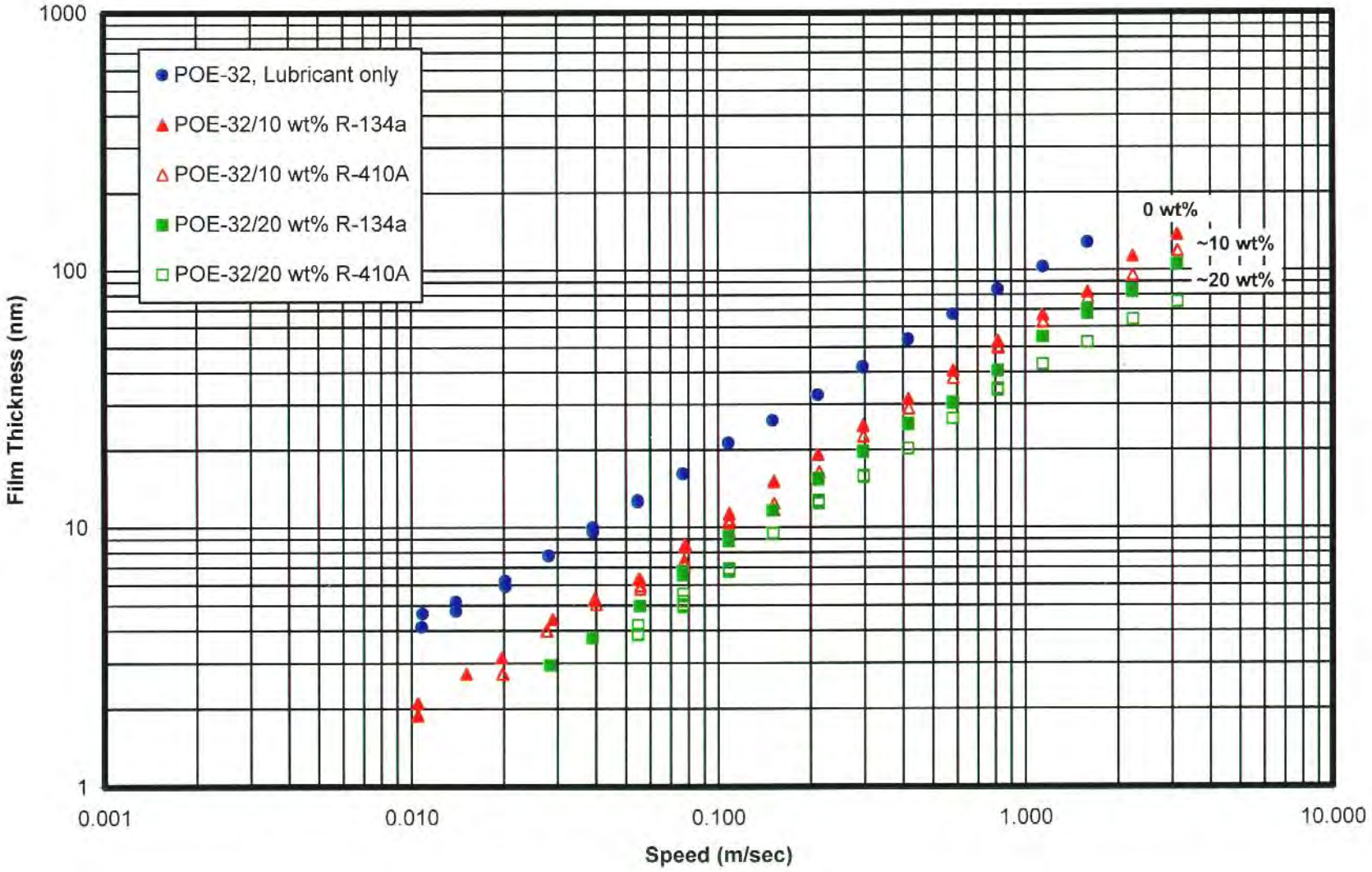

**Figure 128. ISO 68 Polyolester A/R-134a vs. ISO 68 Polyolester A/R-410A Mixtures**
**Film Thickness as a Function of Refrigerant Concentration at 23°C**

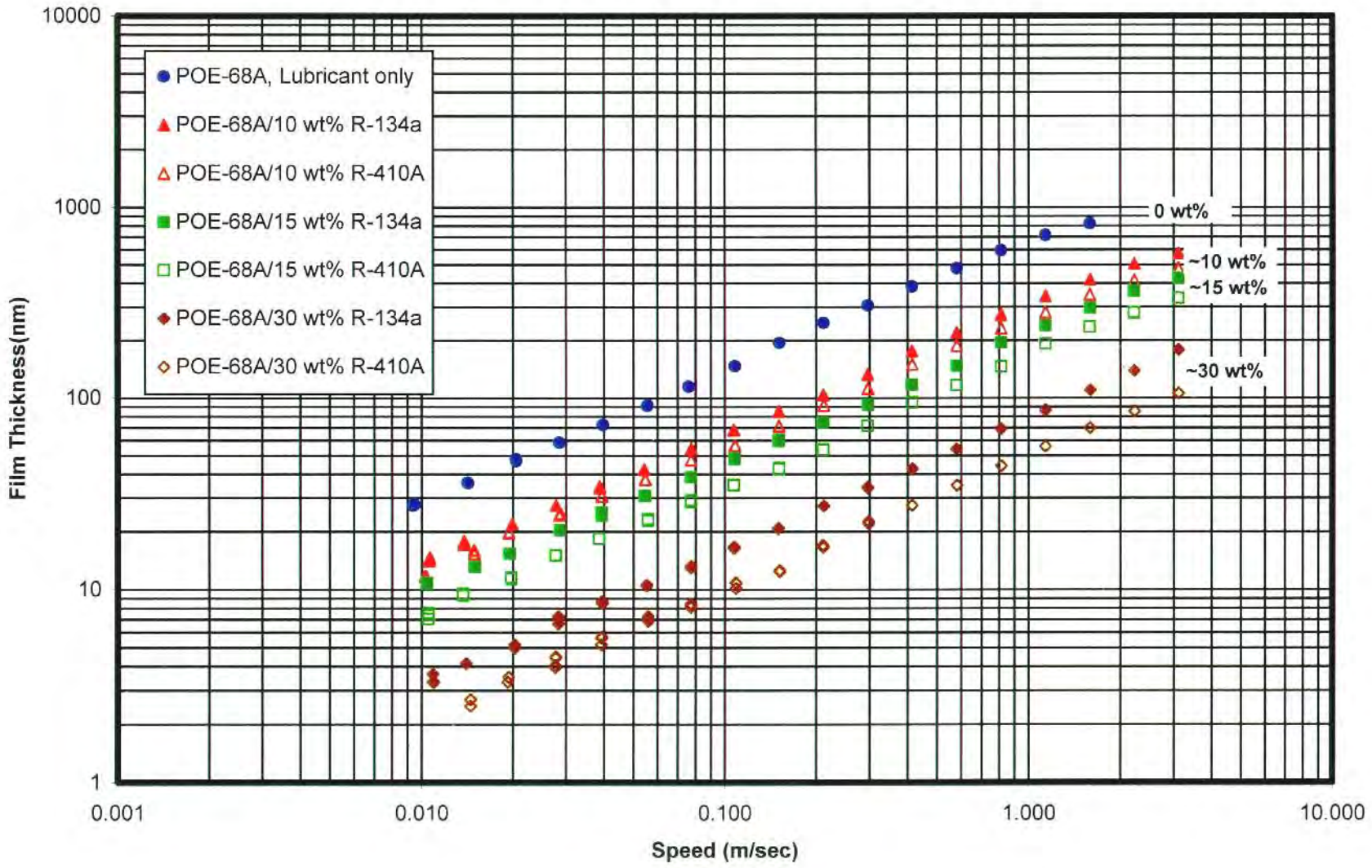

**Figure 129. ISO 68 Polyolester A/R-134a vs. ISO 68 Polyolester A/R-410A Mixtures**
**Film Thickness as a Function of Refrigerant Concentration at 45°C**

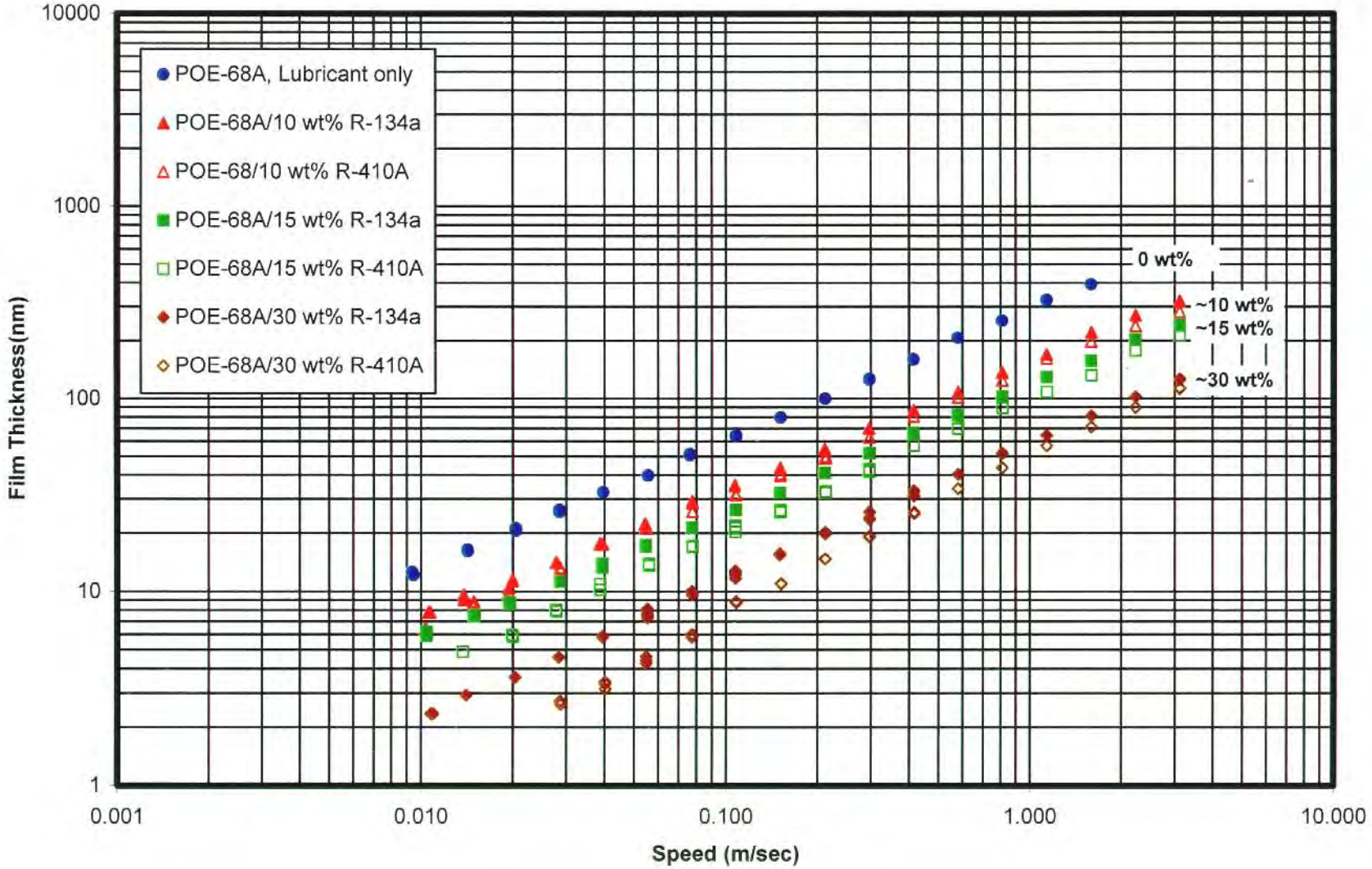

**Figure 130. ISO 68 Polyolester A/R-134a vs. ISO 68 Polyolester A/R-410A Mixtures**
**Film Thickness as a Function of Refrigerant Concentration at 65°C**

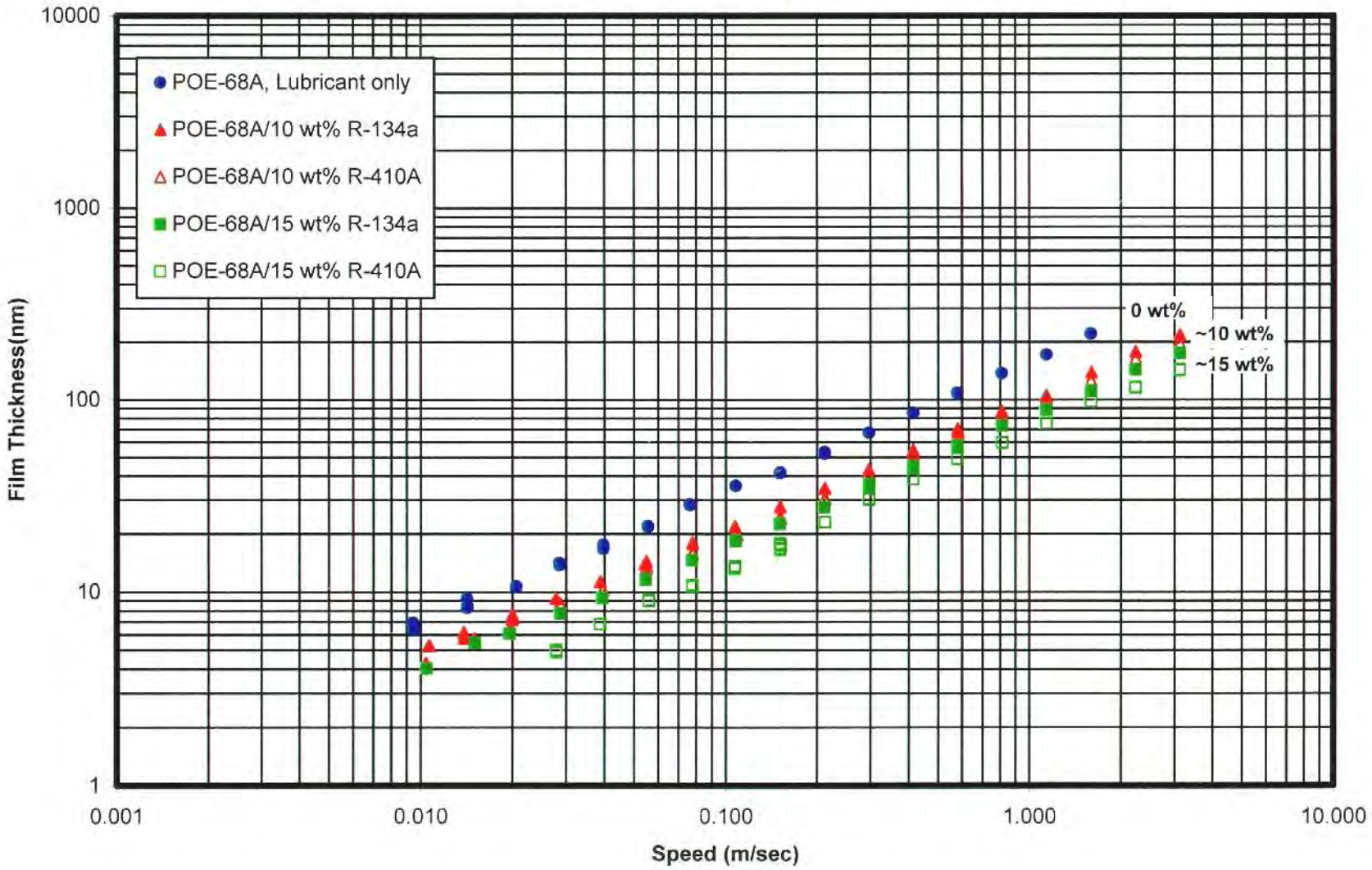

**Figure 131. ISO 32 Polyvinyl Ether/R-134a, vs. ISO 32 Polyvinyl Ether/R-410A Mixtures**
**Film Thickness as a Function of Refrigerant Concentration at 23°C**

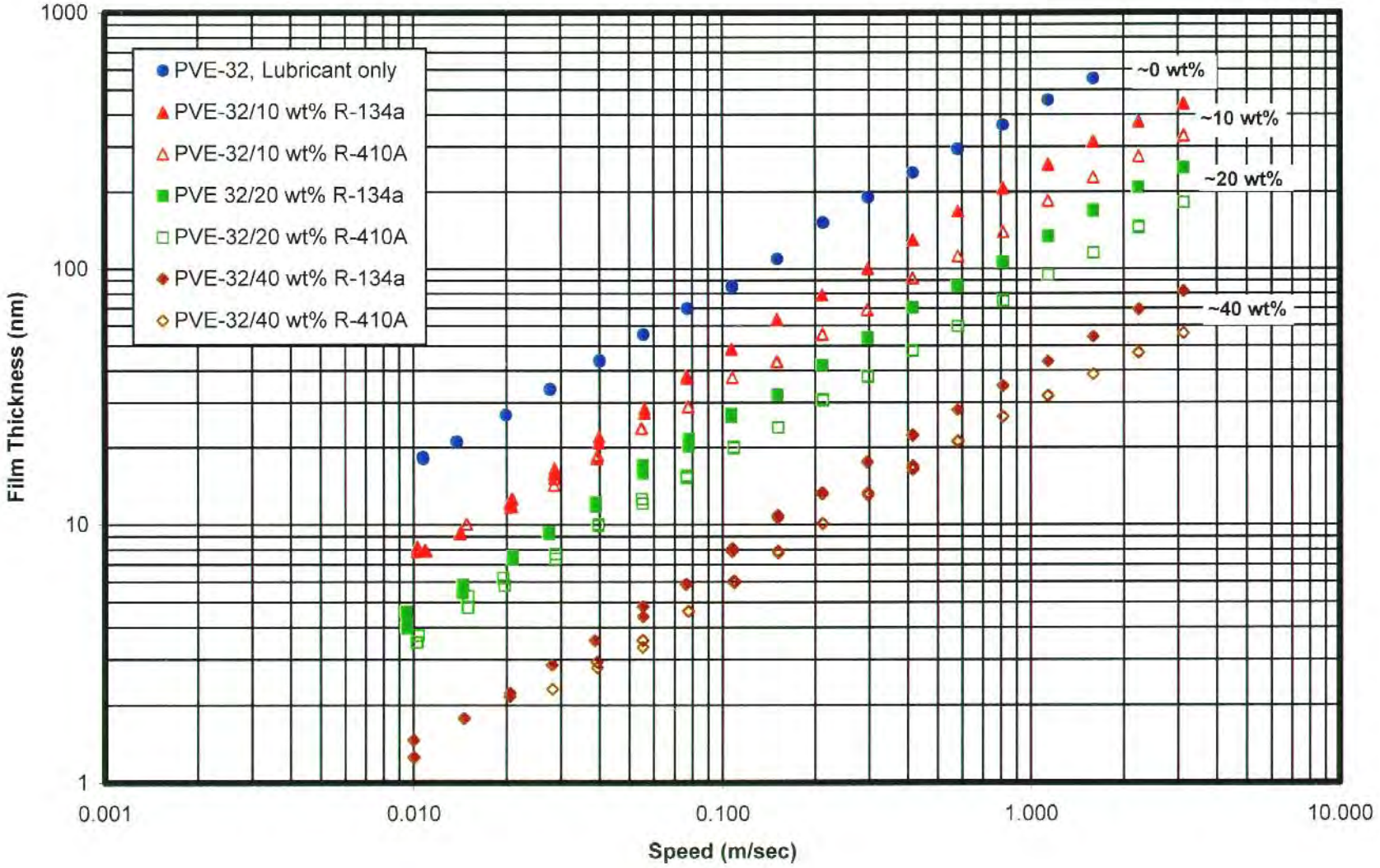

**Figure 132. ISO 32 Polyvinyl Ether/R-134a, vs. ISO 32 Polyvinyl Ether/R-410A Mixtures**
**Film Thickness as a Function of Refrigerant Concentration at 45°C**

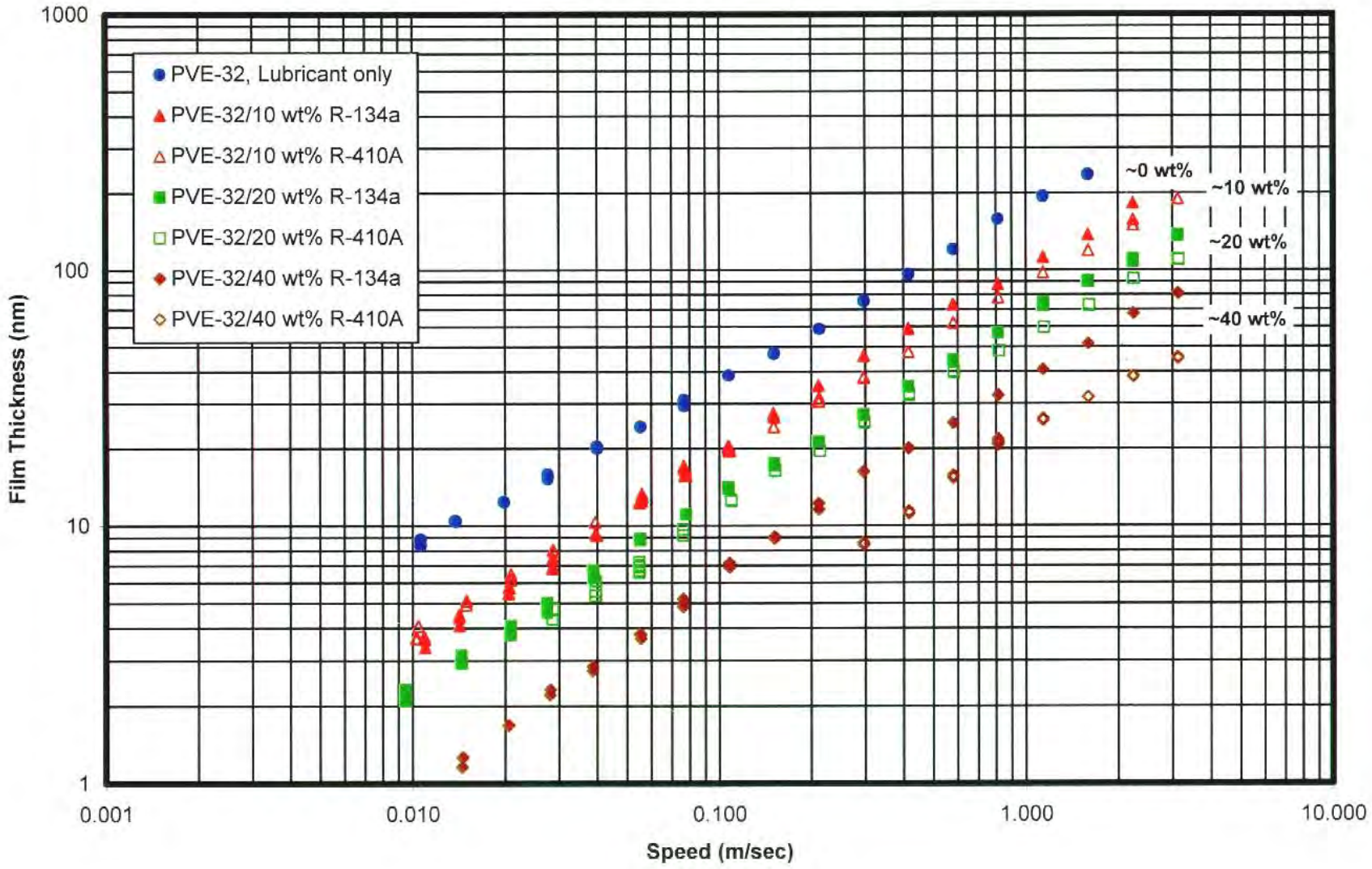

**Figure 133. ISO 32 Polyvinyl Ether/R-134a, vs. ISO 32 Polyvinyl Ether/R-410A Mixtures**
**Film Thickness as a Function of Refrigerant Concentration at 65°C**

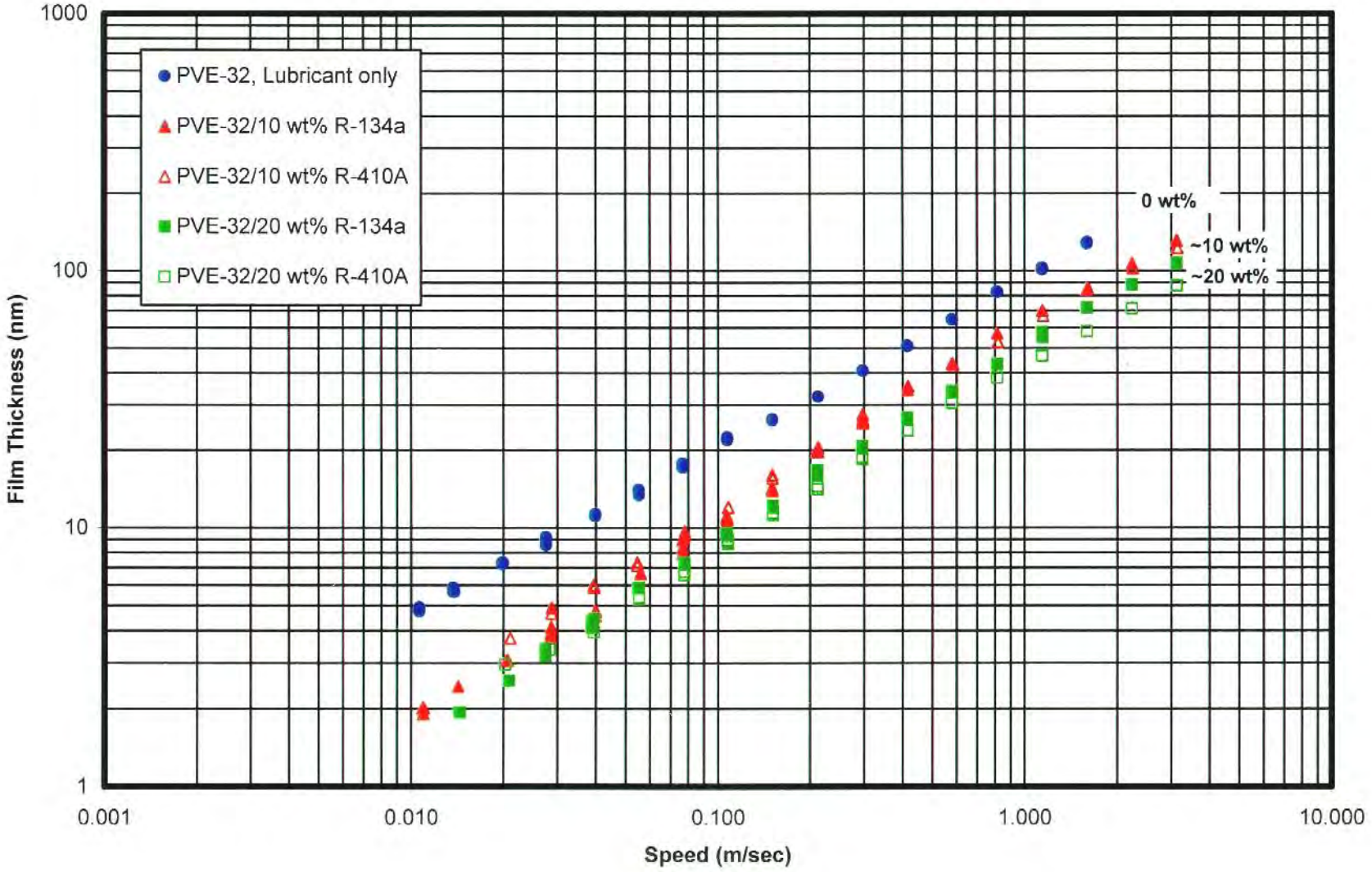

**Figure 134. ISO 68 Polyvinyl Ether/R-134a vs. ISO 68 Polyvinyl Ether/R-410A Mixtures**
**Film Thickness as a Function of Refrigerant Concentration at 23°C**

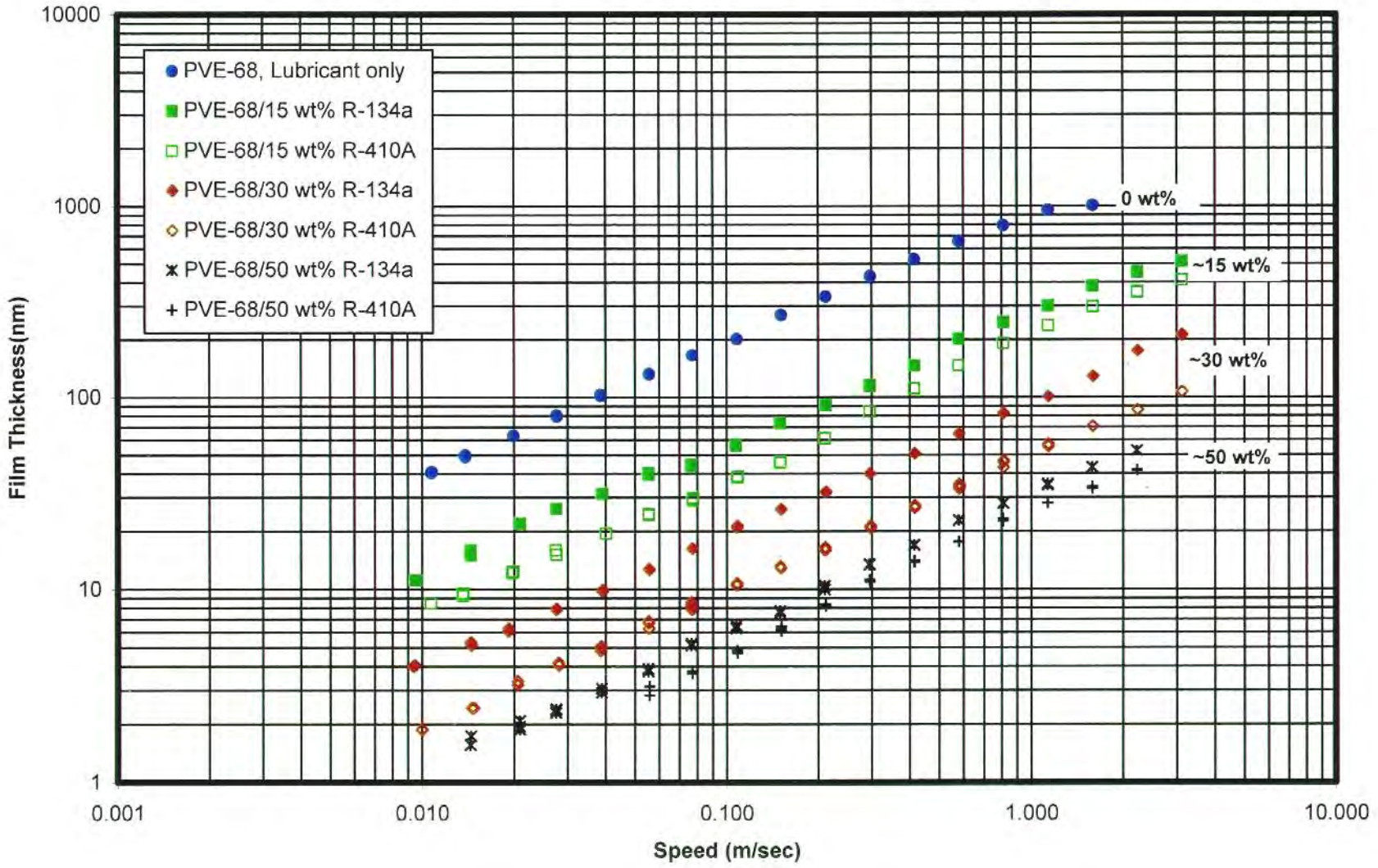

**Figure 135. ISO 68 Polyvinyl Ether/R-134a vs. ISO 68 Polyvinyl Ether/R-410A Mixtures**
**Film Thickness as a Function of Refrigerant Concentration at 45°C**

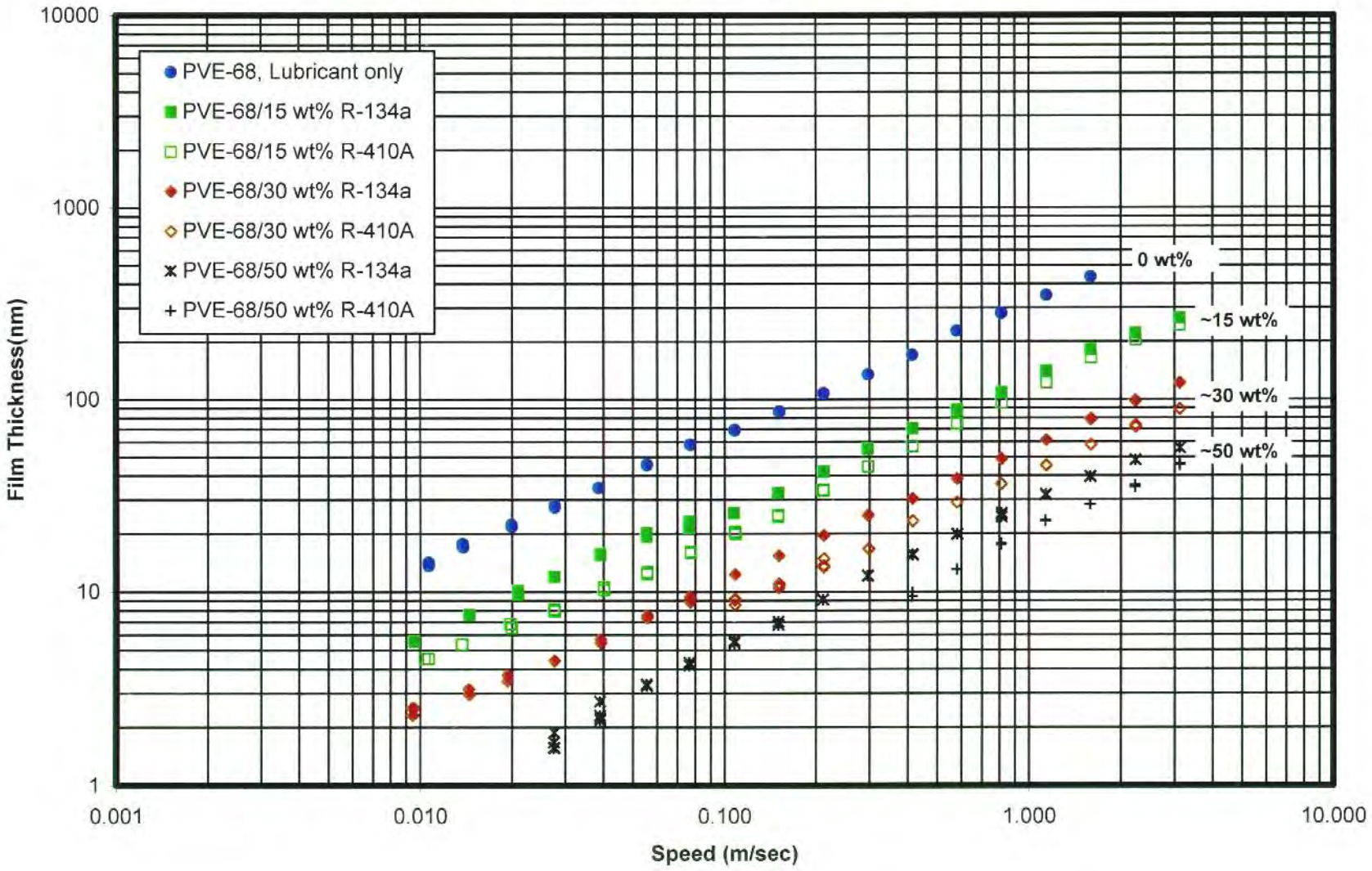

**Figure 136. ISO 68 Polyvinyl Ether/R-134a vs. ISO 68 Polyvinyl Ether/R-410A Mixtures**
**Film Thickness as a Function of Refrigerant Concentration at 65°C**

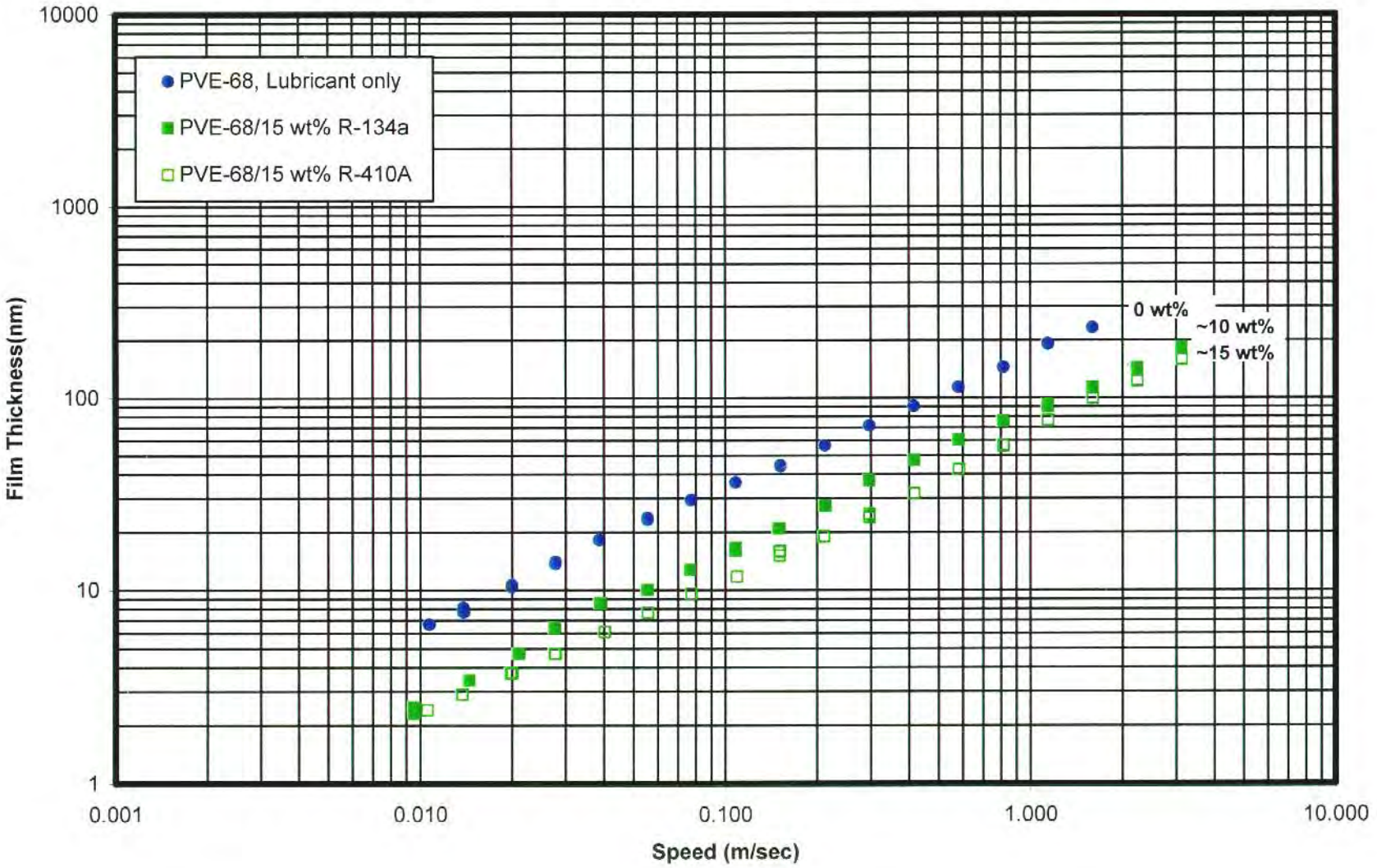

**Figure 137. ISO 32 Polyolester/R-410A vs. ISO 32 Polyvinyl Ether/R-410A Mixtures - Effect of Refrigerant Concentration on Effective Pressure-Viscosity Coefficient**

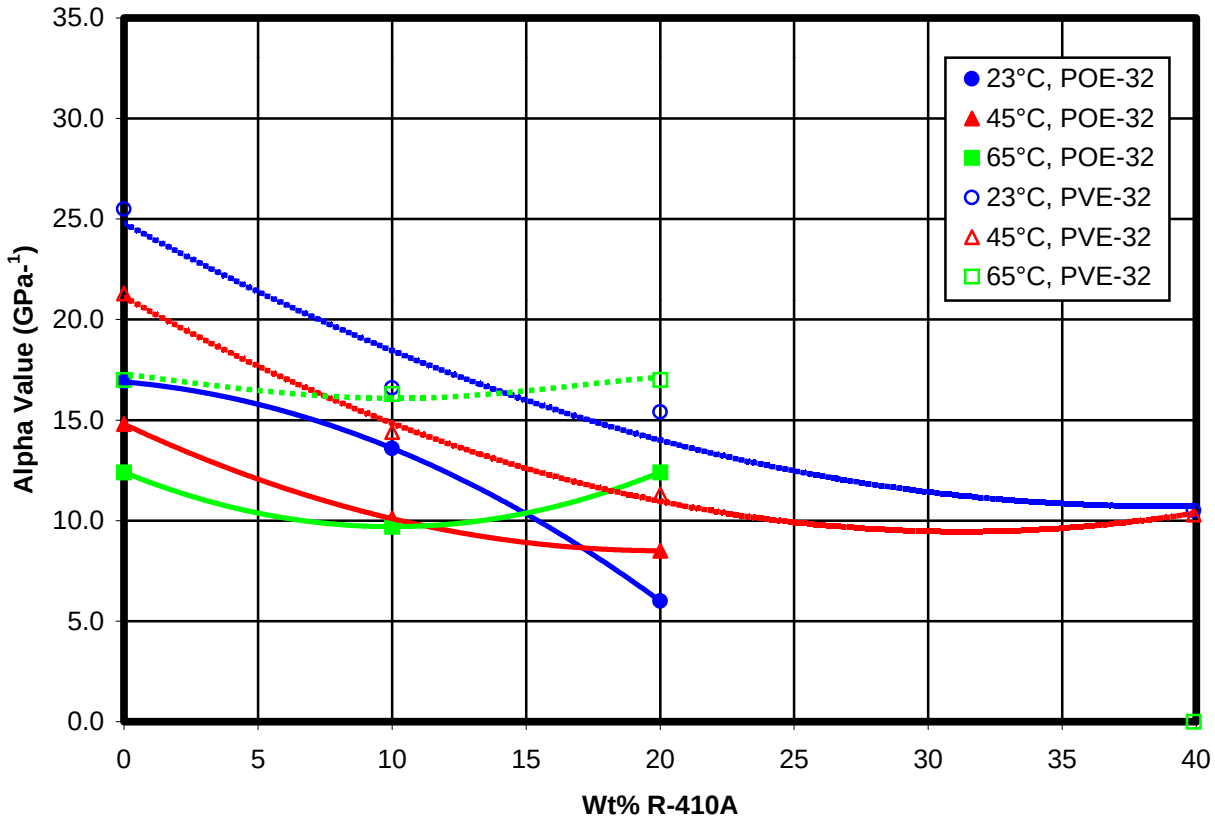

**Figure 138. ISO 32 Polyolester/R-134a vs. ISO 32 Polyvinyl Ether/R-134a Mixtures - Effect of Refrigerant Concentration on Effective Pressure-Viscosity Coefficient**

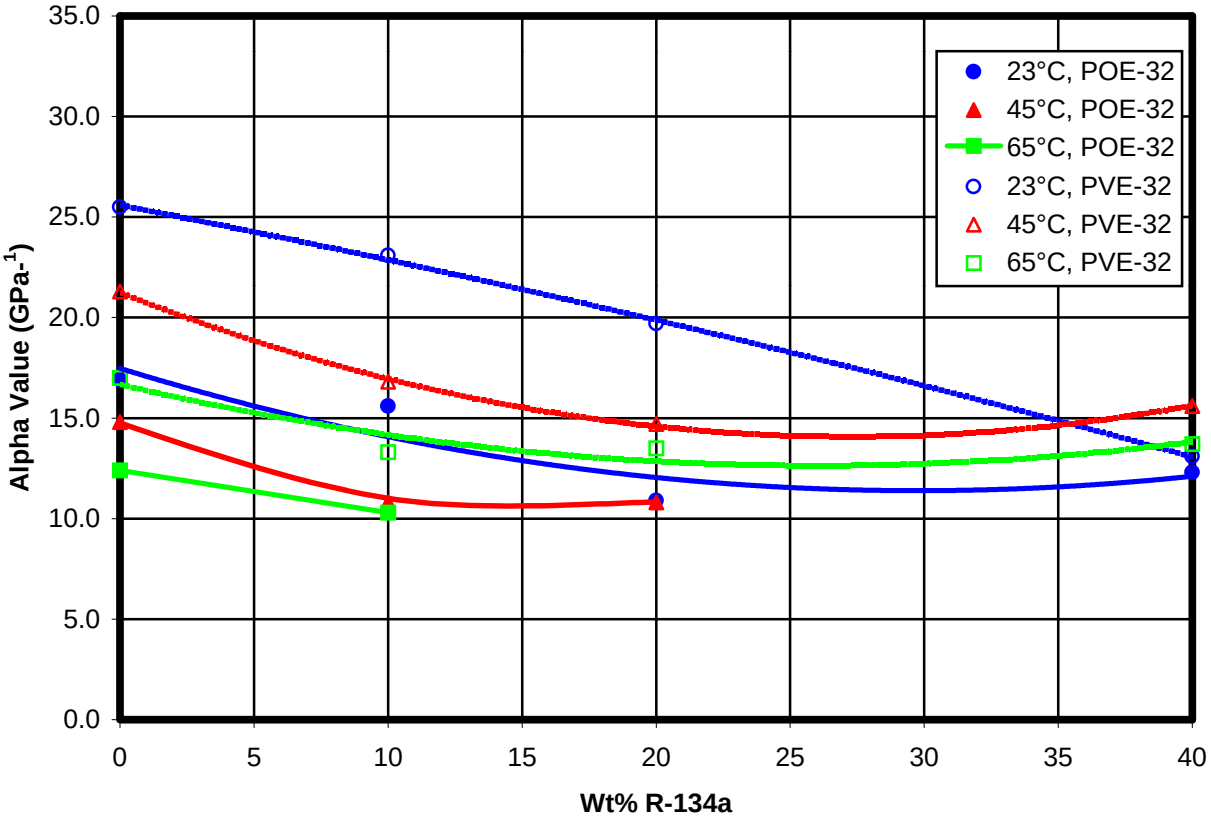

**Figure 139. ISO 32 Polyvinyl Ether/R-134a vs. ISO 32 Naphthenic Mineral Oil/R-22 Mixtures - Effect of Refrigerant Concentration on Effective Pressure-Viscosity Coefficient**

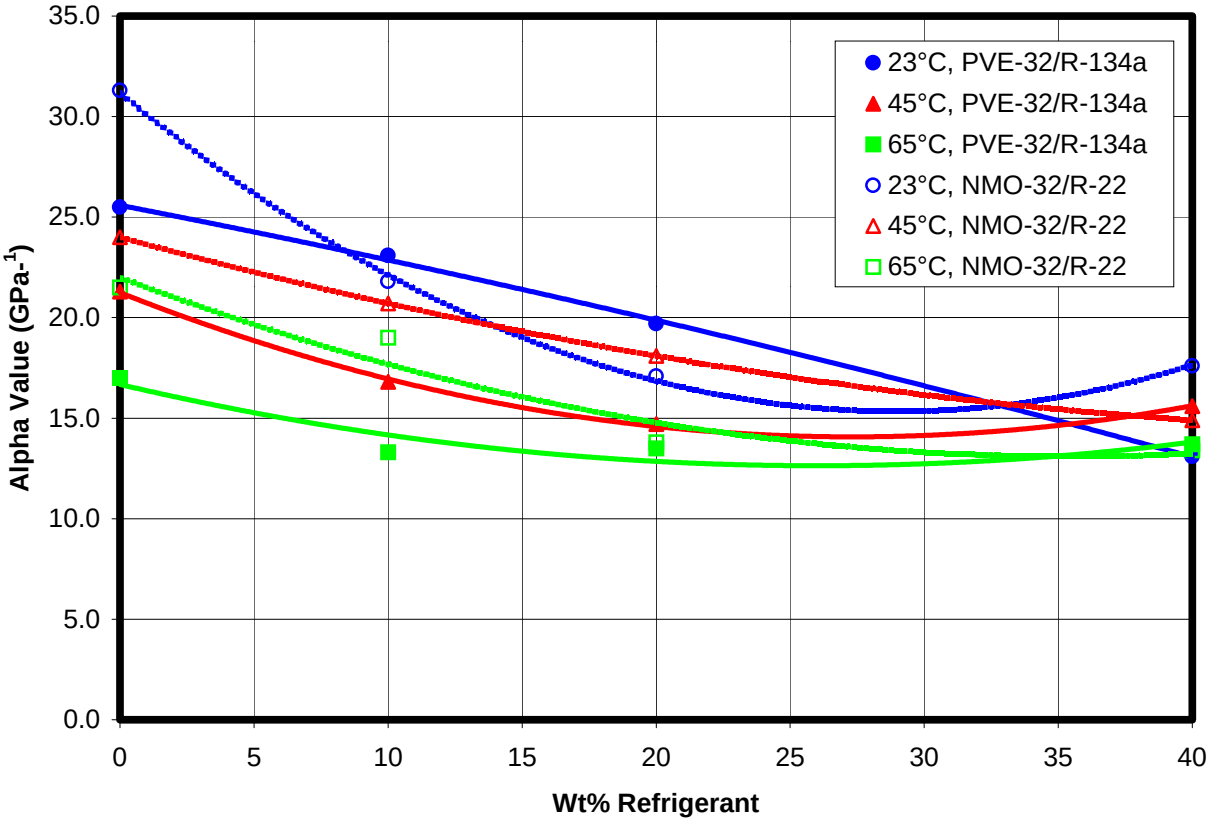

**Figure 140. ISO 32 Polyolester/R-134a vs. ISO 32 Naphthenic Mineral Oil /R-22 Mixtures - Effect of Refrigerant Concentration on Effective Pressure-Viscosity Coefficient**

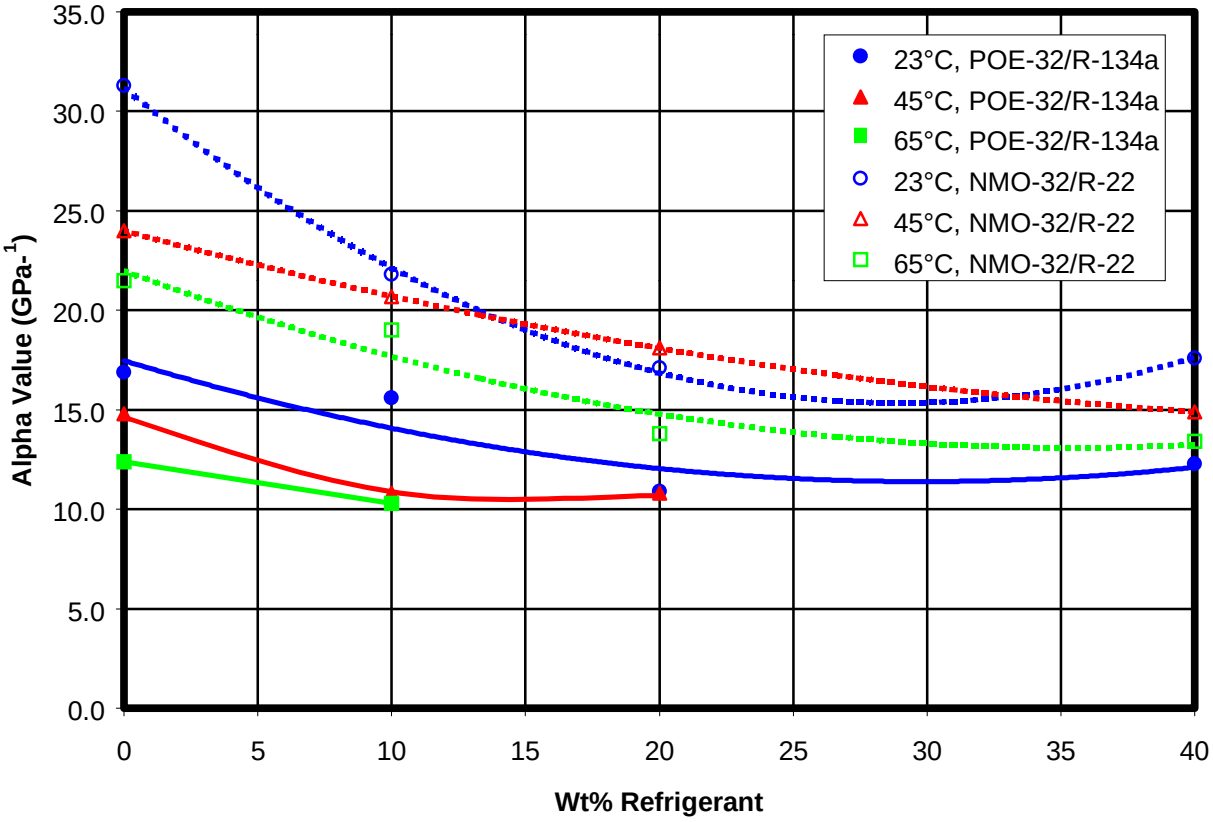

**Figure 141. ISO 32 Polyvinyl Ether/R-410A vs. ISO 32 Naphthenic Mineral Oil/R-22 Mixtures - Effect of Refrigerant Concentration on Effective Pressure-Viscosity Coefficient**

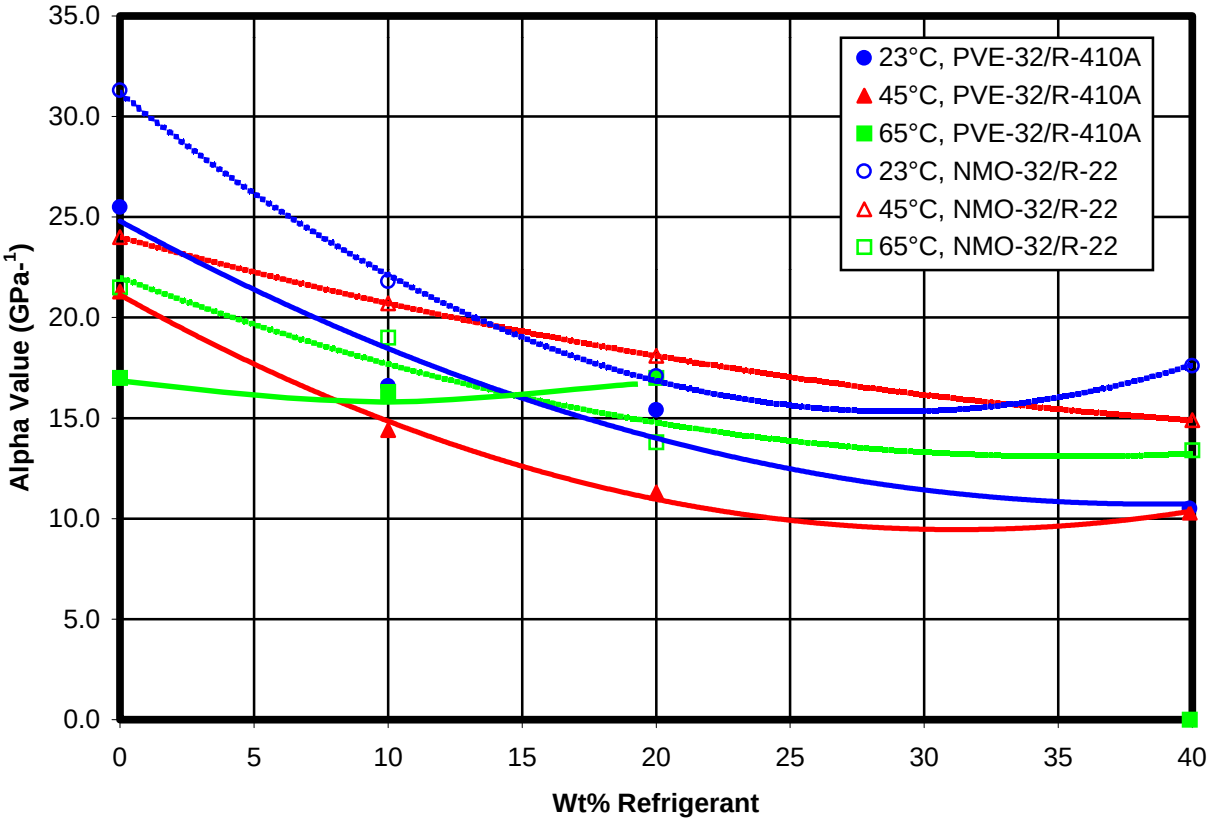

**Figure 142. ISO 32 Polyolester/R-410A vs. ISO 32 Naphthenic Mineral Oil Mixtures - Effect of Refrigerant Concentration on Effective Pressure-Viscosity Coefficient**

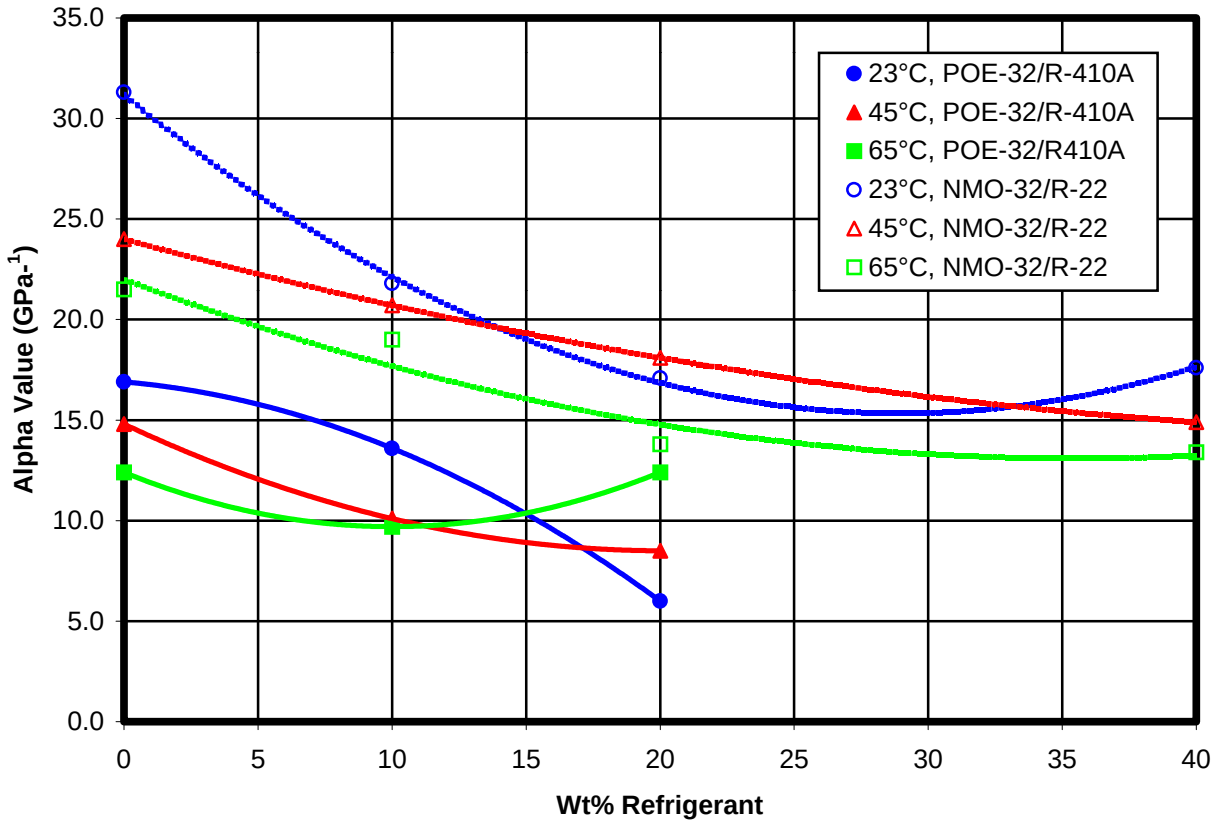

**Figure 143. Comparison of Film Thickness Data for R-134a and R 410A Systems**

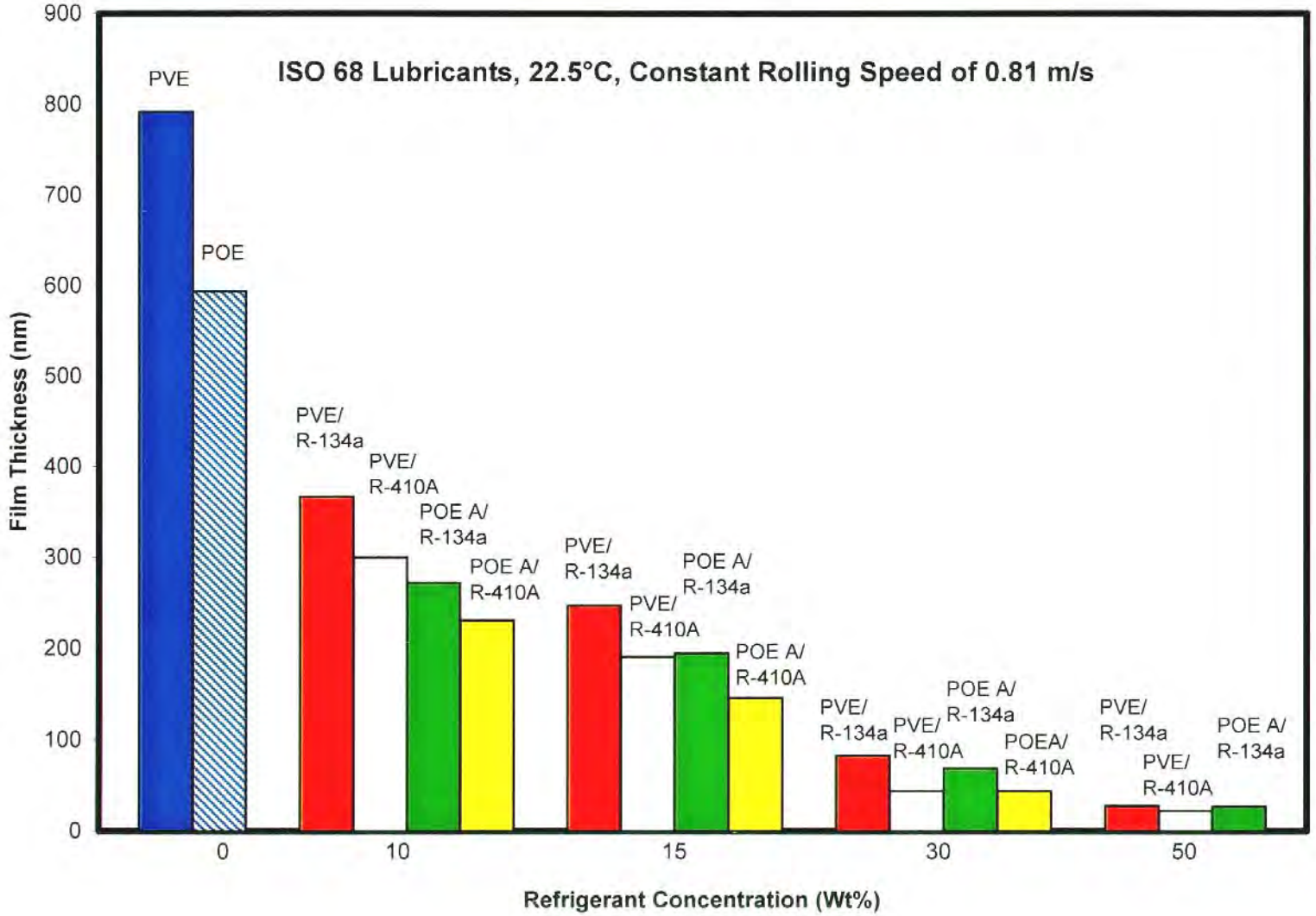

**Figure 144. Comparison of Film Thickness Data for Various Mixtures of ISO 32 Lubricants and Refrigerants**

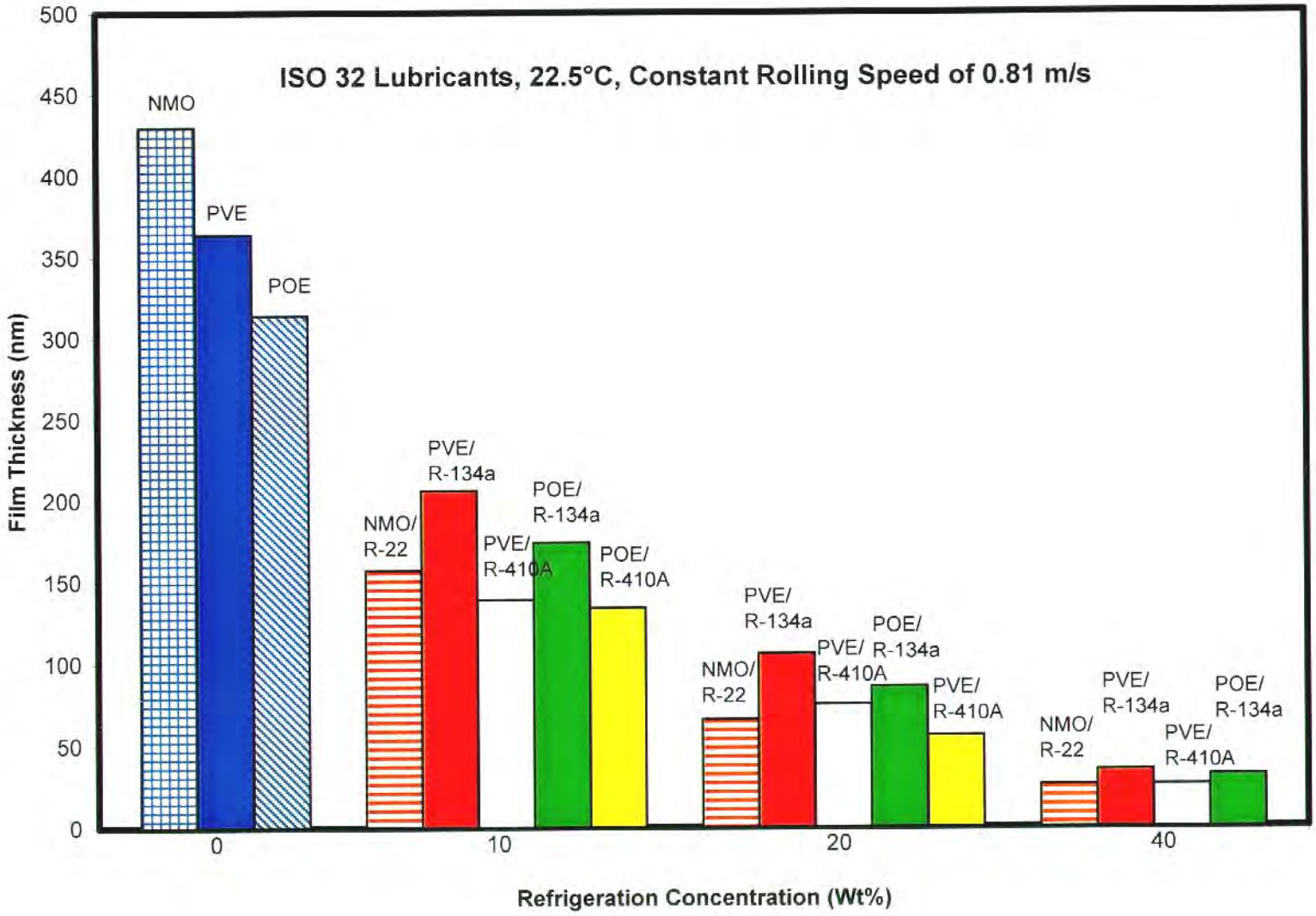

**Figure 145. Comparison of Film Thickness Data for Various Mixtures of ISO 68 Lubricants and Refrigerants**

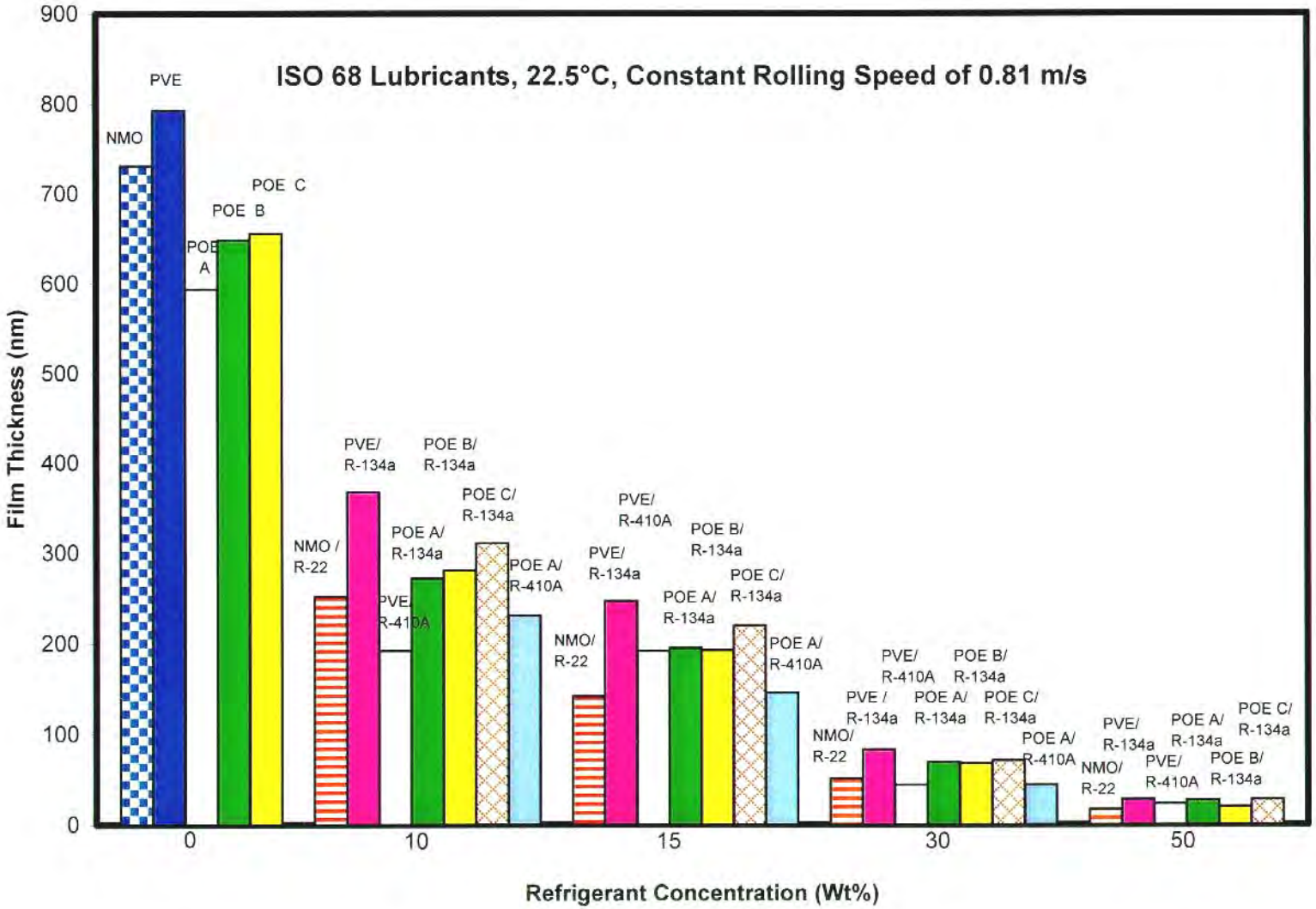

## 7.0 CONCLUSIONS

The ultrathin film interferometry method was modified to operate under a pressurized refrigerant atmosphere in order to investigate the effects of refrigerants on the film formation properties of refrigeration lubricants.

The EHD properties of naphthenic mineral oils, polyolesters and polyvinyl ether lubricants were studied with and without the presence of refrigerants. Under air, all of the lubricants studied behaved as expected from the EHD theory. EHD film thickness increased with speed and viscosity, and decreased with temperature.

Effective pressure-viscosity coefficients calculated from the film thickness data showed the effect of chemical structure on the pressure-viscosity characteristics of the fluids. The fluids were ranked with respect to their pressure-viscosity coefficients in the following order:

naphthenic mineral oils > polyvinyl ethers > polyolesters.

Differences were observed in the pressure-viscosity characteristics of the polyolesters studied. This was related to the degree of branching in the ester structure. Esters with branching have higher $\alpha$-values than those with linear structure. Effective pressure-viscosity coefficients also change with temperature, decreasing as the temperature increases.

Refrigerants have a significant effect on reducing the EHD film formation ability of lubricants. EHD film thickness decreases drastically in the contact as the refrigerant concentration in the lubricant increases. Even at the low refrigerant concentration of 10%, the reduction in film thickness ranges from 30 to 65% depending on the test temperature.

Refrigerants reduce dynamic viscosity as well as the pressure-viscosity coefficients of lubricants. However, this effect decreases as the temperature increases.

The thickness of the EHD film formed by the lubricant/refrigerant mixtures shows a similar dependence on speed as that of the lubricant itself. At high refrigerant concentrations and high temperatures, i.e. under thin film conditions, some deviations from the theoretical slope of 0.67 were observed for the film thickness vs. speed relationship. This discrepancy

might be related to the non-homogeneous nature of the refrigerant and lubricant mixtures at high pressures. This would lead to the formation of a two-phase system in the inlet region of the EHD contact.

Effective pressure-viscosity coefficients for the lubricant/refrigerant mixtures were calculated from the film thickness data using the theoretical relationship of Dowson-Hamrock and viscosity data available for the mixtures in the literature. The accuracy of the calculated pressure-viscosity coefficients depends strongly on the accuracy of the dynamic viscosity data used in the calculations.

For a given fluid and refrigerant mixture, it has been shown that pressure-viscosity coefficient increases linearly in proportion to the logarithm of dynamic viscosity. This suggests that the same fundamental molecular properties govern changes in both dynamic viscosity and pressure-viscosity properties.

The ranking obtained with respect to the pressure-viscosity characteristics of the lubricants under air was also observed under refrigerant environments. However, the differences became smaller as the refrigerant concentration and the temperature increased. In general, refrigerant (R-134a or R-410A) mixtures with polyvinyl ethers have higher $\alpha$-values than those with polyolesters. Mixtures of naphthenic mineral oil and R-22 have higher $\alpha$-values than those of polyolesters or polyvinyl ethers and R-134a or R-410A. The presence of R-410A in the lubricants (polyolesters or polyvinyl ethers) results in thinner EHD films than those produced by the same lubricants in the presence of R-134a.

## 8.0 FUTURE WORK

Future work in this project could focus on the following areas:

In order to improve the accuracy of the film thickness measurements for lubricant/refrigerant mixtures, the refractive index determination method developed in this study needs to be further developed. This would be possible by modifying the optical system and the ultrathin film interferometry software.

The accuracy of the effective pressure-viscosity coefficients determined from EHD film thickness data depends on having a reference fluid with a reliably known pressure-viscosity coefficient. A wider range of fluids would need to be compared using both high-pressure viscometry and film thickness to refine the reference fluid value further.

The accuracy of the effective pressure-viscosity coefficients determined for the lubricant/refrigerant mixtures depends strongly on the accuracy of the dynamic viscosity data available for the refrigerant/lubricant mixtures. Viscosity measurements on refrigerant/lubricant mixtures should be considered in future work. Determination of accurate pressure-viscosity coefficients would allow modeling of the pressure-viscosity characteristics of lubricant/refrigerant mixtures.

More research is needed on the mechanism of the pressure-viscosity characteristics of blends. Studies could be conducted on blends of refrigeration lubricants and liquids similar to refrigerant structures. There are a few studies reported in the literature on liquid blends and pressure-viscosity characteristics (78, 79). For example, for mixtures of high and low $\alpha$-value fluids, such as polyphenyl ethers and diesters, it has been shown that a small amount of ester causes an almost complete loss of the high $\alpha$-value of the ether (78). The rapid fall in the $\alpha$-value is related to the plasticizing effect of the ester to lower the glass transition temperature of the ether. Another study on monoglycol/polyglycol fluids showed an unusual behavior in pressure-viscosity characteristics for the blends (79). A minimum $\alpha$-value was observed at a 50/50 blend of the two liquids. This corresponded to a maximum in the free volume of the mixture and showed an inverse relationship between $\alpha$-value and free volume. Studies like these could lead to the development of successful modeling for predicting the pressure-viscosity characteristics of lubricant/refrigerant mixtures.

In hydrodynamic contacts, one lubricant property, dynamic viscosity, determines both film thickness and friction properties. On the other hand, in EHD contacts, film formation and friction (traction) are effectively decoupled, and both depend upon different rheological properties. The dynamic viscosity of the lubricant in the contact inlet and its' pressure-viscosity coefficient control film thickness, whereas the limiting shear stress of the lubricant controls friction. In order to extend the life of the lubricated components in compressors and improve efficiency, these three different lubricant properties must be considered. Future work could focus on evaluating the EHD friction properties of the lubricant/refrigerant mixtures. Friction data could then be combined with the film thickness data to develop Stribeck-type curves for lubricant/refrigerant mixtures. This information could be used to determine and thus optimize lubricant behavior in refrigeration compressors.

## COMPLIANCE WITH AGREEMENT

No significant modifications or deviations from the technical performance of work as described in the contact agreement have been necessary during this reporting period.

## PRINCIPAL INVESTIGATOR EFFORT

During the course of this project, Dr. Selda Gunsel directed and/or performed the following activities:

- Project management
- Test equipment design and manufacturing
- Laboratory supervision
- Data analysis
- Reporting

## REFERENCES


1. Kruse, H. H. and Schroeder, M., “Fundamentals of Lubrication in Refrigeration Systems and Heat Pumps”, *ASHRAE J.*, 26, 5, 5, 1984.

2. Spauschus, H. O., “Evaluation of Lubricants for Refrigeration and Air Conditioning Compressors”, *ASHRAE J.*, 26, 5, 59, 1984.

3. Short, G. D., “Synthetic Lubricants and Their Refrigeration Applications”, *Lubr. Eng.*, 46, 4, 1990.

4. Bosworth, C. M., “Predicting the Behavior of Oils in Refrigeration Systems”, *Refrig. Eng*., 160, 6, 617, 1952.

5. Spauschus H. O. and Doderer G. C., “Reaction of Refrigerant-12 with Petroleum Oils”, *ASHRAE J*., 2, 65, 1961.

6. Hewitt, N. J., Mcmillan, J. T., Mongey, B., and Evans, R. H., “From Pure Fluids to Zeotropic and Azeotropic Mixtures: The Effects of Refrigerant-Oil Solubility on System Performance”, *International Journal of Energy Research*, 20, 57, 1996.

7. Reyes-Gavilian, J., Eckard, A., Flak, T., and Tricak, T., “A Review of Lubrication and Performance Issues in Refrigeration Systems using an HFC (R-134a) Refrigerant”, *Lubr. Eng*., 52, 4, 317, 1996.

8. Sanvodenker, K. S., “Mechanism of Oil-R12 Reactions - The Role of Iron Catalyst in Glass Sealed Tubes”, *ASHRAE Trans*., 91, 1, 1985.

9. Glova, D., “High Temperature Solubility of Refrigerants in Lubricating Oils”, *ASHRAE J.*, 26, 5, 59, 1984.

10. Spauschus H. O. and Speaker, L. M., “A Review of Viscosity Data for Oil-Refrigerant Solutions”, *ASHRAE Trans*., 93, 2, 1987.

11. Van Gaalen, N. A., Pate, M. B., and Zoz, S. C., “The Measurement of Solubility and Viscosity of Oil/Refrigerant Mixtures at High Pressures and Temperatures: Test Facility and Initial Results for R-22/Naphthenic Oil Mixtures”, *ASHRAE Trans*., 96, 2, 1990.

12. Srinivasan, P., Devotta, S., and Watson, F. A., “Thermal Stability of R11, R12B1, R113 and R114 and Their Compatibility with Some Lubricating Oils”, Chem. Eng. Res. Des., 63, 230, 1985.

13. Burkhardt, J. and Hahne, E., “Surface Tension of Refrigeration Oils”, IIR Commissions B1, B2, E1, E2, Mons, Belgium, 111, 1980.

14. Little J. I., “Viscosity of Lubricating Oil-Freon 22 Mixture”, *Refrig. Eng*. 60, 1191, 1952.

15. *CRC Handbook of Lubrication and Tribology*, Volume III, 387, 1994.

16. Short, G. D. and Rajewski, T. E., “Lubricants for Refrigeration and Air Conditioning”, *Lubr. Eng*., 51, 4, 270, 1995.

17. Hiodoshi, S., Kanayana, T., Matsuma, H., and Nomura, M., “Evaluation of Refrigerant Oils for R410A”, ASHRAE Meeting, Philadelphia, January 1997.

18. Komatsuzaki, S., Homma, Y., Kawashima, K., and Itoh, Y., “Polyalkylglycols as Lubricants for HFC 134a Compressors”, *Lubr. Eng*., 47, 12, 1018, 1991.

19. Komatsuzaki, S., Homma, Y., Itoh, Y., Kawashima, K., and Iizuka, T., “Polyolesters as HFC-134a Compressor Lubricants”, *Lubr. Eng*., 50, 10, 801, 1994.

20. Struss, R. A., Henkes, J. P., and Gabbey, L. W., “Performance Comparison of HFC 134a and CFC-12 with various Exchangers in Automotive Air Conditioning Systems”, SAE 900598.

21. Sanvordenker, K. S., “Experimental Evaluation of an R32/R134 Blend as a Near Drop-in Substitute for R 22”, *ASHRAE Trans*., DE 93-9-3, 773, 1993.

22. Vineyard, E. A., Sand, J. R., and Miller, W. A., “Refrigerator-Freezer Energy Testing with Alternative Refrigerants”, Seminar 89/01 ozone/CFC Alternative Studies ASHRAE Annual Meeting, June 24-28, 1989, Canada, CFC’s Time of Transition, ASHRAE, Atlanta 1989, 205.

23. El-Bourini, R., Hayahi, K., and Adachi, T., “Automotive Air Conditioning System Performance with HFC-134a Refrigerant”, SAE 960214.

24. Bateman, D. J., Bivens, D. B., Gorski, R. A., Wells, W. D., Lindstrom R. A., Morese, R. L., and Shomin, R. L., “Refrigeration Blends for the Automotive Air Conditioning Aftermarket”, SAE 900216.

25. Hourahan, G. and Godwin, D., “ARI’s R-22 Alternative Refrigerants Evaluation Program”, Proceedings of International CFC and Halon Alternatives Conference, Washington D.C., p. 55, 1992.

26. Huttenlocker, D. F., “Bench Scale Test Procedure for Hermetic Compressor Lubricants”, *ASHRAE J*., 11, 6, 85, 1969.

27. Sanvordenker, K. S., “Lubrication by Oil-refrigerant Mixtures: Behavior in the Falex Tester”, *ASHRAE Trans*., 90, 2, 1984.

28. Komatsuzaki, S., Tomobe, T., and Homma, Y., “Additive Effect on Lubricity and Thermal Stability of Refrigerator Oils”, *Lubr. Eng*., 43, 1, 31, 1987.

29. Komatsuzaki, S. and Homma, Y., “Antiseizure and Antiwear Properties of Lubricant Oils under Refrigeration Gas Environments”, *Lubr. Eng*., 47, 3, 193, 1991

30. Sheiretov, T., Glabbeck, W. V., and Cusano, C., “Evaluation of the Tribological Properties of Polyimide and Polyamide-imide) Polymers in a Refrigerant Environment”, *Trib. Trans*., 38, 4, 914, 1995.

31. Jonsson, U., “Elastohydrodynamic Lubrication and Lubricant Rheology in Refrigeration Compressors”, Ph.D. Thesis, Lulea University of Technology, Sweden, 1998.

32. Akei, M., Mizuhara, K., Taki, T., and Yamamoto, T. “Evaluation of Film-forming Capability of Refrigeration Lubricants in Pressurized Refrigerant Atmosphere”, Wear 196, pp. 180-187, 1996.

33. Akei, M. and Mizuhara, K., “The Elastohydrodynamic Properties of Lubricants in Refrigerant Environments”, ASME/STLE Tribology Conference, STLE Preprint 96-TC-1C-1, 1996.

34. Jacobson, Bo., “Lubrication of Screw Compressor Bearings in the Presence of Refrigerants”, Proc. Vol. 1. 115, International Compressor Engineering Conference at Purdue, 1994.

35. Wardle, F. P., Jacobson, B., Dolfsma, H., Höglund, E., and Jonsson, U., “The Effect of Refrigerants on the Lubrication of Rolling Element Bearings Used in Screw Compressors”, Proc. of Int. Com. Eng. Conf. at Purdue, 2, 523, 1992.

36. Jonnson, U. J. and Höglund, E., “Determination of Viscosities of Oil-Refrigerant Mixtures at Equilibrium by means of Film Thickness Measurements”, *ASHRAE Trans*., 99, 2, 1129, 1993.

37. Archard, J. F. and Cowking, F. W., “Elastohydrodynamic Lubrication of Point Contacts”, Proc. I. Mech. E., 180, p. 47, 1965.

38. Hammrock, B. J. and Dowson, D., “Isothermal EHD Lubrication of Point Contacts, Part III, Fully Flooded Results”, *ASME J. Lub. Tech*., 264, 1977.

39. Foord, C. A., Hamman, W. C., and Cameron, A., “Evaluation of Lubricants Using Optical Elastohydrodynamics”, *ASLE Trans*., 11, 31, 1968.

40. Crook, A. W., “The Lubrication of Rollers”, I. Phil. Trans. Roy. Soc. A 250 387, 1987.

41. Alliston-Greiner, A. F., Greenwood, J. A., and Cameron, A., “Thickness Measurements and Mechanical Properties of Reaction Films Formed by ZDDP During Running”, I. Mech. E. C178/87 565, International Conference, Tribology Friction Lubrication and Wear Fifty Years On, 1987.

42. Wilson R. W., “The Contact Resistance and Mechanical Properties of Surface Films on Metals”, Proc. Phys. Soc. 68B, 625, 1955.

43. Cameron, A., “Surface Failure in Gears”, *Jour. Inst. Pet*., 40, 191, 1954.

44. Kimura, Y. and Okade, K., “Film Thickness at Elastohydrodynamic Conjunctions Lubricated with Oil-in-Water Emulsions”, I. Mech. E., C176.87 85, International Conference, Tribology Friction Lubrication and Wear Fifty Years On, 1987.

45. Hoult, D. P., Lux, J. P., Wong, V. W., and Billian, S. A., “Calibration of Laser Fluorescence of Film Thickness in Engines“, SAE Tech. Ser. 881587, Int. Fuels and Lubes Meeting, 1988.

46. Wing, R. D. and Saunders, O. A., “Oil-Film Temperature and Thickness Measurements on the Piston Rings of a Diesel Engine”, Proc. I. Mech. E., 186, 1, 1972.

47. Safa, M. M., Anderson, J. C., and Leather, J. A., “Transducers for Pressure, Temperature and Oil Film Thickness Measurements in Bearings, Sensors and Actuators”, 3, 119, 1982.

48. Moore, S. L., “The Effect of Viscosity Grade on Piston Ring Wear and Film Thickness in Two Particular Diesel Engines”, I. Mech. E. C184/87, 473, International Conference, Tribology Friction Lubrication and Wear Fifty Years On, 1987.

49. Gohar, R. and Cameron, A., “The Mapping of Elastohydrodynamic Contacts”, *ASLE Trans*., 10, 215, 1967.

50. Johnston, G. J., Wayte, R., and Spikes, H. A., “The Measurement and Study of Very Thin Lubricant Films in Concentrated Contacts”, *Trib. Transactions*, 34, 2, 187, 1991.

51. Gunsel, S., Spikes H. A., and Aderin, M., “In-Situ Measurement of ZDDP Films in Concentrated Contacts”, *Trib. Trans*., 36, 2, 276, 1993.

52. Gunsel, S. and Spikes, H., “Film Formation Behavior of Lubricant Base Stocks in Concentrated Contacts”, presented at the 1996 STLE Annual Meeting in Cincinnati, May 1996.

53. Casserly, E. and Gunsel, S., “Elastohydrodynamic Lubrication of Aluminum Cold Rolling Base Oils and Formulated Lubricants”, presented at the 1996 STLE Annual Meeting in Cincinnati, May 1996.

54. Smeeth, M., Spikes, H. A., and Gunsel, S., “The Formation of Viscous Surface Films by Polymer Solutions: Boundary or Elastohydrodynamic Lubrication?”, *Trib. Trans*., 39, 237, 1996.

55. Smeeth, M., Spikes, H. A., and Gunsel, S., “Boundary Film Formation by Viscosity Index Improvers in Lubricated Contacts”, presented at the STLE/ASME Tribology Conference, FL, October 1995, Preprint No. 95-TC-3C-1, accepted for publication in *Trib. Trans*.

56. Gunsel, S., Smeeth, M., and Spikes, H. A., “Friction and Wear Reduction by Boundary Film-Forming Viscosity Index Improvers”, was presented at the 1996 SAE International Fall Fuels and Lubricants Meeting, October 1996, San Antonio, TX, accepted for publication by SAE, SAE 962037.

57. Smeeth, M., Spikes, H. A., and Gunsel, S., “The Performance of Viscosity Index Improvers in Lubricated Contacts”, accepted for publication by Langmuir, September 1995.

58. Gunsel, S., “Elastohydrodynamic Lubrication Properties of Refrigeration Oils”, presented at ASHRAE Meeting, Philadelphia, January 1997.

59. Aggarwal, B. B. and Wilson, W. R. D., “Improved Thermal Reynolds Equations”, Proc. 6th Leeds-Lyon Symposium on Tribology, “Thermal Effects in Tribology”, Lyon, Sept. 1979, Mechanical Engineering Publications, 1980.

60. Kuss, E., “Extreme Values of Pressure Coefficient of Viscosity”, Angew. Chem. Int. Ed. 4, pp. 944-950, 1965.

61. Jones, W. R., Johnson R. L., Winer, W. O., and Sanborn, D. M., “Pressure Viscosity Measurements of Several Lubricants to 5.5 x $10^8$ N/m2 and 149°C”, *ASLE Trans.,* 18, pp. 249-262, 1975.

62. The Theory of Rate Processes, Chapter IX, S. Glasstone, K. J. Laidler and H. Eyring, publ. McGraw Hill, NY and London, 1941.

63. Kyotani, T., Tamia, Y., and Horita, Y., “Flow Properties of Alicyclic Compounds as Traction Fluids”, *ASLE Trans*., 26, pp. 538-544, 1983.

64. Chang, H. S., Spikes, H. A., and Buneman, T. F., “The Shear Stress Properties of Ester Lubricants in Elastohydrodynamic Contacts”, JSL 9, 2, 91-114, 1991.

65. So, B. Y. and Klaus, E. E., “Viscosity-Pressure Correlation of Liquids”, *ASLE Trans.,* 23, 4, pp. 409-21, 1980.

66. Doolittle, A. K., “Studies in Newtonian Flow 11, The Dependence of the Viscosity of Liquids on Free-Space”, J. Appl. Phys., 22, 1471-1475, 1951.

67. Macedo, P. B. and Litovitz, T. A., “On the Relative Rolls of Free Volume and Activation Energy in the Viscosity of Liquids”, J. Chem. Phys., 42, 1, 245-256, 1965.

68. Gunsel, S., Korcek, Stefan, Smeeth, M., and Spikes, H. A., “The Elastohydrodynamic Friction and Film Forming Properties of Lubricant Base Oils”, presented at The World Tribology Congress, London, U.K., September 1997, accepted for publication in Tribology Transactions.

69. LaFountain, A., Johnston, G. J., and Spikes, H. A., “Elastohydrodynamic Friction Behavior of Polyalphaolefin Blends”, Proceedings Leeds-Lyon Symposium, Tribology for Energy Conservation, London, U.K., September 1997, 465-475, Edited by D. Dowson et al, Elsevier, 1998.

70. Henderson, D., “Solubility, Viscosity and Density of Refrigerant/Lubricant Mixtures”, ARTI Report Number DOE/CE/23810-34, 1994.

71. Cavestri, R., “Measurement of Viscosity Density and Gas Solubility of Refrigerant Blends in Selected Synthetic Lubricants”, ARTI Report Number DOE/CE/23810-46.

72. Van Gaalen, N. A., Zoz, S. C., and Pate, M. B., “The Solubility and Viscosity of Solutions of HCFC-22 in Naphthenic Oil and in Alkylbenzene at High Pressures and Temperatures”, *ASHRAE Trans.,* 97 (1): 100, 1991a.

73. Communication with A. Mulay of Copeland Corporation, October 1998.

74. Communication with R. Yost and M. Wilson of ICI Corporation, March-December, 1998.

75. Communication with P. Johnson of Frick Company, July 1997.

76. Communication with V. Cheng of Mobil Corporation, November 1998.

77. Communication with L. Homolish of Idemitsu-Kosan Corporation, November 1997.

78. Spikes, H. and Hammond, C., “Elastohydrodynamic Film Thickness of Binary Ester-Ether Mixtures”, *ASLE Transactions*, 24, 4, 542-548, 1980.

79. Wan, G. and Spikes, H., “The Elastohydrodynamic Lubrication Properties of Water-Polyglycol Fire-Resistant Fluids”, *ASLE Transactions*, 27, 4, 366-372, 1986.

## APPENDIX A
## RI DETERMINATION FOR LUBRICANT/REFRIGERANT MIXTURES

An optical method for measuring refractive index (RI) of lubricant/refrigerant mixtures was developed using the EHD rig and the ultrathin film interferometry technique. This method for measuring the RI of the fluid in the EHD contact is based on the following principles:

Constructive interference obeys the following equation:

$$h = \frac{(N - \Phi)\lambda}{2n \cos\theta} \qquad \textbf{Equation 1}$$

Where h is the film thickness, N is the fringe order, $\Phi$ is the phase change, $\lambda$ is the wavelength, n is the RI, and $\theta$ is the angle of incidence.

For loaded ball on flat (point) contacts, film thickness is related to contact geometry, contact stress and elastic properties of materials as shown below:

$$h = 3.81 \left(\frac{(1 - \sigma_1^2}{E_1} + \frac{1 - \sigma_2^2)}{E_2}\right) \frac{a}{2} \frac{p_{max}}{a} (r - 1)^{1.5} \qquad \textbf{Equation 2}$$

Where h is the film thickness, $\sigma$ is Poisson's ratio, E is Young's modulus, a is the Hertzian diameter, $p_{max}$ is the maximum Hertz stress, r is the radius of the interference fringe's circle. Substituting h from Equation 1 into Equation 2 results in the following equation:

$$\frac{(N - \Phi)\lambda}{2n \cos\theta} = 3.81 \left(\frac{(1 - \sigma_1^2}{E_1} + \frac{1 - \sigma_2^2)}{E_2}\right) \frac{a}{2} \frac{p_{max}}{a} (r - 1)^{1.5} \qquad \textbf{Equation 3}$$

Refractive index for a given fluid in the contact can be calculated from the above equation by measuring the radius of fringes at two different fringe orders (m and m+k). Subtraction of Equation 3 written for fringe order m and m+k gives:

$$\frac{N_{m+k} - N_m}{2n \cos\theta} = 3.81 \left(\frac{(1 - \sigma_1^2}{E_1} + \frac{1 - \sigma_2^2)}{E_2}\right) \frac{a}{2} \frac{p_{max}}{a} \{(r_{m+k} - 1)^{1.5} - (r_m - 1)^{1.5}\} \qquad \textbf{Equation 4}$$

## APPENDIX B
## RI CORRECTION FOR CONTACT PRESSURE

To calculate the film thickness from optical film thickness, it is necessary to know the refractive index of the sample in the contact at the contact pressure. The Lorentz-Lorentz equation given below can be used to relate the refractive index and density as follows:

$$\mu_p = \left[\frac{1 + 2A}{1 - A}\right]^{1/2}$$

where:

$$A = \frac{\rho_p}{\rho_o}\left[\frac{\mu_o^2 - 1}{\mu_o^2 + 2}\right]$$

where $\mu_o$ = RI at atmospheric pressure
$\rho_o$ = density at atmospheric pressure
$\mu_p$ = RI at contact pressure
$\rho_p$ = density at contact pressure

$\rho_p/\rho_o$ is obtained from Hartung's formula given below:

$$\frac{\rho_p}{\rho_o} = 1 + \frac{42.8 \times 10^{-6}\ p^{0.75}}{(\nu_{100})^{0.0385}}$$

where:

$\nu_{100}$ : kinematic viscosity at 100 °F

## APPENDIX C
## COMMERCIAL IDENTIFICATION

| Lubricants | Commercial Identification |
|---|---|
| ISO 32 Naphthenic Mineral Oil | Suniso 3GS |
| ISO 68 Naphthenic Mineral Oil | Suniso 4GS |
| ISO 32 Polyolester | ICI Emkarate RL 32H |
| ISO 68 Polyolester A | ICI Emkarate RL 68H |
| ISO 68 Polyolester B | Mobil EAL 68 |
| ISO 68 Polyolester C | CPI Solest 68 |
| ISO 32 Polyvinyl Ether | Idemitsu Kosan FVC 32B |
| ISO 68 Polyvinyl Ether | Idemitsu Kosan FVC 68B |